

AD-A046 669

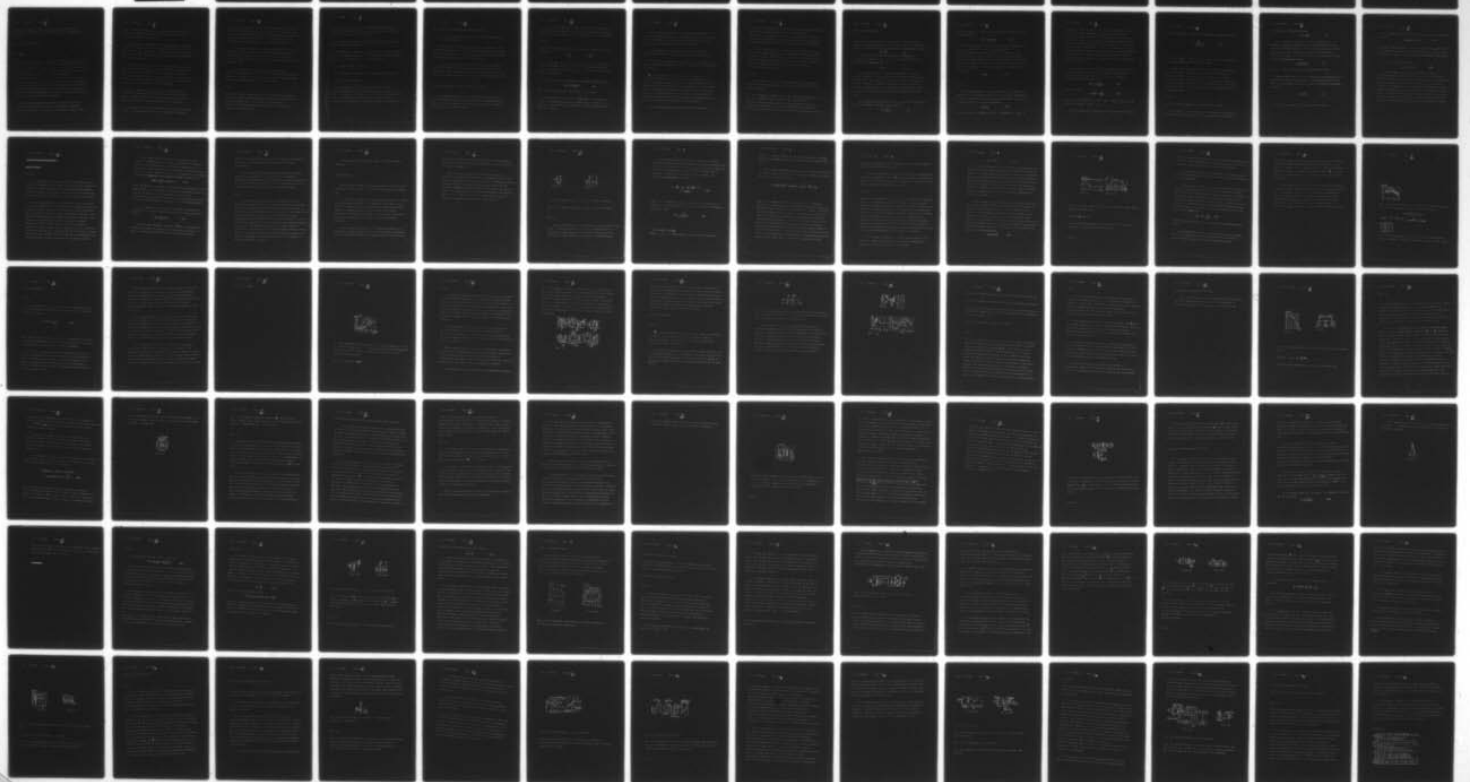
FOREIGN TECHNOLOGY DIV WRIGHT-PATTERSON AFB OHIO
FERROELECTRIC RADIATION DETECTORS, (U)
JUL 77 L S KREMENCHUGSKIY
FTD-ID(RS)T-0846-77

F/G 17/5

UNCLASSIFIED

NL

1 OF
ADA
046669



AD-A046669

1

FOREIGN TECHNOLOGY DIVISION



FERROELECTRIC RADIATION DETECTORS

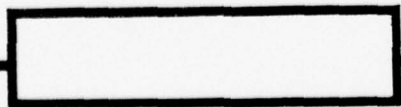
by

L. S. Kremenchugskiy



DDC
RECEIVED
NOV 21 1977
D

Approved for public release;
distribution unlimited.



UNEDITED MACHINE TRANSLATION

FTD-ID(RS)T-0846-77

5 July 1977

MICROFICHE NR: *FTD-77-C-000792*

FERROELECTRIC RADIATION DETECTORS

By: L. S. Kremenchugskiy

English pages: 538

Source: Segnetoelektricheskiy Priyemniki
Izlucheniya, "Naukova Dumka", Kiev,
1971, pp 1-234

Country of origin: USSR

This document is a machine translation

Requester: DRDMI-YDL

Approved for public release; distribution
unlimited

THIS TRANSLATION IS A RENDITION OF THE ORIGINAL FOREIGN TEXT WITHOUT ANY ANALYTICAL OR EDITORIAL COMMENT. STATEMENTS OR THEORIES ADVOCATED OR IMPLIED ARE THOSE OF THE SOURCE AND DO NOT NECESSARILY REFLECT THE POSITION OR OPINION OF THE FOREIGN TECHNOLOGY DIVISION.

PREPARED BY:

TRANSLATION DIVISION
FOREIGN TECHNOLOGY DIVISION
WP.AFB, OHIO.

U. S. BOARD ON GEOGRAPHIC NAMES transliteration SYSTEM

Block	Italic	Transliteration	Block	Italic	Transliteration
А а	<i>А а</i>	A, a	Р р	<i>Р р</i>	R, r
Б б	<i>Б б</i>	B, b	С с	<i>С с</i>	S, s
В в	<i>В в</i>	V, v	Т т	<i>Т т</i>	T, t
Г г	<i>Г г</i>	G, g	У у	<i>У у</i>	U, u
Д д	<i>Д д</i>	D, d	Ф ф	<i>Ф ф</i>	F, f
Е е	<i>Е е</i>	Ye, ye; E, e*	Х х	<i>Х х</i>	Kh, kh
Ж ж	<i>Ж ж</i>	Zh, zh	Ц ц	<i>Ц ц</i>	Ts, ts
З з	<i>З з</i>	Z, z	Ч ч	<i>Ч ч</i>	Ch, ch
И и	<i>И и</i>	I, i	Ш ш	<i>Ш ш</i>	Sh, sh
Й й	<i>Й й</i>	Y, y	Щ щ	<i>Щ щ</i>	Shch, shch
К к	<i>К к</i>	K, k	Ъ ъ	<i>Ъ ъ</i>	"
Л л	<i>Л л</i>	L, l	Ы ы	<i>Ы ы</i>	Y, y
М м	<i>М м</i>	M, m	Ь ь	<i>Ь ь</i>	'
Н н	<i>Н н</i>	N, n	Э э	<i>Э э</i>	E, e
О о	<i>О о</i>	O, o	Ю ю	<i>Ю ю</i>	Yu, yu
П п	<i>П п</i>	P, p	Я я	<i>Я я</i>	Ya, ya

*ye initially, after vowels, and after ъ, ь; e elsewhere.
 When written as ё in Russian, transliterate as yë or ë.
 The use of diacritical marks is preferred, but such marks may be omitted when expediency dictates.

GREEK ALPHABET

Alpha	A	α	α	Nu	N	ν
Beta	B	β		Xi	Ξ	ξ
Gamma	Γ	γ		Omicron	Ο	ο
Delta	Δ	δ		Pi	Π	π
Epsilon	Ε	ε	ε	Rho	Ρ	ρ ϑ
Zeta	Z	ζ		Sigma	Σ	σ ς
Eta	H	η		Tau	Τ	τ
Theta	Θ	θ	θ	Upsilon	Υ	υ
Iota	I	ι		Phi	Φ	φ φ
Kappa	K	κ	κ	Chi	Χ	χ
Lambda	Λ	λ		Psi	Ψ	ψ
Mu	M	μ		Omega	Ω	ω

RUSSIAN AND ENGLISH TRIGONOMETRIC FUNCTIONS

Russian	English
---------	---------

sin	sin
-----	-----

cos	cos
-----	-----

tg	tan
----	-----

ctg	cot
-----	-----

sec	sec
-----	-----

cosec	csc
-------	-----

sh	sinh
----	------

ch	cosh
----	------

th	tanh
----	------

eth	coth
-----	------

sch	sech
-----	------

csch	csch
------	------

arc sin	\sin^{-1}
---------	-------------

arc cos	\cos^{-1}
---------	-------------

arc tg	\tan^{-1}
--------	-------------

arc ctg	\cot^{-1}
---------	-------------

arc sec	\sec^{-1}
---------	-------------

arc cosec	\csc^{-1}
-----------	-------------

arc sh	\sinh^{-1}
--------	--------------

arc ch	\cosh^{-1}
--------	--------------

arc th	\tanh^{-1}
--------	--------------

arc eth	\coth^{-1}
---------	--------------

arc sch	sech^{-1}
---------	----------------------------

arc csch	csch^{-1}
----------	----------------------------

rot	curl
-----	------

lg	log
----	-----

GRAPHICS DISCLAIMER

All figures, graphics, tables, equations, etc. merged into this translation were extracted from the best quality copy available.

Table of Contents

U.S. Board on Geographic Names Transliteration System.....	11
Russian and English Trigonometric Functions.....	111
Preface.....	2
Chapter I. Thermal Radiation Detectors.....	6
Chapter II. Bases of Physics of Ferroelectric.....	98
Chapter III. Pyroelectric Coefficient and Dielectric Constant of Ferroelectric.....	174
Chapter IV. The Theory of Pyroelectric Radiation Detectors.....	238
Chapter V. Pyroelectric Radiation Detectors.....	292
Chapter VI. Ferroelectric Bolometers.....	407
Chapter VII. Equipment and Procedures for Determining the Characteristics of Material and Parameters of Ferroelectric Radiation Detectors.....	435
Chapter VIII. Limited Applications of Ferroelectric Thermal Radiation Detectors.....	500

ACCESSION FOR	
NTIS	White Section <input checked="" type="checkbox"/>
DDC	Buff Section <input type="checkbox"/>
UNANNOUNCED	<input type="checkbox"/>
JUSTIFICATION.....	
BY.....	
DISTRIBUTION/AVAILABILITY CODES	
DIV.	AVAIL. AND/OR SPECIAL
A	

FERROELECTRIC RADIATION DETECTORS.

L. S. Kremenchugskiy.

Page 1.

Page 2.

Monograph is dedicated to the new class of the thermal radiation detectors, develop/processed at present on the basis of ferroactive materials.

Is given the basic information about ferroelectricity of radiation detectors and are given their equivalent replacement schemes. Is given the procedure of calculation of the fundamental receiver responses and the methods of their agreement with measuring device. are described equipment and procedures for determining the basic parameters of receivers.

Monograph is designed to scientific and technical-engineering

workers, who are occupied by the development of radiation detectors, by the measurement of electromagnetic radiation and by the construction of spectral and radiometric instrumentation.

The chief editor is Candidate of Physics and Mathematical Sciences A. F. Yatsenko.

Pages 3-4.

No typing.

Page 5.

The preface

The problem of emission/radiation measurement belongs to the urgent problems of physics technicians.

The creation of new radiation sources in the different regions of the electromagnetic spectrum and whole being expanded range of the measured super-weak and high-power flows present new requirements for radiation detector - to the central cell/element of radiation instrument.

The thermal radiation detectors are universal detectors in all electromagnetic range. They found wide use in spectrometry and radiometry.

From the torque/moment of the appearance of the book of R. Smith, F. Jones and R. Chesmer "detection and the measurement of infrared radiation", significant part of whom is dedicated to thermal radiation detectors, pass more than 10 years. During this period thermal radiation detectors received further development mainly in the direction of an increase in sensitivity and reduction in the inertness. An increase in the sensitivity of thermal receivers proceeded successfully by the creation of the cooled and superconducting bolometers, and a reduction in the inertness - by the development of pyroelectric receivers.

These successes in part of the development of pyroelectric receivers were not reflected in the left in 1968 book of M. N. Markov "infrared receivers", or in the translated to the Russian language in 1969 book of Zh. Shol, I. Marfan, M. Myunsh, P. Torelya and P. Kombet from themes by name.

At present ferroelectric radiation detectors are utilized in the various regions of metrology, and the interest in them with each year grow/rises.

The basic content of the proposed book precedes survey/coverage on thermal radiation detectors (chapter I). In the second chapter are presented the bases of physics of ferroelectric, necessary for the understanding of the operating principle of radiation detector. Chapter III is dedicated to the description of the experimental studies of the derivatives of spontaneous polarization - pyroelectric coefficient and dielectric constant. The theory of pyroelectric radiation detectors is the content of chapter IV. In chapter of V is given the information about developments and parameters of pyroelectric radiation detectors. The examination of ferroelectric bolometers is given in chapter VI.

Page 6.

Special section (chapter VII) is dedicated to the description of equipment and procedures for determining the parameters of ferroelectric receivers. And finally, in the last/latter chapter are presented the limited applications of receivers and prospect for their development.

The present monograph, apparently, is the first attempt at the generalization of material on ferroelectric radiation detectors;

therefore the author is previously grateful to all for critical observations in its address.

The author is sincerely grateful Cand. the physico-mathematical of the sciences of O. V. Raytsinoy, to V. B. Samoilov, to M. A. Itskovskiy and G. S. Danil'chuk for the survey of the separate chapters of the manuscript and the made observations. The author is also grateful to the chief editor of Cand.'s book the physico-mathematical of A. F. Yatsenko's sciences for a series of councils and observations about contents of the book.

Page 7.

Chapter I

THERMAL RADIATION DETECTORS.

The radiation detector is one of the basic links of the channel of information between the radiating body or the medium, through which it passes emission/radiation, and the recorder, which transmits this information to observer.

Relative spectral radiant energy of bodies, which are located at different temperatures, in the optical wavelength range is represented in Fig. to 1.1. This range is spread from extreme ultraviolet to far-infrared region and includes spectral range from 0.1 to 1000 μ [3].

The human eye - one of the radiation detectors - is characterized by remarkable properties. It is equipped with the adjustable pupil, capable of changing its aperture depending on the degree of illumination, it can produce automatic focusing and distinguish the brightness levels, which are changed into a million

once. In the visible region of the spectrum of eye it is one of the most sensitive optical instruments. However, its spectral interval is very limited and it is 450-700 μ .

The large part of the object/subjects, which are located on the earth/ground and surrounding us, has a temperature, close to 300°K. These object/subjects emit infrared radiation in the range 2-100 μ with the maximum of emission/radiation of approximately 10 μ . Unfortunately, the emission/radiation object/subjects with the temperature of less than 800°K (boundary of red heat) eyes completely does not feel.

For the perception of the radiation of invisible objects were developed the radiation detectors - thermal and photoelectric.

The operating principle of thermal radiation detector (TPI) is based on thermal effect. The quanta of the radiation flux being investigated affect the receiving surface of detector.

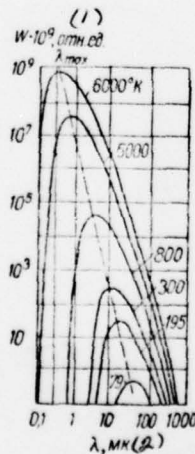


Fig. 1.1.

Fig. 1.1. Relative spectral radiant energy of bodies, which are located at the different temperatures in the optical wavelength range.

Key: (1). rel. un. (2). μ .

Page 9.

Their energy, in essence, is distributed between free electrons and the molecules of the layer, which absorbs emission/radiation, and then it is transferred to sensing element of receiver. This leads to an increase in the temperature of sensing element and a change in the parameter, which depends on temperature (resistance, capacitance/capacities, etc.). A change in the value of the latter is recorded by measuring circuit. Since an increase in the temperature of sensing element connected with its heat capacity and heat-transfer conditions from sensing element in the environment, the set-up time of the equilibrium temperature at the suddenly applied radiation flux of the majority of receivers is 10^{-1} - 10^{-3} s.

Unlike the thermal receivers whose reaction depends on the common/general/total absorbed energy, photoelectric radiation detectors react only to a quantity of effectively absorbed quanta

whose energy is sufficient for the release of bound electrons and emergence of photo effect. For photoelectric receivers there is a long-wave boundary of detection.

The set-up time of photoelectric processes small as compared with the set-up time of temperature balance into TPI and does not depend on the heat capacity of sensitive layer. By this is explained the operating speed of photoelectric receivers with comparatively thick sensing elements.

In the past decade were reached the considerable successes in the creation of the new types of photoelectric receivers and the displacement of the boundary of their sensitivity in long-wave region. In connection with this were assumed about the wide prospect of developing photoelectric receivers in the near future their and universal use in radiation instrument manufacture.

However, recently and TPI received new development. The development of the cooled and superconducting bolometers made it possible to raise threshold sensitivity TPI, and the creation of pyroelectric receivers is to sharply lower their inertness.

The appearance of intense radiation sources - lasers - supplied a series of the new problems before the developers of radiation

detectors. Along with high threshold sensitivity and rapid response to radiation detectors they began to present the requirements for wide dynamic range, ability to maintain/withstand large radiation and mechanical effects, the stabilities of the parameters in time, uniformities of zonal sensitivity and a series of others.

Was outlined at present the following tendency in the use of radiation detectors in optical range. In ultraviolet, visible and near infrared the regions of the spectrum more frequently are utilized photoelectric receivers, while in far-infrared region find a larger use TPI.

It is natural that this division very conditionally. Photoelectric receivers possess the limited spectral characteristic, caused by the nature of photo effect, but they have high sensitivity in working spectral interval and rapid response.

Page 9.

TPI in principle are nonselective, if are covered with the layer of substance, which absorbs emission/radiation in the assigned spectral interval. Majority of TPI are inertia in comparison with photoelectric receivers, but exceed them in the relation to the stability of characteristics.

Thus, the selection of receiver for a radiation instrument depends on the specific conditions, under which it is possible to return advantage to one type or the other.

Depending on the operating principle of TPI it is possible to divide into the following types:

1) bolometers are metallic, semiconductor and dielectric (among other things ferroelectric); the use of cryogenics made it possible to create the superconducting and cooled bolometers;

2) radiation thermal elements;

3) optico-acoustic (pneumatic) and dilatometric receivers;

4) pyroelectric receivers.

The classification of thermal receivers it is possible to conduct also depending on the designation/purpose of this form of receiver - receivers for spectral target/purposes, receivers for the absolute measurements of emission/radiation, receivers for the measurement of the signals of very small intensity or receivers for

the measurement of powerful radiation fluxes, etc.

As the basis below description of TPI is placed the physical principle of their action.

For using TPI in radiation instrument it is necessary to know their characteristics. The set of characteristics must be so complete in order that it would be possible to predict the possibility of the develop/processed on the basis of receivers device.

In spite of works [1-2, 4-16] on classification and metrics of radiation detectors, frequently into determining one and the same characteristics the different authors pack different sense. Therefore one should at first determine the fundamental characteristics of TPI.

§1. Characteristics of thermal radiation detectors.

The conversion factor of TPI is determined by the ratio of the value of output signal to the flow value of the emission/radiation, which falls to it. Radiant flux is expressed in watts or joules, and output signal - in volts or amperes.

In work on the modulated radiant flux, the input signal most frequently is determined by effective power coefficient W (in watts), and exit - by the effective value of voltage/stress of V (in volts).

Page 10.

In this case the conversion factor is called the volt-watt or voltage sensitivity

$$S = \frac{V}{W}. \quad (1.1)$$

If input signal is emission impulse whose energy is expressed in joules, the output signal is determined from the maximum value in volts. The conversion factor during pulse irradiation is called pulse voltage sensitivity.

Function $S(t)$ can be decomposed into Fourier integral [12]:

$$S(t) = \int_{-\infty}^{+\infty} S(f) e^{2\pi i f t} df, \quad (1.2)$$

where $S(f)$ - spectral volt sensitivity; f is frequency.

The RMS value of the noise of TPI $V_{\overline{\epsilon^2}}$. Noises are called the irregular disturbance/perturbations, which appear in receiver in the absence of signal. Noise sets limitations on lower boundary of the detectable signal.

Since the mean deviation of the fluctuating value from equilibrium value at averaging for sufficiently large time interval is equal to zero, the most important characteristic is the mean square of noise or square root of this value [17].

The threshold of sensitivity of TPI in the general case is limited to three forms of noises, fundamental by its nature [6].

1. By thermal or Johnson noises, caused by the fluctuations of charge carriers in resistance and which do not depend on the material of receiver.

2. By the radiation or photon noises, determined by the instantaneous fluctuations of the number of photons, which are emitted by radiation sources at the given instant. Radiation noises appear also from the emission of the background of the which surround receiver object/subjects (housing of receiver). For a reduction in this type of noises the housing of receiver cools and utilize the optical filters, inswept the spectral range of emission/radiation to the spectral interval of the source being investigated.

3. By the temperature noises, connected with temperature

fluctuations, which appear into TPI due to the statistical nature of heat exchange between sensing element of receiver and the environment. In this case, if the heat exchange because of thermal conductivity and convection is small and in essence is determined by emission/radiation, the temperature noises are identical radiation.

Into TPI sometimes there are noises, which are not fundamental and can be removed by improvement in technology of obtaining sensing element and by the construction of receiver. These are current and microphonic noises, the noises, which appear as a result of boiling the cooling fluid in cryostat, is clever repolarization in ferroelectric receivers, etc.

Page 11.

Since of the noise sources enumerated above are statistically independent, the mean square of noise is the sum of the mean squares of its components.

The threshold of response of TPI (the equivalent horsepower of noises) is determined by the amount of the rate of flow of emission/radiation, which creates in sensing transducer, equal in magnitude to the RMS value of its noise. Virtually the threshold sensitivity is equal to RMS value bag, divided into conversion factor

(volt-watt sensitivity):

The threshold of sensitivity one ought not to identify with the minimally detectable aerial input. The latter can be determined with different degree of reliability in different signal-to-noise ratios.

$$\mathcal{P} = \frac{\sqrt{\epsilon^2}}{S} \quad (1.3)$$

Threshold of sensitivity (capability for detection) is introduced by Jones into 1952 and is the reciprocal value of the threshold of sensitivity [4]:

$$\mathcal{DP} = 1. \quad (1.4)$$

Jones noted that the threshold of sensitivity as receiver response suffers one logical deficiency/lack, which consists in the fact that than the receiver is better, the lower its threshold of response. Threshold sensitivity as parameter is free from this defect. The more the parameter \mathcal{D} , the more signal-to-noise ratio it is reached at the given receiver at the fixed/recorded radiation flux.

The threshold of sensitivity from energy is defined as ratio of value signal/noise to energy of input pulse E:

$$\Delta = \frac{U_{\max}}{\sqrt{\epsilon^2} \cdot E} \quad (1.5)$$

The maximum value Δ is characterized according to Jones [12] by the relationship/ratio

$$(\Delta_{\max})^2 = 4 \int_0^{\infty} |D(f)|^2 df. \quad (1.6)$$

Spectral sensitivity TPI $S(\lambda)$. Signal at the output/yield of TPI in principle must not depend on wavelength λ the emission/radiation of source, if receiver is covered with the substance, which completely absorbs emission/radiation at all wavelengths. Unfortunately, the absorbing coatings are nonselective only in small spectral intervals. The spectral sensitivity of TPI is defined as dependence of conversion factor on the wavelength of radiant flux:

$$S = S(\lambda). \quad (1.7)$$

Page 12.

The zonal sensitivity of TPI characterizes its coefficient of conversion in the different sections of sensor during irradiation by the light probe whose size/dimensions are considerably less than the size/dimensions of the receiving area/site:

$$S = S(x, y). \quad (1.8)$$

Sensitivity on the receiving area/site of receiver, as a rule, is

nonuniform. Of the bolometers of the zone of sensor, the close to contacts and having temperature lower than maximum, possess understated sensitivity [21]. The investigations of recent years showed that in work on the modulated emission/radiation the zonal sensitivity of thermal elements is also nonuniform due to more powerful thermal conductivity in the area of joints, than between joints. Besides the basic reasons, which lead to the nonuniformity of sensitivity due to receiving area/site, are possible the local heterogeneities of material of sensitive cell/element, that affect receiver responses.

Time constant of TPI. The phenomenological time constant of TPI is determined from its amplitude-frequency characteristic. If amplitude-frequency characteristic of TPI it is possible to approximate the curve of form [8]

$$S(f) = \frac{S_0}{(1 + \omega^2 \tau_s^2)^{0.5}}, \quad (1.9)$$

that time constant

$$\tau_s = (2\pi f_0)^{-1} = \frac{\sqrt{3}}{2\pi f_{0.5}}, \quad (1.10)$$

where f_0 is the frequency, at which $S(f_0) = 0.71 S_0$; $f_{0.5}$ - the frequency, at which $S(f_{0.5}) = 0.5 S_0$.

The more fundamental determination of the inertness of receiver

is the time constant on threshold sensitivity, introduced by Jones:

$$\tau_d = \frac{\mathcal{D}_{\max}^2}{4 \int_0^{\infty} \mathcal{D}^2(f) df} . \quad (1.11)$$

In this case τ_d does not depend on the frequency characteristic of amplifier and is in this sense invariant.

Besides phenomenological time constants for the calculations of TPI (specifically, bolometers), is utilized the physical time constant, equal to the ratio of heat capacity of the sensitive cell/element to the coefficient of heat losses. Work [7] shows, that in dynamic behavior effective the heat capacity and the coefficient of heat losses are the complex functions of the modulation frequency of radiation flow.

Page 13.

Therefore the term physical time constant loses meaning.

More logical is the introduction of the concept of the factor of the inertness of TPI, equal to the ratio effective heat capacities to

the coefficient of the heat losses:

$$\tau(\omega) = \frac{c(\omega)}{G(\omega)} . \quad (1.12)$$

This parameter is convenient for the calculations of amplitude-frequency and phase-frequency characteristics of TPI. Experimentally the parameter $\tau(\omega)$ at sinusoidal modulation can be determined by angle measurement ϕ , which characterizes phase displacement between the radiant flux and the signal, which appears in receiver during irradiation:

$$\tau(\omega) = \operatorname{tg} \varphi / \omega; \quad (1.13)$$

$$\varphi = \operatorname{arc} \operatorname{tg} \tau(\omega) \cdot \omega, \quad (1.14)$$

where $\varphi = \phi(\omega)$ - phase-frequency characteristic of TPI.

Dynamic range of TPI. L [8] is determined by the relation of the maximum power coefficient (energy) of radiant flux $W_{\max}(E_{\max})$ in the range of the linearity of amplitude receiver response to threshold of response:

$$L = \frac{W_{\max}(E_{\max})}{\mathcal{P}(\Delta)} . \quad (1.15)$$

§2. Bases of the theory of thermal radiation detectors.

The threshold of response of TPI in general form can be written as follows:

$$\mathcal{P} = |\bar{W}_r^2 + \bar{\epsilon}_J^2 S^{-2} + \bar{\epsilon}_A^2 S^{-2}|^{0.5}, \quad (1.16)$$

where \bar{W}_r^2 is the mean square of the fluctuations of the power of heat flux, caused by radiation or temperature noises; $\bar{\epsilon}_J^2$ and $\bar{\epsilon}_A^2$ is the mean square of Johnson and supplementary interferences respectively.

Of the ideal thermal receiver

$$\bar{W}_r^2 > \bar{\epsilon}_J^2 S^{-2} + \bar{\epsilon}_A^2 S^{-2}. \quad (1.17)$$

All effort/forces of developers are directed toward investigation of the possibilities of increase in the conversion factor S a decrease in the value of Johnson and supplementary noises. If supplementary interferences can be excluded by the rational selection of technology of the production of receiver, then Johnson noises are fundamental by their nature and are inherent in all TPI, with the exception acousto-optical. Inequality (1.17) is fulfilled at present not for one of the TPI, and better/best TPI at least by an order worse on the threshold of response of ideal thermal receiver.

~~MICROFILM HEADER ESR 77020846~~~~MT/ST-77-00006~~

Page 14.

The calculation of TPI consists of the determination of the composite coefficient of the conversion, which makes it possible to simultaneously determine amplitude-frequency and phase-frequency receiver responses. If we assume that are absent the supplementary noises, then it is not difficult to find its threshold of response.

There are two approaches for calculation of TPI. In the first case TPI is considered as system with the concentrated constants [2, 6, 20, 27 28, 83]. Solution to the equation of thermal equilibrium for sensing element of the receiver, irradiated by radiation flux and cooled caused by thermal conductivity and intrinsic emission, makes it possible to determine the conversion factor of receiver. Examination of TPI as lumped systems can be, for example, is justified only for a vacuum metallic bolometer 0.1-0.5 μ thickness in the ratio of the length of sensing element l to its width b , which exceeds 10-15. For another TPI this assumption is erroneous, and the calculations lead to large with errors or to incorrect results.

In the second case the receiver is characterized by the distributed parameters. On this basis is constructed the dynamic theory of TPI, which considers volumetric nonuniformity of the distribution in sensing element of receiver and its ambient medium [7, 8, 21, 25, 26]. The basic link in the calculation is the solution to the three-dimensional nonhomogeneous equation of form [25]

$$\frac{\partial \theta(\vec{r}, t)}{\partial t} = k \nabla^2 \theta(\vec{r}, t) + A \theta(\vec{r}, t) + B, \quad (1.18)$$

where $\theta(\vec{r}, t)$ is a temperature increment during irradiation in any point of TPI; k - the coefficient of thermal conductivity; A and B - values which depend on the construction of TPI, from the thermophysical and electrical properties of the material, from which is made the receiver, and the circuits of its connection/inclusion.

For determining the signal, taken from TPI, is necessary the calculation of the mean temperature increment of sensing element by volume v

$$\bar{\theta}(t) = \frac{1}{v} \int_0^v \theta(\vec{r}, t) d\vec{r}. \quad (1.19)$$

On the average temperature increment $\bar{\theta}(t)$ it is possible to determine the composite coefficient of transformation of TPI. In a number of cases the determination of the average temperature

increment on the strength of the symmetry of problem is reduced to the solution to the one-dimensional equations of thermal conductivity.

Dynamic theory of TPI still it is not possible to consider final. Series of problems is solved under the simplifying assumptions. For example, upon consideration of boundary conditions it is assumed that the radiation losses are characterized not by Stephan-Boltzmann law, but by Newton's simplified formula.

Page 15.

Are possible other methods of the calculation of TPI, in particular bolometers [27, 34, 39, 41]. In work [27] is constructed the phenomenological theory of bolometers in their examination as cell/elements of electrical circuit. In this case it was assumed that the characteristics of bolometer remain adequate both during irradiation of it by radiation flux and during scattering in it the power of the Joule loss of the same value. on the measured dependence of resistance of bolometer R on current I it is possible to rate/estimate the basic parameters of the prepared bolometer at this operating point, not by wave of radiation measurements, and if the noises of bolometer are assumed Johnson, then it is possible to determine threshold of response.

We will consider the different forms of thermal radiation detectors.

§3. bolometers.

Bolometers are utilized in metrology about 100 years, but also now because of the new successes in their development are promising TPI.

The action of bolometer in the general case is based on a change in its impedance, which leads to modulation of the stress in the electrical circuit, in which is included the bolometer. Are known metallic, semiconductor and dielectric (among other things ferroelectric) bolometers. Depending on the selection of operating temperature distinguish the uncooled and cooled (cryogenic) bolometers.

Metallic bolometers [30-67]. The temperature dependence of resistance of metallic film was used for the creation of bolometer. The best results were obtained with nickel [37, 40, 42, 44, 53, 66]

and bismuth [30, 31, 33, 35, 51, 54, 57, 58, 59, 61] bolometers, although gold [38, 52, 63] and platinum [20, 32, 36] were close to them in the parameters.

Basic during the development of metallic bolometers is technology of obtaining the lamellar cell/elements, close in their physical characteristics (mainly in the value of temperature specific resistance α_t) to the massive specimen/samples also of the not generating supplementary noises during the passage of the current through the film and through the contact with holder. The analysis of works for the latter of 20 years [21] showed that the optimum thickness of bolometric cell/element is 0.07-0.15 μ .

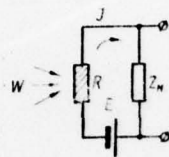


FIG. 1.2.

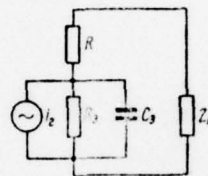


FIG. 1.3.

Fig. 1.2. Fundamental circuit diagram of metallic bolometer.

Fig. 1.3. Equivalent replacement scheme of metallic bolometer.

Page 16.

Sensing cell/elements are utilized either in the form of films, which are found in free state or they are spray-coated to the support/base, which possesses heat capacity smaller or by that comparable in value with the heat capacity of sensing element.

Fundamental circuit diagram and the simplified equivalent replacement scheme of metallic bolometer (temperature coefficient $\alpha_c > 0$) are given in Fig. 1.2 and 1.3 [5, 27]. The effect of radiation absorption by bolometer is represented in the form of current generator i_r , connected in parallel to resistance R , and capacitance/capacity C . With $Z_n = \infty$

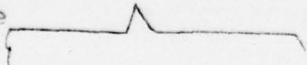
$$i_r = \frac{W}{2RJ}; \quad \frac{1}{R_s} = \frac{1}{2R} \left(\frac{G}{\alpha_c J^2 R} - 1 \right);$$

$$C_s = \frac{c}{2\alpha_c J^2 R^2}, \quad (1.20)$$

where G - the coefficient of heat losses; c is heat capacity of bolometer. By using equivalent circuit, it is possible to determine conversion factor

$$|S| = \frac{\alpha_c J R}{G_0 (1 + \omega^2 \tau^2)^{0.5}}, \quad (1.21)$$

$$G_0 = G - \alpha_c J^2 R; \quad \tau = \frac{c}{G - \alpha_c J^2 R}$$

where  This solution is correct, when bolometer

possesses one time constant and identical temperature on sensing element, for example for the vacuum bolometer, when relation $l/b \gg \gg 10$.

More precise calculation gives the dynamic theory of bolometers [7, 19, 21, 23-25]. the threshold of response of metallic bolometers can be written in the form [21].

$$\mathcal{P} = \left[16K\sigma_c \epsilon_0 A_0 T^3 \Delta f + (4KTRAf) S^{-2} + \Gamma \frac{T^2}{f^2} \Delta f \cdot S^{-2} \right]^{0.5}, \quad (1.22)$$

where K - is constant of stefana - Boltzmann; σ_c - Stephan's constant; ϵ_0 - emissivity. The first canoe in expression (1.22) we characterize the dependence of the threshold of response of bolometer on radiation noises, and the second - on Johnson. The value of the third term depends on technology of the production of thin-film cell/element, its thickness, method of joining with holder and can change from one copy to the next. By the rational selection of technological operations with the thicknesses of sensing element of approximately 0.1μ it is possible in order that the additional noise would not exceed Johnson and temperature. If supplementary noises are small, dynamic theory makes it possible to calculate the basic

parameters of bolometer. The calculations are in a good agreement with experiment [7, 19, 21, 25].

Composite conversion factor S can be written in canonical form (1.21) by replacement G_0 and by τ with an equivalent coefficient of heat losses of $G(\omega)$ and by factor of inertness $\tau(\omega)$, which are the complex functions of modulation frequency.

Page 17.

Dynamic theory explains why bolometer it is not possible to describe by one time constant, is which the character of the distribution according to sensing element at different modulation frequencies and is which the optimum selection of the geometric and thermophysical characteristics of the high-speed bolometer. Although real bolometer it is not possible to describe by one time constant, for the comparison of TPI and for the calculation of radiation instrument convenient the amplitude-frequency characteristic of bolometer to approximate by curve, described by expression (1.9) with the constant of time τ , which will subsequently figure as in tables.

If the noises of bolometer in essence Johnson, then as the factor of quality of the material of bolometer, according to expressions (1.21) and (1.22), can serve value

$$M_0 = \frac{\alpha_c R^{0.5}}{c}. \quad (1.23)$$

The spectral characteristic of bolometer is determined by the selection of the absorbing coating, i.e., features (Fig. 1.4). To selection of the optimum relationship/ratio between the thicknesses of black and sensitivity are dedicated [46, 68]. Work [68] shows, that is advisable a decrease in the thickness of metallic film less than 0.07-0.1 μ , since with more thin films the heat capacity of bolometer in essence is determined by the heat capacity of black, additional noises grow/rise and the temperature coefficient of resistance α_c falls.

Metallic bolometers possess nonuniform zonal sensitivity [7, 8, 18, 20, 60, 63, 64] on sensor (Fig. 1.5). With an increase in the length of sensing element, and also with the decrease in its thickness the nonuniformity decreases [19]. The boundary effect connected with certain increase in the zonal sensitivity near contacts with an increase of frequency, is caused themes that for the given modulation frequency is a optimum coefficient of heat losses, by which volt-watt sensitivity is maximum [6, 21] and which it is determined by the relationship

$$G_{\text{opt}}(\omega) \approx \omega c(\omega). \quad (1.24)$$

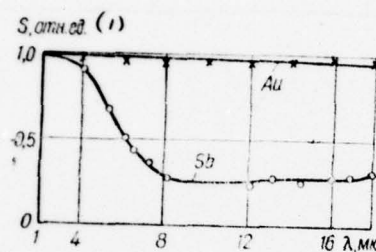


FIG 1.4.

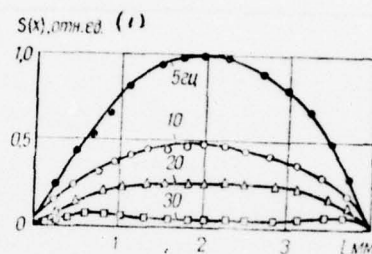


FIG. 1.5.

Fig. 1.4. Spectral characteristics of bolometers with gold (Au) and antimony (Sb) black [8].

Key: (1). S , rel. un.

Fig. 1.5. Zonal sensitivity of nickel bolometer of receiving area/site 4 x 0.5 mm in size/dimension [19].

At low frequencies the maximum of zonal sensitivity is located in the center of strip, while with higher frequencies it is moved to the contacts, where the coefficient of heat losses is more.

The threshold sensitivity of bolometers is improved during the size decrease of receiving area/site; however, not always according to the law $A_0^{0.5}$ [22].

Bolometers are the most high-speed receivers among TPI, with the exception pyroelectric. Figure 1.6 gives the amplitude-frequency characteristic of gold bolometer in pressure dependence of helium in tank/bottle [52]. Calculation of the high-speed bolometers for a thermal replacement scheme (Fig. 1.7) is given in works [23, 24]. In order that the bolometer would possess uniform amplitude-frequency characteristic in the assigned frequency interval Δf , must be made the following conditions:

$$\frac{k_2}{\pi d_2 c_2} \gg \Delta f \gg \frac{k_2^2}{\pi d_2^2 h_3 c_3}. \quad (1.25)$$

Experimentally [8] confirmed the correctness of relationship/ratio (1.25).

The mode/conditions of the work of bolometer with the assigned design and at pressure in container depends on the selection of operating current. Typical for metallic bolometers static

characteristics are given in Fig. 1.8. Dependence $R = R(Q)$ makes it possible to rate/estimate the dynamic range of bolometer L. By knowing dependence of $R = R(T)$, and also $R = R(T)$, it is possible to determine optimum the operating current, with which $T = 1, 2 T_0$ (T_0 - ambient temperature) and the threshold of response reaches minimum [6].

Metallic bolometers are low-resistance. Therefore the question of their agreement with measuring circuit is of independent interest [8, 69-76]. Figure 1.9 depicts the possible circuit diagrams of bolometer. For the agreement of low-resistance bolometer with electron-tube (transistor) amplifier are utilized the step-up transformers, if we do not consider the bridge circuits - galvanometer, which rarely are utilized at present (see Fig. 1.9a).

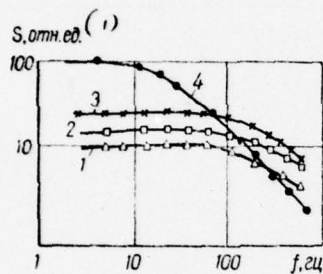


Fig. 1.6. Amplitude-frequency characteristics of gold bolometer at the different pressures of helium in tank/bottle [52]:

1 — $p = 760$ мм рт. ст.; 2 — $p = 20$ мм рт. ст.; 3 — $p = 3$ мм рт. ст.; 4 — $p = 10^{-1}$ мм рт. ст.

KEY: S . rel. un. \uparrow
мм рт. ст. = мм Hg.

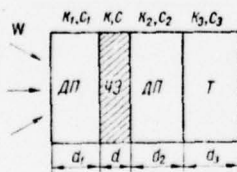


Fig. 1.7. The thermal analog simulator of the metallic bolometer:
dielectric constant - dielectric support/base; ЧЗ - sensing element;

t - heat withdrawal.

Page 19.

The total mean square of the noise of the preamplifier, led to the primary winding of transformer, and the noise of the bridge of bolometer is equal to

$$\bar{e}^2 = \bar{e}_b^2 + \bar{e}_{tp}^2 + \frac{\bar{e}_a^2}{K_{yc}^2(f)}, \quad (1.26)$$

where \bar{e}_b^2 , \bar{e}_{tp}^2 and \bar{e}_a^2 - the mean squares of the noises of the bridge of bolometer, transformer and lamp respectively; $K_{yc}(f)$ - the factor of amplification of transformer at operating frequency.

With the use of transformer with sufficiently small inherent noise and sufficiently large amplification factor it is possible to achieve that the total noise will be in essence determined by the noises of bolometer. To the calculation and the construction of transformers with optimum frequency and dimensional characteristics are dedicated [8, 71, 72].

The widest use received bridge circuits (see Fig. 1.9b and e), although are possible in principle the circuits with separating capacitance/capacity (see Fig. 1.9c) and with the compensation constant component in the primary winding of transformer with the aid of battery E_1 (see Fig. 1.9d). The selection of the optimum relationship/ratios in the bridge of bolometer is examined in [40, 66, 73, 76].

During the modulated irradiation in the case of the supply of direct-current bridge along with the bolometers, which possess the working and compensative films of equal resistance, are utilized single-film bolometers. By working with asymmetric bridge ($R_2 = nR_1$; $R_3 = R_1/n$; $R_4 = R_1$), it is possible to raise the coefficient of its transmission to unit. Analogous results can be obtained by making working and compensative film with different resistance [66].

With the supply of the bridge of bolometer by alternating current (see Fig. 1.9f) for the purpose of a decrease in the imbalance of bridge and improvement in the work of measuring circuit the nonoperative film of bolometer is led to thermal contact with the compensative cell/element, through which is realized the feedback. Relationship/ratio of ratio arms following: $R_1 = R_2$ and $R_3 = R_4$, with

DOC = 77020846

PAGE

~~37~~
38

this $R_2 \gg R[76]$.

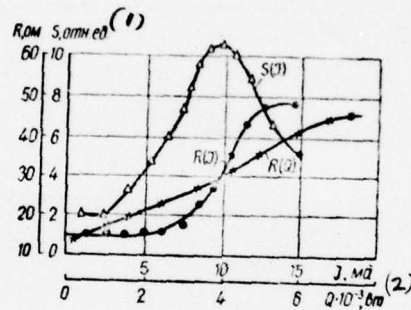


Fig. 1.8. The static characteristics of the nickel bolometer: $F = R(T)$, $S = S(T)$, $R = R(Q)$, where $Q = T^2 R$. By asterisk is noted value $T_K(Q_K)$, corresponding to the "infinite" heating of bolometer - to the boundary of its stability.

key: (1). rel. units. (2) W.

Page 20.

Modulation of emission/radiation during the use of single-film bolometer brings $\approx 50\%$ to the power loss of radiation flux. The bridge circuit, which consists of four single-film bolometers (see Fig. 1.9d), makes it possible this deficiency/lack and to raise two times threshold sensitivity [44]. The alternating irradiation of opposite ratio arms also decreases the faults of measurement of the low-level radiation, connected with a change in the temperature of modulator.

Metallic bolometers widely are applied in metrology for the emission/radiation of the heat fluxes of cumulative effect - radiation and convective. For example, during the determination of the time/temporary dependence of the energy losses of plasma [45, 47, 49, 50, 55, 56, 62].

Semiconductor bolometers [77-102]. The temperature coefficient of resistance of semiconductor materials by an order is higher than of metals. This was one of the reasons for the creation of semiconductor bolometers on the basis of oxides of nickel, cobalt and manganese, and also of the films of germanium and silicon.

The thicknesses of sensing elements of semiconductor bolometers

are 5-50 μ . During a decrease in the thickness of the layer appear large current of noise, which leads to deterioration of the threshold sensitivity. But in spite of the fact that the semiconductor bolometers possess large heat capacity, their volt-watt sensitivity 10-100 times higher than of the metallic bolometers, which work at room temperature. For a decrease in the inertness sensing elements of semiconductor bolometers are located in thermal contact with massive support/base.

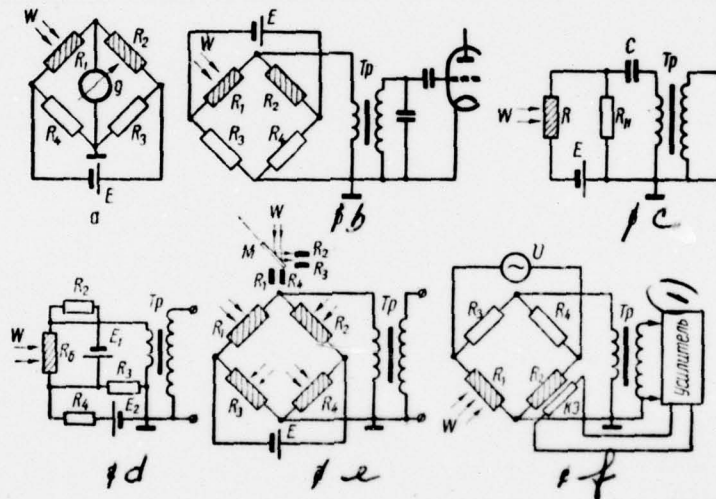


FIG. 1.9.

Fig. 1.9. Circuit diagrams of the low-resistance bolometers: a) bridge with galvanometer; b) direct-current bridge with the raising transformer; c) circuits a with separating capacitance/capacity; d) the compensation for the constant component in the primary winding of transformer; e) the alternating irradiation of opposite ratio arms; f) alternating-current bridge with transformer and with the compensation (kOe) for the imbalance of bridge.

Key: (1). Amplifier.

Page 21.

The oxide semiconductor bolometers, known abroad as thermistor [8, 77-80, 84, 86, 87, 91], from their parameters exceed the bolometers, prepared on the basis of the films of pure/clean germanium [82] and of silicon.

The schematic electrical diagram of semiconductor bolometer and the equivalent circuit of its substitution [5, 27] are given in Fig. 1.10 and 1.11. Unlike metallic bolometer, the effect of effect of radiation is represented by the equivalent generator of emf E_r with $Z_n = \infty$

$$\begin{aligned}
 E_r &= \frac{RW}{2E}; \\
 R_s &= \frac{R}{2} \left(\frac{GR}{|\alpha_c|E^2} - 1 \right); \\
 \mathcal{L}_s &= \frac{R^2}{2} \cdot \frac{c}{|\alpha_c|E}. \quad (1.27)
 \end{aligned}$$

For the conversion factor of semiconductor bolometer, according to Fig. 1.11, can be obtained the expression, analogous (1.21), while for a threshold of response - analogous (1.22).

The threshold of response of semiconductor bolometers is approximately directly proportional $\Lambda_0^{0.5}$. Decrease in the value of receiving area/site is related to the complexity of the creation of the optical focusing systems. For this purpose were developed immersion bolometers [87, 88, 92, 102]. In immersion receivers sensing element is located in optical contact with the lens, which has high refractive index. The calculation of the threshold of response of immersion receivers is carried out in work [89].

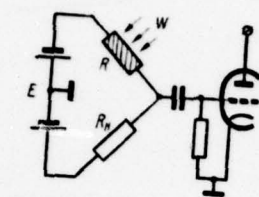


FIG. 1.10

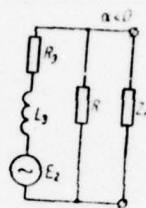


FIG. 1.11.

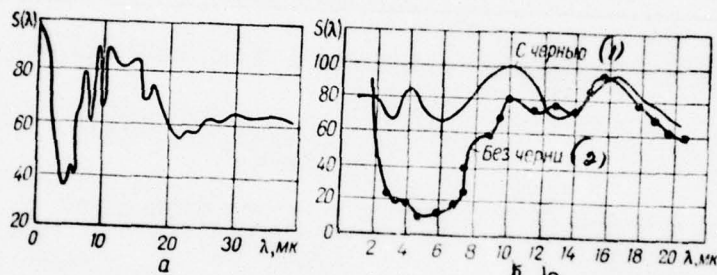


FIG. 1.12.

Fig. 1.10. Fundamental circuit diagram of semiconductor bolometer.

Fig. 1.11. Equivalent replacement scheme of semiconductor bolometer.

Fig. 1.12. The spectral characteristics of the thermistor bolometer:
a) unimmersed (window KRS is 5) (see [66, chapter V]); b) immersed
with germanium lens [102].

Key: (1). With black. (2). Weight of black.

Page 22.

If the threshold of response of receiver is not limited to radiation noises, then the effect of immersion makes it possible to increase calibrated threshold sensitivity $\Phi^* n_0^2$ once, where n_0 - is the smallest of three refractive indices: lens, layers and sensing element. The practical realization of the calculation conducted showed that with the size/dimensions of the sensor of immersion bolometer 0.1×0.1 mm it is possible to obtain gain in threshold of response into 3.5, time with respect to receiver of receiving area/site 1×1 mm in size/dimension, other conditions being equal. Due to reflection losses and absorption in immersion system it is impossible to obtain the calculated improvement in the sensitivity 10

times.

The spectral characteristics of unimmersed and immersion bolometers are given in Fig. 1.12. It is possible to improve the spectral sensitivity of semiconductor bolometers, by using that which absorb by coating the type of gold black, divided from higher-impedance than this coating, sensing element by dielectric layer with large thermal conductivity [99].

Cooling thermistor bolometers down to temperatures 210°K makes it possible several to increase the standardized/normalized threshold sensitivity. The compact device with thermoelectric cooling, described in work [93, 97], makes it possible to obtain value $\mathcal{D}^* = 0.8 \cdot 10^9 \text{ (cm.} \cdot \text{Hz}^{1/2})/\text{W.}$

Semiconductor bolometers are applied mainly in instruments for the measurement of the total radiant flux: in radiometers [85, 95], in solar thermometers [90, 98] and in the scanning image converters [85]. Abroad the thermistor bolometers widely are utilized as sensors in the orientation system of spacecraft [87, 92].

Because of high internal resistance the agreement of semiconductor bolometer with measuring circuit is not represented as complex as for metallic bolometers, and together with electron-tube

preamplifiers are utilized transistor.

Figure 1.13 depicts the amplitude-frequency characteristic of immersion bolometer, while Fig. 1.14 - the distribution of sensitivity according to the area/site of cell/element [79].

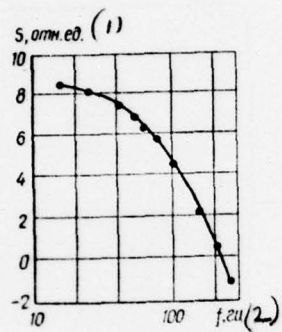


FIG. 1.13.

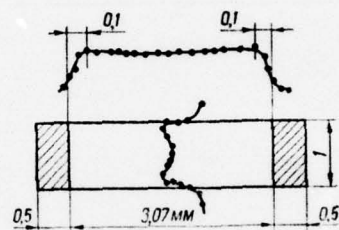


FIG. 1.14.

Fig. 1.13. Amplitude-frequency characteristic of immersion bolometer [102].

Key: (1). S, rel. un. (2) Hz.

Fig. 1.14. Zonal sensitivity of thermistor bolometer [79].

Page 23.

Cryogenic bolometers [94, 96, 103-159]. Cooling sensing elements of metallic bolometers leads to the reduction of Johnson and radiation noises, and also to rapid decrease at the low temperatures of heat capacity, proportional T^3 [108]. In addition to this, according to the data [160], during a reduction in the temperature it decreases the component of supplementary (current) noise.

For a series of metals, which are found at temperature lower than the Debye temperature (θ_D) in range from $\frac{\theta_D}{3}$ to $\frac{\theta_D}{10}$, grow/rises the temperature specific resistance α_c . As shown in [109], for the nickel plate of purity 99.990/o at the temperature of liquid oxygen value α_c grow/rises four times in comparison with room. However, in thin layers due to the defects of crystal lattice and size effect α_c under these conditions it grow/rises not more than two times. Cooling down to the temperature of liquid nitrogen makes it possible to raise α_c [109] and to improve the threshold characteristics of nickel bolometers more than five times [8, 120]. An improvement in the threshold of response during cooling was establish/installed also for gold bolometers [21]. According to the data [127], during cooling one should expect gain in sensitivity for bismuth bolometers. The calculation of cooled platinum bolometers [6] showed that during a

reduction in the temperature from 290 to 20°K it is possible to decrease the threshold of response to ten times and to obtain values $\mathcal{P} = 6 \times 10^{-12}$ W/Hz^{1/2} and $\tau = 0.3$ ms. However, in practice these numerals were not realized.

Along with a monotonic improvement in the parameters of bolometers during cooling are purely the cryogenic effects: the superconductivity and the electrical conductivity of the small impurity levels of the semiconductors, on the basis of which are developed TPI.

The threshold of response of cryogenic bolometer can be written in the form, analogous (1.22), but with the difference in the term, which characterizes radiation noises [136]:

$$\mathcal{P} = \left[(4KTR\Delta f) S^{-2} + 4KT^2 G \Delta f + 8\epsilon_0 \sigma_c K A_0 T^5 \Delta f + \right. \\ \left. + 8\epsilon_0 \sigma_c K A_0 T_\phi^5 \sin^2 \theta \Delta f + \Gamma \frac{T^4}{T_\phi} S^{-2} \right]^{0.5} \quad (1.28)$$

The second term in expression (1.28) characterizes the noise, connected with thermal conductivity G between sensing element and the medium at temperature $T_\phi = T$ (Fig. 1.15); the third - is caused by the radiation fluctuations of sensing element of receiver; the fourth

is the contribution of radiation hum noises with temperature T_ϕ (2θ - cone-apex angle, hearth by which sensing element it receives the radiation of background).

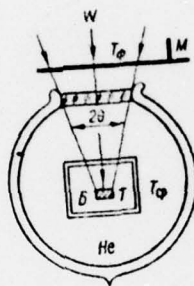


FIG. 1.15.

Fig. 1.15. Circuit of cryogenic bolometer; M - modulator; E - bolometer; T , T_{cp} , T_{ϕ} - the temperature of the bolometer, medium and background respectively; He - liquid helium.

Page 24.

According to the establish/installled terminology, the threshold of response of ideal thermal radiation detector kharaterizuyetsya by the third and fourth terms in expression (1.28), when S - is great, and G - is small. In cryogenic TPI decrease G leads to the very large inertness of receiver, since radiation losses at low temperatures are small. Therefore in the developed receivers the third term is considerably lower than the second and the fourth, if $T_{\phi} \gg T$ [136, 138].

The high temperature specific resistance of superconductors in transient region, approximately 10^3 - 10^4 times larger than of metals at room temperature, it drew the attention of the developers of TPI into the period of the Second World War. Superconducting bolometers from nitride of niobium NbN [104-106, 112] were the result of low-temperature investigations. However, they did not exceed the limits of laboratories due to insufficient high the threshold sensitivity, cause of which were the noises of the superconducting

transition "rigid" (type NbN) superconductors [107, 123, 138].

In work [123] are established/installed the correlations between the noises of the superconducting transition and the surface energy of domain wall, which relate to the superconducting and normal state and which simultaneously exist in transient region. The author of the work established that the noises of "rigid" superconductors on several orders exceed the noises "rigid" (tin, indium, etc.), and proposed criterion for the selection of materials and size/dimensions of sensing elements for the creation of the effective superconducting bolometers.

By the new jerk/impulse, which woke up the interest of workers of TPI in the phenomenon of superconductivity, was creation by Khalbert and Jones into 1955 superconducting bolometer on the basis of lamellar tin and the conducted investigations in research on low-temperature objects ($T = 120^{\circ}\text{K}$) in the far-infrared region of the spectrum [110]. In work with galvanometer they reached sensitivity $3 \cdot 10^{-12}$ W. Then were made the tin superconducting bolometers QMC, working during modulated emission/radiation [116, 121, 124, 125, 129, 130], and were used in the infrared spectrometers of submillimeter range. Their sensitivity more than 50 times exceeded the sensitivity of acousto-optical detector. the qmc-bolometers are called isothermal unlike the nonisothermal, the different sections of

sensing elements of which they are located in normal and superconducting states [134]. Of nonisothermal bolometers resistance change, caused by the absorption of radiation flux, occurs mainly not because of a change in the specific resistance of film, but because of an increase in the section of sensing element, which is found in normal state.

Page 25.

By regulating the coefficient of heat losses, it is possible to lower the time constant of superconducting bolometers. As it was communicated in work [157], was reached time constant $\tau = 2 \cdot 10^{-8}$ s with threshold of response $P = 10^{-9}$ W/Hz^{1/2}.

On the basis of the carbon thermometers of Allen - Bradleys, who possess the large values of the temperature specific resistance $\alpha_c = -2$ at 2°K, were developed in Bell Telephone Lab [96, 117, 118, 122] carbon cryogenic bolometers. Their high sensitivity made it possible to conduct the number of initial experiments in the distant infrared region of the spectrum [118, 122].

However, considerable current noises did not make it possible to achieve the theoretical sensitivity of bolometer.

Most sensitive of all known at present TPI is Low's bolometer [94, 128, 132, 135, 136, 147, 154, 158]. Bolometer is developed on the basis of the lamellar germanium, alloyed by gallium (good results were obtained also with alloying with indium). At temperature of 2°K threshold of response of cryogenic germanium bolometer comprised order 10^{-14} W/Hz^{1/2}. Low's bolometers were used in the radiometer, establish/installed on rocket for space research [143], and also for fu46e-spectroscopy in far-infrared region [141, 155] and microwave range [139]. In addition to this, they were utilized as detectors of thermal momentum/impulse/pulses [114, 150].

Development the investigation of cryogenic bolometers on the basis of the germanium, alloyed by gallium and antimony, are carried out also by N. A. Pankratov with the colleagues [8, 148].

The amplification of the weak signals, taken from low-resistance sensing elements of bolometers, which are located at low temperatures, represents complex radio engineering problem. The agreement of the cell/element of bolometer with amplifier is realized with the aid of the raising transformer (Fig. 1.16), cooled by liquid helium and placed into tin screen for electromagnetic protection [6, 130, 137, 145]. The given circuit serves simultaneously for the electronic regulation of the temperature of bolometer. With the supply of alternating-current bridge the signal of the imbalance of

DOC = 77020846

PAGE

~~44~~
56

bridge will contain the information about the modulated optical signal and about a change in the temperature of bolometer.

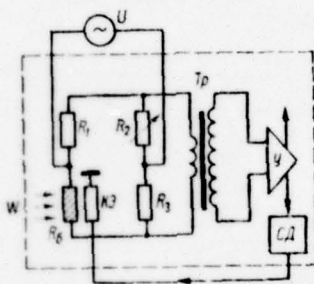


Fig. 1.16. Bridge circuit with superconducting bolometer R_6 . R_1 , R_2 , R_3 are ratio arms; TP - matching transformer; Y is an amplifier, SD - sun sensor - synchronous detector; kOe - compensative cell/element for the automatic balance of bridge.

The band of amplification at the output/yield of synchronous detector SD it is possible to separate/liberate optical signal from the signal of thermal regulation, connected with temperature changes in the environment, by utilizing filters with different time constants. The signal of thermal regulation through the channel of feedback is supplied to heating element R_n . In this case the rough calibration of the temperature is realized manostat that supports the constant vapor pressure of boiling helium [8, 119, 140], and precise - by electronic circuit. The total accuracy of maintaining temperature is approximately $5 \cdot 10^{-5}$.

The use of the superconducting devices for the amplification of the weak signals, taken from low ohmic resistance at low temperatures, is described in publications [111, 113, 114, 133, 146, 149]. Some of them were intended for the measurement of small constant stresses on low-ohmic resistances, connected in it with transformer consecutively with superconducting modulator [111, 113, 114]. For analogous target/purposes were developed magnetic and devices on the basis of Josephson tunnel effect [146]. amplifiers [149]. Such devices can be used also for the measurement of the optical signals, taken from superconducting bolometers; however, they fairly complicated and thus far they did not find use into reliably working the use of parametric amplifiers, possessing lower inherent noise level, than lamp and transistors. The description of such amplifiers is given in works [131, 151]. Figure

1.17 gives the circuit of the parametric amplifier used for a work with the bolometer of Low and which uses nonlinear properties of capacitance/capacity conversely displaced p - n-transfer (diodes D_1 and D_2) [131]. The capacitance/capacity of diodes is modulated by radio frequency voltage e through Tp_1 . Fine-adjustment of capacitors C_n are intended for the compensation for a difference in the capacitance/capacities of diodes and for the balance of the bridge, which consists of secondary windings Tp_1 and diodes D_1 and D_2 . Capacitive the imbalance, which appears as a result of the action of radiant flux W , leads to appearance on the output of the bridge of amplitude-modulated signal, amplified by tuned amplifier u , and then supplied to detector d . The inherent noise level of parametric amplifier is $3 \cdot 10^{-9} \text{ W/Hz}^{1/2}$.

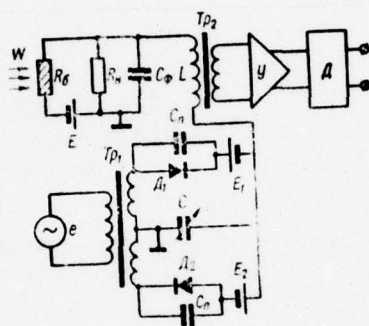


Fig. 1.17. Parametric amplifier to germanium bolometer [131]: R_b is resistance of bolometer; R_n - the resistance of load; E , E_1 and E_2 - battery; Tp_1 , Tp_2 - transformers; e is a high-frequency oscillator; C_n - capacitance/capacity; u - amplifier; d - detector; D_1 and D_2 - diodes.

To the use of field triodes, which work with $T = 4.2^{\circ}\text{K}$ and which possess the high the entry impedance ($R_{\text{ex}} = \text{to } 10^8 \text{ ohm}$) and the low noise level $(2.5-6) \cdot 10^{-8} \text{ W/Hz}^{1/2}$ in the range $f = 25-1000 \text{ Hz}$, are dedicated [152, 159]. Positive results were obtained during parallel connection of of nevistor type lamps [8, 142, 153, 156].

§4. Radiation Thermoclements (155-185).

The measuring the emission/radiation thermal element of the simplest case consists of receiving part p and thermocouple (Fig. 1.18). The receiving part, which absorbs radiation, is located in thermal contact with hot end (g). The cold-soldered joint (x) of thermocouple, isolate/insulated from the accepting emission/radiation area/site and connected towards hot, serves for a decrease in the effect of ambient temperature. The thermal elements, utilized for the measurement of the modulated radiant flux, consists of two hot junctions (Fig. 1.19) (positive (p) and negative (o), creating the thermoelectromotive force (thermo-emf \mathcal{P}_T) of opposite signs and connected so that thermo-emf would store/add up [155, 156, 160, 161]. The different constructions of composite and semiconductor thermal

elements are described in works [8, 155-157, 159-166, 168-173, 175-178, 180-184]. The investigations of their basic parameters are given in works [5, 6, 158, 165, 168, 171], and to the theoretical calculations are dedicated to publication [5, 6, 158, 161, 173, 174, 180].

The work of radiation of thermoelement (RTE) can be approximately described, by using the equivalent circuit (Fig. 1.20), proposed in [158]. In this circuit the result of the absorption of radiation power is represented in the form of generator of current J_r , obtained in parallel to dynamic resistance R_d and to capacitance/capacity C_d . The Peltier effect increases the electrical resistance of circuit to value R_d .

The noises of RTE are determined, according to the given circuit, by the Johnson noises of the active resistance R and the real part of the dynamic impedance $R_d/(1 + \omega^2 C_d^2 R_d^2)^{0.5}$. It is interesting to note that the Johnson noise of dynamic resistance is equal to the noise, induced with temperature fluctuations [5].

The conversion factor with load $Z_n = \infty$ in canonical form takes the following form:

$$S = \frac{\epsilon_0 \mathcal{P}_r}{(G^2 + \omega^2 C^2)^{0.5}}. \quad (1.29)$$

In the real cases of G and c they are the complex functions of the frequency of modulation, physical properties of material and geometric dimensions.



FIG. 1.18.

Fig. 1.18. Circuit for switching on the radiation thermal element of direct current (RTE): p - receiving area/site; g - hot junction; x - cold-soldered joint; i - indicator.

~~END OF DOCUMENT~~

Page 28.

The threshold of response of RTE is equal to:

$$\mathcal{P}^2 = 4KT^2\Delta f \left[G + \frac{R(G^2 + \omega^2 c^2)}{v_0^2 \mathcal{P}_r^2 T} \right]. \quad (1.30)$$

First term in (1.30) corresponds to temperature fluctuations, and the second - Johnson. Having assumed $\omega c \ll G$, we will obtain that the relation of terms is proportional R/R_A . The experimental studies, carried out with different RTE, they showed that $R_A \approx (0.1-0.15) R$, and therefore the threshold of response of RTE in essence is determined by Johnson noises.

The analysis of expression (1.30) determines the effect of the different parameters of RTE on threshold of response. The total thermal conductivity G contains the components, caused by the thermal conductivity of gas into RTE, by radiation heat exchange between the sensor and housing, and also the thermal conductivity of conductors. The analogous components are contained in the total heat capacity c .

The threshold of response of the vacuum RTE is always better than nonvacuum ones, independent of the modulation frequency of radiation flux (this confirmation not applicable to bolometers at high

frequencies).

The optimum size/dimensions of sensing element of RTE can be determined from expression (1.30) when the length of conductors is shorter than the half of the length of temperature wave [6]. Since, according to videman - Franz's law, a decrease in resistance R is connected with an increase in the thermal conductivity of conductors G_n , it is necessary to find the condition of the minimum of expression (1.30). This condition is the equality of the ratio of electrical conductivity to the thermal conductivity of each conductor [6]:

$$R = \frac{4\bar{L}T}{G_n}, \quad (1.31)$$

where \bar{L} is averaged Lorentz number:

$$\bar{L} = \frac{1}{4}(L_1 + L_2) + \frac{1}{2}(L_1 \cdot L_2)^{0.5}; \quad (1.32)$$

L_1 and L_2 are Lorentz numbers for thermoelectric materials. From the analysis of expression (1.30) also ensues the equality of heat losses caused by emission/radiation and because of the thermal conductivity of conductors - the condition of Jchansen.

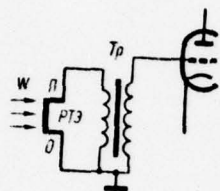


Fig. 1.19.

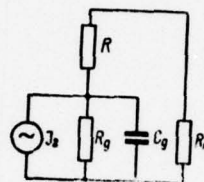


Fig. 1.20.

Fig. 1.19. Circuit diagram of the RTE of alternating current.

Fig. 1.20. The equivalent replacement scheme of the RTE: $J_r = \frac{W}{P_r^2 T}$ - signal generator; $R_d = \frac{P_r^2 T}{G}$ - dynamic resistance; $C_d = \frac{c A_s}{P_r^2 T}$ - dynamic capacitance/capacity; R is resistance of RTE at high modulation frequencies.

Page 29.

The criterion of the quality of thermoelectric material can be

obtained from expressions (1.30) and (1.31):

$$M_r = \frac{\mathcal{P}_r^2}{L}. \quad (1.33)$$

A temperature decrease of RTE does not lead to an improvement in its threshold of response as of bolometers, mainly due to a decrease in value \mathcal{P}_r . Work [167] examines the RTE, which is the combination of thermocouple and bolometer and designed in such a way that thermoelectric and bolometric effects would be summarized. However, practical gain in sensitivity was not obtained due to the emergent noises.

The developed at present RTE are intended for a work on constant and alternating/variable irradiation. RTE of Moll's type, work during constant irradiation, make it possible to realize during connection with photoelectrooptic amplifier threshold of response 10^{-9} - $5 \cdot 10^{-10}$ W/Hz^{1/2}. This system possesses the considerable instability of null reading and for quantitative measurements is hardly suitable. However, for a series of the application/uses where is not essential high sensitivity, but is required simplicity, reliability and mechanical strength, widely are utilized RTE during constant irradiation [175, 180, 182, 183]. For example, in onboard equipment for spacecraft [176, 180, 185] are utilized RTE - economical instruments with the considerable size/dimensions of receiving area/site. Their combinations form the position-sensitive detector,

which is horizontal scanner.

Vacuum RTE, intended for a work on alternating/variable irradiation, possess comparatively slow response and are utilized on low modulation frequencies. However, for the study of the slowly changing processes, in particular, in the receiving-recording equipment/devices of infrared spectrophotometers the vacuum RTE is one of the better/best radiation detectors.

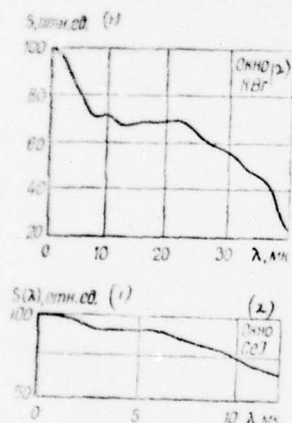


Fig. 1.21.

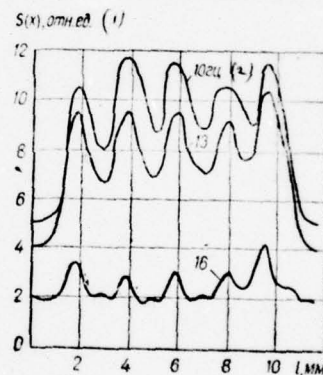


Fig. 1.22.

Fig. 1.21. The spectral characteristics of RTE for two types of thermocouples (see [66, chapter V]).

Key: (1). rel. un. (2). Window.

Fig. 1.22. Zonal sensitivity of RTE, that consists of five joints with the size/dimensions of the receiving area/site $A_0 = 10 \times 2$ mm at different modulation frequencies [184].

Key: (1). rel. units. (2). Hz.

Page 30.

Parallel and series connections of a series of RTE in principle do not give gain on sensitivity. If allows optical system and technology of obtaining sensing elements, RTE one should make with the minimal sizes of receiving area/site. However, in a number of cases - in work in far-infrared region, during the study of radiation fluxes from many radiation sources, when the concentration of emission/radiation is hinder/hampered - is applied RTE with large receiving area/site.

The spectral characteristics of two types of thermocouples are represented in Fig. to 1.21.

The zonal sensitivity $S(x)$ of thermocouples is characterized by large nonuniformity (Fig. 1.22) on receiving area/site - especially near joints and between them. The distribution and the character of value $S(x)$ depends on the form of the utilized amplifier (direct or alternating current), of the modulation frequency and form of the detector of measuring circuit.

The cumulative methods of the signal, taken from RTE, depend on the time constant of RTE. The amplification of signal for the RTE of alternating/variable irradiation is shown in Fig. 1.23 [185]. It is possible to note three cumulative methods of the signals, taken from inertia of RTE, by the way of the conversion of direct current into variable: magnetic amplifier, vibrapack and photo-modulator amplifier. In the last/latter method the pair of neon bulbs N acts as relaxation generator, modulating resistances of photocells PS (CdS). one photoresistor is connected consecutively from RTE and by the step-up transformer, but another - shunts transformer.

§5. Acousto-optical (pneumatic) and dilatometric radiation detectors (186-238).

The phenomenon of the sounding of gases under the action of the interrupted radiant flux, opened by Bell, by Tyndall and Roentgen in 1880, was used by M. L. Veyngerov for the creation of acousto-optical type TPI [186]. The schematic diagram of nonselective optical-acoustic (pneumatic) receiver (OAP) is given in Fig. 1.24.

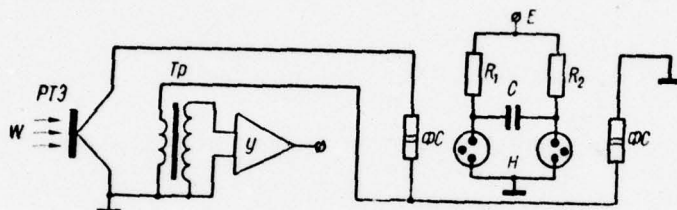


Fig. 1.23. Photo-modulator amplifier to RTE [185]: FS - photoresistor; N - neon bulbs.

Page 31.

The interrupted radiant flux creates the pulsation of pressure in working chamber due to radiation absorption by absorbing coatings (layer of carbon black [189], by gold black [226], charred by organic matter [187], by the semitransparent metallic film, plotted/applied to support/base [189, 192, 212]) or radiation directly is absorbed by

the gas, which fills the chamber. In the first case the accusto-optical detectors are nonselective [187, 189, 192, 193, 213, 214, 217, 226, 229, 235], and in the second - selective [186, 191, 194, 197, 203, 206, 209, 212, 215].

Microphone converts pressure in the chamber into the electrical signal, then amplified by electronic circuit. Are utilized the different forms of the microphones: optical [189, 192, 195, 215, 221, 225, 226], condenser/capacitor [189, 193, 215, 216-218, 221, 222, 237, 235], electrodynamic [186, 191, 212, 215, 221] and some others [187, 236].

The acousto-optical chamber and the microphone are interconnected, and the characteristics of OAP are determined by their total characteristics. Microphone fulfills the functions of optical-electronic or electronic type preamplifier. With correct selection and the construction of microphone, the signal-to-noise ratio at its output/yield must not be worse than gives the chamber.

The operating principle of OAP consists of the following. The modulated emission/radiation of the source W being investigated through the input window passes into the accusto-optical chamber K and is absorbed by film P . Absorbed energy is transferred to the gas, which fills the chamber. In the chamber appear the pulsations of gas

into cycle/stroke to the modulation frequency of the radiation flux, which is transferred to diaphragm/membrane ^M. Diaphragm/membrane is the fire/thin and flexible plate, one side of which is movable chamber wall, and another, covered with the layer of antimony, by the mirror of optico-electronic amplifier. In the absence of pressure (zero sagging/deflection of diaphragm/membrane ^M) the world/light from auxiliary source ^L passes through the upper part of the condenser objective ^O and of raster ^R, it is reflected of film ^M and falls in the lower half of raster in such a way that the images of the slots of the upper half of raster coincide with the opaque bands of its lower half.

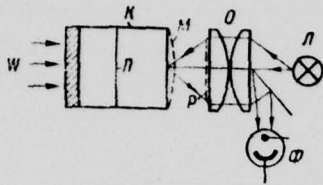


Fig. 1.24.

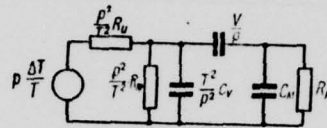


Fig. 1.25.

Fig. 1.24. The diagram of nonselective acousto-optical detector (OAP) with the optical microphone: K - the chamber; P - the absorbing film; M - diaphragm/membrane; R - raster; O - objective, L - lamp; F - photocell.

Fig. 1.25. Equivalent pneumatic diagram of OAP[189]: p - the gas pressure in the chamber; V is a volume of gas in the chamber; R_n and R_{np} are the thermal resistance, caused by emission/radiation and conductivity, C_V - the heat capacity of gas at a constant volume; C_M and R_M are capacitive and active thermal resistance of diaphragm/membrane.

If diaphragm/membrane ^M caves in, then the image of raster will be displaced with respect to the optical axis of system and part of the world/light through the lower half of objective ^O falls on photocell ^F. The optical-electronic system of amplification is very effective, since it makes it possible to feel the sagging/deflection of diaphragm/membrane on the order of 10^{-8} cm.

The threshold of response of OAP can be written by the expression

$$\mathcal{P}^2 = 4KT^2G\Delta f + \overline{W}_M^2 + \overline{W}_A^2. \quad (1.34)$$

First term characterizes radiation fluctuations, the second - is caused by the fluctuations of diaphragm/membrane and third - is connected with the supplementary noises, introduced by measuring circuit.

To the calculation of OAP are dedicated [189, 195, 198, 199, 202, 204, 205, 210, 211, 218, 231, 238]. Golay developed the theory of nonselective pneumatic receiver, considering it as system with the concentrated (and also by distributed) constants and using for the calculation by the method of thermoelectric analogies. The processes, which take place in the acousto-optical chamber, were described by

the equations, used to electrical T-shaped circuit. Figure 1.25 gives the simplified heat-pneumatic circuit OAP, which makes it possible to obtain basic calculated relationship/ratios [189] and to determine the optimum size/dimensions of the chamber, which correspond to the maximum sensitivity. The calculation of microphones in these works was not performed.

N. A. Pancrat conducted the calculations of OAP, considering interconnection in the chamber operation and microphone. Among these calculations are most close for the practical purposes of the work [198, 199, 205 218, 221].

To the experimental study of characteristics of OAP are dedicated works [221, 224-228, 237]. Spectral characteristic of OAP is given in Fig. 1.26, and the distribution of sensitivity according to the surface of the chamber - on Fig. 1.27.

Investigation of OAP with the acousto-optical chamber, adjusted into resonance, is described in works [220, 229].

Selective OAP served as basis for the creation of widely utilized at present gas analyzers [194, 206, 215], and nonselective are known abroad as Golay pneumatic cells - are utilized as radiation detectors in the infrared spectrometers of the middle and distant ranges.

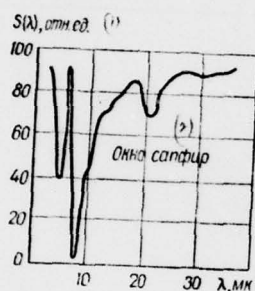


Fig. 1.26

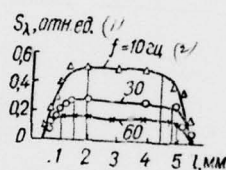


Fig. 1.27.

Fig. 1.26. The spectral receiver response of Golay (see [66, chapter V]).

Key: (1). rel. un. (2). Window is sapphire.

Fig. 1.27. Zonal sensitivity OAP of receiving area 9 x 5 mm in size/dimension at different modulation frequencies [122].

Key: (1). rel. un. (2). Hz.

Page 33.

Close in operating principle to acousto-optical detectors are dilatometric [8, 200, 207, 208, 232, 233], using thermal expansion of solid bodies under the action of radiation fluxes. The idea of the creation of such receivers is not new. Even earlier were developed/processed the radiometers, as active cell/element in which served bimetallic strips [186].

The interesting results were obtained in work [200] during the creation of the detector, in which is used the expansion of fine/thin constantan film for the rotation of galvanometric type mirror system. The sensitivity threshold of this receiver is determined by temperature fluctuations. Figure 1.28 shows the circuit of this receiver. The radiation flux W , absorbed by thermal film E , conducts to its expansion and the rotation of the filament N , during which is fastened the micromirror 7 . The rotation of mirror is recorded by differential type highly sensitive optical balance meter [208]. The authors calculated, that the register system can detect changes in the length of order $5 \cdot 10^{-8}$ cm. Analogous attempts were undertaken on the development of dilatocondensator heat receivers [8].

§6. Thermal image converters [239-262].

one of the basic questions of radiation instrument manufacture is the conversion of the invisible image of objects into visible.

Are observed two tendencies in the development of thermal image converters - the creation of the instruments scanning and not scanning of types.

In the scanning converters, which consist of TPI and optical-mechanical system [3, 240, 243, 251, 254, 260], the obtained information is the totality of electrical signals from the separate cell/elements of the object being investigated, which are amplified and synchronously recorded by the photorecording equipment/device in the form of black-white or colored pictures. As TPI are utilized immersion [3] and unimmersed [240, 243, 260] thermistor bolometers, pyroelectric receivers [260] and the linear batteries of thermal elements [254].

The schematic of the optical-mechanical scanning converter is

given in Fig. 1.29. The mirror of the scanning/sweep of image consecutively projects to TPI emission/radiation from the different sections of the object being investigated. The taken from TPI signal is amplified by electronic circuit and is supplied to neon tube/lamp, modulating its intensity. World/light from lamp, being reflected from the back side of the mirror of scanning/sweep, is focused on the film of camera.

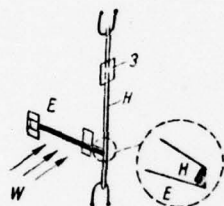


Fig. 1.28. Circuit dilatometric of TPI: E - thermal film, N - filament, Z - micromirror.

Page 34.

Thus, the mirror of scanning/sweep, projecting the emission/radiation of the determined cell/element of object to TPI, produces the synchronous notation of signal from this cell/element with the corresponding to it section of photographic film.

The released in the USA by firm Baroes Engeneering CO thermographs, which act according to the described principle, possess the high resolution (60000 points/frame), are distinguished differences in temperatures 0.1°C and is record/written image for time 30-120 s.

The second direction of works in the creation of image converters is the use of temperature-sensitive layers, different sections of which give the information about the image of object, projected to layer.

one of the first and most widely used instruments of this type is recording evaporimeter [242, 246-248, 253, 255], the operating principle of which is based on a change in the condensation rate or evaporation of the layer of liquid depending on a change in the temperature (Fig. 1.30). The emission/radiation being investigated with the aid of mirror objective is focused on the nitrocellulose diaphragm/membrane, covered with gold black.

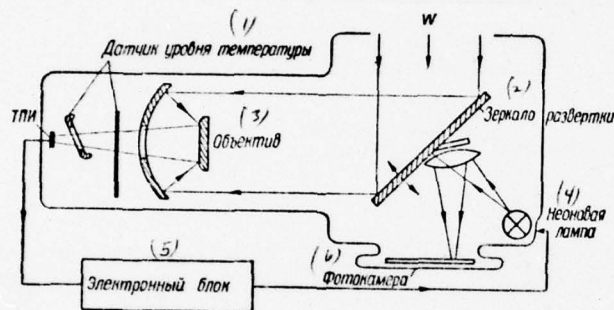


Fig. 1.29. Optical-mechanical scanning converter.

Key: (1). Sensor of the level of temperature. (2). Mirror of scanning/sweep. (3). Objective. (4). Neon tube/lamp. (5). Electronic component. (6). Camera.

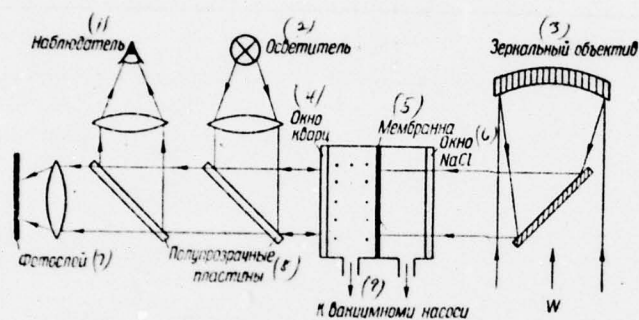


Fig. 1.30. Recording evaporimeter.

Key: (1). Observer. (2) light. (3). Mirror objective. (4). Window of quartz. (5). Membrane. (6). Window. (7). Photosensitive layer. (8). Semitransparent plates. (9). To vacuum pump.

On diaphragm/membrane is created thermal relief. From opposite side of diaphragm/membrane in intake chamber are located the oil vapors. The condensation rate of oil vapors at any point of diaphragm/membrane depends on the temperature in this point. The determined on the surface of diaphragm/membrane oil relief corresponds to temperature. Auxiliary illuminator makes it possible to observe temperature field in interference colors and to photograph. Recording evaporimeter detects differences in temperatures 0.5-2°C at resolution 10 hachure/mm and time constant 10-20 s. The investigation of the resolving and threshold sensitivities of recording evaporimeter is given in works [256, 259].

Another instrument, which belongs to this type of converters, is the converter on boundary/edge absorption - edge graph [241, 244]. As the basis of the work of edge graph is placed the temperature dependence of the edge of fundamental absorption of semiconductor - amorphous selenium. Under effect of radiation in the film of selenium (Fig. 1.31), covered from the flow being investigated with the semitransparent layer of chromium, is created the temperature relief, which is observed with the aid of sodium-vapor lamp. The monochromatic radiation of sodium-vapor lamp ($\lambda = 589 \mu$) lies/rests near the absorption edge of selenium, and depending on temperature

field of sensing element through the equal sections of the latter can pass the large or smaller part of the emission/radiation, which makes it possible for observer direct to examine the image of object. Edge graph distinguishes temperature differentials 10°C at the resolution of 2 dashes/mm and time constant 0.5 s.

The temperature dependence of the intensity of luminescence in the visible range of zinc-cadmium-sulfide phosphoruses, irradiated by ultraviolet radiation source, made it possible to create image converter [239] (Fig. 1.32). The luminous intensity of luminophore changed by 20o/o during a change in the temperature on 1°C .

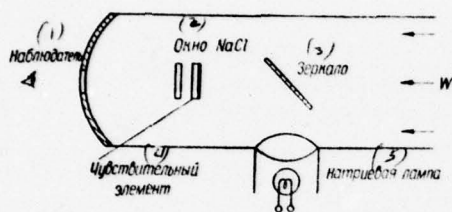


Fig. 1.31.

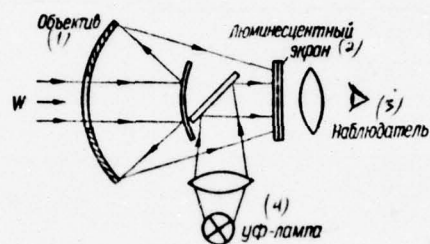


Fig. 1.32.

Fig. 1.31. Edge graph.

Key: (1) Observer. (2). Window. (3). Mirror. (4). Sensing element.
(5). Sodium lamp.

Fig. 1.32. Thermoluminescence converter.

Key: (1). Objective. (2). Luminescent screen. (3). Observer. (4).
UV-lamp.

Page 36.

The threshold of response of instrument comprised $5 \cdot 10^{-4}$ W/cm² (it was possible to distinguish temperature drops 5°C) with resolution 0.5 hachure/mm.

The schematic of photo-thermionic-emitting converter [245] is given in Fig. 1.33. one side of sensing element of converter is the semitransparent layer of gold, plotted/applied to basis from SiO. To another side of basis is plotted/applied photoemitter, sensitive to temperature change. Photoemission occurs from those sections of sensitive layer, which are illuminated by ray/beam from auxiliary kinescope with spotting. The emitted electrons are amplified by multiplier and amplifier. The intensive signal modulates in ray intensity of the kinescope, on which it is possible to observe the image of object. Sweep oscillator synchronizes the work of the basic and auxiliary kinescopes, realizing a survey of all sections of the sensitive layer, to which is projected the image. Photo-thermionic-emitting converter is sensitive to a change in the temperature by 10°C, it possesses time constant 0.1 s and the resolution of 2 dashes/mm.

Recently appeared the report/communications about the use of liquid crystals for the creation of thermal sensors and converters

[249, 262]. Cholesteric type liquid crystals [252] possess the electro-optical properties, which sharply change under the effect of the temperature, electric field [261] and other external agencies. The basic cell/element of converter is the film of liquid crystal, which is located in thermal contact with the layer, which absorbs emission/radiation (Fig. 1.34).

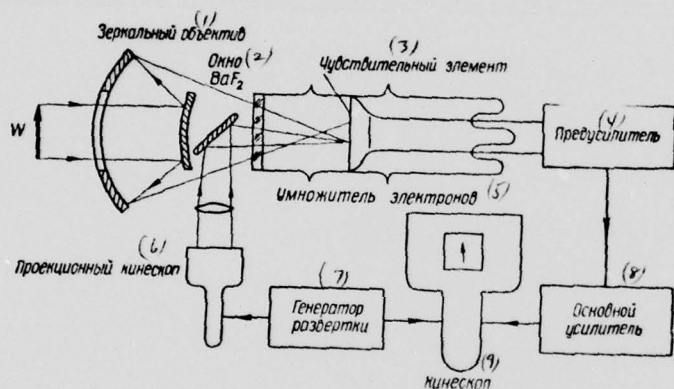


Fig. 1.33.

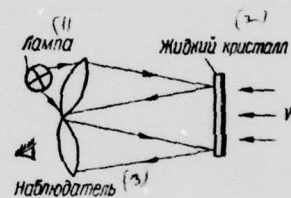


Fig. 1.34.

Fig. 1.33. Photo-thermionic-emitting converter.

Key: (1). Mirror objective. (2). Windows. (3). Sensing element. (4). Preamplifier. (5). Multiplier of electrons. (6). Projector kinescope. (7). Sweep oscillator. (8). Basic amplifier. (9). Kinescope.

Fig. 1.34. Liquid-crystal converter.

Key: (1). Lamp. (2). Liquid crystal. (3). Observer.

Page 37.

The temperature relief of absorbing layer is transferred to the film of liquid crystal. During the illumination of cholesteric film from auxiliary source its color in different sections will depend on temperature. The time constant of equipment/device composes several seconds, and resolution is close to television.

The comparison of the converters not scanning and scanning types can be carried out on the basis of their parameters. The nonscanning converters do not require complex electromechanical and optical node/units, and the visualization of images is reached by comparatively simple methods. To their deficiency/lacks, besides nonuniform sensitivity on receiving area/site, one should relate the powerful effect of the long-wave radiation of background with the maximum of emission/radiation 10μ (300°K) during the study of objects with the temperature, close to room. For conducting such

investigations are required cooling sensing elements, which is connected with supplementary technical difficulties. The scanning image converters although are more complex than not scanning, also more sensitive.

In conclusion of chapter let us note that on the basis of ferroelectric materials in recent years are developed the highly sensitive and low-inertia radiation detectors and target for thermal image converters. To the description of their physical properties, to the calculations of the parameters and to concrete/specific/actual developments are dedicated the subsequent chapters.

BIBLIOGRAPHY

1. Havens R.— J. Opt. Soc., America, 1946, 36, 6, 355.
2. Jones C. R.— J. Opt. Soc., America, 1947, 37, 11, 888; 1949, 39, 5, 327; 1949, 39, 5, 344.
3. Wormser E. M.— Appl. Optics, 1968, 7, 9, 1667.
4. Jones C. R.— Nature, 1952, 170, 29, 937.
5. Jones C. R.— Advances in Electronics, 1953, 5, 1, Acad. Press, New York.
6. Смит Р., Джонс Ф., Чесмер Р. Обнаружение и измерение инфракрасного излучения. ИЛ, М., 1959.
7. Кременчугский Л. С., Мальнев А. Ф., Ройцина О. В.— УФЖ, 1962, 7, 12, 1298.
8. Тепловые приемники излучения. «Наукова думка», К., 1967.
9. Jones C. R.— Proc. IRE, 1959, 47, 9, 1495.
10. Марков М. И.— Оптика и спектроскопия, 1957, 3, 158.
11. Мальнев А. Ф., Кременчугский Л. С., Скачко М. А.— УФЖ, 1960, 5, 5, 634.
12. Jones C. R.— J. Opt. Soc., America, 1960, 50, 9, 883.
13. Jones C. R.— J. Opt. Soc., America, 1960, 50, 11, 1058.
14. Jones C. R.— J. Opt. Soc., America, 1960, 50, 12, 1166.
15. Jones C. R.— J. Opt. Soc., America, 1962, 52, 11, 1193.
16. Мальнев А. Ф., Кременчугский Л. С.— Измерительная техника, 1961, 6, 26.
17. Ван-Дер-Зил Л. Флуктуации в радиотехнике и физике. Госэнергоиздат, М.—Л., 1958.
18. Кременчугский Л. С., Мальнев А. Ф.— ПТЭ, 1963, 5, 182.

AD-A046 669

FOREIGN TECHNOLOGY DIV WRIGHT-PATTERSON AFB OHIO

F/G 17/5

FERROELECTRIC RADIATION DETECTORS, (U)

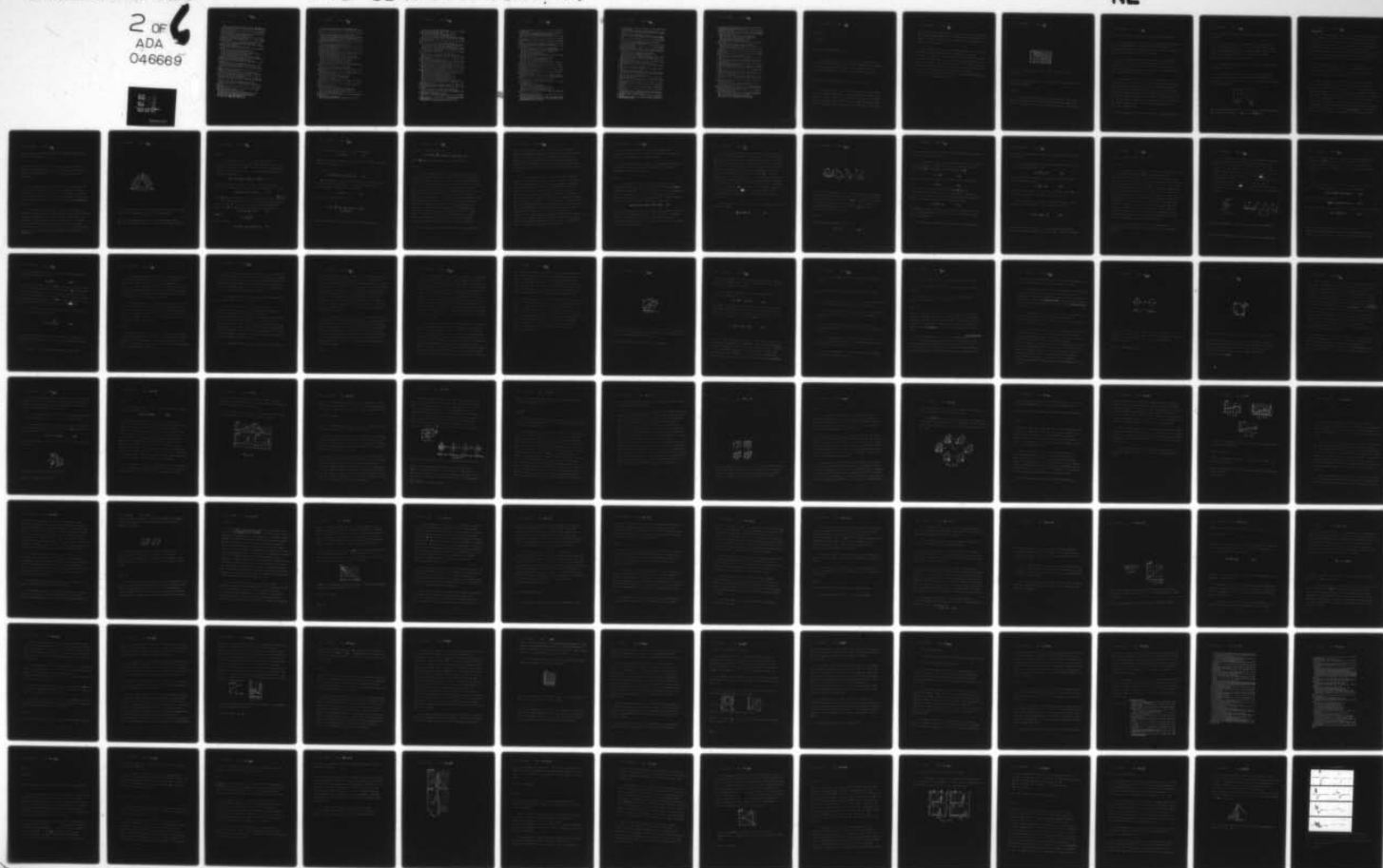
JUL 77 L S KREMENCHUGSKIY

UNCLASSIFIED

FTD-ID(RS)T-0846-77

NL

2 OF
ADA
046669



Pages 38-43.

19. Кременчугский Л. С., Ройцина О. В. — ПТЭ, 1965, 1, 153.
20. Chasmar R. P., Mitchell W. H., Reppie A. — J. Opt. Soc., America, 1956, 46, 7, 469.
21. Кременчугский Л. С. — Автореферат канд. дисс. Институт физики АН УССР, К., 1963.
22. Артюховская Л. М., Кременчугский Л. С., Мальнев А. Ф., Ройцина О. В. — УФЖ, 1964, 9, II, 1240.
23. Ройцина О. В. — ЖПС, 1965, 3, 5, 403.
24. Ройцина О. В., Кременчугский Л. С., Мальнев А. Ф. — Оптико-механическая промышленность, 1965, 12, 9.
25. Ройцина О. В. — Автореферат канд. дисс. Институт физики АН УССР, К., 1968.
26. Strong J., Lawrence P. W. — Appl. Optics, 1968, 7, 1, 49.
27. Jones C. R. — J. Opt. Soc., America, 1953, 43, 1, 1.
28. Jones C. R. — Light and Heat Sensing, 1963, Oxford — London — New York — Paris, Pergamon Press.
29. Gelling L. — Z. angew. Phys., 1951, 3, 467.
30. Mönch G. C., Wichert G., Böttger O. — Ann. Phys., 1953, 6, 12, 4, 183.
31. Wichert G. — Exp. Techn. Phys., 1953, 1, 4, 197.
32. Novak R. — Ceskosl. casop. fys., 1955, 5, 11, 96.
33. Reimann H. — Ann. Phys., 1955, 6, 16, 1, 59; 1955, 6, 16, 1, 52.
34. Urago Y. — J. Phys. Soc. Japan., 1955, 10, 10, 864.
35. Марков М. Н. — ДАН СССР, 1956, 108, 3, 428.
36. Novak R., Resler F. — Ceskosl. casop. fys., 1956, 6, 2, 209.
37. Мальнев А. Ф. — В кн.: Материалы X Всесоюзного совещания по спектроскопии, I. Изд-во Львовского университета, 1957.
38. Archbold E. — J. Scient. Instrum., 1957, 34, 6, 240.
39. Novak R. — Чехословацкий физический журнал, 1957, 3, 3, 284; 1957, 7, 4, 432.
40. Barth G., Zelss C. — Optik, 1958, 15, 11, 694.
41. Novak R. — Чехословацкий физический журнал, 1958, 8, 2, 196.
42. Barth G., Maier W. — Ann. Phys., 1959, 7, 3, 5, 260.
43. Stubbs H. E., Phillips R. G. — Rev. Scient. Instrum., 1960, 31, 2, 115.
44. Мальнев А. Ф., Кременчугский Л. С. — Авт. свид. № 136070. — Бюл. изобретений, 1961, 4.
45. Горелик Л. Л., Лобиков Е. А. — ЖТФ, 1961, 31, 1, 125.
46. Doppecker J., Stecker K. — Wiss. Z. Martin — Luther Univ., Halle — Wittenberg, Math. naturwiss. Reihe, 1961, 10, 5, 917.
47. Горелик Л. Л., Ковальский Н. Г., Подгорный И. М., Синицын В. В. — ДАН СССР, 1962, 147, 576.
48. Ливенцов А. В., Марков М. Н. — ДАН СССР, 1962, 146, 344.
49. Samas M., Feinberg R. M. — Rev. Scient. Instrum., 1962, 33, 9, 344.
50. Gliok H. S. — Rev. Scient. Instrum., 1962, 33, 11, 1268.
51. Жуков А. Г. — Оптика и спектроскопия, 1963, 14, 3, 422.
52. Кременчугский Л. С. — Оптико-механич. промышленность, 1963, 8, 18.
53. Кременчугский Л. С., Мальнев А. Ф., Самойлов В. Б. — УФЖ, 1963, 8, 7, 762.
54. Марков М. Н., Мерсон Я. И., Шалимов М. Р. — Космические исследования, 1963, 1, 2, 235.
55. Горелик Л. Л. — ЖТФ, 1964, 34, 496.
56. Горелик Л. Л., Синицын В. В. — ЖТФ, 1964, 34, 3, 506.
57. Жуков А. Г., Рукман Г. И. — ПТЭ, 1964, 2, 133.
58. Марков М. Н. — Оптика и спектроскопия, 1964, 17, 6, 934.
59. Luck G. — Z. angew. Phys., 1964, 17, 1, 48.
60. Luck G. — Z. angew. Phys., 1964, 18, 2, 84.

61. Марков М. Н.— Оптика и спектроскопия, 1965, 18, 1, 119.
62. Редкобородый Ю. Н., Федулов В. И.— ЖТФ, 1965, 35, 9, 1652.
63. Blevin W. R., Brown W. S.— J. Scient. Instrum., 1965, 42, 1, 19.
64. Deb S., Mukherjee M. K.— Infrared Phys., 1965, 5, 3, 101.
65. Kortum H.— Faengeräte technik, 1965, 14, 11, 484.
66. Kortum H.— Symposium Photon-detectors, Imeko, 1967, Warszawa.
67. Novak R., Hrbek J.— Czech. J. Phys., 1968, 18, 10, 1423.
68. Кременчугский Л. С., Лысенко В. С., Мальнев А. Ф., Ройцина О. В.— ЖПС, 1966, 4, 4, 298.
69. Robinson T. S.— J. Scient. Instr., 1952, 29, 10, 311; 1953, 30, 4, 142.
70. Марков М. Н.— ЖТФ, 1954, 24, 10, 1867.
71. Дианов-Клоков В. И., Стаховский А. Д., Остерман Л. А.— Измерительная техника, 1957, 2, 37.
72. Дианов-Клоков В. И., Палицына Н. А., Стаховский А. Д.— ПТЭ, 1963, 6, 89.
73. Мальнев А. Ф., Есельсон М. П., Кременчугский Л. С.— УФЖ, 1961, 6, 6, 881.
74. Мальнев А. Ф., Есельсон М. П.— ПТЭ, 1961, 1, 137.
75. Есельсон М. П., Кременчугский Л. С., Мальнев А. Ф.— УФЖ, 1961, 6, 3, 420.
76. Карташов А. В., Марков М. Н.— ПТЭ, 1968, 4, 142.
77. Becker G., Moore H.— J. Opt. Soc., America, 1946, 36, 354.
78. Конозенко И. Д.— ЖТФ, 1950, 20, 6, 645.
79. Wormser E. M.— J. Opt. Soc., America, 1953, 43, 15.
80. Конозенко И. Д.— УФИ, 1955, 55, 2, 283.
81. Gilligan E.— J. Scient. Instrum., 1956, 33, 338.
82. Богомолов В. Н., Иллесавский Ю. В., Корнфельд М. Н., Сочава Л. С., Струнин Р. Н.— ЖТФ, 1957, 27, 1, 213.
83. Корнфельд М. Н.— ЖТФ, 1957, 27, 1, 2652.
84. Varica K. M.— Amer. J. Phys., 1958, 26, 8, 561.
85. Astheimer R. W., Wormser E. M.— J. Opt. Soc., America, 1959, 49, 2, 179.
86. Буркин А. Л., Шефтель И. Т.— ФТТ, 1960, 2, 2, 288.
87. Astheimer R. W., De Waard R., Jackson E. A.— J. Opt. Soc., America, 1961, 5, 12, 1387.
88. Dreyfus M. G.— Appl. Optics, 1962, 6, 5, 615.
89. Jones R. C.— Appl. Optics, 1962, 1, 5, 607.
90. Wiley C. M.— Electronics, 1962, 35, 40, 17.
91. Appl. Optics, 1963, 2, 6.
92. Lavan J. T.— Light and Heat Sensing, 1963, Pergamon Press, Oxford — London — New York — Paris.
93. Beerman H. P., Rozett G. C.— Rev. Scient. Instrum., 1965, 36, 8, 1258.
94. Jones C. E., Hilton A. R., Damrel J. B., Helms C. C.— Appl. Optics, 1965, 4, 6, 683.
95. Rev. Scient. Instrum., 1965, 36, 6, 154.
96. Shephard G. G.— J. Appl. Phys., 1965, 36, 10, 3300.
97. Beerman H. P.— Amer. Ceram. Soc. Bull., 1966, 45, 1, 2.
98. Canad. Contr. and Instrum., 1966, 5, 12, 42.
99. Кременчугский Л. С., Лысенко В. С., Мальнев А. Ф., Ройцина О. В.— ЖПС, 1965, 4, 4, 298.
100. Королук В. С., Слободянюк А. И.— Радиоэлектроника, 1967, 10, 1, 82.
101. Electr. Industr., 1967, 104, 537.
102. De Waard R., Weiner S.— Appl. Optics, 1967, 6, 8, 1327.

103. Goetz A.—Phys. Rev., 1939, 55, 1270.
104. Andrews D. H., Milton R. M., Desorbo W.—J. Opt. Soc., America, 1946, 36, 352A; 1946, 36, 9, 518.
105. Fuson N.—J. Opt. Soc., America, 1948, 38, 10, 845.
106. Milton R. M.—Chem. Rev., 1946, 39, 3, 419.
107. Kuol K. S., Volger J.—Physica, 1953, 19, 1, 46.
108. Swenson C. A., Emslie A. G.—Proc. IRE, 1954, 42, 2, 408.
109. Bischoff K., Justi E., Kohler M., Lautz G.—Z. f. Naturforsch., 1955, 10a, 5, 401.
110. Hulbert I. A., Jones G. O.—Proc. Phys. Soc., 1955, 68, 431B, 801.
111. Templeton I. M.—J. Scient. Instrum., 1955, 38, 8, 314.
112. Roberts L. M., Fray S. J.—J. Scient. Instrum., 1956, 33, 3, 115.
113. DeVroomen A. P., Bearle C.—Physica, 1957, 23, 8, 785.
114. Olsen J. L.—Rev. Scient. Instrum., 1958, 29, 6, 537.
115. Biondi M. A., Forrester A. T.—Rev. Mod. Phys., 1958, 30, 1109.
116. Dean T. J., Jones G. O., Martin D. H., Mawer P. A., Perry C. H.—Physica, 1958, 24, 151.
117. Boyle W. S., Rodgers K. F.—J. Opt. Soc., America, 1959, 49, 1, 66.
118. Boyle W. S.—J. Phys. Chem. Solids, 1959, 8, 321.
119. Pestel P., Philip R.—Cryogenics, 1960, 1, 1, 49.
120. Мальнев А. Ф., Кременчугский Л. С.—Оптика и спектроскопия, 1960, 9, 4, 530.
121. Dean T. J., Jones G. O., Martin D. H., Mawer P. A., Perry C. H.—Optica acta, 1960, 7, 2, 185.
122. Ginsberg D. M., Tinha M.—Phys. Rev., 1960, 118, 4, 990.
123. Lalevic B.—J. Appl. Phys., 1960, 31, 7, 1234.
124. Bloor D., Dean T. J., Jones G. O., Martin D. H., Mawer P. A.—Proc. Roy. Soc., 1961, A210, 1303, 510.
125. Bloor D.—Probl. Low Temper. Phys. and Thermod., 1962, 2, 235.
126. Broom R. F.—Nature, 1961, 190, 4780, 992.
127. Holsch H.—Z. Wiss. Z. Martin—Luther Univ., Halle—Wittenberg, Math. naturwiss. Reihe, 1961, 10, 5, 907.
128. Low F. J.—J. Opt. Soc., America, 1961, 51, 1300.
129. Jones G. O., Martin D. H.—Proc. Roy. Soc., 1961, A162, 10.
130. Martin D. H., Bloor D.—Cryogenics, 1961, 1, 3, 1.
131. Biard J. R.—Proc. IEEE, 1963, 51, 2, 327.
132. Hoffman A. R.—Appl. Optics, 1963, 2, 11, 1201.
133. Качинский В. Н.—ПТЭ, 1967, 5, 207.
134. Franzen W.—J. Opt. Soc., America, 1963, 53, 5, 596.
135. Low F. J.—Proc. IRE, 1963, 51, 9, 1171.
136. Low F. J., Hoffman A. R.—Appl. Optics, 1963, 2, 6, 649.
137. Выставки А. Н., Мельник П. Г.—ПТЭ, 1963, 1, 189, ЖЭТФ, 1962, 42, 965.
138. Панкратов Н. А., Виноградова Л. М.—Оптико-механическая промышленность, 1964, 7, 2; 1964, 8, 2; 1964, 9, 1.
139. Galloway D. G., Tolbert C. W.—Rev. Scient. Instrum., 1964, 35, 5, 628.
140. Parkinson D. H.—J. Scient. Instrum., 1964, 41, 2, 68.
141. Richards P. L.—J. Opt. Soc., America, 1964, 54, 1474.
142. Панкратов Н. А., Коротков В. П.—Оптико-механическая промышленность, 1965, 9, 18.
143. Low F. J.—Proc. IEEE, 1966, 54, 4, 37.
144. Andrews J. M., Standberg M. W. P.—Proc. IEEE, 1966, 54, 4, 86.
145. Зайцев Г. А., Хребтов И. А.—Оптико-механическая промышленность, 1966, 1, 34.
146. Clarke J.—The Philosophical mag., 1966, 13, 121, 115.

147. Cavallini M., Gallinaro G., Scoles G.—Z. Naturforsch., 1967, B22a, 3, 413.
148. Пайкратов Н. А., Виноградова Л. М., Пухов Ю. Г., Шибасва О. А.—Оптико-механическая промышленность, 1967, 8, 1.
149. Foils C. L.—Rev. Scient. Instrum., 1967, 38, 6, 9.
150. Cannon W. C., Chester M.—Rev. Scient. Instrum., 1967, 38, 3, 10.
151. Ries P. R., Satterthwaite C. B.—Rev. Scient. Instrum., 1967, 38, 9, 1203.
152. Snively B. B., Yutzy J. C.—Rev. Scient. Instrum., 1967, 38, 5, 125.
153. Коротков В. П., Корнаухов Ю. Н., Робачевский М. В.—Оптико-механическая промышленность, 1967, 5, 21.
154. Merriam J. D., Eisenman W. L., Naugle A. B.—Appl. Optics, 1967, 6, 3, 567.
155. Schwarz E.—Rev. Scient. Instrum., 1949, 20, 12, 962.
156. Hornig D. F., Keefe J. O.—Rev. Scient. Instrum., 1947, 18, 7, 474.
157. Cary H., George K. P.—Phys. Rev., 1947, 71, 4, 276.
158. Fellgett P. B.—Proc. Phys. Soc., 1949, 62, 351.
159. Perkin Elmer News, 1951, 2, 2, 4.
160. Schwarz E.—Research, 1952, 5, 405.
161. Brown D. A. H., Chasmar R. P., Fellgett P. F.—J. Scient. Instrum., 1953, 30, 6, 195.
162. Mönch G. C.—Ann. Phys., 1953, 12, H4—6, 161.
163. Mohr T.—Ann. Phys., 1953, 12, H4—6, 175.
164. Козырев Б. П.—Изв. ЛЭТИ, 1956, 30, 37.
165. Kessler R.—Z. angew. Phys., 1957, 9, 8, 408.
166. Броунштейн А. М., Красильников Л. Б.—Оптика и спектроскопия, 1958, 4, 3, 412.
167. Stecker K.—Wiss. Z. Martin—Luther Univ., Halle—Wittenberg, Math. naturwiss. Reihe, 1958—59, 8, 6, 10.
168. Karoli A. R., Angström A. K., Drummond A. J.—J. Opt. Soc., 1960, 50, 8, 758.
169. Купчинский О. Н., Богомолов П. А.—Оптико-механическая промышленность, 1960, 9, 21.
170. Ожогов Г. Е., Смирнов В. Г., Соковшин Ю. А.—Инж.-физ. журн., 1961, 4, 40, 90.
171. McCarthy D. E.—J. Opt. Soc., America, 1961, 51, 7, 801.
172. Купчинский О. Н., Богомолов П. А., Заболотный И. П., Есаулов Н. А.—Оптико-механическая промышленность, 1961, 8, 27.
173. Козырев Б. П.—Изв. ЛЭТИ, 1960, 44, 3, 22, 44.
174. Черпаков.—Инж.-физ. журн., 1962, № 9, 44.
175. Simms D. L., Rickard R. W., Hinkley P. L.—J. Scient. Instr., 1962, 39, 5, 204.
176. Электроника, 1963, 36, 21, 12.
177. Instr. and Contr. Syst., 1963, 36, 5, 41.
178. Kramer L.—Jenaer Jahrbuch, 1963, 1, 77.
179. Kortum H.—Feingeräte technik, 1964, 12, 561.
180. Козырев Б. П.—Изв. ЛЭТИ, 1966, 55, 3, 59, 190.
181. Slack H. L.—Appl. Optics, 1967, 6, 12, 2151.
182. Drummer L. F., Sanderson J. A.—Appl. Optics, 1967, 6, 12, 2196.
183. Appl. Optics, 1968, 7, 5, A34.
184. Stair R., Schneider W. E., Waters W. R., Jackson J. K.—Appl. Optics, 1965, 4, 6, 703.
185. Astheimer P. W., Weiner S.—Appl. Optics, 1964, 3, 4, 493.
186. Вейнгероу М. Л.—ДАН СССР, 1933, 4, 149; 1938, 19, 9, 687; —Заводская лаборатория, 1947, 13, 4, 426.

187. Теренин А. Н., Ярославский Н. Г.— Изв. АН СССР, сер. физ., 1945, 9, 3, 203.
188. Weiss R. A.— J. Opt. Soc., America, 1946, 36, 6, 356.
189. Goulay M. J. E.— Rev. Scient. Instrum., 1947, 18, 5, 347, 357; 1949, 20, 11, 816.
190. Weber P. F.— Optik, 1950, A6, 3, 152.
191. Степанов Б. И., Гурин О. П.— ЖЭТФ, 1950, 20, 10, 947.
192. Savitsky A., Halford R. G.— Rev. Scient. Instrum., 1950, 21, 3, 203.
193. Васильев Г. А., Жаботинский М. Е.— ЖТФ, 1953, 24, 5, 571.
194. Павленко В. А.— Заводская лаборатория, 1954, 7, 868.
195. Сааль А. О.— ЖТФ, 1956, 26, 1, 157.
196. Панкратов Н. А., Галкин Л. Н.— Оптико-механическая промышленность, 1957, 1, 67.
197. Панкратов Н. А., Нечаева Л. М.— Оптико-механическая промышленность, 1957, 4, 8.
198. Панкратов Н. А.— Оптика и спектроскопия, 1957, 2, 5, 662.
199. Панкратов Н. А.— Оптико-механическая промышленность, 1957, 3, 7; 1957, 2, 6.
200. Jones R. V.— Proc. Phys. Soc., 1958, 71, 458, 280.
201. Yoshihara K.— J. Spectros. Soc. Japan, 1958, 7, 1, 29.
202. Yoshihara K.— Sci of Light, 1958, 7, 3, 67.
203. Слободская П. В.— Оптика и спектроскопия, 1958, 5, 3, 342.
204. Kaiser R.— Canad. J. Phys., 1959, 37, 12, 1499.
205. Панкратов Н. А., Виноградова Л. М.— Оптика и спектроскопия, 1959, 7, 6, 789.
206. Павленко В. А.— В кн.: Теплотехнические и химико-технологические приборы и регуляторы, Машиз, М.— Л., 1959.
207. Jones R. V.— Proc. Roy. Soc., 1959, A249, 1256, 100.
208. Jones R. V., Richards I. C. S.— J. Scient. Instrum., 1959, 36, 2, 90.
209. Yoshihara K.— Sci of Light, 1959, 8, 1, 1.
210. Сааль А. О.— Оптика и спектроскопия, 1959, 6, 556; 1959, 6, 2, 219.
211. Сааль А. О.— ЖТФ, 1959, 29, 3, 324.
212. Панкратов Н. А.— Оптика и спектроскопия, 1960, 8, 1, 109.
213. Панкратов Н. А.— Оптико-механическая промышленность, 1960, 1, 37.
214. Yoshihara K.— Sci of Light, 1960, 9, 2, 75.
215. Панкратов Н. А., Виноградова Л. М. Автоматические газоанализаторы. ЦНИИ, М., 1961.
216. Голубков В. С.— Оптико-механическая промышленность, 1961, 12, 20.
217. Панкратов Н. А., Васильев Э. Ф.— Оптика и спектроскопия, 1961, 10, 127.
218. Панкратов Н. А.— Оптико-механическая промышленность, 1961, 7, 40; 1961, 4, 7.
219. Виноградова Л. М.— Оптико-механическая промышленность, 1962, 1, 26.
220. Сивков А. А., Аверьянов Н. А.— Оптика и спектроскопия 1963, 15, 3, 434.
221. Панкратов Н. А. Автореферат канд. дисс. ГОИ, Л., 1962.
222. Voiteus H. L. J.— Light and Heat Sensing, 1963, 434, Pergamon Press, Oxford — London — New York — Paris.
223. Виноградова Л. М.— Оптико-механическая промышленность, 1963, 10, 58.
224. Панкратов Н. А.— В кн.: Физические проблемы спектроскопии, 2. Изд-во АН СССР, М., 1963.

225. Панкратов Н. А., Васильев Э. В., Корноухов Ю. Н.—*Оптико-механическая промышленность*, 1963, 2, 25.
226. Панкратов Н. А., Голубков В. С.—*Оптико-механическая промышленность*, 1963, 6, 35.
227. Коротков П. В.—*Оптико-механическая промышленность*, 1964, 9, 25.
228. Коротков П. В., Панкратов Н. А.—*Оптико-механическая промышленность*, 1964, 3, 35.
229. Сивков А. А., Попова Э. Т.—*ПТЭ*, 1965, 2, 190.
230. Collins D. A.—*Rev. Scient. Instrum.*, 1965, 36, 6, 850.
231. Schuman M.—*Appl. Optics*, 1965, 4, 11, 1442.
232. Гриценко О. П.—*УФЖ*, 1966, 11, 1, 80.
233. Новиков М. М.—*УФЖ*, 1966, 11, 1, 85.
234. Hennerich K., Lahmann W., White W.—*Infrared Phys.*, 1966, 6, 3, 123.
235. Бреслер П. И.—*Оптика и спектроскопия*, 1967, 23, 6, 973.
236. Сивков А. А., Гуд В. В.—*ПТЭ*, 1967, 1, 195.
237. Hill D. W., Powell T.—*J. Scient. Instrum.*, 1967, 44, 9, 731.
238. Сааль А. О.—*ЖПС*, 1968, 9, 1, 108.
239. Urbach T., Nail N. R., Pearlman D.—*J. Opt. Soc., America*, 1949, 39, 1011.
240. Astheimer R. W., Wormser E. M.—*J. Opt. Soc., America*, 1957, 47, 4, 340.
241. Harding W., Hilsum C., Northrop D.—*Nature*, 1958, 181, 4610, 691.
242. Weike W. K.—*Proc. IRE*, 1959, 47, 9, 1593.
243. Astheimer R. W., Wormser E. M.—*J. Opt. Soc., America*, 1959, 49, 184.
244. Hilsum C., Harding W. R.—*Infrared Phys.*, 1961, 1, 1, 67.
245. Garbung M., Vogl T. P., Hansen J. R.—*J. Opt. Soc., America*, 1961, 51, 3, 261.
246. Фаерман Г. П., Синцов В. Н., Попова К. Б.—*Оптико-механическая промышленность*, 1962, 11, 27.
247. McDaniel G. W., Robinson D. Z.—*Appl. Optics*, 1962, 1, 311.
248. Синцов В. Н.—*Оптико-механическая промышленность*, 1963, 4, 23; 1964, 12, 1.
249. Hansen J. R., Ferguson J. L., Okaа A.—*Appl. Optics*, 1964, 3, 8, 987.
250. Синцов В. Н.—*Оптика и спектроскопия*, 1966, 11, 3, 402.
251. Астгеймер Р.—В кн.: *Измерение нестационарных температур и тепловых потоков*. ИЛ, М., 1966.
252. Чистяков И. Г. *Жидкие кристаллы*. «Наука», М., 1966.
253. Долодугина В. С., Синцов В. Н., Воскресенская В. Н., Левин Б. М.—*Оптико-механическая промышленность*, 1967, 11, 56.
254. Козырев Б. П., Васильев Б. В.—*Оптико-механическая промышленность*, 1967, 11, 61.
255. Koch P. H. B., Oertel H.—*Proc. IEEE*, 1967, 55, 3, 193.
256. Sintsov V. N.—*Appl. Optics*, 1967, 6, 11, 1851.
257. Ицковский М. А., Кременчугский Л. С., Мальнев А. Ф., Склярченко С. К.—В кн.: *Тезисы докладов Всесоюзной межвузовской конференции по элементам радиоэлектронных устройств и микроэлектроники на диэлектриках*. Изд. УкрНИИПИ, К., 1967.
258. Пельц С., Дун Л. М., Новик В. К., Рез Н. С.—*Радиотехника и электроника*, 1968, 13, 1, 183.
259. Синцов В. Н.—*Оптико-механическая промышленность*, 1968, 9, 6.
260. Astheimer R. W., Schwarz.—*Appl. Optics*, 1968, 7, 9, 1687.
261. Surgan D. H.—*Electr. Design*, 1968, 16, 5, 34.
262. Ferguson J. L.—*Appl. Optics*, 1968, 7, 9, 1729.
263. Putley E. H. J.—*Scient. Instrum.* 1966, 43, 12, 857.

Page 44.

Chapter II.

BASES OF PHYSICS OF FERROELECTRIC.

In the present chapter is given the basic information about ferroelectricity and lamellar ferroelectric materials, necessary for the understanding of the physical operating principles of the pyroelectric radiation detectors and ferroelectric bolometers.

§1. Bases of the thermodynamic theory of ferroelectric.

All crystals (Fig. 2.1) in accordance with their cell/elements of symmetry can be distributed to 32 crystallographic classes [25]. twenty of classes, deprived of symmetry center, have one or several polar axes and therefore they can possess piezoelectric properties. From these twenty piezoelectric classes ten they have special polar

axes and are called pyroelectric. The special polar axis it does not have crystallographically to itself equivalent, and its direction cannot be changed to opposite any cell/element of the symmetry of the point group of crystal.

Pyroelectric crystals are spontaneously polarized in the absence external electrical field. However polarization at constant temperature it cannot be reveal/detected from the presence of surface charges, since the latter are compensated for by volumetric and surface conductivity of crystal. But, on the other hand, the value of the spontaneous polarization of pyroelectric crystals it depends on the temperature also during its change on crystal faces, perpendicular to special polar axis, can be reveal/detected charges. Of this consists pyroelectric effect.



Fig. 2.1. Crystal distribution depending on their electrical properties.

Key: (1). Crystals. (2). Piezoelectric materials. (3). Pyroelectrics. (4). Ferroelectric.

Page 45.

The ferroelectric crystals belong to pyroelectric classes and are characterized by the reversible spontaneous polarization. In the presence of field, that more determined (coercive), the direction of

the polarization of ferroelectric can be changed to opposite.

Certain demonstrative representation of spontaneous polarization and the repolarization of ferroelectric can be obtained on hypothetical model. Let us visualize the crystal, which contains two types of ions - A and B (Fig. 2.2) [26, 44].

Possessing high thermal energy and freedom of motion between ions A, ion B it will be equiprobably displaced to one of the adjacent ions A, so that its middle statistical position will be equidistant from them. In this case the curve of potential energy of ion B will have one minimum (Fig. 2.2b).

Certain quantity of ions B with thermal change-overs can simultaneously be displaced in one direction, then in crystal arises internal field. At temperatures, lower than critical (Curie point the intensity of thermal agitation decreases so, that accidentally the emergent internal field be able not only to hold ions B in the displaced position, but also it will displace the adjacent ions B in the same direction. On curved potential energy of ion B will appear two asymmetric minima (Fig. 2.2a). In crystal will arise the spontaneous polarization.

If we increase the applied field, applied to ferroelectric and

directed opposite to polarization, potential minima will begin to be equalized.

In the field, greater than coercive, ion B during thermal agitation will overcome barrier ΔE and will change into the right potential minimum, carrying off after itself other ions B. In this case the right potential minimum will become deeper during removal/taking applied field, than left.

For linear pyroelectrics no fields, up to the disruptive, can repolarize the crystal.

The presence in the ferroelectric crystals of spontaneous polarization in polar phase is interesting not only from the viewpoint of solid state physics, but also in connection with diverse application/appendices.

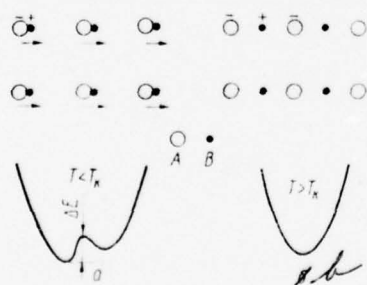


Fig. 2.2. Hypothetical structure and the form of potential energy of ferroelectric for cases of $T < T_K$ (a) and $T > T_K$ (b).

Page 46.

The sharp temperature dependence of spontaneous polarization and its derivative in terms of field - dielectric constant - lay as the basis of the creation of pyroelectric receivers and ferroelectric bolometers. In the range of phase transition a series of the alloyed ferroelectric possesses the anomalous temperature course of resistance. Positive temperature specific resistance in them reaches 20-60o/o in the range of phase transition, which makes it possible to prepare highly sensitive temperature sensors on their basis.

In connection with the fact that the icrm/shaped in ferroelectric sensing transducer is the complex function of the electrical, thermal and mechanical properties of crystal, it is necessary to examine the interrelation between them.

Figure 2.3 gives the relationship/ratio between the values, which characterize the properties of ferroelectric crystal [41 indicated] in thermodynamic equilibrium. In the apex/vertexes of external triangle in symbols T (temperature), σ (mechanical stress), E (electric field) are designated the "forces", which act on crystal, while in the apex/vertexes of internal triangle are shown values s (entropy), D (induction), u (strain), that are the result of the action/effect of the corresponding "forces". The lines, which combine in pairs the near external and internal apex/vertexes of triangles, designate the main effects (for example, $D_i = \epsilon_0 E_i^*$), while the lines,

which connect distant apex/vertexes, the conjugated effects (for example, $\Delta D = 4\pi\gamma\Delta T$). ^{1.}

FOOTNOTE 1. Latin indices here and subsequently designate the components of tensors in the selected coordinates, in this case is implied the summation over the twice being repeated indices.

ENDFOOTNOTE.

For the characteristic of the energy state of crystal in the general case are sufficient to know six components of stress σ_{ij} , three components of electric field E_i and temperature T . With the same law can be selected as the independent variables of the strain tensor component u_{ij} , the vector of induction (polarization) $D_i (P_i)$ and entropy s .

The properties of crystals turn out to be those which were interlocked and one should examine them together. For example, during a change in temperature of T occurs a change in induction D - the pyroelectric effect, caused by direct coupling $T \rightarrow D$. However, along with this communication/connection is possible indirect coupling $T \rightarrow u \rightarrow D$ ($T \rightarrow u \rightarrow \sigma \rightarrow D$), i.e., electrical induction can be caused by thermal expansion and piezoelectric effect.

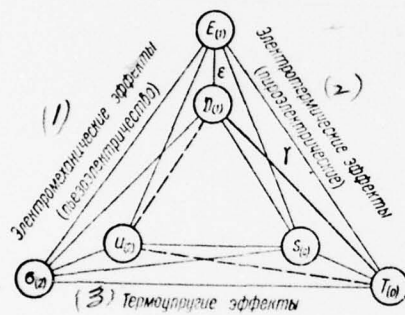


Fig. 2.3. Thermodynamic communication/connection between the thermal, electrical and mechanical properties of ferroelectric.

Key: (1). Electromechanical effects (piezoelectricity). (2). Electrothermal effects (pyroelectric). (3). Thermoelastic effects.

Page 47.

Let us examine in general form piezoelectric effect in ferroelectric. Is decomposed induction \vec{D} crystal in a series in the components of electric field E_i and of stress σ_{ij} . By set/assuming induction changes small, we will be restricted during resolution by first-order derivatives:

$$D_i(E, \sigma, T) = D_i(0, 0, T) + \left(\frac{\partial D_i}{\partial E_j} \right)_{\sigma, T} E_j + \left(\frac{\partial D_i}{\partial \sigma_{jk}} \right)_{E, T} \sigma_{jk}. \quad (2.1)$$

Here indices with the partial derivatives indicate, with which fixed/recorded independent variables are differentiate. Let us write

$$D_i(E, \sigma, T) = D_{i0} + \epsilon_{ij} E_j + 4\pi d_{ijk} \sigma_{jk}, \quad (2.2)$$

where $\frac{\partial D_i}{\partial E_j} = \epsilon_{ij}$ - the components of the tensor of dielectric constant; $\frac{\partial D_i}{\partial \sigma_{jk}} = 4\pi d_{ijk}$

- the components of the tensor of piezoelectric module/modulus.

Taking into account the common/general/total relationship/ratio,

which joins D_i and E_i with the polarization of crystal P_i :

$$D_i = E_i + 4\pi P_i = E_i \delta_{ij} + 4\pi P_{ij}, \quad (2.2a)$$

where

$$\delta_{ij} = \begin{cases} 1 (i = j) \\ 0 (i \neq j), \end{cases}$$

we will obtain

$$P_i = \frac{1}{4\pi} D_{i0} + \frac{1}{4\pi} (\epsilon_{ij} - \delta_{ij}) E_j + d_{ijk} \sigma_{jk}. \quad (2.3)$$

On the basis of Hooke's law it is possible to write

$$\sigma_{jk} = c_{jklm} u_{lm}, \quad (2.4)$$

where c_{jklm} and u_{lm} are components of the tensors of elastic hardnesses and strains respectively.

Thus,

$$P_i = \frac{1}{4\pi} D_{i0} + \frac{1}{4\pi} (\epsilon_{ij} - \delta_{ij}) E_j + d_{ijk} c_{jklm} u_{lm}. \quad (2.5)$$

Let us define the pyroelectric coefficient of crystal γ_i , which it characterizes its pyroelectric activity as derivative of polarization P_i in terms of the temperature:

$$\gamma_i = \frac{\partial P_i}{\partial T}. \quad (2.6)$$

From equation (2.5) we will obtain

$$\gamma_i = \frac{1}{4\pi} \cdot \frac{\partial D_{i0}}{\partial T} + \frac{1}{4\pi} \cdot \frac{\partial}{\partial T} (\epsilon_{ij} - \delta_{ij}) E_j + d_{ijk} c_{jklm} \frac{\partial u_{lm}}{\partial T} + u_{lm} \frac{\partial}{\partial T} (d_{ijk} c_{jklm}).$$

Thus, expression for the total pyroelectric coefficient of free

crystal ($\sigma = \text{const}$) takes the form

$$\gamma_i^o = \gamma_i'' + \frac{1}{4\pi} \cdot \frac{\partial \epsilon_{ij}}{\partial T} E_j + d_{ijk} c_{iklm} a_{lm} + u_{lm} \frac{\partial}{\partial T} (d_{ijk} c_{iklm}), \quad (2.7)$$

where $\frac{\partial u_{lm}}{\partial T} = a_{lm}$ - the coefficient of thermal expansion.

Page 48.

The first term γ_i'' determines the pyroelectric effect of the mechanically jammed crystal ($u = \text{const}$). It they call by primary ("true") pyroelectric effect, since it is caused by a direct/straight change in thermal energy of the lattice of the evenly heated crystal and is not bonded with its strain. The remaining three members characterize the secondary ("false") pyroelectric effect. Far from Curie point, in the ferroelectric phase, when the temperature dependences of dielectric constant, piezoelectric module/modulus and elastic hardnesses are small, the second and fourth terms can be disregarded. However, the third term of many ferroelectric very considerable, and of some introduces the basic contribution to pyroelectric effect. Near phase transition the second and fourth terms can introduce the significant contribution to the total pyroelectric effect due to an abrupt change in the dielectric constant, piezoelectric module/moduli and elastic hardnesses.

In the examination of pyroelectric effect it was assumed that

the crystal is evenly heated (in it there are no temperature gradients). Nonuniform heating of crystal creates the nonhomogeneously stressed state in it, which in turn, leads to a change of the polarization in crystal. This phenomenon is known by the name of tertiary pyroelectricity. Tertiary pyroelectric effect barely was investigated, and at present there are no any even estimated data on its value.

In the general case each of the components of the vector of pyroelectric coefficient contains much terms, since in expression (2.7) enter tensors II, III and IV ranks. However, the number of independent components of tensors considerably is decreased as a result of the symmetry of crystals. The effect of symmetry of crystals on their physical properties is determined by Neumann's principle, according to whom the symmetry of any physical property must include the cell/elements of the symmetry of the point group of the crystallographic class of crystal. In the book J. Naya [41] are given the matrix/dies of equilibrium physical properties for 32 crystallographic classes. If is known the point group of ferroelectric crystal, then of the expressions for the matrix/dies of piezoelectric moduli, elastic hardnesses, coefficients of thermal expansion and dielectric constants it is possible to determine the number of components of pyroelectric coefficient.

Let us examine concrete expressions for spontaneous polarization, a dielectric constant and pyroelectric coefficient at different temperatures and in electric fields.

At present greatest quantity of experimental facts succeeds in explaining within the framework of Ginzburg - Devonshire's thermodynamic theory [19, 44, 64].

Page 49.

Let us assume that free energy of ferroelectric is the single-valued function only of polarization and temperature $A(\vec{P}, T)$, a polarization vector \vec{P} is directed along one of the crystallographic axes. I investigate the range of phase transition, where the polarization is small or equal to zero. Then free energy of crystal can be presented in the form of converging series [26]:

$$A(P, T) = A(0, T) + \frac{1}{2}\beta^\sigma P^2 + \frac{1}{4}\xi^\sigma P^4 + \frac{1}{6}\xi^\sigma P^6. \quad (2.8)$$

The coefficients with odd terms of expansion are equal to zero, since the form of the function A must not depend on sign P . In equation (2.8) the coefficients are determined with constant stresses σ (subsequently index σ let us for simplicity omit) and in the general case depend on temperature.

Let free energy of the nonpolarized crystal be equal to zero: $A(0, T) = 0$, and on temperature depends only one of the coefficients: $\beta = \beta(T)$. The steady state of crystal is determined by the minimum of free energy at the assigned temperature. If ζ and ξ is more than zero in polar and nonpolar phases, then the analysis of expression for free energy of system A (P, T) gives following. With $\beta > 0$ minimum of free energy is located from equation $\frac{\partial A}{\partial P} = 0$ and corresponds to the only condition $P = 0$ (Fig. 2.4a). Physically this means that the spontaneous polarization in crystal exist cannot. In $\beta < 0$ root of equation (2.8) $P = 0$ corresponds already to the maximum of free energy, since $\left(\frac{\partial^2 A}{\partial P^2}\right)_{P=0} < 0$, and to the minimum of function $A(P, T)$ correspond roots $P \neq 0$. The polarized state becomes energetically more favorable, and in crystal appears spontaneous polarization.

If we disregard the term of the sixth order in (2.8), then it is possible to write

$$\frac{\partial A}{\partial P} = E = \beta P + \zeta P^3. \quad (2.9)$$

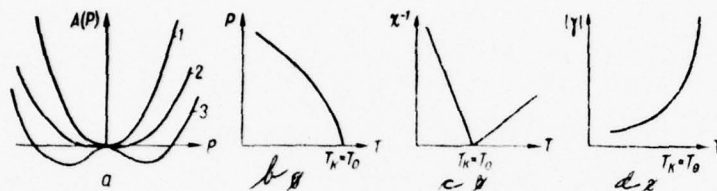


Fig. 2.4. The dependences of some characteristics of ferroelectric during second order phase transition: a is free energy of crystal from polarization $A = A(P)$ with $T > T_K$ (1), $T = T_0$ (2) and $T < T_0$ (3); b - spontaneous polarization from temperature of $P = P(T)$; c is reverse/inverse dielectric susceptibilities χ^{-1} from T ; d - pyroelectric coefficient γ from T .

Page 50.

In the absence of electric field ($E = 0$)

$$P^2 = -\frac{\beta}{\zeta}. \quad (2.10)$$

If dependence $P = P(T)$ is continuous, then such transition is called second order phase transition.

On the basis of common relationship/ratio (2.2a) it is possible to establish/install communication/connection between dielectric constant $\epsilon = \frac{\partial D}{\partial E}$ and dielectric susceptibility $\chi = \frac{\partial P}{\partial E}$:

$$\epsilon = 1 + 4\pi\chi. \quad (2.11)$$

Near Curie point, when dielectric constant reaches large values,

$$\chi \approx \frac{1}{4\pi} \epsilon. \quad (2.12)$$

Differentiating equation (2.9), we obtain $\beta \approx \frac{\partial^2 A}{\partial P^2} \approx \frac{1}{\gamma}$, that characterizing the reverse/inverse susceptibility of crystal. In order to describe Curie-Weiss' experimentally established/installed law, β it is possible to write in the following form:

$$\beta = \frac{4\pi}{C_K} (T - T_0), \quad (2.13)$$

where C_K is constant Curie; T_0 - Curie-Weiss' temperature. In this case one should remember that constant Curie in polar and nonpolar phases is different.

The dependence of spontaneous polarization P on temperature is

constructed on the basis of expressions (2.10), (2.13) and is given in Fig. 2.4b.

For a reverse/inverse dielectric susceptibility higher than the point of phase transition we have

$$\frac{1}{\chi} = \left(\frac{\partial^2 A}{\partial P^2} \right)_{P=0} \approx \beta. \quad (2.14)$$

It is lower than the transition temperature, taking into account relationship/ratio (2.10),

$$\frac{1}{\chi} = \frac{\partial^2 A}{\partial P^2} \approx -2\beta. \quad (2.15)$$

This dependence is given in Fig. 2.4c. At transition point $\frac{\partial^2 A}{\partial P^2}$ it is theoretically equal to zero, a ϵ it becomes infinite.

From expression for spontaneous polarization (2.10) we obtain the temperature dependence of pyroelectric coefficient γ :

$$\gamma = \frac{\partial P}{\partial T} = \frac{1}{2V - \beta_+} \cdot \frac{\partial \beta}{\partial T}. \quad (2.16)$$

At transition point, according to equation (2.13), pyroelectric coefficient becomes infinite, but is above T_K - apparent/imaginary.

Curve $\gamma = \gamma(T)$ is given in Fig. 2.4d.

Page 51.

The dependence of polarization P on electric field E lower than the temperature of transition T_K , constructed according to relationship/ratio (2.9), is represented in Fig. 2.5 (curve ABCD). Section BC does not have the physical sense, and crystal from state B abruptly transfer/converts to state \mathcal{E} , a from C - to F. The obtained figure is called the hysteresis loop of ferroelectric. Experimentally the taken relationship/ratics between P and E take the similar form. The hysteresis loop is not only essential feature of ferroelectrics, but also by evidence of the presence of the reversible spontaneous polarization in it. Cut $GO = OH$ is called coercive field E_K , which necessary to apply to overcome the potential threshold (see Fig. 2.2a) and to convert crystal of one state into another with the equal, but oppositely directed polarization. Extrapolation of the quasi-linear section AF before intersection with axis OP gives the value of spontaneous polarization P_c (cut (ON)).

On the basis of equations (2.9), (2.11) and (2.16) it is possible to find the dependence of values γ and \mathcal{E} from electric field E .

Let us examine now ferroelectric with first-order transition. During the analysis of expression (2.8) they assumed that all coefficients at temperature higher than the Curie point were positive. Let us assume now that $\zeta < 0$, $\alpha > 0$ and $\beta > 0$. from expression (2.8) it is evident (Fig. 2.6a) that in this case free energy can have equal minima with $P = 0$ and $P \neq 0$, which correspond to one value $\beta > 0$ (curve 2). Thus, in $T = T_K$ to crystal correspond two steady states with the different values of polarization ($P = 0$ and $P \neq 0$) - transition of one to another it is completed by jump. This phase transition is called of first-order transition.

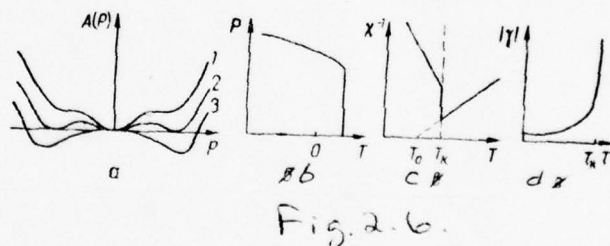
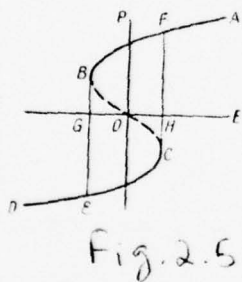


Fig. 2.5. Dependence of polarization P on electric intensity E .

Fig. 2.6. The dependence of some characteristics of ferroelectric

during first-order transition: a is free energy from polarization $A = A(P)$ with $T > T_K$ (1) $T = T_0$ (2) and $T < T_0$ (3); b - spontaneous polarization from temperature of $P = P(T)$; c is reverse/inverse dielectric susceptibilities χ^{-1} from T; d - pyroelectric coefficient γ from T.

Page 52.

The value of free energy at transition point is equal to zero, since it is the continuous function of the polarization:

$$A(0, T) = \frac{1}{2} \beta P^2 + \frac{1}{4} \zeta P^4 + \frac{1}{6} \xi P^6 = 0. \quad (2.17)$$

Let electric field $E = 0$, then

$$\frac{\partial A(0, T)}{\partial P} = E = \beta P + \zeta P^3 + \xi P^5 = 0. \quad (2.18)$$

Solving together (2.17) and (2.18), we find value of $P = P_0$ in point T_K :

$$P_0^2 = -\frac{3}{4} \frac{\zeta}{\xi} \text{ and } P = 0. \quad (2.19)$$

Figure 2.6b shows that function $P = P(T)$ undergoes discontinuity/interruption at point T_K , transfer/converting from one value of $P = 0$ to the next, determined by equation (2.19). In this

case the expression for an inverse dielectric susceptibility at transition point takes the form

$$\frac{1}{\chi_0} = \frac{3}{16} \frac{\epsilon^2}{\epsilon}, \quad (2.20)$$

from which it is clear that value $1/\chi_0$ at transition point is positive and also it experience/tests jump. The dependence $1/\chi$ on temperature is given in Fig. 2.6c. It is analogous with that done for second order phase transition, it is possible to show that with $T < T_0$ the slope/inclination of straight line $1/\chi$ is steeper than with $T > T_0$. of ferroelectric with first-order transition T_0 ~~T_0~~ T_K .

From equation (2.18), by assuming that electric field E does not depend on temperature, we will obtain

$$\gamma = - \frac{P \frac{\partial \beta}{\partial T}}{\beta + 3\epsilon P^2 + 5\epsilon^2 P^4}. \quad (2.21)$$

By putting to use equations (2.18) and (2.21), it is possible to establish/install the dependence γ and ϵ on the value of electric field E .

Dependence $\gamma = \gamma(T)$ is schematically given in Fig. 2.6d.

The given above thermodynamic theory of ferroelectricity bears purely phenomenological character. The molecular mechanism of ferroelectricity is located in the stage of development. The emergence of spontaneous polarization can be considered as result of the equilibrium between two forms of reaction - "that which drive" and "returning" [28]. The "leading" reaction includes in essence electrostatic, while to "returning" - elastic.

The microscopic theory of ferroelectricity, which is based on the dynamic loudspeaker of crystal lattice, is developed by V. L. Ginsburg [19], by P. V. Anderson [4] and by V. Kokren (theory book) [63]. Phase transition in this theory is joined with the loss of stability of lattice relative to the low-frequency optical mode of normal oscillatory mode in crystal.

Page 53.

V. Kokren showed that the square of the frequency of this mode depends on the difference between the forces driving and returning of reactions. With the balancing of reactions the frequency becomes zero, and in crystal it appears the unsteady state of lattice, which leads to ferroelectric transition.

By L. B. Bersuker [5], and then by it and by B. G. Vekhter [6] is developed the "inter-zone" theory of ferroelectricity, according to which under some conditions structural communication/connections in crystal can turn out to be unstable with respect to the dipole nuclear displacement, which lead to the formation of dipole moment and the emergence of spontaneous polarization.

The available at present theoretical works on pyroelectricity are applied mainly to linear pyroelectrics.

As the basis of the theory of S. A. Boguslawski's pyroelectricity [9] is placed the einstein model of crystal as totalities of linear anharmonic oscillators. Author establish/installed the dependence of the appearing dipole moment on temperature. In high-temperature range the theory will agree sufficiently well with experiment; however, in low-temperature range strongly from it it diverges. The drop of the value of pyroelectric coefficient according to the law T^2 at low temperatures gave Born's quantum mechanical theory [10, 11], which is based on the created by it dynamic theory of crystal lattice.

The spontaneous polarization, which appears in ferroelectric in

polar phase, can have different directions in the different parts of the crystal. Crystal is divide/marked off into separate ranges - domains - with identical direction of polarization within the limits of each domain. In the absence of external electrical and mechanical fields the domain structure of real ferroelectric crystals can be different the characteristic of crystal in the general case they depend on its domain structure. So, pyroelectric effect of the crystal, which consists of two domains, which have the equal, but oppositely directed polarization, is equal to zero. In connection with this expedient to examine the question concerning domains in ferroelectric crystals.

In the ideal case the ferroelectric must be divided into domains in connection with the fact that poly-domain state energetically more suitable. Free energy of poly-domain crystal less the monodomain, since with separation into the domains, which have the antiparallel orientation of spontaneous polarization, decreases energy of the depolarizing field. However, in the process of this separation free energy grow/rises because of the formation of domain walls. As a result appears the determined equilibrium domain structure at the assigned temperature.

Due to the presence of defects in real crystal the polarization is not uniform. In the process of crystal growth in it they are formed mechanical strains, and finally conductivity any ferroelectric partially compensates for the charges, which create the depolarizing field. Therefore the actual domain structure of ferroelectric is the result of the energy equilibrium, which conditions the domain configuration of the ideal crystal and perturbation effect of the volume of surface conductivity, mechanical strains and defects. It is necessary to note that they are encountered and monodomain of crystal. Although energetically their state is metastable, they can exist for a very long time. It is completely obvious, that external electric fields and mechanical effects also can influence the domain structure of crystal.

From Ginsburg-Devonshire's thermodynamic theory were obtained the expressions for the pyroelectric coefficient of ferroelectric with the phase transitions of the first (2.16) and second (2.21) order, from which it follows that in polar phase the pyroelectric coefficient is monotonic function with maximum at Curie point, where is observed also the maximum of dielectric constant. The experimental data, obtained recently [3, 15, 32, 35], they showed that the maximums γ and ϵ can not coincide, also, besides the basic maximum γ , near Curie point they can appear supplementary peaks [35]. 91

Possible explanation of this phenomenon is given by V. Kh. Kozlovskiy

[29]. The author examined free energy of the broken into domains ferroelectric crystal, consisting of energy of two sublattices of domains and interaction energy of their through interfaces and external faces. The investigation of the temperature dependence of free energy of this ferroelectric indicated the possibility of the phase transformations, bonded with transition from energetically unstable monodomain to energetically stable poly-domain state.

Schematically this process is represented in Fig. 2.7. From the figure one can see that the monodomain state is metastable, since with the same temperature its free energy is higher than of poly-domain state. Point M_1 limits that part of the branch of the curve 1, after which the square of the amplitude of the oscillations of the adjacent sublattices of domains u^2 begins to fall with an increase of temperature (unsteady state). Crystal with $T > T'_n$ transfer/converts to poly-domain state. The reflection of this process is the abrupt change in the polarization (peak of pyroelectric coefficient).

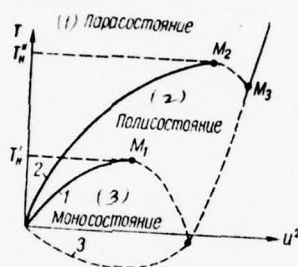


Fig. 2.7. The diagrammatic representation of part of free energy u^2 , which depends on temperature (u is amplitude of the oscillations of the adjacent sublattices of domains).

Key: (1). Parastate. (2). Poly-state. (3). Monostate.

At temperature $T > T_n$ the crystal transfer/converts from poly- to parastate, nonpolar, state. This is exhibited also in the anomalous course of pyroelectric coefficient.

The formally total polarization of ferroelectric can be presented as follows [35]:

$$P_{\text{изм}} = \Theta_y P_c \quad (0 \leq \Theta_y \leq 1), \quad (2.22)$$

where P_c is the spontaneous polarization, measured in high electric field; Θ_y - coefficient of unipolarity, which is the ratio of the value of the polarization of domains in this direction to the overall value of the polarization of all domains (P_c). Let us write

$$\gamma = \frac{\partial P_{\text{изм}}}{\partial T} = \Theta_y \frac{\partial P_c}{\partial T} + P_c \frac{\partial \Theta_y}{\partial T}. \quad (2.23)$$

First term (2.24) characterizes part of the pyroelectric coefficient, determined by temperature course $P_c(T)$; the second - the rearrangement of domain structure. If $\Theta_y = \text{const}$ in an entire temperature range Δ $T < T_K$,

that pyroelectric coefficient has one maximum, which coincides with maximum ε with $\bar{T} = T_K$. If at certain temperature $\bar{T}_H < \bar{T}_K$ specimen/sample made of monodomain state changes in poly-domain ($\Theta_y(T_n)$)

= 0), then at point T_H pyroelectric coefficient will achieve maximum.

§2. Ferroelectric crystals for thermal radiation detectors.

The basic requirements, presented to the ferroelectric materials of sensing elements of thermal receivers, are determined:

a) by the high value of the measured parameter - pyroelectric coefficient, of the temperature coefficient of permittivity or resistance;

b) by the low level of supplementary noises (noises of repolarization, Barkhausen's jumps, current noises, the vibrations of some others);

c) by the possibility of obtaining the thin layers of ferroelectric with the preservation/retention/maintaining in it of the properties of massive material;

d) by the invariability of characteristics under climatic, mechanical and radiation exposure;

e) by the stability of the parameters in the course of time;

f) by the technologically simple and cheap method of obtaining material.

Are unknown at present the ferroelectric materials, which satisfy the requirements enumerated above.

Page 56.

However, among open ferroelectric [43] whose number exceed 150, for developing receivers are utilized the single crystals of the group of triglycine sulfate, titanate of barium and its derivatives, ceramics of titanate of zirconate of lead, the single crystals of niobate of lithium and SBN ($\text{Sr}_{1-x}\text{Ba}_x\text{Nb}_2\text{O}_6$). Let us examine the properties of basic of them.

Group of triglycine sulfate (TGS). Triglycine sulfate $(\text{NH}_2\text{CH}_2\text{COOH})_3 \text{H}_2\text{SO}_4$ \wedge

is a comparatively young representative of ferroelectric, open by Mathias, Miller and Remeyka [84] into 1956. Because of its good dielectric properties and convenient technology this crystal began to be utilized as memory element in computers [52], in instruments for

temperature self-stabilization [25], in dielectric amplifiers and as sensing element in thermal radiation detectors [33, 34].

The crystals TGS grow from its aqueous solutions [37] by gradual cooling from 55 to 20°C with reversive mixing. Basis for the preparation of solution is glycine and sulfuric acid. For obtaining triglycinefluoroberyllate $(\text{NH}_2\text{CH}_2\text{COOH})_3 \text{H}_2\text{BeF}_4$ instead of sulfuric acid is applied fluoroberyllium, while for triglycineselenate $(\text{NH}_2\text{CH}_2\text{COOH})_3 \text{H}_2\text{SeO}_3$ is selenate.

Into crystallizer with the solution of TGS or its isomorphous is placed the seeding, cut out along Z-axis, and during the automatically adjustable slow cooling for 2-3 weeks it is possible to grow crystals 400-800 g in weight.

Higher than the temperature of phase transition the crystals of the group of TGS are related to centrally symmetrical class $2/m$ monoclinic system (Fig. 2.8). Lower than the temperature of phase transition the mirror plane m disappears, and crystal transfer/converts to the ferroelectric phase, which relates to point group 2 of monoclinic system [41]. Crystals possess the axis of the symmetry of the 2nd order - by the monoclinic axis b , which is special polar axis. Along it are exhibited the ferroelectric properties of the crystals of the group of TGS. The adopted crystalphysic system of coordinates for TGS is represented in Fig. 2.9 [36].

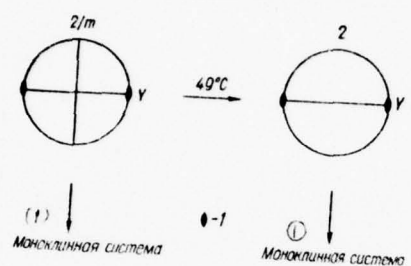


Fig. 2.8. A change in the cell/elements of the symmetry of the crystals of the group of TGS during the phase transition: 1 - twofold axis; m is a mirror plane of symmetry; y - crystallographic coordinate axis.

Key: (1). Monoclinic system.

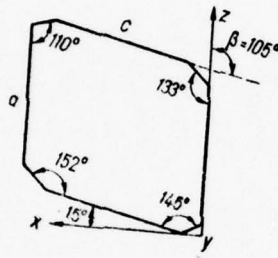


Fig. 2.9. Selection of crystallophysic system in the crystal of TGS.

Page 57. Crystal shape is complex, but axis b sufficiently marked. With the aid of saw for cutting water-soluble crystals it is possible to easily obtain plates, perpendicular axes b (plane 010). The obtained by the method described above plates are called y -section/shear (axis $y \parallel b$).

There is a series of works, dedicated to the investigation of the nature of ferroelectricity in the crystals of the group of TGS [7, 18, 22, 24, 26, 31, 45, 65, 72, 86, 87]. Detailed X-ray diffraction examination of TGS was carried out Hoshino, Okaya and Pepinskiy [72]. Figure 2.10 gives part of the unit cell of TGS from by their this structural analysis. According to findings, molecule TGS consists of three glycine groups and one sulfate group. Glucinum I and III are record/written in the form $\text{NH}_3^+\text{CH}_2\text{COOH}$, a glycine II $\text{NH}_3^+\text{CH}_2\text{COO}^-$.

The latter is dipolar ion ("zwitter-ion"). Glucinum I and III planes, and glycine II is partially plane, since in it the atom of nitrogen somewhat emerges the plane of two atoms of carbon and two atoms of oxygen. Ion SO_4^{2-} connects groups glucinum I and III through the system of hydrogen bonds and is the slightly distorted tetrahedron, whereupon the degree of its distortion is different in ferroelectric and paraelectric phases.

The investigations of the infrared spectra of the group of TGS in polarized light, carried out in works [7, 24], they showed that the initiating cell/element in the emergence of ferroelectric activity are the quasi-tetrahedral anions (of type XY_4^{2-}), which acquire their own dipole moment as a result of Jan-Ieller's pseudoeffect.

In mechanical relationship the ferrocrystals of the type TGS are brittle. This one of the reasons, on which sensing elements of triglycinesulfate receivers do not make thinner. 50 μ . Crystals possess noticeable cleavage in plane (010).

The heat capacity of crystals TGS and it isomorphous was studied in works [46-49, 73, 94] in the range of temperatures 0-65°C.

From equation (2.8) for the value of free energy of crystal, it is possible to obtain expression for entropy $s = \left(\frac{\partial A}{\partial T} \right)_p$ and the jump of entropy during the phase transition

$$\Delta s = s_0 - s = \frac{1}{2} \left(\frac{\partial \chi_0}{\partial T} \right) P^2. \quad (2.24)$$

where s_0 is entropy in nonpolarized state, but s - in that which was polarized.

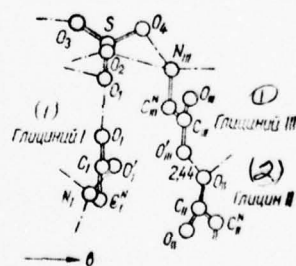


Fig. 2.10. Part of the unit cell of TGS [72].

Key: (1). Glucinum. (2). Glycine.

Page 58.

Then expression for the jump of heat capacity (during constant polarization) takes the form

$$\Delta c = c_p - c_{p_0} = \beta T \frac{\partial p^2}{\partial T} \quad (2.25)$$

By taking into account dependence of P on E , it is possible to predict that the electric field also will render/show the determined effect on the jump of heat capacity in the region of phase transition. The results of experimental studies are given in Fig. 2.11. Temperature course of heat capacity is quantitatively not subordinated to the relationship/ratios, which escape/ensue from Ginzburga - Devonshire's thermodynamic theory. Electric field decreases the maximum of heat capacity at point curie, but it increases its value in paraelectric phase. Since the experimental data indicate an increase in the peak of heat capacity several times in comparison with thermodynamic calculation, was assumed [46] about effect on its value of the fluctuations of polarization.

It is impossible to observe the domain structure of of TGS with the aid of polarizing microscope. Therefore is utilized the etching method, which lies in the fact that two end/leads of the polar

crystal index they have different rate of solution (etching), whereupon crystal boundary from the positive end/lead of polar axis it is etched faster than of negative.

Domain picture can be determined by pyroelectric effect during the probe irradiation of the γ -section/shear of crystals.

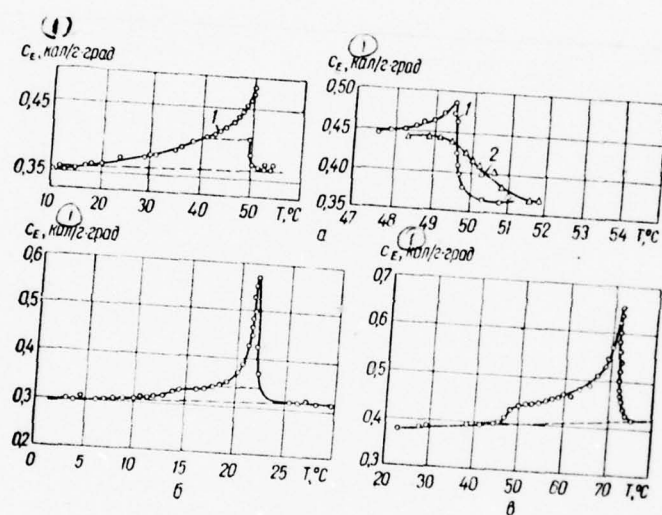


Fig. 2.11.

Fig. 2.11. The temperature dependence of heat capacity c_E : a) for single crystals of TGS with $E = 0$ (1) and $E = 450$ V/cm (2) [46, 47]. b) for single crystals TGSe [48], c) for single crystals TGFB [49].

Key: (1). Cal/g·deg.

Page 59. The superficial dimensions of domains can change over wide limits. In cross section the domains have oval form.

Titanate of barium (BaTiO_3) and its derivatives. Ferroelectric titanate of barium was opened by B. M. Vul and I. M. Gol'dan in the USSR into 1945 and independent of them by the American and Japanese scientists. Single crystals BaTiO_3 , its ceramicist and derivatives most in detail are studied in detail.

Temperature of the phase transition of crystals BaTiO_3 about 120°C . Higher than this temperature crystal belongs to the centrally symmetrical class $m\bar{3}m$ cubic system [41]. Crystal BaTiO_3 has perovskite structure ABO_3 , characteristic for calcite CaTiO_3 . Unit cell BaTiO_3 is given in Fig. 2.12. The stereographic projection of the cell/elements of symmetry of crystal BaTiO_3 is shown in Fig. 2.13 [41]. The presence of symmetry center among the cell/elements of the symmetry of this class makes this phase nonpolar.

Lower than the Curie temperature crystal BaTiO_3 belongs to class $4mm$ tetragonal system. The rotary tetrad axis is special polar axis. Hence it follows that spontaneous polarization \vec{P}_c can be directed only along this axis. Such axes in initial cubic lattice three (direction $\langle 100 \rangle$); therefore the vector of spontaneous polarization can be directed along one of the six equivalent directions $\langle 100 \rangle$. The tetragonal unit cell BaTiO_3 appears as a result of distortion by initial cubic, in which one fin/edge is lengthened and becomes tetragonal axis (Fig. 2.14^a), but two others are reduced along axis a .

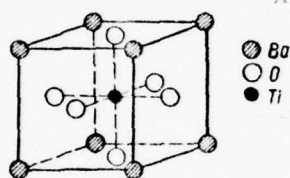


Fig. 2.12.

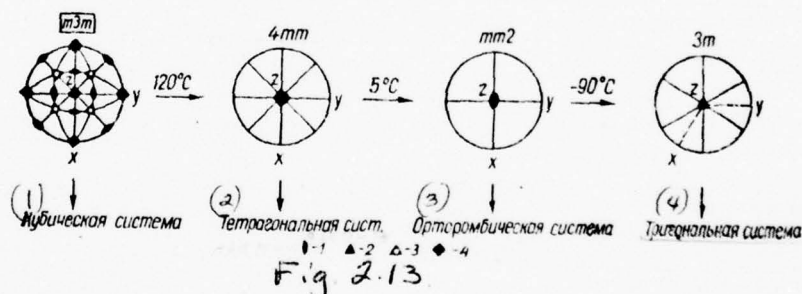
Fig. 2.12. The unit cell of the cubic perovskite structure BaTiO_3 .

Fig. 2.13. The stereographic projection of the elements of the symmetry of crystal BaTiO_3 : 1 - twofold axis; 2 - triad axis; 3 - inversion triad axis; 4 - tetrad axis; continuous straight lines and circumference - the plane of symmetry (π); x, y, z - crystallographic coordinates.

[Key appears on following page.]

Key: (1). Cubic system. (2). Tetragonal syst. (3). Orthorhombic system. (4). Triangular system.

Page ⁶⁰~~59~~:
1

The tetragonal phase BaTiO_3 is most studied, since it is related to the range of room temperatures, where the crystals have the basic practical application/appendix.

At temperatures below 5°C crystals of titanate of barium undergo new phase transition, but already of one polar state to another. Below 5°C BaTiO_3 it belongs to class $mm2$ orthorhombic system (see Fig. 2.13). As a result of the fact that the axis of 2 orders here is special, the vector of spontaneous polarization is directed along this axis (diagonal of the face of the initial cubic cell). Such axes in cubic lattice 6 (direction $\langle 110 \rangle$) or 12, equivalent to the direction of polarization. Orthorhombic phase is stable in the range from 5 to -90°C . At lower temperature is observed one additional phase transition to new polar state. Crystal BaTiO_3 below -90°C belongs to class $3m$ trigonal (rhombohedral) system. Figure 2.13 shows that the axis of third order is special and polarization vector can be directed along one of the eight of possible equivalent directions $\langle 111 \rangle$ four triad axes of the initial cubic lattice. The distortion of

the initial cubic lattice, depicted on Fig. 2.14a consists of its elongation along body diagonal.

There are several methods of single crystal growing BaTiO_3 . Most widely used is the Remeyka method [85]. They grow crystals from the fusion/melt synthesized BaTiO_3 and solvent KF. Relationship/ratio between solvent and titanate of barium 5:1 (3:1). Important conditions during single crystal growing are the degree of the cleanliness of the initial materials, the degree of dispersion and the gradient of the temperature in furnace. The initial material thoroughly is mixed and grind in agate mortar. Growing in all cases produces in the platinum crucibles, which, in turn, are establish/installed in corundum. Crucible with solution/opening is extracted from furnace in hot state. Fusion/melt KF they pour, and crucible again is placed into furnace for complete cooling down to room temperature. Crystals disengage solvent KF by flushing in water. The washed clean crystals are sweat/dried. The selection of crystals according to the character of domain structure and according to thickness conducts with the aid of polarizing microscope.

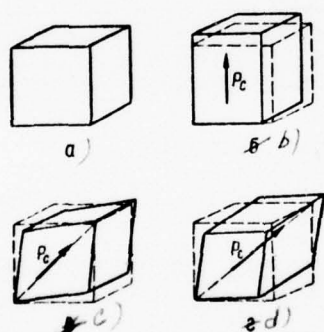


Fig. 2.14. The unit cells of four phases of crystal BaTiO_3 : a) cubic (above 120°C); b) tetragonal (from $+120$ to $+5^\circ\text{C}$); c) orthorhombic (from $+5$ to -90°C ; d) trigonal (rhombohedral), stable are below -90°C . As broken lines is depicted the initial cubic cell.

Page 61.

For a single crystal growing 30-50 μ m thickness the most suitable, according to data of RGU (Rostov), are the following conditions: BaTiO_3 : KF = 1:5; maximum temperature 1140°C; delay at this temperature 2.5 h; cooling down to 950°C with speed (20-25) deg/h the gutter of fusion/melt at $T = 950^\circ\text{C}$.

Crystals grow in the form of the twin/counterparts and have a form of wings of butterfly. Grown crystals BaTiO_3 have more complex domain structure, than the single crystals of TGS. This is connected with the fact that on the strength of the cubic symmetry of crystal in nonpolar phase it is a system of several equivalent axes, using which can be directed the vector of the spontaneous polarization of crystal in ferroelectric (polar) phase.

Figure 2.15 gives the schematic of the possible orientations of the vector of spontaneous polarization \vec{P}_c [26]. During transition from the tetragonal phase into rhombic of crystal B large probability of changing into state D, than in E, since in this case is required the rotation of vector \vec{P}_c only through 45°, but not through 90°. For crystal C transitional probability according to the considerations

pointed out above is one and the same (rotation through 45°). In rhombic phase there is one direction \vec{P}_c .

Figure ^{2.16}~~4.16~~ gives the temperature dependence of spontaneous polarization for crystal BaTiO_3 . The relationship of the dielectric constants ϵ_a and ϵ_c , measured in weak electric fields, is given in Fig. 2.17.

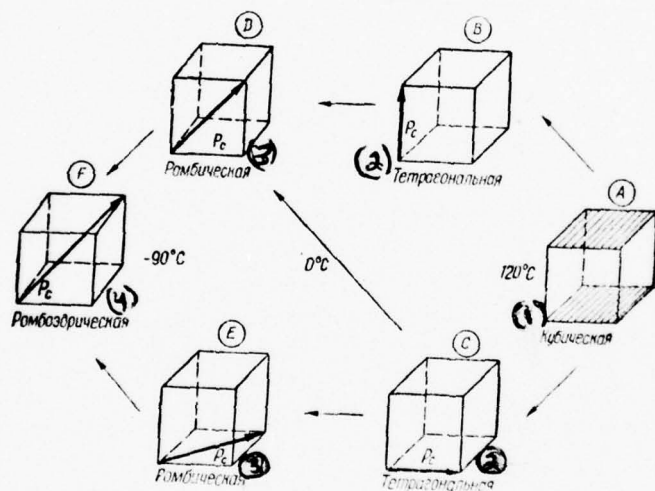


Fig. 2.15.

Fig. 2.15. Schematic of the possible orientations of the vector of spontaneous polarization \vec{P}_c in single crystal BaTiO_3 [26].

Key: (1). Cubic. (2). Tetragonal. (3). Rhombic. (4). Rhombohedral.

Page 61.

In tetragonal phase $\epsilon_a = 4000$, $\epsilon_c = 200$ at room temperature [83]. The value of dielectric constant in rhombic phase is lower than in tetragonal. The modification E is the continuation of branch tetragonal phase, while modification ϵ_a is the continuation of branch ϵ_c . The presence of two branches in trigonal (rhombic) phase thus far not found explanation.

The phase transition of crystal BaTiO_3 theoretically is first-order transition. However, during experiment due to the combined effect of internal stresses, inhomogeneity and surface phenomena transition is close to the second order. By this also is explained insufficiently sharp (for first-order transition) jump of polarization, and also heat capacity at Curie point. The dependence of heat capacity on temperature is given in Fig. 2.18 [88].

Unlike TGS the domain structure of crystals BaTiO_3 can be

observed with the aid of polarizing microscope. If the polarized light beam is directed along polar (optical) axis in crystalline plate, then plate to all positions will remain dark. But if angle is 90° (world/light is perpendicular polar axis), then during the rotation of plate will be observed light picture with the exception of two positions, in which the polar axis of plate is parallel to the plane of the polarization of the Niccl prisms of microscope.

For the observation of domain structure can be used also other methods: research on the etch figures or figures, which appear during precipitation on the crystal boundary of charged particles [26], the visualization of domain structure with the aid of local pyroelectric signal, etc.

Domains with the polar axis, perpendicular to the plane of plate, are called c-domains a with parallel - by a-domains (Fig. 2.19).

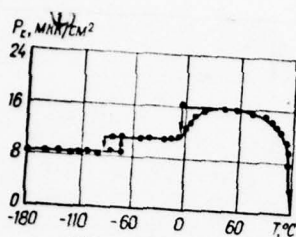


Fig. 2.16.

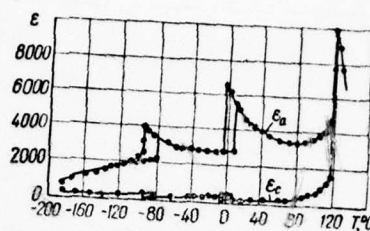


Fig. 2.17.

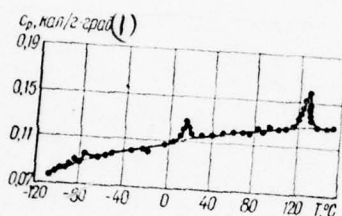


Fig. 2.18.

Fig. 2.16. The temperature dependence of spontaneous polarization for single crystal BaTiO_3 [83].

Key: (1). $\mu\text{k}/\text{cm}^2$.

Fig. 2.17. Temperature dependence of dielectric constant ϵ for crystal BaTiO_3 [83].

Fig. 2.18. Dependence of the heat capacity polycrystalline BaTiO_3 on temperature [26].

Key: $\text{cal/g} \cdot \text{deg}$.

Page 63.

The real domain configuration of single crystals BaTiO_3 is considerably more complex: in just one crystal can be interwoven c- and the a-domains with 90- and 180- degree domain walls and the direction of polarization "head - tail", "head to head" and "tail to tail".

According to existing representations [28], during transition from nonpolar to polar phase at transition point are formed the nuclei of domains. Their appearance bears accidental character, and at the first torque/moment are possible the configuration of domain structure, not corresponding to the minimum of free energy. This metastable changes gradually to more stable. The instability of domain configuration is one of the reasons for the rare utilization of single crystals BaTiO_3 for the creation of thermal radiation detectors.

Conducted investigations [26, 79] made it possible to determine the structure, necessary for the understanding of the mechanism of ferroelectricity in crystals BaTiO_3 . The loose packing of atoms in

unit cell (see Fig. 2.12), that is one of the reasons for the emergence of spontaneous polarization, can be understood from the following reasonings. A comparatively large ionic radius Ba^{2+} (1.43 Å) leads to the fact that in oxygen octahedron the ion Ti^{4+} , which possesses a small ionic radius (0.64 Å), in ferroelectric phase is displaced to one of oxygens O^{2-} . It should be noted that another representative of perovskite CaTiO_3 is not ferroelectric, since ionic radius Ca^{2+} (1.0 Å) is less than of Ba^{2+} , and the anharmonicity of the fluctuations of ion Ti^{4+} in lattice CaTiO_3 is expressed weakly.

Polycrystalline ceramic specimen/samples BaTiO_3 and its derivatives find at present a large practical use. Therefore to investigation ceramicist BaTiO_3 is devoted the considerable number of works. The possibility in principle of the unlimited variation of structural/design forms open/discloses the great possibilities of the technical utilization of ceramics for developing receivers with various forms of sensing element.

The ceramic specimen/samples BaTiO_3 are the totality of the separate crystallites, connected by glassy phase.

The dielectric constant of nonpolarized ceramics is the result of averaging ϵ_c and ϵ_o separate crystallites in the assigned direction. Experimentally obtained values ϵ compose 1000-1500 for

ceramics BaTiO_3 . The analyses of the domain structure of ceramics BaTiO_3 showed, that are observed thin plates 90- and 180-degree domains 0.5-2 μm wide.

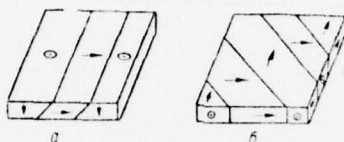


Fig. 2.19. The domain structure of single crystal BaTiO_3 in tetragonal phase (arrow/pointers indicate the direction of polarization in crystal): a) two c-domainnes and a-domains between them; b) a-domains divided by 90-degree walls (arrangement "degree - tail").

Page 64.

The value of spontaneous polarization for ceramic BaTiO_3 is 5-10 $\mu\text{k}/\text{cm}^2$, i.e., into two and a half times less than of single crystal. This is explained themes which in the process of polarization is completely oriented part of the domains, and fields, even close to disruptive, not in state to orient all domains along the direction of

polarization.

Ceramics BaTiO_3 is obtained by sintering the mixture of the TiO_2 and barium carbonate dioxide of titanate BaCO_3 at temperature of 1400°C . In the process of sintering the carbon dioxide is volatilized, and is formed ceramics BaTiO_3 . This material possesses considerable mechanical strength, moisture resistance and can be processed by known technological methods. The electrophysical characteristics of ceramics BaTiO_3 depend on the technological mode/conditions of sintering and presence of impurity/admixtures. With a change in the temperature of annealing from 1180 to 1400°C dielectric constant of ceramics at room temperature it differs three times [1]. Furthermore, depending on the conditions of production in ceramic specimen/sample can be located the crystallites of tetragonal and hexagonal modifications. Since at room temperature the tetragonal modification possesses ferroelectric properties, the necessary measure for its obtaining and stabilization is the introduction of additions (Ca, Sr, etc.).

The electrical resistance of ceramics BaTiO_3 depends substantially both on the impurity/admixtures in the initial material and the conditions of production and on electric field and the temperature, by which conducts the measurement. In weak fields at room temperature the volume resistivity of ceramics BaTiO_3 is $10^{12}-10^{13}$ ohm \cdot cm. the additions of oxides of metals and especially

oxides of rare-earth elements (cerium - Ce_2O_3 , samarium - Sm_2O_3 , lanthanum - La_2O_3 , neodymium - Nd_2O_3) lower resistance of ceramics. With the alloying of ceramics with oxides of rare-earth elements near Curie point occurs an abrupt change in resistance; in temperature interval of 20-30°C resistance changes on several orders. Anomalous positive specific resistance in this region can reach 50-600/o.

The introduction of additions Ca, Co, Zr, Sr, Sn and some others [26] lowers the Curie temperature (Fig. 2.20), but of the compositions, which contain, except BaTiO_3 , titanate or zirconate of lead (PbTiO_3 and PbZrO_3) Curie point it is raised.

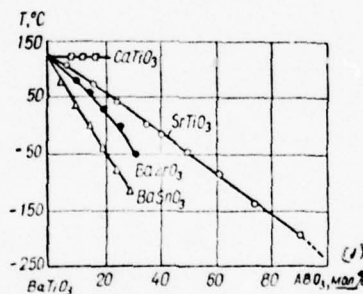


Fig. 2.20. The temperature dependence of Curie point for the assorted composition of solid solution BaTiO_3 [26].

Key: (1) is small.

Different additions can be used for a control of the value of the dielectric constant of ceramics [2, 21]. So, ferroelectric ceramics SM-1 on the basis of titanate of barium with the addition of oxides Zr and Bi is characterized by the smoothed temperature dependence ϵ in the range of room temperatures. Large dielectric constant with maximum in the range of room temperatures has ceramics T-7500, which contains titanates of barium, calcium and strontium. With addition to titanate of barium of small quantities of oxides of tin and zirconium, and also stannates and zirconate of barium and other connections [8] is obtained ceramics with the strongly depending on field dielectric constant. On its basis are develop/processed varicaps [16].

Ceramics BaTiO_3 and its derivatives all the same possesses lower ferroelectric characteristics, than monocrystals BaTiO_3 , although as previously it was indicated, it has a series of technological advantages. Therefore were carried out studies on the investigation of the single crystals of solid solutions BaTiO_3 with the variable Curie point and the controlled properties.

Solid solutions BaTiO_3 and SrTiO_3 form continuous series [26] and comparatively easily are crystallized. This offers the possibility of obtaining single crystals with assigned values of Curie temperatures in wide temperature range (see Fig. 2.20).

Negative is the active depression SrTiO_3 growth of the lamellar twin/counterparts even with the small additions Fe_2O_3 , which facilitate their formation. The obtained single crystals with c-domain structure have size/dimensions of more several square millimeters. Analogous phenomena are observed for single crystals of solid solutions $\text{Ba}(\text{TiSn})\text{O}_3$, and also of the single crystals of solid solutions BaTiO_3 with additions Fe_2O_3 , CoCO_3 , etc.

The prolonged investigations of the ferroelectric specimen/samples, especially polarized, they showed that occurs in the course of time a slow change in their characteristics [40]. This effect, known by the name of aging, many authors are explained by the reorientation of the domain structure of specimen/sample, bonded with different factors, for example, as consequence of the release of internal mechanical stresses in ceramics. By utilizing the forced methods of the aging of ceramics immediately after its production, it is possible then to retain stable the characteristics of specimen/samples during long time.

§3. Thin-film ferroelectric.

The properties of substance change during transition to thin

layers. This is explained themes that in obtaining the thin layers, sprayed on support/base, the structure of the formed film to a considerable degree is determined by the relief of support/base and disturbance/breakdowns of the regularity of lattice in thin layers considerably more than of massive material.

Page 66.

The surface layer of material, appearing as a result of the break of the periodicity of crystal lattice and deposition of electrodes, also differs in its properties from massive specimen/sample. When the thickness of specimen/sample decreases, surface layer begins to affect its properties.

The threshold of response of all thermal radiation detectors is improved during a decrease in the thickness of sensing element to a definite limit. Although a decrease in the thickness of film logically decreases its heat capacity, this favorable fact, however, is bonded with a decrease in parameter value of the receiver, which depends on temperature, beginning with some thicknesses of sensing element.

Therefore one of the basic questions during the development of thermal radiation detectors is the determination of the optimum

thickness of sensing element. As criterion can be selected the value of the ratio of dependent from the temperature of the parameter to heat capacity (thickness) sensing element. A decrease in the thickness of sensing element leads to an increase in the receiver sensitivity with an increase in this relation. When relation reaches a constant value or it begins to fall, a further decrease in the thickness of cell/element becomes already unsuitable, since in this case deteriorates the threshold of response of receiver.

The optimum ratio of the value of the parameter, which depends on temperature, to the thickness of sensing element is located experimentally. In this case important role play the supplementary noises, which appear in layer as a result of its thinning, and reduction in the mechanical strength of sensing element.

Of metallic bolometers with thinning of sensing element decreases the temperature specific resistance and coefficient of thermal conductivity, is increased specific resistance and they grow/rise noises during the passage of the exciting current through the film. Experimentally the obtained value of the optimum thickness 0.05-0.5 μ .

The optimum thickness of sensing elements of semiconductor bolometers is 5-50 μ m.

The values of pyroelectric coefficient and dielectric constant in the thin layers of ferroelectric also differ from volumetric specimen/samples. Surface layer with the thicknesses of specimen/sample less than 30-50 μm already considerably influences its ferroelectric properties. The nature of the surface layer of ferroelectric up to now is insufficiently clear and is the object/subject of continuous investigation.

The greatest number of works on the study of the properties of surface layer is related to titanate of barium [14, 20, 39, 56, 60, 69, 75].

Immediately after growing energy state of c-domain crystal PbTiO_3 is unsuitable, if it is not affected by any of the mechanisms of screening.

Page 67.

Are possible at least three mechanisms of shielding [27]:

a) settling ions from atmosphere to crystal boundary;

b) the formation of a-domains on crystal boundary with the vector of spontaneous polarization, perpendicular to the vector of spontaneous polarization in c-domain crystal;

c) the inleakage of charges from the thickness of crystal to surface because of its final electroconductivity.

Each of these mechanisms leads to decrease in the energy of system and the formation of stable (metastable) state. But in this case on crystal is formed the surface layer, which leads to a change in its ferroelectric properties.

Kentsig assumed for the first time about the existence of surface layers [53, 77]. The X-ray and electron-graphic examinations showed that with decrease of the size of particles BaTiO_3 the phase transition is eroded of to increasing to temperature interval. For particles 1000 \AA in diameter was observed the presence of tetragonal phase with 500°C. The explanation of this fact was made on the basis of the representations of the presence of surface field in crystal. Was presented the model of crystal with surface layer (Fig. 2.21).

By set/assuming the thickness of the surface layer of constant/invariable and by varying the thickness of crystal d , it is possible from the relationship/ratio

$$\frac{d}{\epsilon} = \frac{2d_n}{\epsilon_n} + \frac{d_u}{\epsilon_u} \quad (2.26)$$

to find the thickness of surface layer t_n and its dielectric constant ϵ_n , if are known the values d_n and ϵ_n , which relate to material. The thickness of surface layer according to the data of Kentsig is 10^{-6} cm.

At the present time were accumulated many experimental facts, attesting to the presence of surface layer of ferroelectric and the explained on the basis of representations of the determined form of the model of surface layer.

Mertz [82], studying time of repolarization in single crystals BaTiO_3 , establish/installed the dependence of this value from the thickness of crystal.

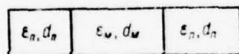


Fig. 2.21

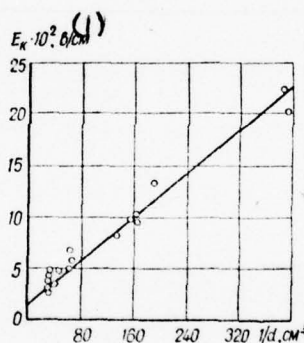


Fig. 2.22

Fig. 2.21. The model of crystal with the surface layer: ϵ_n and d_n - are dielectric constant and the thickness of surface layer; ϵ_M and d_M - crystal.

Fig. 2.22. Dependence of the value of coercive field E_K on the

thickness of crystal BaTiO_3 at frequency 60 Hz [82].

Key: (1). V/cm.

Page 68. Also experimentally they establish/installed the dependence of the value of coercive field (Fig. 2.22) from the thickness of crystal, which took the following form:

$$E_k = E_{k0} \left(1 + \frac{d_n}{d} \right), \quad (2.27)$$

where E_{k0} is the coercive field of massive specimen/sample, a d_n is thickness of surface field.

To explain this dependence it was possible, after assuming the existence of capacitive surface layer with dielectric constant $\epsilon_n \approx 5$ and the thickness of order 10^{-4} cm. The model of this crystal is given in Fig. by 2.21.

The dependence of coercive field E_k from the thickness of crystal BaTiO_3 was studied also in works [55, 57, 66, 70, 71].

Brzhezina and Yanovets [55] for the explanation of the experimental data unlike Mertz assumed that on surface the layer possesses the nonhomogeneous dielectric constant ϵ , which constantly decreases in the direction of surface. Glogar and Yanovets [71] measured the coercive field of single crystals BaTiO_3 , gradually bronzed by phosphoric acid, and they established that during a decrease in the thickness occurs an increase in the coercive field:

$$\frac{\partial E_k}{\partial d} = -1.5 \cdot 10^5 \text{ V/cm}^2$$

For layers by thickness $(1-2) \cdot 10^{-3} \text{ cm}$, the coercive field increases more slowly: $\frac{\partial E_k}{\partial d} \approx 7 \cdot 10^3 \text{ V/cm}^2$.

The nature of surface layer according to the model, proposed by Mertz and Fattuzo [70] (MF-model), assumes existence on crystal boundary BaTiO_3 the electrically charged and mechanically strained layer, caused by impoverishment by the ions of oxygen (by defects according to Schottky). In powerful electrical and mechanical fields the dielectric constant of this layer (occasionally referred to as Kentsig) is small.

However, the calculations, carried out by Dvorak [67], they showed that only at temperatures more than 400°C origin of surface layer can be explained by the presence of Schottky defects. At the lower temperatures in the formation of surface layer participate the electrons and the ions of impurity/admixtures, which are located in real crystal.

The investigation of the electroconductivity of the fine-grained sintered powders BaTiO_3 [91] was one additional argument, denying the existence of the impoverished surface layer. Data on electroconductivity indicate the complex nature of surface layer even in the absence of electrodes.

Draugard and Landauyer also expressed doubt apropos of MF-model [66], after indicating the unreality of the existence of repolarizing surface layer with low dielectric constant.

The proposed by them model of surface layer (^{DL}~~MF~~-model) proceeded of the presence repolarizing thin (less than 50 Å) surface layer with low dielectric constant and dielectric losses.

Page 70.

The appearing in this case electric fields composed $3 \cdot 10^6$ V/cm. Such

fields can lead to electron emission from metal electrode in surface layer and cause electroluminescence [74]. In turn, this model also could not explain a series of the facts, bonded with the motion of domain walls in the crystals of different thickness.

To the questions of the interrelation between optical absorption and surface layer is dedicated work of the Tsoufova and Arend [61]. The dependence of optical absorption at wavelengths 0.48 and 0.64 μm on the thickness of crystal the authors explained by the presence of defects, in particular by the oxygen vacancy of surface layer.

A series [54, 57] on the study of the motion of domain walls in the process of changeover introduced the supplementary information about the properties of surface layer.

Important practical value has an effect of geometric dimensions of film on the value of spontaneous polarization P_c , of dielectric constant ϵ and of pyroelectric coefficient γ . The overwhelming majority of publications [13, 42, 51, 76] testifies to a reduction in the spontaneous polarization P_c and in the dielectric constant with the thicknesses of crystals BaTiO_3 less than 15-25 μm . Exception is [17]. According to the data of M. M. Nekrasov and B. A. Khrashchevskiy [45, 51], thickness of the layer, with which begins sharp deterioration in the dielectric properties, it is approximately

25 μm . Figure 2.23 gives the dependence of spontaneous polarization on thickness for single crystals BaTiO_3 . F. V. Bursian and N. P. Smirnovoy [13] establish/installed that films BaTiO_3 with thickness up to 1 μm retain tetragonality and exhibit spontaneous polarization. The coercive field grow/rises, but films do not lose capability for ferroelectric polarization. With the thicknesses of specimen/samples less than 1 μm the coercive field becomes more than disruptive, reversible spontaneous polarization it disappears and ferroelectric it degenerates into linear pyroelectric. The authors investigated films BaTiO_3 in tetragonal, orthorhombic and trigonal phases. Figure 2.24 gives the temperature dependence of the dielectric constant of films BaTiO_3 different thickness.

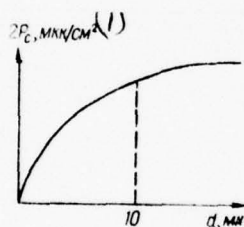


Fig. 2.23.

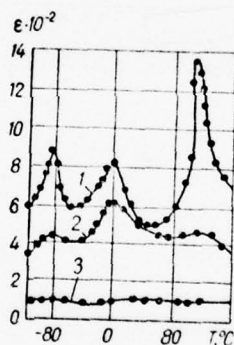


Fig. 2.24.

Fig. 2.23. Dependence of spontaneous polarization P_s on thickness for single crystal BaTiO_3 , [90].

Key: (1) $\mu\text{K}/\text{cm}^2$. (2) μm .

Fig. 2.24. Temperature dependence ϵ films BaTiO₃ the different thickness: 1 - 27 μm ; 2 - 6 μm ; 3 - 1 μm ; [Bursian E. V., Smirnova ⁴ p. - Izv. the Academy of Sciences of the USSR the ser. of phys., 1965, 29, 6. 1016].

Page 70.

A decrease in the thickness of film first of all manifests itself the value of the maximum of dependence $\epsilon = \epsilon(T)$ at 120°C, then disappears the maximum of dielectric constant with 80°C, remaining clearly expressed at +5°C. With the thicknesses of specimen/samples less than 1 μm disappear everything three maximums.

On the basis of the experimental data is made a conclusion about the fact that in phases with lower symmetry due to a decrease in the coercive field and degree of ferroelectric "hardness" decreases the thickness, by which the ferroelectric transfer/converts to linear pyroelectric. This fact was explained themes that during the transition of ferroelectric axis from direction $\langle 100 \rangle$ to directions $\langle 110 \rangle$ and $\langle 111 \rangle$ (see Fig. 2.14) the angle between the ferroelectric axis and the internal field in crystal, directed perpendicularly to surface, it is increased from 0 to 45 and 55°, but therefore the degree of the attachment of domains it must decrease.

Chaynoviz investigated surface layer in BaTiO_3 [62] with the aid of the proposed by it dynamic method for the measurement of pyroelectric current. They establish/installed that the pyroelectric current appears above Curie point in the fine/thin crystals BaTiO_3 even in the absence of applied fields. Remanent polarization higher than the Curie point can be explained by the field of space charges. Studying temperature dependence $\gamma(T)$ with the periodically modulated flow of radiation, Chaynoviz drew the conclusion about the existence of the charged surface layer of order 10^{-5} cm. thickness, which creates electric field within crystal. It also assumed the presence of two potential thresholds for each of the crystal boundaries. As the proof of the presence of potential threshold served the dependence of photo-voltaic effect higher than the Curie point on temperature and asymmetry of hysteresis loops. Chaynoviz also showed that the field of residual charges influences the domain structure of crystal lower than the Curie point, conditioning the determinate direction of spontaneous polarization after cooling the preheated for Curie point crystal.

The analogous character of pyroelectric current in paraelectric titanate of barium was establish/installed in work [58]. The authors of this work observed large thermocurrent (pyroelectric current)

higher than the Curie point and established that besides the basic maximum of pyroelectric current with $T = 120^\circ\text{C}$, was observed the second maximum with $T = (160-200^\circ\text{C})$ (Fig. 2.25). The region of the existence of thermocurrent was spread for 200°C .

The simple model of surface layer could not explain all the observed in lamellar ferroelectric anomalies.

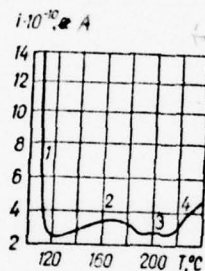


Fig. 2.25. Dependence of pyroelectric current on the temperature in paraelectric phase for single crystal BaTiO_3 .

Page 71. In connection with this they were proposed to the model of dual (and more complex) surface layer [38, 50, 55, 80, 81]. A. V. Turik [50] examined a model of the surface layer, which consists of two layers, with the considerably differing thicknesses and

dielectric constants. With a decrease in the thickness of crystal the role of its internal part begins to play near-surface layer. Its thickness according to the calculations is approximately $2 \cdot 10^{-3}$ cm.

T. N. Lezgintseva [38] reveal/detected tendency toward an increase in the thickness of surface layer with an increase in the thickness of crystal. It noted many complicating facts during the determination of the thickness of surface layer and its properties. As the source of contradictory information can serve measurements in different in value and nonhomogeneous in structure electric fields [61]. Characteristic measurements of specimen/samples BaTiO_3 , scoured in hot phosphoric acid, strongly depend on time of measurement, since domain structure near the surface of layer immediately after etching differs from the structure, which is establish/installed after certain time.

It was establish/installed that of monocrystals BaTiO_3 , grown in one crucible according to the method of Remeyka, the concentration of a-domains with an increase of thickness grow/rises, and this by the determining form manifests itself the value of the total dielectric constant of layer.

Figure 2.26 gives the model of the dual surface layer, utilized in work [59] for the explanation of the dependence of dielectric

constant on the thickness of crystal.

Considerably less works is devoted to the investigation of characteristics of TGS in thin layers [23, 30, 89, 92]. The value of pyroelectric coefficient up to thicknesses on the order of 200 μm differs little from massive material. At thicknesses on the order of 50 μm value γ composes the half of the value, measured with 200 μ .

The results of the investigation of the dependence of dielectric constant ϵ on thickness d for the crystal of TGS are given in Fig. 2.27 [92].

Thus, are at present many experimental facts, which confirm the existence of surface layer in ferroelectric.

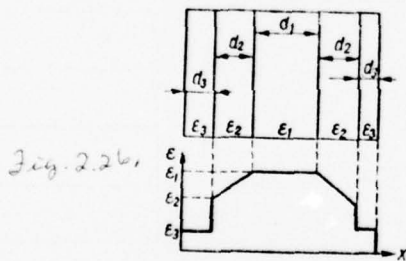


Fig. 2.26. Model of dual surface layer [59].

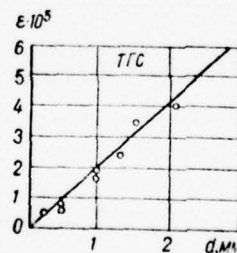


Fig. 2.27

Fig. 2.27. Dependence ϵ on thickness d of the single crystal of TGS ($E = 0.7 \text{ V/cm}$, $f = 10 \text{ Hz}$).

The physical picture of the processes, which lead to the formation of surface layer, is not still finally clear, but the proposed models for the explanation of experiment are limited and often contradictory.

But, in spite of the available contradictions in the physical treatments, it is solidly establish/installated that the surface layer plays the determining role in tape/film ferroelectric, influencing the existence of reversive polarization. In lamellar ferroelectric dielectric constant and pyroelectric coefficient cannot be designed on the basis of the data on massive specimen/samples. The characteristics of lamellar ferroelectric to a considerable degree depend on technology of obtaining layers and in each specific case must be determined experimentally.

The powerful effect of surface layer on the properties of thin-film ferroelectric led to the fact that the optimum thickness of sensing elements of ferroelectric receivers considerably more than of metallic and semiconductor bolometers, and is 50-200 μm . Are known the following methods of obtaining the fine/thin ferroelectric films BaTiO_3 :

- a) vacuum evaporation or the inert medium;

b) cathode sputtering;

c) obtaining films from fusion/melt with the subsequent etching;

d) injection molding with plasticizer.

The method of obtaining the thin gauge sheets BaTiO_3 by thickness several microns is described in work [68]. Powder-like BaTiO_3 vaporized at high temperature from tantalum boat to the preheated support/base. Then films were calcined at temperature of 500-1000°C.

In films were observed the hysteresis loops. The value of spontaneous polarization P_c composed 0.53 $\mu\text{k}/\text{cm}^2$ (for the massive BaTiO_3 $P_c = (20-30) \mu\text{k}/\text{cm}^2$). A deficiency/lack in this method it is expansion BaTiO_3 on BaO and TiO_2 with evaporation in vacuum and in summation, the loss of oxygen. The reduction of oxygen with puncturing to end/lead does not occur, and the lattice of crystals is obtained that which was distorted. The obtained thus films are polycrystalline.

E. V. Bursianom and to N. P. Smirnovoy [13] is proposed the method of obtaining single-crystal films by growing from fusion/melt in the atmosphere of oxygen. To platinum foil will be deposited the

layer of powder BaTiO_3 , and foil during several minutes is heated in the furnace, where is maintained temperature 1600-1700°C, in the atmosphere of oxygen or air. After this platinum support/base with molten BaTiO_3 is driven out from the test section of the furnace, and fusion/melt hardens with considerable temperature gradient. Platinum foil is one of the electrodes, and as the second serve sprayed in vacuum silver. Films are obtained sufficiently monocrystalline with 5-50 μ thickness.

Fig 73.

In works [76, ⁷⁸97] is described the procedure of obtaining the thin gauge sheets BaTiO_3 of approximately 1 μ thickness by cathode sputtering at pressure 0.05-3 mm Hg on platinum, glass or aluminum support/bases.

The thin layers BaTiO_3 5-10 μ m thickness can be obtained from the plates, which have the form of the "wings of butterfly", by means of growing from fusion/melt according to the method of Remeyka with the subsequent their letting out in hot phosphoric acid [90-93]. Good results are obtained with the plates, which have faultless surface with monodomain structure.

Analogously can be obtained the thin layers of TGS 20-200 μ m

thickness by the letting out of the plates, pre-cut out by saw for water-soluble crystals and the polished in solution TGS with water and ethyl alcohol. For obtaining isometric surface etching it is better to conduct with temperature higher than the Curie point. By this method it is possible to obtain layers up to $5 \mu\text{m}$ thickness; however, they are more brittle than the layers of the same size/dimensions BaTiO_3 .

The procedurally important method of obtaining the thin ceramic layers of ferroelectric of approximately $20\text{-}50 \mu\text{m}$ thickness is the injection molding of dross with organic cementing and plasticizing substance [12]. This method makes it possible to obtain the thin large-size layers and complex form with a good reproducibility of characteristics.

БИБЛИОГРАФИЯ.

Pages 74-75.

1. Ананьева А. А., Стрижков Б. В., Угрюмов М. А. — Изв. АН СССР, сер. физ., 1960, 24, 11.
2. Ананьева А. А. Керамические приемники звука. Изд-во АН СССР, М., 1963.
3. Артюховская Л. М., Кременчугский Л. С., Мальнев А. Ф., Самойлов В. Б., Яценко А. Ф. — Изв. АН СССР, сер. физ., 1965, 29, 11, 2110.
4. Андерсон П. В. Физика диэлектриков. Изд-во АН СССР, М., 1960.
5. Bersuker I. B. — Phys. Lett. 1966, 20, 589.
6. Берсукер И. Б., Вехтер Б. Г. — ФТТ, 1967, 9, 9, 2652; — Изв. АН СССР, сер. физ., 1969, 33, 2, 199.
7. Берсукер И. Б., Вехтер Б. Г., Данильчук Г. С., Кременчугский Л. С., Музалевский А. А., Рафалович М. Л. — ФТТ, 1969, 11, 9, 2452.
8. Богородицкий Н. П., Волокобинский Ю. М., Воробьев А. А., Тареев Б. М. Теория диэлектриков. «Энергия», М.—Л., 1965.
9. Богуславский С. А. — В кн.: Избранные труды по физике. «Наука», М., 1961.
10. Борн М., Гепперт-Майер М. Теория твердого тела. ГИТТЛ, М.—Л., 1938.
11. Борн М., Кунь Х. Динамическая теория кристаллических решеток. ИЛ, М., 1953.
12. Богородицкий Н. П., Кальмане Н. В., Нейман М. И. и др. Радиокерамика. Госэнергоиздат, М.—Л., 1963.
13. Бурсиан Э. В., Смирнова Н. П. — ФТТ, 1962, 4, 1675; 1964, 6, 1818.
14. Бурсиан Э. В., Смирнова Н. П. — Ученые записки ЛПИ им. Герцена, 1966, 303, 151.

15. Бородин В. З., Гах С. Г., Крамаров О. П., Кременчугский Л. С., Ливанская Л. П., Мальнев А. Ф.— Электронная техника, 14. Материалы, 1967, 8, 141.
16. Вербицкая Т. Н.— Электричество, 1956, 6, 90.
17. Вербицкая Т. Н., Александрова Л. М., Ширококова Е. Н.— Изв. АН СССР, сер. физ., 1965, 29, 11, 2104.
18. Галанов Е. К.— ФТТ, 1966, 8, 3386.
19. Гинзбург В. Л.— УФН, 1949, 38, 4, 490; ЖЭТФ, 1949, 19, 36; ФТТ, 1960, 2, 2031.
20. Гуенок Е. П., Кудзин А. Ю.— Изв. АН СССР, сер. физ., 1967, 31, 7, 1188.
21. Глозман И. А. Пьезоэлектрические материалы в электронной технике. «Энергия», М.—Л., 1965.
22. Гуревич В. М., Желудев И. С.— Изв. АН СССР, сер. физ., 1960, 24, 10, 1342.
23. Данильчук Г. С., Кременчугский Л. С., Мальнев А. Ф.— Изв. АН СССР, сер. физ., 1967, 31, 1754.
24. Данильчук Г. С., Ицковский М. А., Кременчугский Л. С.— Кристаллография, 1969, 14, 998.
25. Желудев И. С. Физика кристаллических диэлектриков. «Наука», М., 1968.
26. Иона Ф., Шпране Д. Сегнетоэлектрические кристаллы. «Мир», М., 1965.
27. Иванчик И. И.— ФТТ, 1961, 3, 3731.
28. Кенциг В. Сегнетоэлектрики и антисегнетоэлектрики. ИЛ, М., 1960.
29. Козловский В. Х.— Изв. АН СССР, сер. физ., 1965, 29, 6, 882.
30. Кладкевич М. Д., Кременчугский Л. С., Мальнев А. Ф.— УФЖ, 1968, 13, 4, 629.
31. Кисловский Л. Д., Галанов Е. К., Шувалов Л. А.— Оптика и спектроскопия, 1968, 24, 137.
32. Кременчугский Л. С., Самойлов В. Б.— Кристаллография, 1967, 12, 6, 1077.
33. Кременчугский Л. С., Мальнев А. Ф., Самойлов В. Б.— В кн.: Электрические и оптические свойства диэлектриков. Изд. Укр. НИИТИ, К., 1968, 65.
34. Кременчугский Л. С., Мальнев А. Ф., Самойлов В. Б.— ПТЭ, 1966, 6, 169.
35. Копчик В. А., Гаврилова Н. Д.— Изв. АН СССР, сер. физ., 1965, 29, 11, 1969.
36. Константинова В. П., Сильвестрова И. М., Александров К. С.— Кристаллография, 1959, 4, 69.
37. Колдобская М. Ф., Гаврилова И. М.— В кн.: Рост кристаллов. «Наука», М., 1961, 3, 278.
38. Лезгинцева Т. Н.— ФТТ, 1965, 7, 4, 975.
39. Лурье М. С., Игнатьева И. В.— В кн.: Физика твердого тела, I. Изд-во АН СССР, М., 1959.
40. Мисарова А.— ФТТ, 1960, 2, 1276.
41. Най Дж. Физические свойства кристаллов. «Мир», М., 1967.
42. Некрасов М. М., Храшевский В. А.— Изв. АН СССР, сер. физ., 1965, 29, 11, 2107.
43. Рез И. С.— Изв. АН СССР, сер. физ., 1969, 33, 2, 289.
44. Смоленский Г. А., Крайник Н. Н. Сегнетоэлектрики и антисегнетоэлектрики. «Наука», М., 1968.
45. Сильвестрова И. М.— Кристаллография, 1961, 6, 4, 582.
46. Струков Б. А.— ФТТ, 1964, 6, 9, 2362.
47. Струков Б. А., Тараскин С. А., Скоморохова Т. Л., Минаева К. А.— Изв. АН СССР, сер. физ., 1965, 29, 6, 982.
48. Струков Б. А., Тараскин С. А., Варикаш В. М.— ФТТ, 1968, 10, 6, 1836.

49. Струков Б. А., Тараскин С. А., Копчик В. А.—ЖЭТФ, 1966, 51, 4 (10), 1037.
50. Турик А. В.—ФТТ, 1963, 5, 9, 2102.
51. Хращевский В. А.—Вестник КПИ. Серия радиоэлектроника, 1965, 2, 141.
52. Червинский М. М. Сегнетоэлектрики и перспективы их применения в вычислительной технике. «Энергия», М.—Л., 1962.
53. Anliker M., Brugger H. R., Kanzig W.—Helv. Phys. Acta, 1951, 27, 99.
54. Březina B., Fotcencov A. A.—Czech. J. Phys., 1964, 14, 1, 21.
55. Březina B., Janovec V.—Czech. J. Phys., 1964, 14, 1, 44.
56. Buchanan P.—Solid State Electronics, 1968, 11, 8, 767.
57. Callaby D. R.—J. Appl. Phys., 1965, 36, 9, 2751; 1966, 37, 6, 2295.
58. Chanussot G., Arend H.—Phys. Stat. Sol., 1968, 29, 2, K149.
59. Chincholkar V. S., Unruh—Phys. Stat. Sol., 1968, 29, 2, 669.
60. Crawford J. C., Dragsdorf R. D.—J. Appl. Phys., 1965, 9, 2764.
61. Coufova P., Arend H.—Czech. J. Phys., 1962, 12, 4, 308; 1960, 10, 9, 663.
62. Chynoweth A. G.—Phys. Rev., 1956, 102, 3, 705.
63. Cochran W.—Phys. Rev. Lett., 1960, 9, 387; 1961, 40, 401; Adv. Phys., 1959, 3, 412.
64. Devonshire A. F.—Phil. Mag. Suppl., 1954, 3, 85.
65. Dodd D. M.—Spectrochim. Acta., 1966, 16, 413.
66. Drougard M. E., Landauer R.—J. Appl. Phys., 1959, 30, 11, 1663.
67. Dvofak.—Czech. J. Phys., 1959, 9, 710.
68. Feldman C.—Rev. Scient. Instrum., 1955, 26, 5, 463.
69. Feldman C.—J. Appl. Phys., 1956, 27, 8, 870.
70. Fatuzzo E., Merz W. J.—J. Appl. Phys., 1961, 32, 9, 1685.
71. Glogar P., Janovec V.—Czech. J. Phys., 1963, 13, 4, 261.
72. Hoshino S., Okaya G., Pepinsky R.—Phys. Rev., 1959, 115, 323.
73. Hoshino S., Mitsui T., Jona F., Pepinsky R.—Phys. Rev., 1957, 107, 1255.
74. Harman G. G.—Phys. Rev., 1959, 3, 1, 27.
75. Heywang W.—Z. Naturforsch., 1965, 20a, 7, 981.
76. Huydat R. Vu., Baumberger C.—Phys. Stat. Sol., 1967, 22, 2, K67.
77. Kanzig W.—Phys. Rev., 1955, 98, 2, 549.
78. Kalisz L.—Acta Phys. Polon., 1968, 33, 3, 381.
79. Last J. T.—Phys. Rev., 1957, 105, 1740.
80. Liesk W.—Appl. Phys., Lett., 1961, 5, 4, 69.
81. Liesk W.—Z. angew. Phys., 1966, 21, 3, 205.
82. Merz W. J.—J. Appl. Phys., 1956, 27, 8, 938.
83. Merz W. J.—Phys. Rev., 1948, 76, 1221.
84. Mattias B. T., Miller C. E., Remeika J. P.—Phys. Rev., 1956, 104, 849.
85. Remeika J. P.—J. Amer. Chem. Soc., 1954, 76, 940.
86. Sato G.—J. Chem. Phys., 1966, 45, 275.
87. Shibuya J., Mitsui T.—J. Phys. Soc., Japan, 1961, 16, 479.
88. Shirane F., Takeda A.—A. J. Phys. Soc., Japan, 1952, 7, 1.
89. Savage A., Miller R.—J. Appl. Phys., 1959, 30, 11, 1616.
90. Shibata H., Toyoda H.—J. Phys. Soc., Japan, 1962, 17, 404.
91. Schoijet M.—Phys. Stat. Sol., 1964, 4, 3, 639.
92. Sekido T., Mitsui T.—J. Phys. Chem. Solids, 1967, 28, 6, 967.
93. Tanaka M., Kitamura N., Houjo G.—J. Phys. Soc., Japan, 1962, 17, 7, 1197.
94. Wieder H. H., Parkenson—J. Phys. Chem. Solids, 1966, 27, 2, 247.

Page 76.

Chapter III.

PYROELECTRIC COEFFICIENT AND DIELECTRIC CONSTANT OF FERROELECTRIC.

Research on pyroelectric effect in ferroelectric is conducted by two methods: static [6-14, 24, 29, 31, 61, 62, 67, 73, 91] and dynamic [1-4, 28, 30, 32-34, 36, 64, 65, 83, 86]. As shown in work [1], is observed the difference in values static γ_c and dynamic γ_d pyroelectric coefficients, which is explained by the different contribution to the pyroelectric effect of the separate mechanisms of a change in the polarization with temperature.

If the static pyroelectric coefficient γ_c is defined by the contribution both of rapid and slow mechanisms, then value γ_d is determined only by comparatively rapid processes in the course of time of relaxation $\tau_p \leq \frac{1}{2\pi f_m}$ (f_m - modulation frequency). Differences in the temperature dependences of pyroelectric coefficients γ_c and γ_d for single crystals TGS and BaTiO₃ are

insignificant; however, at the ceramicist of value γ_c can 2.5-3 times exceed values γ_A .

The findings [1,2] indicate the need for characteristic measurement of ferroactive materials under conditions, close to the operational conditions of radiation detectors. Below in essence is given the information about measurements γ_A and ϵ by dynamic method for lamellar ferroelectric.

§1. Crystals of the group of TGS.

The investigations of pyroelectric effect in the single crystals of TGS and its isomorphous were conducted by dynamic method [1, 2, 32, 33, 34, 63, 65, 66, 70, 74, 76].

Work [33] gives the results of the measurements of the temperature dependence of the pyroelectric coefficient of single crystals TGS at the different values of electric field E . For measurements were utilized the specimen/samples in the form of plates, cut out perpendicularly to axis Y made of the large single crystal of TGS [35]. Then they bronzed in aqueous solution to the necessary thickness and on them were spray-coated in the vacuum of

the order of 10^{-5} torr silver electrodes 1000 Å thickness. To the irradiated electrode was deposited gold black.

Page 77.

Its heat capacity composed $c_0 = 2.5 \cdot 10^{-5}$ J/deg·cm² and absorptivity $\epsilon_0 = 0.95$ in spectral range 0.5-10 μm . At the radiation flux density $2 \cdot 10^{-4}$ W/mm², it is established/installed that the specimen/samples being investigated were reheated by radiation flux not more than to 0.1°C.

The significant part of the specimen/samples had clearly expressed maximum pyrocoefficient in range 47.5-48.5°C, exceeding its values at the room temperature 12-15 times. The value and the position of this maximum changed from temperature training/aging and the conditions of polarization. Part of the samples did not possess the clearly expressed maximum $\gamma_A = \gamma_A(T)$ with $E = 0$. The maximum of pyroelectric coefficient was reached in area 35-45°C.

In work [33] also were investigated the specimen/samples, polarized slow cooling from 60°C to the room temperature in field 2 kV/cm. Figure 3.1 gives temperature dependences of absolute values $|\gamma_A|$ for different electric fields.

FOOTNOTE 1. Subsequently the sign on module/modulus for γ_A will be lowered. ENDFOOTNOTE.

Measurements were conducted in the following order. At the determined temperatures were measured the values γ_A in fields 0, 60, 100, 1000, 8000 V/cm of one polarity (E_+). After the repeated polarization of the specimen/sample being investigated under the same conditions was determined dependence $\gamma_A = \gamma_A(T)$, but in the fields of opposite polarity (E_-). Then were constructed dependences $\gamma_A(T, E_+)$ and $\gamma_A(T, E_-)$. The presented in the figure curves are related to these two cycles of measurements.

The curves of Fig. 3.1b are typical for a monodomain specimen/sample, with an increase in the field they become more washed away and the absolute values of maximum γ_A descend.

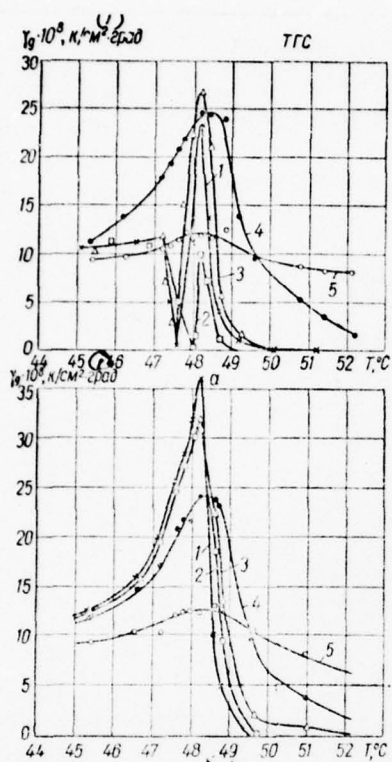


Fig. 31.

Fig. 3.1. Temperature dependences γ_A on the value of electric field for the cases of the positive (a) and negative (b) polarity: 1 - $E = 0$; 2 - $E = 60$ V/cm; 3 - $E = 100$ V/cm; 4 - $E = 1000$ V/cm; 5 - $E = 8000$ V/cm.

Key: (1). $k/cm^2 \cdot deg.$

Page 78.

In high fields is observed the insignificant displacement (to $0.2-0.3^\circ C$) of the maximum of pyroelectric coefficient to the side of large temperatures.

Figure 3.1a gives curves γ_A removed in the field of opposite polarity. Is observed a sharp decrease in the pyroelectric coefficient in fields less than 300 V/cm, during approach/approximation to phase transition. It is possible to select this field, in which γ_A in all area of phase transition is less than at room temperature.

Sharp reduction γ_A at some fields and temperatures is explained by the rearrangement of domain structure. In this case the pyroelectric signals, given by domains with opposite orientation,

compensate for each other, and total pyroelectric coefficient it becomes equal to zero. The given above curves, taken in the fields of different polarity, are typical for many specimen/samples being investigated.

Investigation of the dependence γ_A on the thickness of the specimen/samples, prepared according to one and the same technology from the large single crystal of TGS, gave the following results. During a decrease in the thickness is observed tendency toward reduction γ_A , especially this noticeably beginning with thicknesses 50-100 μ . However, powerful spreads in values γ_A separate copies and even the party/batches of specimen/samples did not make it possible to derive reliable dependences. Of the majority of specimen/samples 200-500 μ thickness the maximum γ_A was located in area 48.2-48.4°C, while of specimen/samples 50-100 μ thickness - in range 47.5-47.8°C.

Work [29] gives the information about the considerable displacement of the maximum of pyroelectric coefficient γ_c for single crystals of TGS ($T_m = 40^\circ\text{C}$) during static measurements. The measurements of sublimity γ_A conducted also showed that the maximum of pyroelectric coefficient was displaced to the side of the lower temperatures with respect to the maximum of dielectric constant at very weak fields.

This displacement was not so/such considerable and of some specimen/samples it was 0.3-0.5°C, so that could arise the doubts of the nonidentity of ferroelectric states during measurement γ_A and ϵ and of the accuracy of measurements. For the more convincing proof of the displacement of maximums was carried out the measurement of relation γ_A/ϵ , since in this case it was eliminated the error, caused by the heterochronism of the measurements of these values. Figure 3.2 gives typical for the majority of specimen/samples temperature dependence γ_A/ϵ , made of which evident that the maximum γ_A is displaced more left than the maximum ϵ (curve 1).

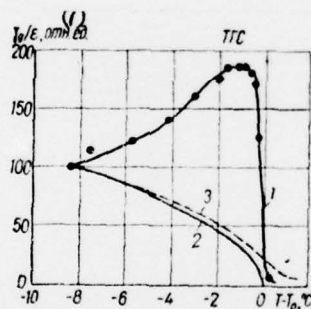


Fig. 3.2. Dependences of relation γ_A/ϵ on value $T-T_0$: 1 - experimental; 2 - designed with $E = 0$; 3 - designed with $E = 300$ V/cm.

key: (1). rel. un.

Page 79.

There are given temperature dependences γ_A/ϵ , designed in accordance with thermodynamic theory. According to equation (2.16), the temperature dependence γ/ϵ is similar to dependence $P = P(T)$ and in the absence of field must change according to the law $(T-T_0)^{1/2}$. The given theoretical relative dependences γ_A/ϵ strongly differ from the experimental. This difference it is not possible to explain by the presence of internal field in crystal. Calculated curve γ_A/ϵ in the field, comparable with coercive, is given in the same figure (curve 3). The displacement of maximum γ_A into the range of lower temperatures with respect to maximum ϵ must be explained by other reasons.

The dependences of pyroelectric coefficient γ_A and of dielectric constant ϵ on temperature for single crystals TGS, deuterized TGS, TGFB and TGSe are represented in Fig. 3.3 [18]. The values of pyroelectric coefficient for all crystals, except TGSe, at room temperature have identical order of magnitude. In the crystals TGFB and TGSe an increase in value γ_A and in the especially dielectric constant near the temperature of phase transition sharper

in comparison with single crystals TGS and DTGS.

In all crystals is observed the characteristic shift/shear of the temperature of maximum T_m^y in comparison with the temperature of maximum T_m^e to 0.3-1.0°C to the side low-temperature.

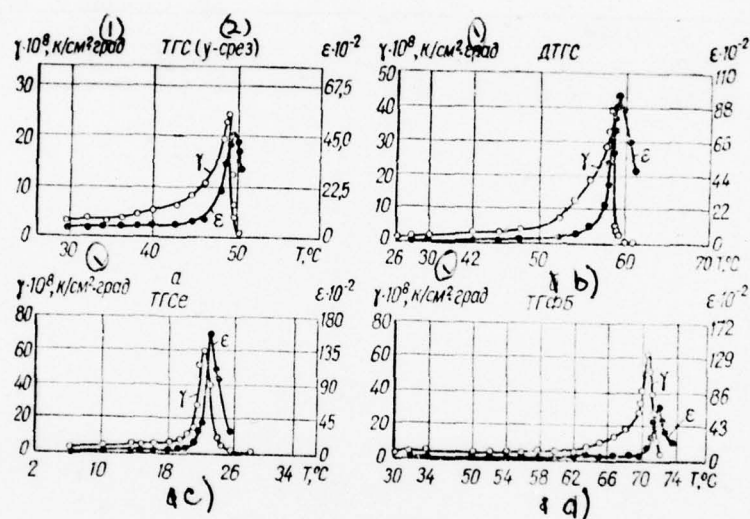


Fig. 3.3.

Fig. 3.3. Dependences of pyroelectric coefficient γ and of dielectric constant ϵ on temperature for the single crystals of the group TGS [18]: a) TGS (y -section/shear); b) DTGS (y -section/shear); c) TGSe (y -section/shear); d) TGFb (y -section/shear).

Key: (1). $\text{k/cm}^2 \cdot \text{deg.}$ (2). (y -section/shear).

Page 80.

Sometimes are observed supplementary peaks in curve $\gamma(T)$, displaced with respect to the Curie temperature T_K to the side low-temperature on 2-6°C. These supplementary maximums disappear during the imposition of external electric field larger than coercive, at room temperature. The displacement of the temperature of the basic maximum T_m^y on relation T_m^e can be explained by appearance in the vicinity of the temperature of the phase transition of the considerable polarization for thin-film ferroelectric, induced with the fields of volumetric and surface charges, and also with terminal assemblies. This induced polarization gives the supplementary contribution to pyroelectric coefficient in the form of term $\frac{1}{4\pi} \cdot \frac{\partial \epsilon_{ij}}{\partial T} E_j$. The maximum of this contribution corresponds to point of inflection in curve $\epsilon(T)$ and leads to the displacement of maximum $\gamma_\lambda(T)$ to

the side low-temperature.

The appearance of a supplementary maximum in curve $\gamma_n(T)$ (see Fig. 3.1a, curved 1 and 2) it is explained within the framework of the Kozlovskiy model [29] as effect of the rearrangement of domain structure, which corresponds in thermodynamic description to an abrupt change of the coefficient of unipolarity θ , (see 2.24).

In works [34, 65] were observed remanent/residual pyrosignals at the temperatures, exceeding Curie temperature, whereupon the sign of these signals were changed by opposite during the transition through the Curie point. The appearance of these signals and a change in their sign also can be explained by the emergence of the induced polarization, proportional to value $\frac{\partial p}{\partial T}$ and which changes sign during the transition through the Curie point (Fig. 3.4).

The investigation of pyroelectric effect in the single crystals of triglycine sulfate during rapid heating specimen/samples was carried out by the authors [34].

Figure 3.5 shows the oscillograms of the pyroelectric current in the range of phase transition at the different heating rates from powerful source (see Chapter VII). Before each measurement the specimen/sample was polarized in field 5 kV/cm. In the torque/moment

of the inclusion of radiation sources the temperature in the thermostatically controlled container was 46°C . Are in parallel given the curves of pyroelectric current, taken in the absence of the modulated signal. The first peak to the left in these curves characterizes the transient process, bonded with the connection/inclusion of radiation sources. The manifestation of the second and third (lower) peaks can be explained by displacement T_m^y and T_m^e (see Fig. 3.4).

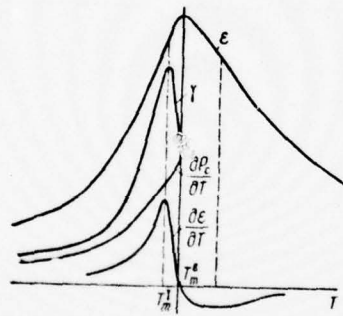


Fig. 3.4. The diagrammatic representation of the displacement of values T_m^y and T_m^e . Page 81.

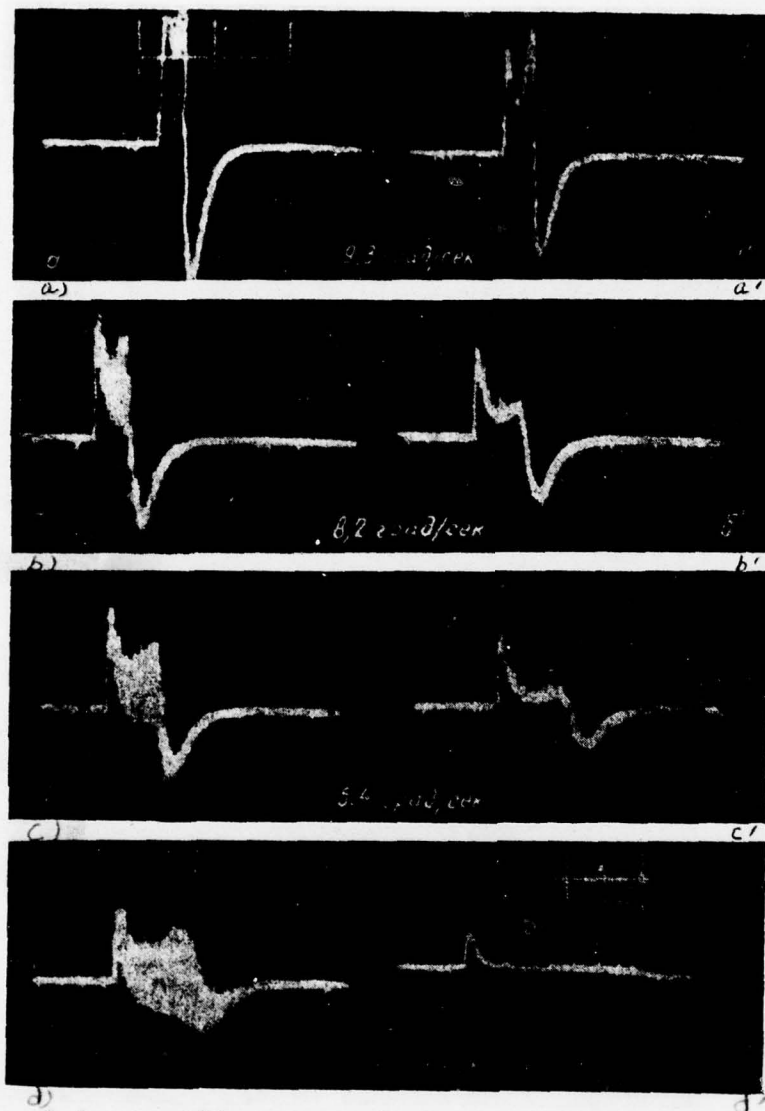


Fig. 3.5. Oscillograms of the pyroelectric current for single crystals TGS in the range of phase transition at the different heating rates: a, b, c, d - with modulation of flow; a', b', c', d', in the absence of modulation.

$$[2 \text{ rad/sec} = \text{deg/s}]$$

AD-A046 669

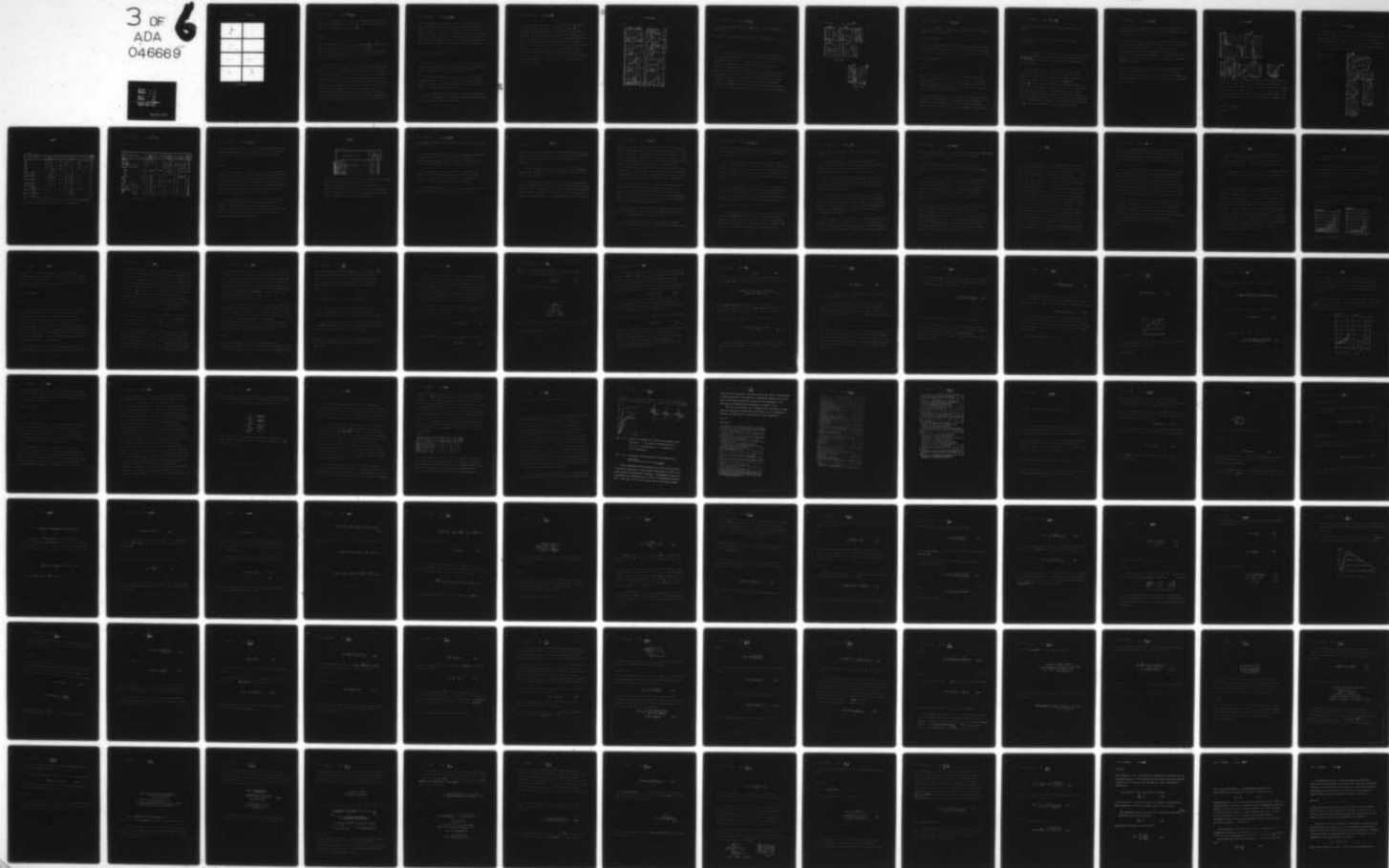
FOREIGN TECHNOLOGY DIV WRIGHT-PATTERSON AFB OHIO
FERROELECTRIC RADIATION DETECTORS, (U)
JUL 77 L S KREMENCHUGSKIY
FTD-ID(RS)T-0846-77

F/G 17/5

UNCLASSIFIED

3 OF 6
ADA
046669

NL



Page 82.

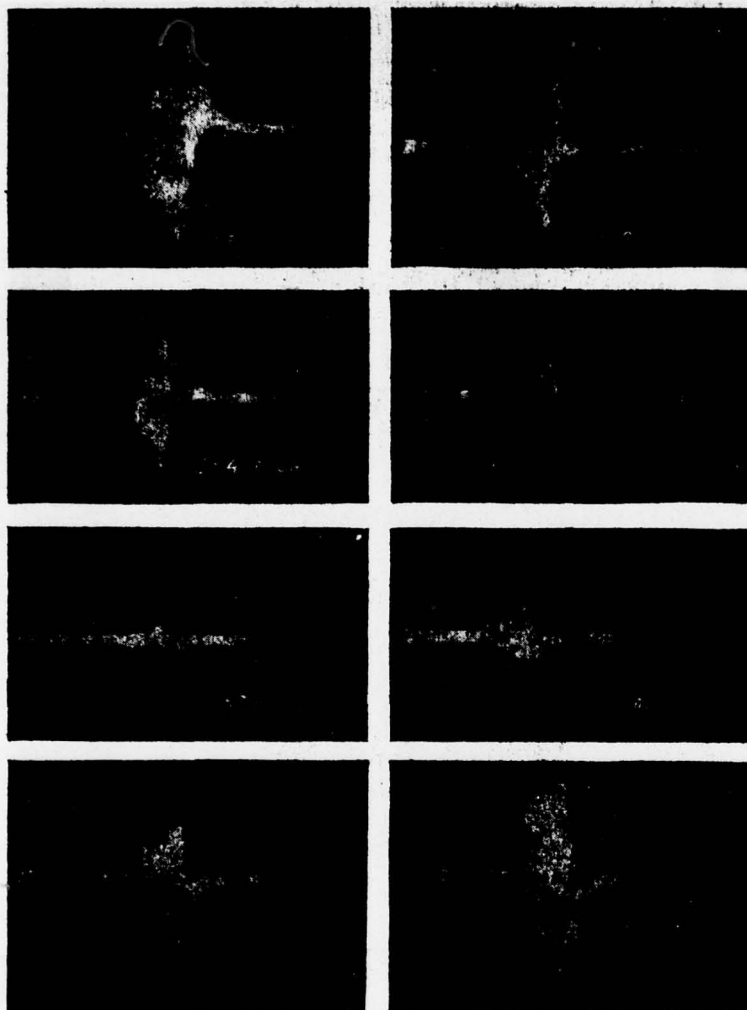


Fig. 36.

$$[B/cm = V/cm]$$

Fig. 3.6. Oscillograms of the pyroelectric current during heating the unipolar specimen/sample, which possesses certain internal field, at the different values of applied field E .

Page 83.

Certain the tightening of discharging curve ($t_{\text{dis}} \approx 10^{-4}$), apparently, can be explained by the rescription of space charges in specimen/sample. During the transition through the Curie point are visible Barkhausen's jumps, which can be observed at the rates of heating more than 1 deg/s.

The oscillograms of the pyroelectric current during heating the unipolar specimen/sample, which possesses certain internal field, are given in Fig. 3.6. During cooling preliminarily reheated for Curie point specimen/sample the internal field polarizes it in determinate direction. The direction of polarization can be judged from of the initial peak, caused by the connection/inclusion of luminous flux. By applying applied field, it is possible to compensate for effective internal field. According to the figure, the applied field of approximately 60 V/cm, directed oppositely internal, completely compensates for the latter, and during cooling the specimen/sample, preheated above the Curie point, single crystal transfer/converts to

poly-domain state, and pyroelectric signal virtually it is absent. A further increase in the applied field leads to the appearance of a polarity of opposite sign. In the figure it is evident that the initial peak to fields 60 V/cm is directed down, and with the higher strengths of field - upward. The determination of the displacing (internal) fields employing the described procedure can be conducted more accurately than by the oscillography of hysteresis loops.

§2. Crystals of group BaTiO_3 .

Ferroelectric of the type BaTiO_3 possess more complex domain structure, than the crystals of TGS; therefore the information about their pyroactivity bears often contradictory character.

Single crystals BaTiO_3 possess, as a rule, unstable domain configuration and the unstable coefficient of unipolarity. This is one of the reasons for the rare utilization of single crystals of titanate of barium in radiation detectors.

However, ceramicist BaTiO_3 , polarized under certain conditions, possesses the stable value of pyroelectric coefficient and widely is utilized as sensing elements of receivers.

Figures 3.7 and 3.8 depict the dependence of pyroelectric coefficients γ_A and γ_C and also dielectric constant ϵ on temperature for single crystals the ceramicist of group BaTiO_3 . The distinctive special feature/peculiarities of these curves are the powerful displacement of the maximum of pyroelectric coefficient in relation to the maximum of dielectric constant, considerable difference in value and position of the maximums of the pyroelectric coefficients, measured by static and dynamic methods, and the existence of pyroelectric current higher than the Curie point. Apparently, besides ferroelectric polarization, an essential effect on the pyroelectric effect have other forms of polarization (for example, interlayer).

Page 84.

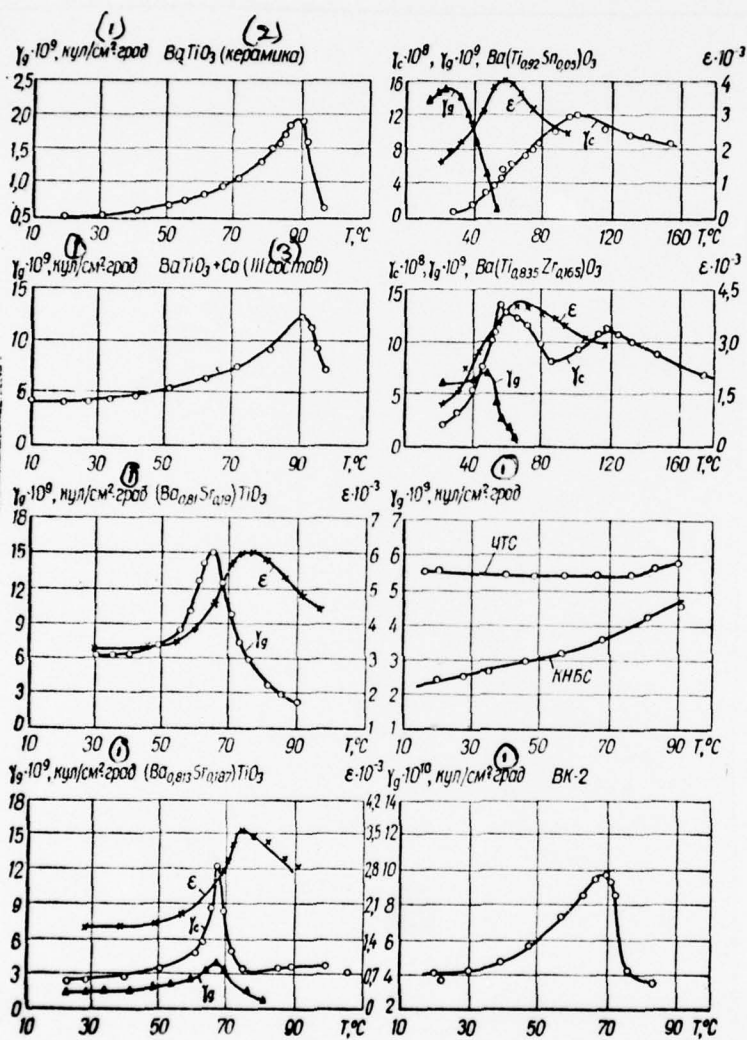


Fig. 3.7

Fig. 3.7. Temperature dependences γ_A , γ_C and ϵ for the ceramicist of group BaTiO_3 .

Key: (1). $\text{cul/cm}^2 \cdot \text{deg.}$ (2). ceramic. (3). III composition.

Page 85.

In work [30] was conducted research on the infralow-frequency dispersion of pyroelectric coefficient and dielectric constant of the derivatives BaTiO_3 in the range of frequencies 0.05-10 Hz. Interesting are presented the results of the investigation of temperature dependence γ_A for ceramics BaTiO_3 with the impurity/admixture of tin Va ($\text{Ti}_{0.92}\text{Sn}_{0.08}\text{O}_3$) (Fig. 3.9). The curves of pyroelectric current in an interval of temperatures 20-30°C are little affected at different frequencies. At temperature of 48°C is observed the maximum of pyroelectric coefficient γ_A , apparently, caused by maximum $\frac{\partial \epsilon}{\partial T}$, according to Fig. 3.7. These curves illustrate the effect of the different mechanisms of polarization on dispersion γ_A .

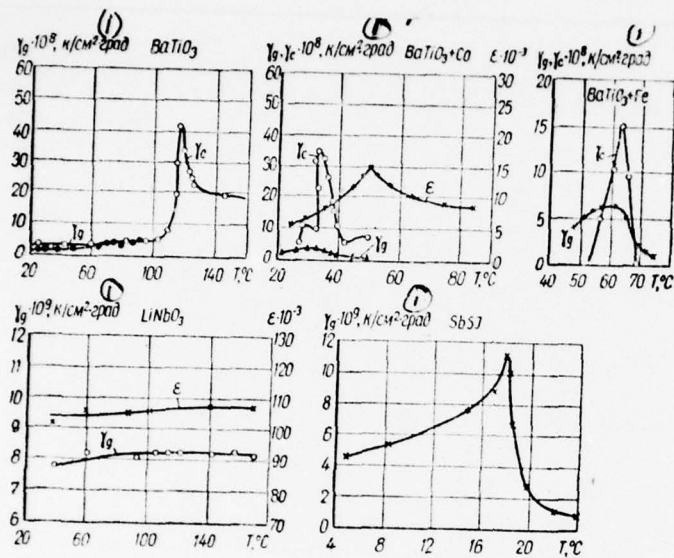


Fig. 3.8.

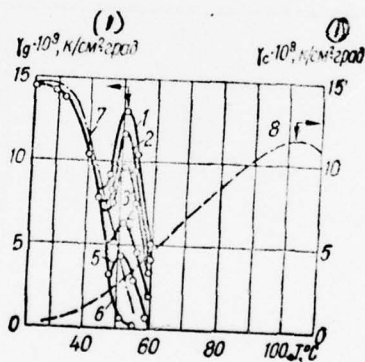


Fig. 3.9.

Fig. 3.8. Temperature dependences $\rho_{\alpha\gamma_e}$ and for the single crystals of group BaTiO_3 and some others.

Key: (1) $\cdot \text{k/cm}^2 \cdot \text{deg.}$

Fig. 3.9. The temperature dependence of the pyroelectric coefficient of ceramics γ_a ($\text{Ti}_{0.92}\text{Sn}_{0.08}$) O_3 at different modulation frequencies: 1 - 0.05; 2 - 0, 1; 3 - 0.2; 4 - 0.5; 5 - 1; 6 - 2; 7 - 40 Hz; 8 - γ_e .

Key: (1) $\cdot \text{k/cm}^2 \cdot \text{deg.}$

Page 86.

If at room temperature the dominant role in formation γ_a plays spontaneous polarization, then during an increase in the temperature a more noticeable role begins to play the relaxation processes of volumetrically-charge polarization. Dispersion γ_a in the range of frequencies $10\text{-}10^4$ Hz is insignificant.

The obtained results are not only supplementary material for the explanation of the nature of the infrared-frequency mechanism of polarization in ferroelectric, but also they have the determined practical value in connection with the utilization of pyroelectrics

for producing the radiation detectors and temperature-sensing devices.

§3. Pyroelectric effect in other ferroelectric and linear pyroelectrics.

For developing pyroelectric radiation detectors, besides TGS and BaTiO_3 , are utilized the crystals of niobate of lithium LiNbO_3 , SBN ($\text{Sr}_{1-x}\text{Ba}_x\text{Nb}_2\text{O}_6$),
ceramics of titanate of zirconate of lead and sulfate of lithium Li_2SO_4 .

Niobate of lithium of all known at present ferroelectric possesses the greatest value of the Curie temperature, which according to the data [48] is 1245°K . Pyroelectric coefficient of niobate of lithium at room temperature small ($\gamma_A = 8 \cdot 10^{-9}$ $\mu\text{k}/\text{cm}^2 \cdot \text{deg}$). However, small changes in this value up to 100°C and its stability make it possible to recommend crystal for the creation of the receivers, intended for the measurement of intense radiant fluxes. The pyroelectric characteristics of tantalate of lithium LiTaO_3 are described in works [41, 44, 71, 73]. In the data of Glass [71], the pyroelectric coefficient of tantalate of lithium comprises (0.8 ± 0.1) the coefficient of titanate of barium at room

temperature. The dependences of the pyroelectric coefficient of niobate of lithium and tantalate of lithium on temperature are given in Fig. 3.8 and 3.10 f.

The investigation of pyroelectric effect in the single crystals of potassium ferrocyanide (see Fig. 3.10 c, d, and e) is carried out in work [31]. Under the condition of repeated preliminary polarization were reached the large values of pyroelectric coefficient in Curie point ($\gamma_c = 10^{-5} \div 10^{-6}$ K/ (cm²•deg)). However, these values were unstable. The value of spontaneous polarization at (-33°C) was 50 $\mu\text{C}/\text{cm}^2$.

In work [24] was investigated the dependence of pyroelectric effect in the single crystals of Rochelle salt at different pressures. For determined polarizable mechanical stresses (Y_2), is an optimum value, by which the pyroelectric coefficient reaches maximum (see Fig. 3.10a).

Page 87.

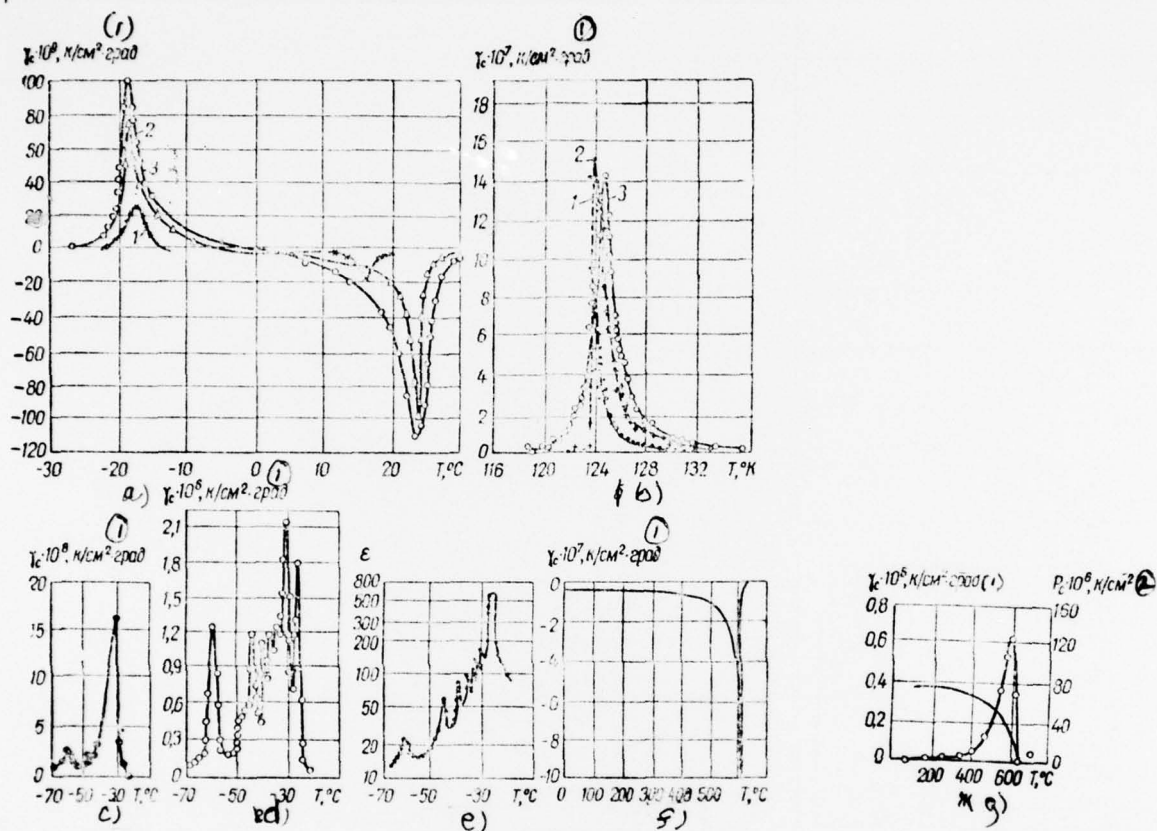


Fig. 3.10. Dependences of values γ and ϵ from the temperature: a) the X-cut of Rochelle salt [24] at the different pressures (1 - 0, 2 - 2280, 3 - 4500 kg/cm²); b) of the dihydrogen phosphate of potassium KH_2PO_4 (KDP) in different DC fields (1 - 2.5; 2 - 4.9; 3 - 7.4 kV/cm [10]); c, d, e) (101) section of potassium ferricyanide ($\text{K}_3\text{Fe}(\text{CN})_6$) [31]; f) tantalate of lithium LiTaO_3 [71]; g) tantalate of lithium LiTaO_3 [41].

Key: (1) $\text{N/cm}^2 \cdot \text{deg}$.

Page 88.

Fig. 3.11. The dependences of value γ_e from temperature for some linear pyroelectrics: a) green tourmaline [8]; b) sulfate of lithium Li_2SO_4 (1), ethylenediaminetartrate (2) guanidine is aluminum is sulfate of hexahydrate (3) [39]; c) nitrate cesium [12]; d) nitrite of barium [11]; e) sulfate of lithium (1) and of nitrate barium (2) [12]; f) glycine (1) and potassium distilled (2) [12].

Key: (1) - $\text{k/cm}^2 \cdot \text{deg}$.

Page 89.

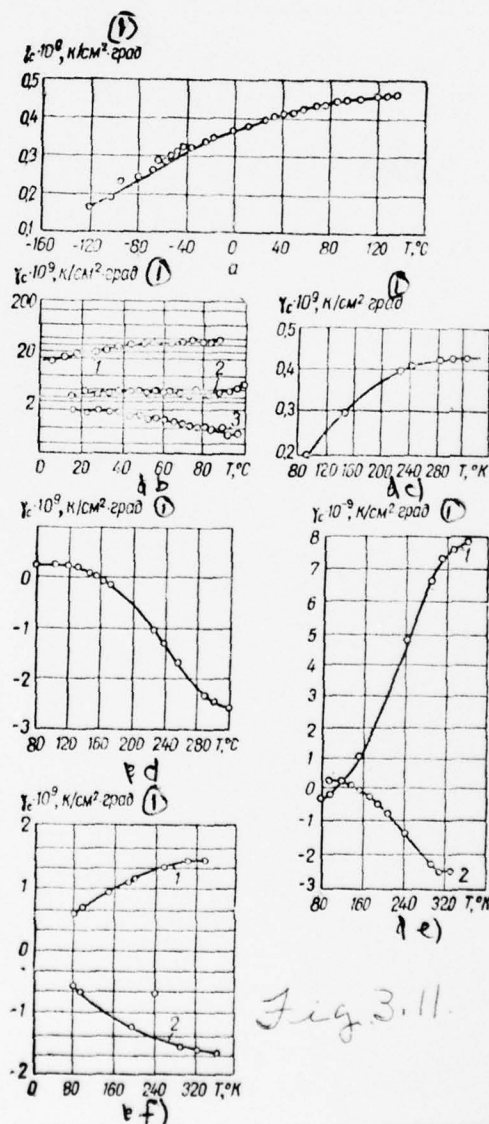


Fig. 3.11.

Table 3.1

(1) Наименование материала	$T_c, ^\circ\text{C}$	$\gamma_d (T = 20^\circ\text{C}),$ (2) $\mu\text{K}/\text{cm}^2 \cdot \text{град.}$	$\epsilon (T = 20^\circ\text{C})$	$T_{\text{пр}}, ^\circ\text{C}$	$\gamma_{\text{max}},$ (3) $\mu\text{K}/\text{cm}^2 \cdot \text{град.}$	ϵ_{max}	$P_c (T = 20^\circ\text{C})$	(3) Лите- рату- ра
ГТС	49	0,03	300	48,8	0,25	4500	2,8	[18]
ДТГС	59	0,01	50	58,2	0,4	10 200	—	[18]
ГТСе	23	0,10	400	22	0,6	16 000	3,2	[18]
ГГФБ	72	0,015	100	71	0,63	6700	3,2	[18]
BaTiO ₃	—	0,0005	—	90	0,002	—	—	[1]
BaTiO ₃ + Co (керамика)	—	0,005	—	90	0,012	—	—	[1]
(BaSr)TiO ₃ (керамика)	75	{0,01 0,025 (γ_c)}	1700	67 67	{0,04 0,13 (γ_c)}	3500	—	[1]
Ba(TiSn)O ₃ (керамика)	60	{0,014 0,005 (γ_c)}	1600	30 100	{0,015 0,12 (γ_c)}	4000	—	[1]
Ba(TiZr)O ₃ (керамика)	72	{0,006 0,02 (γ_c)}	1300	50 50	{0,007 0,14 (γ_c)}	4200	—	[1]
BaTiO ₃ (монокристалл)	120	0,02	—	118	0,42	26,0	—	[1]
BaTiO ₃ + Co (твердый раствор)	50	0,02	6000	33 34	{0,05 0,35 (γ_c)}	15 000	—	[1]
BaTiO ₃ + Fe (твердый раствор)	—	—	—	63	{0,07 0,16 (γ_c)}	—	—	[1]
BaTiO ₃ + Ni (твердый раствор)	100	—	—	95	{0,3 0,75 (γ_c)}	—	—	[1]

Key: (1). Designation of material. (2). $\mu\text{K}/\text{cm}^2 \cdot \text{deg.}$ (3). Literature.

(4). ceramics. (5). single crystal. (6). solid solution.

Page 90.

Table 3.2.

(1) Наименование материала	$T_K, ^\circ\text{C}$	$\gamma_d (T = 20^\circ\text{C}),$ мкК/см ² ·град (2)	$\epsilon (T = 20^\circ\text{C})$	$T_m, ^\circ\text{C}$	$\gamma_{\text{max}},$ мкК/см ² ·град (2)	ϵ_{max}	$P_C,$ мкК/см ² (3)	Литера- тура (4)
(5) Сегнетовая соль	-18; 24	0,1 (24°С) (γ_c)	—	—	0,1 (γ_c)	—	—	[24]
КДР (KH_2PO_4)	-150	—	—	-149	1,4 (γ_c)	10 ⁶	4,75(-177°С)	[10]
ЖКС (6) тетрагональный (10 $\bar{1}$)-срез	-26	—	—	-32	2,2 (γ_c)	600	35(-70°С)	[31]
(7) ЖКС моноклинный (10 $\bar{1}$)-срез	—	—	—	-30	6,0 (γ_c)	—	50(-70°С)	[31]
LiTaO ₃	618	0,016 (γ_c)	80—100	—	1,0 ₁ 0,6 ₁ (γ_c)	—	50(20°С)	[71, 41]
SbSI	21	—	—	18	0,012	—	—	—
LiNbO ₃	1245	0,007	100	—	—	—	14(350°С)	—
КНБС	250	0,003	1500	—	—	—	—	[1]
ВК-2	70	0,0004	200	69	0,001	—	—	[1]
ЦТС-19	330	0,005	1100	—	—	—	—	[1]
Pb(Zr _{0,95} Ti _{0,05})O ₃ (8) (керамика)	—	-0,02 (γ_c)	300—400	—	—	—	—	[92]
Sr _{1-x} Ba _x Nb ₂ O ₆ { x = 0,25	40	0,31	—	—	—	—	—	[92]
Твердые растворы) { x = 0,33	60	0,11	—	—	—	—	—	[92]
(9) { x = 0,41	78	0,07	—	—	—	—	—	[92]
{ x = 0,52	105	0,06	—	—	—	—	—	[92]

[Key on following page.]

Key: (1). Designation of material. (2). $\mu\text{k}/\text{cm}^2\cdot\text{deg}$. (3). $\mu\text{k}/\text{cm}^2$. (4). Literature. (5). Rochelle salt. (6). tetragonal (101) section. (7). monoclinic (101) section. (8). ceramics. (9). Solid solutions.

Page 91.

Is of also interest the investigation of the single crystals of the dihydrogen phosphate of potassium (KDP) in different DC fields. On the data of the authors [10], pyroelectric coefficient lower than the Curie point is very low in the absence of electric field and it reaches large values only in the range of phase transition (see Fig. 3.10b). During the imposition of DC field the range of the large values of the pyroelectric coefficient is expanded.

Figure 3.11 gives the curves of the temperature dependence of the pyroelectric coefficients of some linear pyroelectrics. The values of the quantities of pyroelectric coefficients are considerably less than of ferroelectric crystals. Table 3.1-3.3 gives the basic information about the electrical characteristics of ferroelectric and linear pyroelectrics.

Table 3.3.

(1) Наименование материала	$\gamma_T = 20^\circ\text{C} \cdot 10^6$, K/cm ² ·deg (2)	Литература (3)
(4) Зеленый турмалин	0.04	[8]
(5) Сульфат лития	12	[39]
(6) Этилендиаминтарtrat	0.3	[39]
(7) Гуанидин-алюминий сульфат гексагидрат	0.14	[39]
(8) Азотнокислый цезий	0.04	[12]
(9) Нитрит бария	0.25	[11]
(10) Азотнокислый барий	0.7	[12]
(11) Глицин	0.14	[12]
(12) Калий виннокислый	0.15	[12]
(13) Кадмий сернистый	0.04	[93]
(14) Кадмий селенистый	0.02	[93]

Key: (1). Designation of material. (2). K/cm²·deg. (3). Literature.

(4). Green tourmaline. (5). Sulfate of lithium. (6).

Ethylenediaminetartrate. (7). Guanidine-aluminum sulfate is

hexahydrate. (8). Nitrate cesium. (9). Nitrite of barium. (10).

Nitrate barium. (11). Glycine. (12). Potassium distilled. (13).

Cadmium is sulfurous. (14). Cadmium is selenious.

§4. Effect of gamma-radiation on the electrical characteristics of ferroelectric.

The stability of the characteristics of ferroelectric radiation detectors is bonded with the stability of the spontaneous polarization in crystals, which depends on the internal electric field, which is determined by space charges and contacts.

The systematic investigation of value and reasons for the emergence of considerable internal fields in ferroelectric they became to be occupied in connection with the utilization of ferroelectric films as memory elements in computers.

The basic investigations were directed toward research on the factors, lowering the value of internal field in crystal.

From practical point of view this was especially important, since it made it possible to obtain cell/elements with the identical reversible characteristics, necessary for the normal operation of memory elements.

The wide utilization of ceramic materials in electromechanical transformers is caused by the sufficient stability of the internal field of their material.

The investigation of the stability of pyroelectric coefficient ceramicist BaTiO_3 showed that, at least, during half a year the value of quantity γ_A is changed not more than to $\pm 10\%$. Are considerably more complex the processes of the stabilization of unipolar state in ferroelectric crystals [15, 25, 45]. Frequently are encountered the

monodomain crystals, when pyroelectric effect in them is observed without preliminary polarization by stationary field. After several cycles the heating - cooling the high degree of unipolarity in these crystals disappears. However, through certain it can again be reduced to the original value. Are encountered such single crystals, of which the value of pyroelectric effect it does not decrease after temperature effects. A quantity of such single crystals is small. If we obtain ceramic cell/elements with the close values of pyroelectric coefficient it is sufficiently easy, then obtaining single crystals with the identical values of quantity γ_n presents difficulties.

It is appropriate to still note that a series of the physical phenomena finds its satisfactory explanation only under the assumption of the existence of internal field in crystal. These phenomena include the dependence of coercive field and changing over characteristics on the thicknesses of crystals [59], the Barkhausen effect [58] gamma-irradiated crystals, etc.

The problem of the stabilization of spontaneous polarization in ferroelectric, thus, is reduced to the stabilization of polarized state of those oriented in one direction domain.

There are several methods of the stabilization of domain structure. Basic made of them - irradiation X-ray and by gamma rays,

the introduction of impurity/admixtures, the processing/treatment of crystal boundary and the deposition of electrodes from different by work function.

Gamma- and X-rays produce ionization in all solid bodies. The reaction of gamma-radiation with substance is realized mainly because of three mechanisms: the photoelectric effect, the Compton effect and vaporization. The first effect is that which predominate with low energies of gamma-quanta, the second - with middle, the third - with high.

In all three processes are driven out the electrons with the energies, comparable with energy of the initial gamma-quanta, which leads to the internal bombardment of substance. The large part of their energy is expend/consumed on further ionization, but frequently occurs atomic displacement as a result of elastic collisions.

Page 93.

The gamma irradiation of solid dielectrics leads to a change in their electroconductivity and dielectric constant, it produces polarizational effects. The appearing as a result of irradiation space charges contribute to the formation of internal fields. These fields can exist after the cessation of irradiation, but at

sufficiently high temperature they can change or to completely disappear.

Gross [69] developed the phenomenological theory of the weakening of radiation flux in solid dielectrics, based on the theory of Compton effect and the experimental data on the radiogionno-induced in the irradiated substance charges.

There is special interest in the investigation of the effect of radiation on structural-sensitive crystals whose properties very strongly change during insignificant changes in structure. Such crystals are the ferroelectric.

I. V. Kurchatov and M. A. Yeremeyev [21] for the first time reveal/detected the effect of impurity/admixtures on the properties of Rochelle salt. They showed, that the addition to the solution of pure/clean Rochelle salt of one percent of tartrate sodium-ammonium narrows at the obtained crystals the temperature interval of ferroelectric range double.

I. S. Zheludev and V. A. Yurin [22, 23] reveal/detected that the radiation defects have an analogous effect on the properties of Rochelle salt. the gamma- irradiated Rochelle salt has a hysteresis loop, sharply different from the normal. With an increase in the dose

of gamma-radiation the loop is bifurcated, and in large doses ($D_p \geq 10 \text{ Mrad}$) Rochelle salt begins to be polarized similar to linear dielectric.

Rogers [81] established that dielectric constant BaTiO_3 decreases and its peak at Curie point disappears in large radiation doses.

V. A. Yurin et al. [54, 56, 57] showed, that during irradiation the range of ferroelectric phase becomes narrow. The gas analysis conducted showed that the irradiated Rochelle salt is subjected to noticeable resolution. One molecule decomposes approximately on several thousands. The abnormal polarization of the irradiated Rochelle salt is caused by the formation of the products of radiolysis.

I. Ya. Bysner [50], being based on the obtained by it results about the narrowing of the existence domain of spontaneous polarization and the distortion of hysteresis loops, it noted the analogy between the effect on the ferroelectric of radiation defects and impurity/admixtures. Apparently, during the introduction of small quantities of impurity/admixtures into ferroelectric its domain structure acquires considerable stability with respect to external agencies (electric field, high temperature, etc.).

Page 94.

For the first time the effect of X-radiation on the crystals of TGS was studied by Chaynoviz [65]. The author showed that during irradiation of the nonpolarized specimen/sample is formed the dual hysteresis loop, and during irradiation of the polarized specimen/sample - the displaced single loop. Coercive field E_k also changes with irradiation, in this case first is observed an increase in value E_k , and then decrease. The annealing of the specimen/samples, irradiated during 10-15 min with 80°C converts the dual loops into normal, which after delay at room temperature again become dual. Chaynoviz assumed that the mechanism of the radiation damage in the crystals of TGS consists in the rearrangement of atomic structure as a result of the secondary chemical reactions. However, in connection with the complexity of radiation effects and nature of ferroelectricity into TGS Chaynoviz proposed the phenomenological treatment of effect, considering that the accumulation of radiation damages in crystal leads to a gradual decrease in depth of one of potential wells, which characterize energy of the ion (see Fig. 2.2), critical for the emergence of spontaneous polarization. As a result of this strain one of the directions of spontaneous polarization P_s is made energetically more favorable than another, thanks to which

and occurs the displacement of hysteresis loops along the axis of fields. Subsequently the dielectric properties of the crystals TGS, which contain defects, were investigated by a number of the authors both in powerful and in weak electric fields [19, 20, 38, 40, 51-56, 82].

For single crystals TGS it was established that the achromatic before irradiation specimen/samples acquire uniform greenish-yellow coloration, also, in the doses, greater than 5 Mr, is observed a sharp decrease in the spontaneous polarization. If we irradiate single domain by external stationary field specimen/sample, then after irradiation and removal/taking of the field the sample exhibits the normal hysteresis loop, displaced along the axis of fields. The amount of this displacement is equal to the value of internal field.

During irradiation by gamma-quanta in the crystal of TGS is formed either stable monodomain state (displaced loop), or stable poly-domain state (dual propeller-shaped loop). Is secured that picture by the domain structure, which occurs in the process of irradiation. The stability of domain structure is caused by formation in the crystal of the products of radiolysis, which are arranged/located in lattice in places with the minimum energy.

Internal field acts on crystal to analogously external - stabilizes its spontaneous polarization. The analogy between the external and internal field is exhibited also in effect on the position of Curie point and the value of dielectric constant.

External electric field reduces the value of dielectric constant and it displaces its maximum to the side of higher temperatures.

Page 95.

In the gamma-irradiated crystals of TGS in comparison with those which were not irradiated is reduced the value of the maximum of dielectric constant and is displaced Curie point to the side of lower temperatures. However, in this case appears no contradiction in the fact that during irradiation the value of Curie point does not grow/rise, but it is reduced. ^{TP} The irradiated crystal TGS can be considered as ferroelectric in another state with new Curie point. New Curie point it is possible to determine, by compensating for internal field by external electric field, in this case her value lower than the value of the temperature of the phase transition of the uncompensated for gamma-irradiated crystal. Possible explanation of this effect on the basis of a decrease in the number of ferroactive dipoles is given in work [40].

Under the effect of ultraviolet radiation also are observed analogous phenomena, but to considerably smaller degree [47].

The effect of gamma-radiation on crystal BaTiO_3 bears similar character. The results of these investigations are presented in works [26, 27, 46, 68, 72, 81, 90], and the property of crystals BaTiO_3 , grown with additions, are described in work [49].

The experimental study of the effect of gamma-radiation on the electrical and spectral characteristics of TGS is carried out in works [19, 20].

The authors studied the pyroelectric effect of the crystals TGS, possessing the low degree of unipolarity, during irradiation by small doses of gamma-radiation for the purpose of their single domainization.

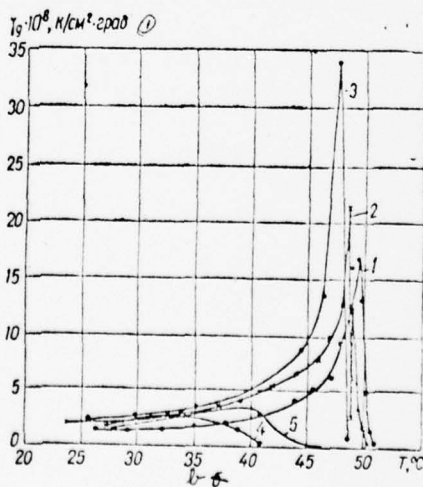
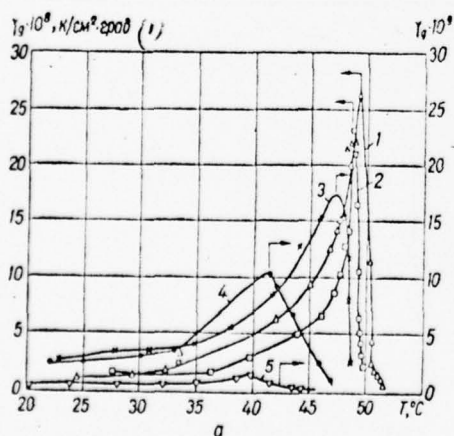


Fig. 3.12. (Caption next page.)

Fig. 3.12. The temperature dependences of the pyroelectric coefficient γ_A in different radiation doses D_p for the crystals: a) with the high degree of unipolarity (1 - $D_p = 0$; 2 - 6; 3 - 50; 4 - 100 crit.; 5 - 0.5 mr); b) with the low degree of unipolarity (1 - $D_p = 0$; 2 - 60; 3 - 130; 4 - 530 crit.).

Key: (1). $k/cm^2 \cdot deg.$

Page 96.

As specimen/samples for investigation were used the plates of the y-section/shear of TGS. Specimen/samples had an area 1-2 mm² and a thickness 100 μ . In vacuum on them were deposited silver electrodes, and the irradiated surface they cover/coated with the layer of gold black. The determination of values γ_A and ϵ conducted by means of direct measurement γ_A and of relation γ_A/ϵ . The source of radiation was Co⁶⁰ specimen/samples during irradiation were maintain/withstood under DC field ($E_m > E_k$). Their temperature did not exceed 40°C. Measurements were conducted before irradiation also in the interval/gaps between to irradiations.

Figure 3.12 depicts the temperature dependences of γ_A on radiation dose for two specimen/samples, which possess the different

degree of unipolarity (strongly differing in γ_a). From the figure one can see that with an increase in the dose occurs the displacement of Curie point T_K to the side of lower temperatures. However, if for the first specimen/sample (with the high degree of unipolarity before irradiation, see Fig. 3.12a) occurs the monotonic incidence/drop in the pyroelectric coefficient γ_a with an increase of dose, then for the second (with the low degree of unipolarity before irradiation, see Fig. 3.12^b) it is observed a considerable increase in the coefficient γ_a in the determined interval of doses, and already subsequently, in large doses, is observed its decrease, i.e., occurs an improvement in the pyroelectric properties of poly-domain specimen/sample under the effect of small radiation doses.

The value of the maximum of curve $\epsilon(T)$ in these measurements, independent of the degree of the unipolarity of specimen/samples, with an increase in the dose it was reduced and the position of maximum was moved to the side of lowest temperatures.

In work [20] was carried out the investigation of the stability of this effect in time. The investigated specimen/samples possessed before irradiation by the low degree of unipolarity $\Theta_y = 0,1 \div 0,5$. The degree of unipolarity was defined as ratio of pyroelectric signal in the absence of field to signal in the field, greater than coercive E_K . After the irradiation of crystals in field $E > E_K$ by the dose of

gamma-radiation on the order of 10^5 p were measured the values of quantities Θ_y, γ_A and ϵ . Such measurements were carried out three times: immediately after irradiation, in two months and through half a year. After irradiation of the majority of specimen/samples the value Θ_y rose. With the very low coefficient of unipolarity before irradiation after irradiation the value of pyroelectric coefficient grew/rose; however, at values $\Theta_y = 0.3 \div 0.5$ to irradiation after irradiation was observed both an increase γ_A for some specimen/samples and decrease for others.

As it was earlier said, the temperature maximums of dielectric constant T_m^e and of pyroelectric coefficient T_m^y for single crystals TGS, as a rule, do not coincide, their shift/shear relative to each other can reach about 1.5°C . The effect of gamma-radiation leads to the fact that an interval $T_m^e - T_m^y$ for the majority of specimen/samples noticeably decreases. However, after semimonthly aging the value of shift/shear again grows/rises, which is bonded, apparently, with the "annealing" of radiation defects.

Page 97.

In this case somewhat decrease the values Θ_y and γ_A . The measurements, carried out through half a year after irradiation, they showed that values Θ_y and γ_A continue to fall. Furthermore, of some

specimen/samples an interval $T_m^e - T_m^y$ with aging becomes narrow. ¹¹ Given information can be useful for the explanation of the effect of radiation exposure on the parameters of ferroelectric radiation detectors. The method of the stabilization of the spontaneous polarization with the aid of gamma-radiation is insufficiently reliable.

§5. Contact system is metal - ferroelectric-metal.

The study of system metal - dielectric - metal (MDM) (for example, [17]) shows that in lamellar crystal the different electrodes can lead to the different distribution of electric field.

Let us examine the sandwich system metal - ferroelectric; metal (MSM [MCM - Ministry of Medium Machinery Manufacture]) when metals they possess different work function (ϕ_1 and ϕ_2) ¹.

FOOTNOTE 1. The problem of the contact of ferroelectric semiconductor with two identical metals was recently examined in work [16].

ENDFOOTNOTE.

We will be restricted to the case of uniform ferroelectric. Let χ be energy of the affinity of electron for ferroelectric - the work, which must be expended for the translation/conversion of electron from the infinitely moved away point of space into the energy state in ferroelectric, which corresponds to the bottom of conduction band. The thermodynamic equilibrium condition of electrons in the contact system of MSM is the equality of chemical potential in all parts of the system (common/general/total Fermi level) (Fig. 3.13).

For finding the distribution of electric field and concentration of electrons it is necessary to together solve the equation of electroconductivity and diffusion

$$j = eUnE - eD_n \frac{dn}{dx} \quad (3.1)$$

and the equation of Poisson, which will be written in the form

$$\frac{dD}{dx} = 4\pi en(x). \quad (3.2)$$

\mathcal{D}_3 - the diffusion coefficient, which is bonded with electron mobility U by Einstein's relationship/ratio

$$\mathcal{D}_3 = \frac{KT}{e} U, \quad (3.3)$$

and $n(x)$ - the electron concentration.

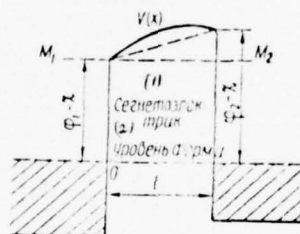


Fig. 3.13. The diagram of the energy bands of the system of metal is a ferroelectric - metal.

Key: (1). Ferroelectrics. (2). Fermi level.

The solution to equations (3.1) and (3.2) is given in work [17], when the dependence between the induction D field E is linear ($D = \epsilon E$). In ferroelectric the dependence between induction and field is described by the more complex relationship/ratio, in which for crystals with the phase transition of the first type the electrical field is approximately bonded with polarization (see Chapter II):

$$E = \beta P + \zeta P^3 + \xi P^5. \quad (3.4)$$

In this case the system of equations (3.1) and (3.2) can be accurately solved only by numerical methods for a concrete ferroelectric. However, approximate solution for real ferroelectric can be obtained during the following simplifications.

Let us present the complete polarization of ferroelectric in the form

$$P = P_c + P_{\text{ind}}, \quad (3.5)$$

where P_c - spontaneous polarization of the massive ferroelectric, when the wobble of electrodes can be disregarded; P_{ind} is the polarization, caused by the electric field of contacts and which depends on coordinate. Numerical estimation shows that of ferroelectric with first-order transition is fulfilled well in ferroelectric phase the inequality

$$P_{\text{ind}} \ll P_c. \quad (3.6)$$

Substituting expression (3.5) in (3.4) and retaining the terms, linear on P_{ind} , taking into account relationship/ratio (3.6) we have

$$\begin{aligned} E &= \beta(P_c + P_{\text{ind}}) + \xi(P_c + P_{\text{ind}})^3 + \xi(P_c + P_{\text{ind}})^5 \approx \\ &\approx P_{\text{ind}}(\beta + 3\xi P_c^2 + 5\xi P_c^4) = P_{\text{ind}}/\chi_{\text{эф}}, \end{aligned} \quad (3.7)$$

where $\chi_{\text{эф}} = (\beta + 3\xi P_c^2 + 5\xi P_c^4)^{-1} = \frac{4}{3} \cdot \frac{\xi}{\xi^2}$ taking into account relationship/ratios (2.19) and (3.4): $\beta P_c + \xi P_c^3 + \xi P_c^5 = 0$, since with the absence of contacts field in ferroelectric is equal to zero.

Expression for induction D is taken in the form

$$\begin{aligned} D &= E + 4\pi P_c + 4\pi P_{\text{ind}} = \epsilon_{\text{эф}} E + 4\pi P_c, \\ \epsilon_{\text{эф}} &= 1 + 4\pi\chi_{\text{эф}}. \end{aligned} \quad (3.8)$$

Since the spontaneous polarization P_c does not depend on coordinate x , the equation of Poisson (3.2) can be written in the form

$$\frac{dE}{dx} = \frac{4\pi e}{e_{sp}} n(x). \quad (3.9)$$

Thus, in the simplified version problem is reduced to the solution of problem for a system MDM.

The theory of contact system MDM (MSM) with the different metals, when the thickness of crystal excludes the possibility of tunneling junction, gives three types of solutions depending on the value of a contact potential difference of V (2), and also values l and T .

Page 99.

The analysis of these solutions, carried out in work [17], shows that in the case of a large difference in the work functions of metals ($\phi_2 - \phi_1$) occurs a monotonic increase in the potential energy of $V(x)$. In the case of metals with one and the same work function dependence of $V(x)$ has a maximum, and the curve of $E(x)$ - opposite signs in ferroelectric.

Let us examine, as influences the field of the contact system of MSM value and position of pyroelectric coefficient in crystal. In accordance with formulas (2.13) and (2.16)

$$\gamma_A = \frac{\partial P}{\partial T} = \frac{B_0}{2} \times \frac{1}{\sqrt{T_0 - T}}, \quad (3.10)$$

where B_0 is is constant, not depending on the temperature.

The experimental dependences of the maximum of pyroelectric coefficient on the value of the applied field are given in Fig. 3.14. In not very high fields the dependence $T_0' \approx T_K + f[E(x)]$ is quasi-linear. Then, after presenting $f[E(x)] = bE(x)$, we convert expression (3.10):

$$\gamma_n = \frac{B_0}{2l} \int_0^l \frac{dx}{\sqrt{V T_K + bE(x) - T}}. \quad (3.11)$$

Calculation γ_n in the general case is difficult, since dependence $E(x)$ is complex. However, it is possible the curve of potential energy of electron (see Fig. 3.13) to approximate the curve of the form

$$V(x) = V(0) - B(x - x_m)^2. \quad (3.12)$$

If we designate by x_1 and x_2 points of parabola (3.12), that correspond to the left and right interfaces, then are possible the case, when these points are arranged along one side to the left of x_m (point of maximum of $V(x)$), or they are located through different sides from x_m .

From expression (3.12) it follows:

$$E(x) = -2B(x - x_m). \quad (3.13)$$

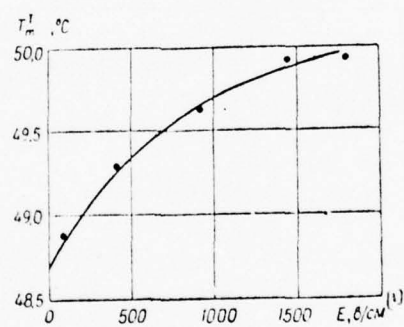


Fig. 3.14. Dependence of the temperature maximum of pyroelectric current T_m^y on electric intensity.

Key: (1) = V/cm.

With this form $E(x)$ the integration of expression (3.11) is conducted simply:

$$\gamma_A = \frac{B_0}{2Bbl} [\sqrt{T_K + bE(x_1) - T} - \sqrt{T_K + bE(x_2) - T}]. \quad (3.14)$$

Expressing B through $E(x_1)$ and $E(x_2)$, we find

$$B = \frac{E(x_1) - E(x_2)}{2l}. \quad (3.15)$$

Then expression (3.14) assumes the form

$$\gamma_A = \frac{B_0}{b} \cdot \frac{\sqrt{T_K + bE(x_1) - T} - \sqrt{T_K + bE(x_2) - T}}{E(x_1) - E(x_2)}. \quad (3.16)$$

The analysis of expression (3.16) makes it possible to draw the conclusion about the character of pyroelectric coefficient γ_A depending on difference $E(x_1) - E(x_2)$. The more this difference, the smaller and more washed away maximum possesses pyroelectric coefficient.

The minimum diffuseness of value γ_A is obtained in the case of contacts with a large difference of $\phi_2 - \phi_1$, and maximum, when $E(x_1) = -E(x_2)$. The last/latter case is realized with contacts with the metals, which have identical work function.

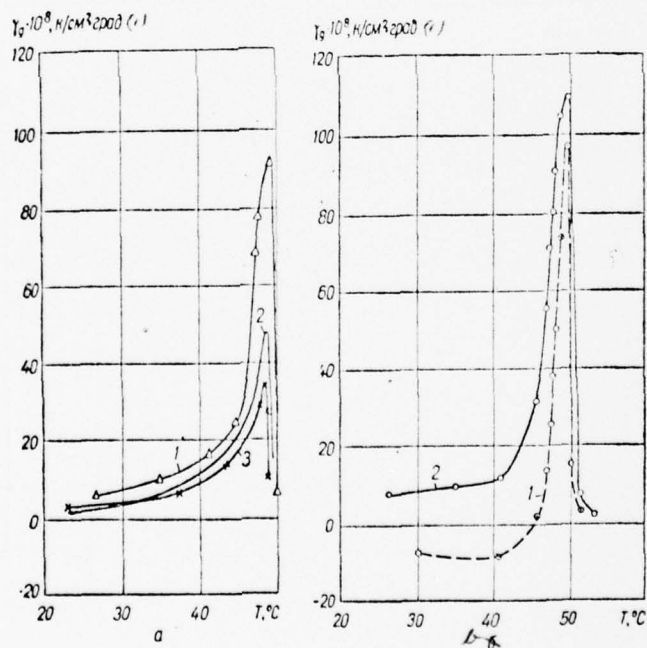


Fig. 3.15. Caption next page.

Fig. 3.15. The temperature dependences of pyroelectric coefficient for specimen/samples TGS with the different electrodes: a) electrodes In - Au (1); Bi are In (2); Ag - Ag (3); b) electrodes In - Bi (1 - primary heating; 2 - secondary).

Key: (1) $\mu\text{K}/\text{cm}^2 \cdot \text{deg}$.

Page 101.

Although a potential difference is equal to zero, electric intensity in ferroelectric is nonhomogeneous; therefore transition from ferrophase to paraphase more washed away. During the utilization of contacts with the large difference of the work functions $\phi_2 - \phi_1$ in ferroelectric are created the sufficiently high fields, which lead to an increase in the coefficient of unipolarity Θ_y .

The experimental studies of the effect of the material of electrode on the pyroelectric effect and other electrical properties were carried out on the lamellar crystals of TGS and BaTiO_3 [2, 4, 37, 60, 79, 80, 89]. The observed effects of control of the physical properties are caused both effect of electrodes and by surface condition with the deposition of electrodes [75, 85, 87, 88].

The amplification of unipolarity and pyroelectric effect in the single crystals of TGS with the deposition of different electrodes was observed in work [4]. The plates of TGS were cut out perpendicular to polar axis whose thickness is 80-200 μ and whose area is 1-3 mm². As materials for electrodes were utilized aqueous solution of lithium chloride LiCl (liquid electrodes), Aquadag C, silver Ag (vacuum evaporation and chemical precipitation), indium In (vacuum evaporation and rubbing in with $T = 150^{\circ}\text{C}$), gold Au, bismuth Bi and antimony Sb (vacuum evaporation), nickel Ni , copper Cu (chemical precipitation). Figure 3.15 depicts the curves of the temperature dependence of pyroelectric coefficient γ_A , obtained by dynamic method. In the case of the symmetrical electrodes Ag - Ag, the pyroelectric effect is caused only by the the natural unipolarity of crystal, electrodes Bi - In amplify pyroelectric effect. Especially strongly grow/rises γ_A during the utilization of electrodes In - Au (see Fig. 3.15). The application/appendix of DC field $E = 100 \text{ V/cm}$ before measurements did not change the value of pyroelectric signal. One and the same signal was reduced after each cycle of heating above T_K , and cooling down to room temperature. Are of interest curves $\gamma_A(T)$ for the specimen/sample, in which during primary heating the direction of internal field, caused by electrodes, is opposite to the direction of remanent polarization in crystal (see Fig. 3.15b). It was establish/install that the direction of the polarization in specimen/sample, directed by the

internal field of electrodes In - Au, does not depend on the material of ferroelectric (BaTiO_3 or TGS), is always directed from one In to Au. Next it is 100-150 V/cm for specimen/samples 100 μ thickness.

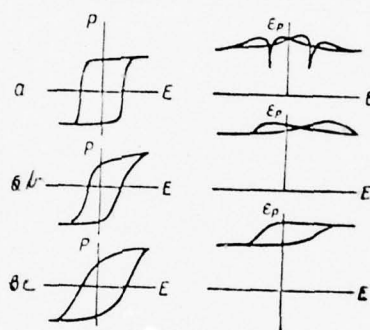


Fig. 3.16. Hysteresis loops and the reversible characteristics of single crystals BaTiO_3 : a) liquid electrodes; b) electrodes Ag - Ni; c) electrodes Sh - Ag.

Page 102.

The investigations of pyroelectric effect and nonlinear properties of crystals BaTiO_3 , obtained from the method of Remeyka, were carried out in the laboratory of RGU [4]. Crystals took the form of plates whose thickness is 100-300 μ whose area is 4-15 mm^2 . In a number of cases were utilized the single crystals 15-100 μ thickness.

Were studied the hysteresis loops, on which was estimated the spontaneous polarization P_c , coercive field E_K and effective dielectric constant $\epsilon_{\text{eff}}^m = 4\pi \frac{P_m}{E_m}$ (where P_m and E_m - the maximum values of polarization and applied electric field respectively). Furthermore, was studied the dependence of reversible dielectric constant ϵ_p [3] on the value of guiding field E at the frequency of the weak measuring field $f = 150 \text{ kHz}$ even 1 kHz . During the utilization of liquid electrodes the unipolarity of single crystals BaTiO_3 was not detected: hysteresis loops were symmetrical (Fig. 3.16a), dielectric constant ϵ_p had sharp minima in field $E = E_K$, caused by the effect of "domain pressings" [5].

The replacement of liquid electrodes by electrodes Ag, as a rule, was not accompanied by substantial changes in the properties of crystals. Somewhat they grow/rose value P_c maximum ϵ_{eff}^m ; in this case considerable unipolarity was exhibited only in weak fields with $E_m \ll E_K$.

Natural unipolarity stops distinct with deposition of electrodes made of In, C, Sb, ~~Ni~~⁶, Au. The utilization of these materials leads to a reduction in the squareness of hysteresis loop and decrease P_c .

Reversive characteristics become asymmetric (especially in the case of the indium electrodes, obtained by rubbing in). Table 3.4 illustrates the effect of the material of electrodes on the value of spontaneous polarization (are represented greatest value P_c , obtained during the utilization of this material). Of a series of the most ideal crystals chemically pure BaTiO_3 with silver electrodes were observed the values P_c exceeding value $26 \mu\text{k}/\text{cm}^2$. The values of remanent/residual polarization $P_{\text{ост}}$ are obtained by the integration of curves γ_c .

Table 3.4.

(1) Материал электрода и способ его нанесения	(2) P_c , $\mu\text{k}/\text{cm}^2$	(3) γ_c , $\mu\text{k}/\text{cm}^2 \cdot \text{град}$	$P_{\text{ост}}$, (4) $\mu\text{k}/\text{cm}^2$
(4) Жидкие электроды (LiCl)	25	—	—
(5) Серебро (химическое осаждение)	30	10.1	30
(6) Серебро (испарение в вакууме)	26	5.5	16
(7) Никель (химическое осаждение)	24	1.05	15
(8) Сурьма (испарение в вакууме)	22	0.55	8
(9) Индий (втирание)	20	—	—
(10) Индий (испарение в вакууме)	6	0.4	3
(11) Золото (испарение в вакууме)	8	0.76	7.3

Key: (1). Material of electrode and the method of its deposition. (2). $\mu\text{k}/\text{cm}^2$. (3). $\mu\text{k}/\text{cm}^2 \cdot \text{deg}$. (4). Liquid electrodes (LiCl). (5). Silver (chemical precipitation). (6). Silver (vacuum evaporation). (7). Nickel (chemical precipitation). (8). Antimony (vacuum evaporation). (9). Indium (rubbing in). (10). Indium (vacuum

evaporation). (11). Gold (vacuum evaporation).

Page 103.

Figure 3.17 depicts basic the curves of polarizations, obtained on the apex/vertexes of hysteresis loops. In the curve of polarization it is possible to distinguish three ranges of the fields: a) the range of weak fields ($E < 0.5 \text{ kV/cm}$), where the polarization smoothly grow/rises with an increase in the field, mainly, because of the contribution of the motion of domain boundaries; b) the range of the sharp increase in the polarization, caused by implication in the process of the repolarization of basic part of the domains; c) the saturated region of polarization. From Fig. 3.17 it follows that range; b) narrowest for electrodes LiCl, while of specimen/samples with metal electrodes it is expanded, being displaced to the side of stronger fields. The expansion of this range is a characteristic feature of the weakening of nonlinear properties. The investigation logically of unipolar crystals (without preliminary polarization) showed that is most pronounced the pyroelectric effect of specimen/samples with electrodes In and Ni.

In work [2] were investigated the volt-amperes characteristic of single crystals BaTiO_3 with different electrodes, at temperatures of

200-500°C (Fig. 3.18). The character of these curves indicates the presence of rectifying contact as one of the reasons for unipolarity.

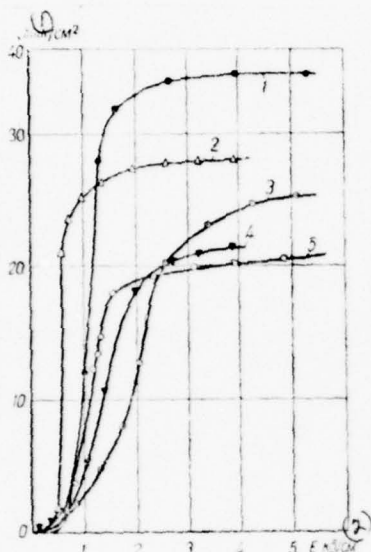


Fig. 3.17

Fig. 3.17. Curves of polarization of BaTiO_3 monocrystals with electrodes: 1- Ag (chemical precipitation); 2- LiCl ; 3- Sb (sublimation); 4- In (rubbing in); 5- Ni (sublimation)

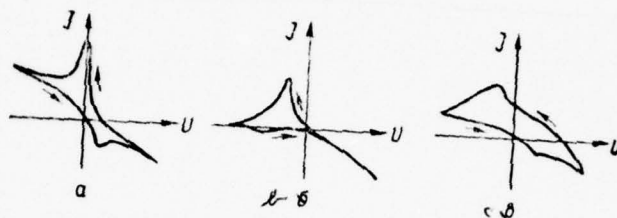


Fig. 3.18

Fig. 3.18. Volt-ampere characteristics of monocrystals with electrodes:

a - Cu - Ag ($T = 310^\circ \text{C}$); b - Ni - Ag ($T = 275^\circ \text{C}$); c - Sb - Ag ($T = 260^\circ \text{C}$).

Thus, experimental data indicate the effect of the control of physical properties of thin-layered ferroelectrics using electrodes having different work functions. Experimental curves can be qualitatively explained on the basis of a theoretical examination. From Fig. 3.15 it can be seen that in the case of ferro-

electrics with different electrodes (In-Au) the value of the maximum of the pyroelectric coefficient is considerably higher than in the case of identical electrodes (Ag-Ag) and the spreading is less. The latter is qualitatively determined by formula (3.16).

The use of electrodes with different work functions to create sensitive elements of pyroelectric receivers can be recommended to increase the sensitivity and stability of their parameters.

Page 104.

BIBLIOGRAPHY

1. Бородин В. З., Барберова Л. М., Гах С. Г., Крамаров О. П., Кременчугский Л. С., Мальнев А. Ф., Самойлов В. Б., Шолохович М. Л. — Изв. АН СССР, сер. физ., 1967, 31, 1818.
2. Бородин В. З., Гах С. Г., Крамаров О. П., Кременчугский Л. С. — УФЖ, 1969, 14, 2, 179.
3. Бородин В. З., Крамаров О. П., Кравцова С. П., Турик А. В., Янвич В. А., Дорошенко В. А. — Изв. АН СССР, сер. физ., 1969, 33, 7, 1101.
4. Бородин В. З., Гах С. Г., Крамаров О. П., Кременчугский Л. С., Ливанская Л. П., Мальнев А. Ф. — Электронная техника (материалы), 1967, сер. 14, в. 8, 141.
5. Бородин В. З. — Изв. АН СССР, сер. физ., 1965, 29, 1986.
6. Гаврилова Н. Д., Новик В. К., Кошчик В. А. — Кристаллография, 1968, 13, 6, 1088.
7. Гаврилова Н. Д. — Кристаллография, 1965, 10, 1, 114.
8. Гаврилова Н. Д. — Кристаллография, 1965, 10, 3, 346.
9. Гаврилова Н. Д., Новик В. К., Кошчик В. А., Цвилова С. В. — Изв. АН СССР, сер. физ., 1969, 33, 2, 306.
10. Гладкий В. В., Желудев И. С., Сиденко Е. В. — Изв. АН СССР, сер. физ., 1969, 23, 2, 300.
11. Гладкий В. В., Желудев И. С. — Кристаллография, 1967, 12, 5, 905.
12. Гладкий В. В., Желудев И. С. — Кристаллография, 1965, 10, 1, 63.
13. Григас Б. П. — ФТТ, 1967, 9, 8, 2430; 1967, 9, 10, 2998.
14. Гаврилова Н. Д., Новик В. К. — Вестник МГУ, сер. III, 1967, 4, 121.
15. Гавриляченко В. Г., Дудкевич В. П., Фесенко Е. Г., Лайкова А. Ю., Постриганов Е. И. — Кристаллография, 1968, 13, 1, 175.
16. Гуро Г. М., Иванчик И. И., Ковтонюк Н. Ф. — ФТТ, 1969, 11, 7, 1953.
17. Гифейсман Ш. Н. — ФТТ, 1969, 11, 8, 2097.
18. Данильчук Г. С., Ицковский М. А., Кременчугский Л. С. — УФЖ, 1969, 14, 6, 975.
19. Данильчук Г. С., Кременчугский Л. С., Мальнев А. Ф. — Изв. АН СССР, сер. физ., 1967, 31, 11, 1754.
20. Данильчук Г. С., Кременчугский Л. С. — В кн.: Новые пьезо- и сегнетоматериалы и их применение. Изд-во Рото МДНТП, М., 1969.
21. Еремеев М. А., Курчатова И. В. — ЖЭТФ, 1932, 2, 5, 329.
22. Желудев И. С., Проскурина М. А., Юрин В. А., Берберкин А. С. — ДАН СССР, 1955, 103, 207.

23. Желудев И. С., Юрин В. А.— Изв. АН СССР, сер. физ., 1956, 2, 211.
24. Желудев И. С., Гладкий В. В.— Кристаллография, 1966, 11, 3, 415.
25. Кудзин А. Ю., Гускина Л. Г., Петрушкевич И. С.— ФТТ, 1964, 6, 1, 92.
26. Кузьмин Н. И., Соловьев С. П., Вербницкая Т. Н.— ФТТ, 1967, 9, 3, 918.
27. Кузьмин Н. И., Соловьев С. П., Закуркин В. В.— Изв. АН СССР, сер. физ., 1969, 33, 2, 354.
28. Кладкевич М. Д., Кременчугский Л. С., Мальнев А. Ф.— УФЖ, 1968, 13, 4, 629.
29. Ковчик В. А., Гаврилова Н. Д.— Изв. АН СССР, сер. физ., 1965, 29, 11, 1969.
30. Кладкевич М. Д., Кременчугский Л. С.— УФЖ, 1969, 14, 5, 816.
31. Красникова А. Я., Гаврилова Н. Д., Новик В. К., Копчик В. А.— Вестник МГУ, 1968, 4, 111.
32. Кременчугский Л. С., Мальнев А. Ф., Самойлов В. Б.— В кн.: Электрические и оптические свойства диэлектриков. Изд. КПИ, К., 1966, 65.
33. Кременчугский Л. С., Самойлов В. Б.— Кристаллография, 1967, 12, 6, 1077.
34. Кременчугский Л. С., Самойлов В. Б.— УФЖ, 1968, 13, 2, 215.
35. Константинова В. П., Сильвестрова И. М., Александров К. С.— Кристаллография, 1959, 4, 125.
36. Константинова В. П., Юрин В. А.— Кристаллография, 1957, 2, 2, 294.
37. Лурье М. С., Васильева Е. И., Игнатьева И. В.— Изв. АН СССР, сер. физ., 1960, 24, 11, 1376.
38. Мелешкина В. А., Рез И. С.— Изв. АН СССР, сер. физ., 1964, 28, 4, 735.
39. Новик В. К.— Кристаллография, 1965, 10, 1, 113.
40. Пешиков Е. В., Стародубцев С. В.— Изв. АН СССР, сер. физ., 1967, 31, 11, 1759.
41. Ройтберг М. Б., Шапиро З. И., Рабинович А. З.— ФТТ, 1967, 9, 12, 3613.
42. Романюк Н. А., Пидзырайло Н. С.— Кристаллография, 1964, 9, 6, 870.
43. Ринкявичус В. С., Микалкевичус— ФТТ, 1967, 9, 10, 2997.
44. Ройтберг М. Б., Рабинович А. З., Ригерман Л. Г., Шапиро З. И., Томашпольский Ю. Я., Виневцев Ю. Н.— Неорганические материалы, 1969, 5, 1, 188.
45. Селюк Б. В.— Кристаллография, 1968, 13, 3, 447.
46. Соловьев С. П., Кузьмин Н. И., Харченко В. А.— Изв. АН СССР, сер. физ., 1967, 31, 11, 1757.
47. Сильвестрова И. М., Романюк Н. А.— Кристаллография, 1960, 5, 1, 147.
48. Шапиро З. И., Федудов С. А., Веневцев Ю. Н.— Неорганические материалы, 1967, 3, 1, 208.
49. Шолохович М. Л., Берберова Л. М., Бородин В. З., Лежгинцева Т. Н.— Изв. АН СССР, сер. физ., 1965, 29, 6, 1005; 1956, 20, 2, 215.
50. Эйслер Н. Я.— Изв. АН СССР, сер. физ., 1957, 21, 334; 1965, 29, 11, 2014.
51. Юрин В. А.— Кристаллография, 1956, 1, 6, 734.
52. Юрин В. А., Желудев И. С.— Кристаллография, 1959, 4, 2, 253.

53. Юрий В. А.—Изв. АН СССР, сер. физ., 1960, 24, 11, 1329.
54. Юрий В. А., Баберкин А. С., Корниленко Э. Н., Гаврилова Н. В.—Изв. АН СССР, сер. физ., 1960, 24, 1334.
55. Юрий В. А., Желудев И. С.—Изв. АН СССР, сер. физ., 1964, 28, 4, 726.
56. Юрий В. А.—Изв. АН СССР, сер. физ., 1965, 29, 11, 2000.
57. Юрий В. А.—Изв. АН СССР, сер. физ., 1957, 21, 329.
58. Шувалов Л. А., Рудяк В. М., Комлякова Н. С., Камарев В. Е.—Изв. АН СССР, сер. физ., 1967, 29, 11, 2007.
59. Abe R.—J. Appl. Phys., Japan, 1965, 4, 11, 906.
60. Brandwood, Hugnes O. H., Hurd J. D., Tredgold R. H.—Proc. Phys. Soc., 1962, 79, 1161.
61. Berlincourt D. A., Jaffe H., Shiozawa L. R.—Phys. Rev., 1963, 129, 3, 1009.
62. Berlincourt D. A., Cook W. R., Rauder M. E.—Acta Cryst., 1963, 16, 163.
63. Bury P. C., McLaren A. C.—Phys. Stat. Sol., 1969, 31, 2, 799.
64. Chynoweth A. G.—Acta Cryst., 1957, 10, 511.
65. Chynoweth A. G.—Phys. Rev., 1960, 117, 5, 1235; 1959, 113, 1, 159.
66. Chanoussot G., Godefroy G.—C. r. Ac. Sc., 1968, 266, 12, B793.
67. Cook W. R., Berlincourt D. A., Scholz T. J.—J. Appl. Phys., 1963, 34, 5, 1392.
68. Glower D. D., Hester D. L.—J. Appl. Phys., 1965, 36, 2175.
69. Gross B.—J. Appl. Phys., 1965, 36, 1635.
70. Guy C., Lucien G.—C. r. Ac. Sc., 1967, 265, 21, 1189.
71. Glass A. M.—Phys. Rev., 1968, 172, 2, 564.
72. Hilezer B.—Phys. Stat. Sol., 1962, 2, 4, 447.
73. Iwasaki H., Uchida N.—J. Appl. Phys., 1967, 6, 11, 1336.
74. Jimenez B., Mendiola J., Maurer E.—Phys. Stat. Sol., 1967, 19, 2, 865.
75. Janovec V., Brezina B., Glanc A.—Czech. J. Phys., 1960, 10, 9, 690.
76. Krajewski T.—Acta Phys. Polon., 1966, 30, 6, 1015.
77. Luiz A. M.—J. Appl. Phys., Japan, 1968, 8, 50.
78. Minkus W. J.—Phys. Rev., 1965, 138, A, 1277.
79. Murakami—J. Phys. Soc., Japan, 1967, 23, 457; 1968, 24, 2, 282.
80. Northrip J.—J. Appl. Phys., 1960, 31, 2293.
81. Rogers F. T.—J. Appl. Phys., 1956, 27, 9, 1066.
82. Rewajt—Acta Phys. Polon., 1964, 26, 6, (12), 1093.
83. Rice R. R., Fay H.—J. Appl. Phys., 1969, 40, 2, 909.
84. Saburi O.—J. Phys. Soc., Japan, 1959, 14, 1159.
85. Savage A., Miller R. C.—J. Appl. Phys., 1959, 30, 11, 1646.
86. Savage A.—J. Appl. Phys., 1966, 37, 8, 3071.
87. Takagi M., Suzuki S., Tanaka K.—J. Phys. Soc., Japan, 1967, 23, 1, 134.
88. Toyada H., Itakura U.—J. Phys. Soc., Japan, 1962, 17, 924.
89. Vemuri V.—Ind. J. Pure Appl. Phys., 1967, 5, 10, 484.
90. Welk H., Schneider J.—Phys. Lett. (Netherland), 1966, 19, 8, 619.
91. Wentz J. L., Kennedy L. Z.—J. Appl. Phys., 1964, 35, 6, 1767.
92. Glass A. M.—Appl. Phys. Lett., 1968, 13, 4, 147.
93. Minkus W. J.—Phys. Rev., 1963, 129, 3, 1009.

Chapter IV.

THE THEORY OF PYROELECTRIC RADIATION DETECTORS.

Page 107.

The first theory of pyroelectric radiation detectors was proposed by Cooper [9]. The author examined receiver as lumped system and gave the equivalent electrical circuit of its substitution.

The dynamic theory of pyroelectric receiver in its examination as distributed systems is described in works [1-3, 7]. To the theoretical questions of the work of pyroelectric receiver is also dedicated a series of publications [6, 8, 10].

§1. Calculation pyroelectric receiver as lumped systems.

Equivalent replacement scheme of pyroelectric radiation detector. Let us examine pyroactive crystal (Fig. 4.1) in the form of

plane-parallel plate with an area of A_0 and by thickness d .

Subsequently let us assume that the temperature in crystal does not depend on coordinate and is only function of time.

Communication/connection between induction \vec{D} , by electric field \vec{E} polarization \vec{P} (dipole moment per unit of volume) of crystal in general form can be written in the form

$$\vec{D} = \vec{E} + 4\pi\vec{P}. \quad (4.1)$$

If crystal monodomain and its polarization vector is directed along X-axis, then is current density in crystal in this direction

$$j = j_{\text{ex}} + \frac{1}{4\pi} \cdot \frac{\partial D_x}{\partial t}, \quad (4.2)$$

where $j_{\text{ex}} = \sigma_{xx}^0 E_x$ - the current density of conductivity σ_{xx}^0 - electroconductivity.

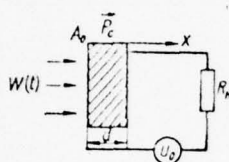


Fig. 4.1. Diagram of pyroelectric receiver.

Page 109.

In this case

$$P_x = P_{xc} + \chi_{xx} E_x, \quad (4.3)$$

where P_{xc} - the component of spontaneous polarization \vec{P}_c ; a χ_{xx} is dielectric susceptibility in direction x . (It is assumed that

$$\chi_{xy} = \chi_{xz} = 0 \text{ and } \sigma_{xy}^* = \sigma_{xz}^* = 0.)$$

The continuity condition of current requires, in order to $\text{div } j = 0$. In the case $\frac{dj}{dx} = 0$ and the current density j is

only function of time t .

From equation (4.2) taking into account equations (4.1) and (4.3) we will obtain

$$j = \sigma_{xx} E_x + \frac{1}{4\pi} \cdot \frac{\partial}{\partial t} (\epsilon_{xx} E_x + 4\pi P_{xc}), \quad (4.4)$$

where $1 + 4\pi\chi_{xx} = \epsilon_{xx} = \epsilon$.

If crystal is not connected to measuring circuit and current in external circuit is absent ($j = 0$), then

$$\sigma_{xx} E_x + \frac{1}{4\pi} \cdot \frac{\partial}{\partial t} (\epsilon E_x + 4\pi P_{xc}) = 0. \quad (4.5)$$

Let us integrate expression (4.5) with respect to the volume of the crystal:

$$A_0 \sigma_{xx} \int_0^d E_x dx + \frac{\partial}{\partial t} \left(\frac{A_0 \varepsilon}{4\pi} \int_0^d E_x dx + A_0 \int_0^d P_{xc} dx \right) = 0. \quad (4.6)$$

Let us designate $\bar{P}_c d = \int_0^d P_{xc} dx$ (\bar{P}_c - the average value of polarization in crystal; $\int_0^d E_x dx = R_{kp} i_a$ (R_{kp} - the equivalent resistance of crystal, i_a - the active component of the crystal current)). Then expression (4.6) after division into value d will take the following form:

$$\frac{\sigma_{xx} A_0}{d} R_{kp} i_a + \frac{\partial}{\partial t} \left(\frac{A_0 \varepsilon}{4\pi d} R_{kp} i_a + \bar{P}_c A_0 \right) = 0. \quad (4.7)$$

If we consider, $\frac{d}{\sigma_{xx} A_0} = R_{kp}$ and $\frac{\varepsilon A_0}{4\pi d} = C_{kp}$, then

$$i_a + R_{kp} \frac{d}{dt} (C_{kp} i_a) + \frac{d(A_0 \bar{P}_c)}{dt} = 0. \quad (4.8)$$

Numerical estimations, given below, they showed that far from Curie point value $\frac{dC_{kp}}{dt} \sim \frac{d\epsilon}{dT} \cdot \frac{dT}{dt}$ was low in view of the smallness of derivative $\frac{d\epsilon}{dT}$.

Page 109.

Pyroelectric current it is possible to write in the form

$$J_0 = - \frac{d(A_0 \bar{P}_c)}{dt}. \quad (4.9)$$

Minus sign shows that during a decrease in the value of spontaneous polarization \bar{P}_c the current grow/rises. In this case equation (4.8) is simplified:

$$i_n + R_{kp} C_{kp} \frac{di_n}{dt} = I_0. \quad (4.10)$$

Expression (4.10) corresponds to the equivalent circuit, given in Fig. 4.2a. It is possible to change from the equivalent oscillator circuit of current (see Fig. 4.2a) to the oscillator circuit of stress (see Fig. 4.2b).

Let us examine now the pyroactive crystal, connected to load resistance R_n and the external source of stress U_0 . Then it is possible to write

$$U_0 = jA_0 R_n + \int_0^d E_x dx. \quad (4.11)$$

Integrating equation (4.4) for the volume of crystal taking into account expression (4.11), we will obtain

$$dA_0j = \sigma_{xx}^2 A_0 (U_0 - jA_0 R_n) + \frac{d}{dt} \left[\frac{\epsilon A_0}{4\pi} (U_0 - jA_0 R_n) \right] + A_0 \int_0^d P_{xc} dx. \quad (4.12)$$

After designating $A_0j = \mathcal{J}$ and after dividing into thickness d , let us find

$$\mathcal{J} = \frac{\sigma_{xx}^2 A_0}{d} (U_0 - \mathcal{J} R_n) + \frac{d}{dt} \left[\frac{\epsilon A_0}{4\pi d} (U_0 - \mathcal{J} R_n) + A_0 \bar{P}_c \right]. \quad (4.13)$$

Let us write

$$\mathcal{J} = \frac{U_0}{R_{kp}} - \mathcal{J} \frac{R_n}{R_{kp}} + \frac{d(C_{kp} U_0)}{dt} - R_n \frac{d(\mathcal{J} C_{kp})}{dt} + \frac{d(A_0 \bar{P}_c)}{dt} \quad (4.14)$$

or

$$R_n \frac{d(\mathcal{T}C_{kp})}{dt} + \mathcal{T} \left(1 + \frac{R_n}{R_{kp}} \right) = \frac{d(\bar{A}_0 \bar{P}_c)}{dt} + \frac{U_0}{R_{kp}} + \frac{d(C_{kp}U_0)}{dt} \quad (4.15)$$

In steady state we will obtain

$$\mathcal{T}_0 = \frac{U_0}{R_{kp} + R_n} \quad (4.16)$$

During a change in the parameters of crystal the current changes: $\mathcal{T} = \mathcal{T}_0 + \mathcal{T}'$. After designating $\Delta V = \mathcal{T}'R_n$, from equation (4.15) taking into account relationship/ratio (4.16) let us find

$$\frac{C_{kp}d\Delta V}{dt} + \Delta V \left(\frac{1}{R_n} + \frac{1}{R_{kp}} \right) = \frac{d(\bar{A}_0 \bar{P}_c)}{dt} + (U_0 - \Delta V) \frac{dC_{kp}}{dt} \quad (4.17)$$

Expression (4.17) becomes (4.10) with $R_n \rightarrow \infty$ and $\frac{dC_{kp}}{dt} \rightarrow 0$.

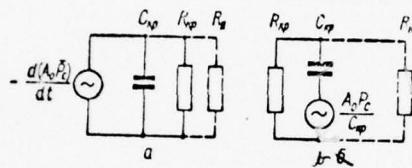


Fig. 4.2. Simplest circuit of the replacement of the pyroelectric receiver: a) the oscillator circuit of current; b) the oscillator circuit of stress.

Page 110.

The first term to the right in expression (4.17) characterizes the contribution to the value of output signal, brought about a change in the spontaneous polarization, and the second term is the contribution, bonded with capacitance change.

Relation of these contributions

$$\eta^0 = \frac{(U_0 - \Delta V) \frac{dC_{kp}}{dt}}{\frac{d(\Lambda_0 \bar{P}_c)}{dt}} = \frac{E \alpha_e}{4\pi\gamma}, \quad (4.18)$$

where $\frac{U_0 - \Delta V}{d} = E$ - electric intensity; $\gamma = \frac{dP_c}{dT}$ - pyroelectric coefficient; $\alpha_e = \frac{de}{dT}$ - the temperature coefficient of dielectric constant.

Numerical estimates of the magnitude η^0 for single crystals BaTiO₃ and TGS at electric intensity $E = 10$ kV/cm and at temperature of 300° K give the following values: $\eta_{BaTiO_3}^0 < 10^{-3}$; $\eta_{TGS}^0 \approx 2 \cdot 10^{-2}$. In the absence of the external voltage sources these values are still less. Therefore the last/latter term, which contains $\frac{dC_{kp}}{dt}$, in equations (4.9) and (4.17) can be disregarded.

The thermal design of the irradiated pyroelectric radiation detector. Let us examine the thermal processes in pyroactive crystal under the action/effect of the sinusoidally modulated radiant flux w

$(t) = W_0 (1 + e^{i\omega t})$ (where W_0 is amplitude of the radiation flux density in W/cm^2). ^PLet us assume that of all modulation frequencies the length of temperature wave greater than the thickness of crystal, but therefore temperature T in any point of crystal does not depend on coordinate, but it is only the function of time ¹.

FOOTNOTE ¹. Analogous results can be obtained, after assuming that the mean temperature of crystal T does not depend on modulation frequency. ENDFOOTNOTE.

The irradiated electrode of the crystal in question possesses absorptivity ϵ_1 . Then the equation of heat balance for a pyroactive crystal can be written thus:

$$c \frac{dT}{dt} + GT = \epsilon_1 W_0 A_0 (1 + e^{i\omega t}), \quad (4.19)$$

where c is heat capacity of crystal; G - the coefficient of heat losses.

The solution to this equation for steady conditions takes the following form:

$$T = \frac{e_1 W_0 A_0 e^{i\omega t}}{G + i\omega C} + \frac{e_1 W_0 A_0}{G}. \quad (4.20)$$

The first term of equation (4.20) characterizes the variable component of temperature increment, which directly influences signal conditioning in crystal, and the second term determines constant heating crystal.

Page 111.

Appearing during irradiation by the modulated flow pyroelectric current taking into account expression (4.20)

$$J = A_0 \frac{dP}{dt} = \gamma A_0 \frac{dT}{dt} = \frac{e_1 \gamma W_0 A_0^2 i\omega e^{i\omega t}}{G + i\omega C}. \quad (4.21)$$

Putting to use equivalent circuit (see Fig. 4.2a), let us determine

exit voltage taking into account load resistance R_n :

$$U_{\max} = \frac{i\omega\epsilon_1 R_0 W_0 A_0^2 e^{i\omega t}}{(G + i\omega C)(1 + i\omega C_0 R_0)}, \quad (4.22)$$

where $C_0 = C_{kp} + C_{nx}$ (C_{nx} - the input capacitance of measuring circuit);

$$R_0^{-1} = R_n^{-1} + R_{kd}^{-1}.$$

Expression for the volt-watt sensitivity of pyroelectric receiver will take the form

$$S = \frac{U_{\max}}{W_0 A_0} = \frac{A_0 \omega \epsilon_1 \gamma R_0 e^{i\left(\omega t + \frac{\pi}{2} - \varphi_1 - \varphi_2\right)}}{(G^2 + \omega^2 C^2)^{0.5} (1 + \omega^2 C_0^2 R_0^2)^{0.5}}, \quad (4.23)$$

where

$$\varphi_1 = \arctg \frac{C}{G} \omega; \quad \varphi_2 = \arctg \omega C_0 R_0.$$

It is possible to write

$$|S| = \frac{A_0 \omega \varepsilon_1 \gamma R_0}{(G^2 + \omega^2 c^2)^{0.5} (1 + \omega^2 C_0^2 R_0^2)^{0.5}}. \quad (4.24)$$

Let us designate relation $\frac{c}{G} = \tau_r$ and let us call/name it thermal time constant, a $C_0 R_0 = \tau_e$ by electrical time constant. Then

$$|S| = \frac{A_0 \omega \varepsilon_1 \gamma R_0}{C_0 G (1 + \omega^2 \tau_r^2)^{0.5} (1 + \omega^2 \tau_e^2)^{0.5}}. \quad (4.25)$$

Let us estimate the values of time constants τ_r and τ_e for sensing elements from single crystals of TGS and BaTiO₃. In the case when the coefficient of heat losses is determined only by emission/radiation $G = 4\varepsilon_1 \sigma_c T_0^3 A_0$ ^{and} $R_n \ll R_{np}$, it is possible to write:

$$\tau_r = \frac{c_{yd} V}{G_{изл}} = \frac{c_{yd} A_0 d}{4 (\epsilon_1 + \epsilon_2) T_0 A_0}, \quad (4.26)$$

$$\tau_r = \frac{\epsilon A_0}{4 \pi d} R_n, \quad (4.27)$$

where c_{yd} is heat capacity of unit volume.

Page 112.

At values $A_0 = 10^{-2} \text{ cm}^2$; $d = 5 \cdot 10^{-3} \text{ cm}$; $\sigma_c = 5.67 \cdot 10^{-12}$; $T = 300^\circ \text{K}$; K ; $\epsilon_1 + \epsilon_2 = 1$; $\epsilon_{\text{BaTiO}_3} = 200$; $\epsilon_{\text{TGC}} = 50$; $R_n = 10^6$ we obtain:

Материал	τ_r , ⁽¹⁾ сек	τ_r , ⁽²⁾ сек
BaTiO ₃	12	$3.5 \cdot 10^{-5}$
TGC	10	$8.8 \cdot 10^{-6}$

Key: (1) . Material. (2) . s.

In order that $\tau_r \approx \tau_n$ it is necessary to increase load resistance 10^6 times. In this case value $R_n = 10^{12} \text{ ohm}$ becomes comparable with the equivalent resistance of crystal R_{kp} at low frequencies.

Let us conduct the analysis of expression (4.25). Function $S(\omega, \tau_r, \tau_s)$ reaches the maximum value with

$$\omega_{\max} = \frac{1}{\sqrt{\tau_r \tau_s}} \quad (4.28)$$

and is equal to:

$$S_{\max} = \frac{A_0 \varepsilon_1 \gamma \tau_s}{C_0 G (\tau_r + \tau_s)} \quad (4.29)$$

Let us assume that $\tau_s = a_0 \tau_r$ with $0 \leq a_0 \leq 1$. Then

$$S = \frac{A_0 \varepsilon_1 \gamma \omega a_0 \tau_r}{C_0 G (1 + \omega^2 \tau_r^2)^{0.5} (1 + \omega^2 a_0^2 \tau_r^2)^{0.5}}; \quad (4.30)$$

$$S_{\max} = \frac{A_0 \varepsilon_1 \gamma}{C_0 G} \cdot \frac{a_0}{1 + a_0}; \quad (4.31)$$

$$\omega_{\max} = \frac{1}{\tau_r \sqrt{a_0}} \quad (4.32)$$

By putting to use equations (4.30) - (4.32), let us construct the frequency dependence of volt-watt sensitivity at four values of parameter a_0 .

The dependence of the conversion factor in unity $A_0 e_1 \gamma / C_0 G$ at the frequencies, expressed in unity $\omega \tau_L^{-1}$, is given in Fig. 4.3.

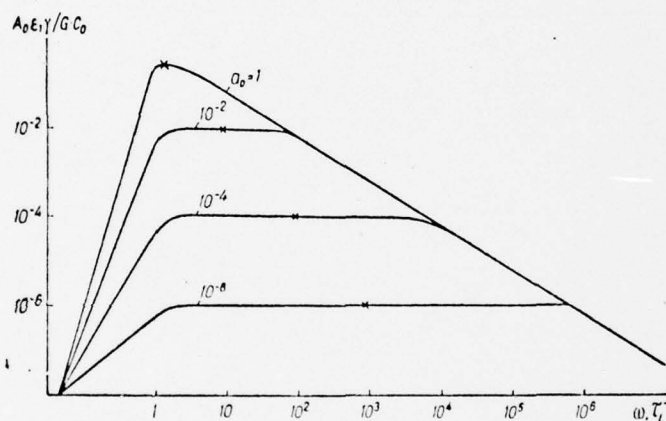


Fig 4.3. Caption next page.

Fig. 4.3. The frequency dependence of relative receiver sensitivity at the different values of parameter a_0 (angular frequency ω is expressed in unity τ^{-1}).

Page 113.

If one assumes that the noises of pyroelectric radiation detector are temperature and (possibility of the emergence of the supplementary noises, bonded with the fluctuations of polarization, will be examined below), then its threshold of response takes the following form:

$$\mathcal{P}^2 = \overline{W}_T^2 + \overline{e}_J^2 S^{-2}, \quad (4.33)$$

where

$$\overline{W}_T^2 = 4KT^2 A_0 G; \quad \overline{e}_J^2 = \frac{4KTR_0 \Delta f}{1 + \omega^2 C_0^2 R_0^2}.$$

By substituting the value $\overline{W}_T^2, \overline{e}_J^2$ and S (from equation (4.24)) in equation (4.33), we will obtain

$$\mathcal{P}^2 = 4KT^2 A_0 G + \frac{4KT\Delta / (G^2 + \omega^2 c^2)}{A_0^2 \omega^2 \epsilon_1^2 \gamma^2 R_0} . \quad (4.34)$$

If $\omega^2 c^2 \gg G^2$, then

$$\mathcal{P}^2 = 4KT^2 A_0 G + \frac{4KT\Delta / c^2}{A_0^2 \epsilon_1^2 \gamma^2 R_0} . \quad (4.35)$$

From equation (4.35) it is evident that the threshold of response of pyroelectric receiver under the made assumptions does not depend on modulation frequency, with the exception of very low frequencies.

Let us examine the work of pyroelectric receiver in pulsed operation. Under instantaneous thermal effect on crystal the equation of heat balance can be written thus:

$$c \frac{d\bar{T}}{dt} \approx e_1 A_0 W(t) \quad (4.36)$$

where $W(t)$ - the radiation flux density; \bar{T} is the mean temperature of crystal.

Then equation (4.17) taking into account (4.36) and on the assumption that $\frac{dC_{kp}}{dt} \approx \frac{dC_0}{dt} = 0$, assumes the form

$$C_0 \frac{d\Delta V}{dt} + \frac{\Delta V}{R_0} = \frac{e_1 A_0^2 \gamma}{c} W(t). \quad (4.37)$$

By integrating expressions (4.37) under the initial conditions $t = 0$ and $\Delta V = 0$, we will obtain ($C_0 = C_{kp}$)

$$\Delta V = \frac{4\pi\gamma e_1}{ec_{yA}} e^{-\frac{t}{R_0 C_0}} \int_0^t e^{\frac{\tau}{R_0 C_0}} W(\tau) d\tau. \quad (4.38)$$

We examine the limiting cases, when $R_0 C_0 \gg t_{\max}$ ^{and} $R_0 C_0 \ll t_{\min}$ ^{and} (t_{\max} ^{and} t_{\min} - the maximum and minimum duration of radiation pulse)

Page 114.

In the first case

$$\Delta V_1 = \frac{4\pi\gamma e_1}{ec_{yA}} \int_0^t W(\tau) d\tau. \quad (4.39)$$

Output signal is proportional to energy of emission impulse. If we conduct electronic differentiation, output signal will be proportional to radiant flux:

$$\frac{d\Delta V_1}{dt} = \frac{4\pi\gamma e_1}{\epsilon c_{y\lambda}} W(t). \quad (4.40)$$

If the time constant of input circuit is low ($R_0 C_0 \ll t_{\min}$), expression (4.38) is simplified:

$$\Delta V_2 = \frac{4\pi\gamma e_1}{\epsilon c_{y\lambda}} W(t) R_0 C_0. \quad (4.41)$$

Relationship/ratios (4.³⁹~~38~~) and (4.41) determine two very important mode/conditions of the work of pyroelectric receiver - the mode of the measurement of energy of momentum/impulse/pulse ($R_0 C_0 \gg t_{\max}$) and the mode/conditions of the measurement of its power ($R_0 C_0 \ll t_{\min}$).

§2. Dynamic theory of pyroelectric radiation detector.

The developed in the preceding/previous paragraph theory did not explain the reason for the rapid response of pyroelectric receiver. By considering pyroelectric receiver as system with distributed parameters, it is possible to rate/estimate its cut-off frequencies.

Determination of the sensitivity of pyroelectric receiver. Let us examine the pyroelectric receiver, sensing element of which consists of pyroactive crystal 2, covered from the irradiated side with absorbing layer (black) 1, and basis/base 3, to which is fastened the crystal (Fig. 4.4). The polarization vector of crystal \vec{P} is directed along y axis, perpendicular to the irradiated surface.

During irradiation of crystal by radiation flux the temperature in the arbitrary point of the crystal

$$T(y, t) = T_0 + \Theta(y, t), \quad (4.42)$$

where T_0 is temperature of crystal to irradiation; $\Theta(y, t)$ - temperature increment during irradiation.

Let the operating temperature of crystal T_0 to irradiation be close to Curie point T_K $[(T_K - T_0) = (1-5)^\circ\text{C}]$.

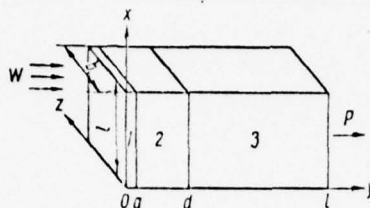


Fig. 4.4. Circuit of sensing element of the pyroelectric receiver: 1 - black; 2 - pyroactive crystal; 3 - basis/base.

Page 115.

If the crystal is ferroelectric with second order phase transition, for example single crystal TGS, then its pyroelectric coefficient according to expression (2.16) is written:

$$\gamma(T) = - \sqrt{\frac{\pi}{C_K \xi (T_K - T)}}, \quad (4.43)$$

where C_K and ξ are constants for this crystal. Pyroelectric coefficient taking into account expression (4.42), if we disregard the terms of the second and of the higher orders of smallness, it is possible to present in the following form:

$$\begin{aligned} \gamma(T) &= - \sqrt{\frac{\pi}{C_K \xi (T_K - T_0) \left(1 - \frac{\Theta(y, t)}{T_K - T_0}\right)}} = \\ &= \gamma(T_0) \left[1 + \frac{\Theta(y, t)}{2(T_K - T_0)}\right], \end{aligned} \quad (4.44)$$

where

$$\gamma(T_0) = - \sqrt{\frac{\pi}{C_{K5}(T_K - T_0)}}.$$

Pyroelectric current, which appears in any element of crystal $\delta x \cdot \delta y \cdot \delta z$,

$$i(y) = \delta x \cdot \delta z \gamma(T) \frac{d\Theta(y, t)}{dt}, \quad (4.45)$$

a average current in elementary rectangular prism $\delta x \cdot \delta z \cdot d$

$$\bar{i} = \frac{\delta x \cdot \delta z}{d} \int_0^d \gamma(T) \frac{d\Theta(y, t)}{dt} dy. \quad (4.46)$$

Then the total pyroelectric current of the crystal

$$J = \frac{\gamma(T_0) bl}{d} \int_0^d \left[1 + \frac{1}{2} \frac{\Theta(y, t)}{T_K - T_0} \right] \frac{d\Theta(y, t)}{dt} dy, \quad (4.47)$$

where l , b , d - respectively length, the width and the thickness of crystal.

The irradiation of crystal by the modulated flow leads not only to the emergence of pyroelectric current, but also to a change in the capacity of crystal due to critical dependence of dielectric constant ϵ on temperature. If the capacity of the irradiated crystal is presented in the form of the infinite number of series-connected condenser/capacitors with surface bl and thickness Δy in so small that within its limits value $\epsilon[T(y, t)]$ remains constant/invariable, then it is possible to write

$$C(T) = bl/4\pi \int_0^d \frac{dy}{\epsilon[T_0 + \Theta(y, t)]}, \quad (4.48)$$

where

$$\epsilon [T_0 + \Theta(y, t)] \approx \epsilon(T_0) + \frac{d\epsilon(T_0)}{dT} \Theta(y, t). \quad (4.49)$$

Page 116.

After using value for $\epsilon(T_0)$, let us write expression (4.48) in the form

$$C(T) \approx b\epsilon(T_0)/4\pi \int_0^d \left[1 - \frac{\Theta(y, t)}{T_K - T_0} \right] dy. \quad (4.50)$$

The conversion conducted is correct, when $T_K - T_0 > \Theta$.

The equivalent replacement scheme of the pyroelectric receiver, which works near Curie point, is represented in Fig. 4.5. From equivalent circuit it follows that stress U on load resistance R_n ($R_{kp} \gg R_n$) takes form $U = \mathcal{T}R_n / 1 + i\omega[C_{px} + C(T)]R_n$. After using formulas (4.47), (4.50) and (4.51), we will obtain for the volt-watt

sensitivity $S = U/Wble^{i\omega t}$ the following expression:

$$S = \frac{\gamma(T_0) R_u \int_0^d \left[1 + \frac{1}{2} \cdot \frac{\Theta(y, t)}{T_K - T_0} \right] \frac{d\Theta(y, t)}{dt} dy}{W_0 \left\{ 1 + i\omega R_u \left[C_{BX} + \frac{ble(T_0)}{4\pi \int_0^d \left[1 - \frac{\Theta(y, t)}{T_K - T_0} \right] dy} \right] \right\} e^{i\omega t}} \cdot (4.52)$$

Expression for the Johnson noises of pyroelectric receiver can be written thus:

$$V_{\bar{e}_J}^2 = (4KT\Delta f R_u)^{0.5} \left(1 + \omega^2 R_u^2 \left\{ \frac{ble(T_0)}{4\pi \int_0^d \left[1 - \frac{\Theta(y, t)}{T_K - T_0} \right] dy} \right\}^2 \right)^{0.5} \cdot (4.53)$$

Then the threshold of response of the pyroelectric receiver whose noises in essence Johnson, let us write in the form

$$\mathcal{P} = \frac{V_{e_j}^2}{S} = (4KT\Delta f)^{0.5} W_0 d/\gamma(T_0) R_n^{0.5} \int_0^d \left[1 + \frac{1}{2} \cdot \frac{\Theta(y, t)}{T_K - T_0} \right] \frac{d\Theta(y, t)}{dt} dy. \quad (4.54)$$

For obtaining concrete results it is necessary to determine value $\Theta(y, t)$.

The thermal design of pyroelectric receiver.

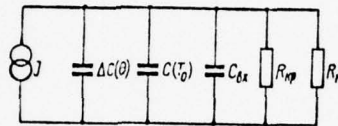


Fig. 4.5. The equivalent replacement scheme of the pyroelectric receiver: γ is a generator of pyroelectric receiver; $\Delta C(\theta)$ - a change in the capacity of crystal during irradiation; $C(T_0)$ - the capacity of crystal before irradiation; R_{kp} is the equivalent resistance of the losses of crystal; R_n - load resistance.

Page 117.

If the thickness of crystal d considerably shorter than its length l width b , it is possible to disregard heat losses from the lateral faces. Then the solution to the equation of the thermal conductivity of the heated by irradiation vacuum receiver comes to the one-dimensional case.

For determining temperature increment in each point of the crystal (see Fig. 4.4) is necessary to solve the equations of thermal conductivity for all three ranges of receiver (black - crystal - basis/base)

$$\frac{\partial \Theta_n(y, t)}{\partial t} = \frac{k_n}{c_n} \cdot \frac{\partial^2 \Theta_n(y, t)}{\partial y^2} \quad (4.55)$$

under following boundary conditions:

$$\begin{aligned} - \left[\frac{\partial \Theta_1(y, t)}{\partial y} \right]_{y=0} + h_1 [\Theta_1(y, t)]_{y=0} &= \frac{W_0}{k_1} (1 + e^{i\omega t}); \\ [\Theta_1(y, t)]_{y=a} &= [\Theta_2(y, t)]_{y=a}; \\ k_1 \left[\frac{\partial \Theta_1(y, t)}{\partial y} \right]_{y=a} &= k_2 \left[\frac{\partial \Theta_2(y, t)}{\partial y} \right]_{y=a}; \\ [\Theta_2(y, t)]_{y=d} &= [\Theta_3(y, t)]_{y=d}; \quad [\Theta_3(y, t)]_{y=l} = 0; \\ \left[\frac{\partial \Theta_2(y, t)}{\partial y} \right]_{y=d} + h_2 [\Theta_2(y, t)]_{y=d} &= \frac{k_3}{k_2} \left[\frac{\partial \Theta_3(y, t)}{\partial y} \right]_{y=d}. \end{aligned} \quad (4.56)$$

In equations (4.55) and (4.56) are used the following designations: k_n is a coefficient of thermal conductivity; c_n - the heat capacity of unit volume. Index n means that the values pertain respectively to ranges 1, 2 or 3; $h_n = 4\sigma_c \epsilon_n T_0^3 / k_n$; ϵ_1 ^{and} ϵ_2 the absorptivity of black and crystal; σ_c - is constant of stefana -

Eoltzmann; ω - cyclic modulation frequency; $i = \sqrt{-1}$; $W_0(1 + e^{i\omega t})$ - the sinusoidally modulated radiation flux.

The solution to equation (4.55) let us search for in the form

$$\Theta_n(y, t) = \varphi_n(y) + \chi_n(y) e^{i\omega t}, \quad (4.57)$$

where first term it is solution for the time-constant component of temperature increment, and the second - for a variable.

Page 118.

If one assumes that the emission/radiation is absorbed evenly by all volume of black (this equivalent $a \rightarrow 0$), we will obtain the temperature distribution in pyroactive crystal [3]:

$$\begin{aligned}
\Theta_2(y, t) = & \frac{\epsilon_1 W_0 b l \{ (d-y) [k_3 + h_2 k_2 (l-d)] + k_2 (l-d) \}}{\{ k_3 (k_2 b l + 4 \epsilon_1 \sigma_C T_0^3 b l d) + k_2 [4 \epsilon_1 \sigma_C T_0^3 b l d + \\
& + h_2 (4 \epsilon_1 \sigma_C T_0^3 b l d + k_2 b l) (l-d) \}} + \\
& \frac{\epsilon_1 W_0 b l \operatorname{ch} \eta (d-y) \{ \operatorname{th} \eta (d-y) [\eta + H h_2 \operatorname{th} \psi (l-d)] + \\
& + H \eta \operatorname{th} \psi (l-d) \} e^{i \omega t}}{\operatorname{ch} \eta d \{ k_2 b l \eta [\eta + H h_2 \operatorname{th} \psi (l-d) + H \eta \operatorname{th} \psi (l-d) \operatorname{th} \eta d] + \\
& + (4 \epsilon_1 \sigma_C T_0^3 b l + i \omega c_0) [\operatorname{th} \eta d (\eta + H h_2 \operatorname{th} \psi (l-d) + H \eta \operatorname{th} \psi (l-d))] \}} , \quad (4.58)
\end{aligned}$$

where $\eta = (1+i) \sqrt{\omega c_2 / 2k_2}$; $\psi = (1+i) \sqrt{\omega c_3 / 2k_3}$; $\frac{2k_n}{\omega c_n} = \lambda_n$ - the length of temperature wave; $H = (k_2 c_2 / k_3 c_3)^{0.5}$; c_0 - the heat capacity of black.

First term in expression (4.58) determines time-constant, and the second - the variable component of the increment of temperature. Obtained expression (4.58) is complex and for a series of special cases can be simplified.

Let us examine the construction of pyroelectric radiation detector, at whose sensing element is located in vacuum and is fastened during very fine/thin suspensions, so that losses to thermal conductivity through suspensions can be disregarded. In this case $k_3 = 0$ and expression (4.58) assumes the form

$$\begin{aligned} \theta_1(y, t) = & \frac{e_1 W_0 [1 + h_2 (d - y)]}{4\sigma_C T_0^3 (e_1 + e_2)} + \\ & + \frac{e_1 W_0 e^{i\omega t} \left[\frac{h_2}{\eta} \operatorname{sh} \eta (d - y) + \operatorname{ch} \eta (d - y) \right]}{k_2 \eta \operatorname{ch} \eta d \left(\frac{h_2}{\eta} + \operatorname{th} \eta d \right) \left[1 + \right.} \\ & \left. + \frac{(4e_1 \sigma_C T_0^3 b l + i\omega c_0) \left(1 + \frac{h_2}{\eta} \operatorname{th} \eta d \right) \right]}{k_2 b l \eta \frac{h_2}{\eta} + \operatorname{th} \eta d} \Bigg] \end{aligned} \quad (4.59)$$

By substituting expression (4.59) in equation (4.47), it is possible to find the total pyroelectric receiver current of the

emission/radiation, which works in vacuum, and then, by utilizing equation (4.52), to obtain expression for a volt-watt sensitivity. The obtained expression sufficiently cumbersome and therefore is not given. However, for the procedurally important cases, when

$$i\omega R_n C(T) \gg 1; \quad C(T) \gg C_{nx}$$

and

$$|4e_1 \sigma_c T_0^3 b l + i\omega c_0 / k_2 b l \eta| \ll 1,$$

O. V. Roytsinoy [3] obtained expression for the volt-watt sensitivity

$$S = \frac{4\pi e_1 \gamma (T_0)}{i\omega c_0 b l e (T_0)} \left(\frac{h_2 + \eta \operatorname{th} \eta d - h_2 \operatorname{sch} \eta d}{h_2 + \eta \operatorname{th} \eta d} + B_1 + B_2 \right) (1 - \Gamma_1 - \Gamma_2), \quad (4.60)$$

where

$$B_1 = \frac{e_1 W_0 [\operatorname{th} \eta d (\eta^2 + \eta^2 d - h_2^2) + d h_2^2 \eta^2]}{8 (T_K - T_0) \sigma_c T_0^3 (e_1 + e_2) (\eta h_2 + \eta^2 \operatorname{th} \eta d)};$$

$$B_2 = \frac{e_1 W_0 e^{i\omega t}}{4 (T_K - T_0) k_2 \eta} \left[\frac{\operatorname{th} \eta d (\eta^2 + h_2^2) + 2h_2 \operatorname{th}^2 \eta d + \eta d (\eta^2 - h_2^2) \operatorname{sch}^2 \eta d}{(h_2 + \eta \operatorname{th} \eta d)^2} \right];$$

$$\Gamma_1 = \frac{e_1 W_0}{4\sigma_c T_0^3 (e_1 + e_2) (T_K - T_0)}; \quad \Gamma_2 = \frac{e_1 W_0 e^{i\omega t} (\eta \operatorname{th} \eta d + h_2 - h_2 \operatorname{sch} \eta d)}{(T_K - T_0) d c_2 i \omega (\eta \operatorname{th} \eta d + h_2^2)}.$$

Page 119.

The coefficients B_1 , B_2 , G_1 and G_2 caused by temperature dependence of pyroelectric coefficient γ and of dielectric constant characterize the nonlinearity of vacuum pyroelectric receiver. This nonlinearity the greater, the nearer to critical temperature is selected the operating point of receiver.

Let us examine the case, when pyroelectric crystal is mounted on the solid basis/base whose thickness is much greater than the length of temperature wave $(l-d) \gg \lambda_3$. Then, assuming that $h_2 = 0$, $k_2 \gg 4\epsilon_1 \sigma_C T_0^3 [d + k_2(l-d)/k_3]$ ^{and} $|(4\epsilon_1 \sigma_C T_0^3 b l + i\omega c_0) / k_2 b l \eta| \ll 1$ equation (4.58), we will obtain from equation (4.52)

$$S = \frac{\gamma(T_0) \epsilon_1 R_{II} \left[\frac{1 + H \operatorname{th} \eta d - \operatorname{sch} \eta d}{\operatorname{th} \eta d + H} + N_1(\gamma) + N_2(\gamma) \right]}{c_2 d [1 + i\omega R_{II} (C_{BX} + C(T_0)/l - M_1(e) - M_2(e))]}, \quad (4.6)$$

where

$$N_1(\gamma) = \frac{\epsilon_1 W_0 d}{2(T_K - T_0) k_2} \left[1 + \frac{k_2(l-d) \operatorname{th} \eta d \left(H + \operatorname{th} \frac{\eta d}{2} \right)}{k_3 d (1 + H \operatorname{th} \eta d)} - \frac{\operatorname{th} \eta d \left(1 + H \operatorname{th} \frac{\eta d}{2} \right)}{\eta d (1 + H \operatorname{th} \eta d)} \right];$$

$$N_2(\gamma) = \frac{\{\epsilon_1 W_0 e^{i\omega t} [\operatorname{th} \eta d - d \eta \operatorname{sch}^2 \eta d + H^2 (\operatorname{th} \eta d + d \eta \operatorname{sch}^2 \eta d + 2H(1 - \operatorname{sch}^2 \eta d))]\}}{4(T_K - T_0) k_2 \eta (1 + H \operatorname{th} \eta d)^2};$$

$$M_1(e) = \frac{\epsilon_1 W_0 [k_3 d + 2k_2(e-d)]}{2k_2 k_3 (T_K - T_0)};$$

$$M_2(e) = \frac{\epsilon_1 W_0 \left(H + \operatorname{th} \frac{\eta d}{2} \right) \operatorname{th} \eta d e^{i\omega t}}{(T_K - T_0) i\omega c_2 d (1 + H \operatorname{th} \eta d)}.$$

Coefficients $N_1(\gamma)$, $N_2(\gamma)$, $M_1(\epsilon)$ and $M_2(\epsilon)$ characterize an increase in the pyroelectric current and capacity of crystal due to temperature dependence γ and ϵ near Curie point. Numerical estimation for the receiver, prepared from the single crystal of TGS 10^{-2} cm. thickness and strengthened to copper basis/base by thickness $2 \cdot 10^{-1}$ cm., it showed that formula (4.61) was valid during the assigned simplifications in the range of frequencies 0.04-20000 Hz.

Page 120.

In this case for $W_0 \leq 10^{-3}$ W/cm² of value $N_1(\gamma)$, $N_2(\gamma)$, $M_1(\epsilon)$ and $M_2(\epsilon)$ on several orders are less than unity. Therefore in the frequency band

$$S = \frac{\gamma(T_0) e_1 R_n \left| \frac{1 + H \operatorname{th} \eta d - \operatorname{sch} \eta d}{\operatorname{th} \eta d + H} \right|}{c_2 d \{1 + i \omega R_n [C_{0x} + C_0(T)]\}} \quad (4.62)$$

From equation (4.62) for a frequency region $20 \cdot 10^3$ Hz at the length of temperature wave in crystal $\lambda_2 \ll d$ ($\eta d \gg 1$) we will obtain

376

$$S_{\lambda, < d} = \frac{\gamma(T_0) \epsilon_1 R_H}{c_2 d (1 + i\omega R_H [C_{nx} + C(T_0)])}, \quad (4.63)$$

since $\text{th } \eta d \rightarrow 1$, as $\text{sch } \eta d \rightarrow 0$. For infra-low modulation frequencies (0.04-2 Hz) at the length of temperature wave $\lambda_2 \gg d$ ($\eta d \ll 1$) equation (4.62) acquires the following form:

$$S_{\lambda, > d} = \frac{(1 + i) \gamma(T_0) \epsilon_1 R_H \sqrt{\omega}}{\sqrt{2k_2 c_2} (1 + i\omega R_H [C_{nx} + C(T_0)])} \quad (4.64).$$

At very low modulation frequencies ($\omega R_H [C_{nx} + C(T_0)] \ll 1$) expression (4.64) is simplified:

$$|S_{\lambda, d}| = \frac{\gamma(T_0) \epsilon_1 R_{11} \sqrt{\omega}}{\sqrt{k_2 c_2}} \quad (4.65)$$

Volt-watt sensitivity in a low-frequency range inversely proportional to square root on cyclic modulation frequency and does not depend on the thickness of crystal.

Pyroelectric receivers of the longitudinal and cross types. Let us examine in more detail of two forms of pyroelectric receivers - the longitudinal type, whose radiation flux is parallel or antiparallel to the direction of the spontaneous polarization of crystal, and cross, at whose radiation flux is perpendicular to the direction of spontaneous polarization (Fig. 4.6).

In working frequency band above 20 Hz for crystals with the thickness of sensing element, greater than 50 μ , equation (4.59) for the temperature increment of a crystal under the action/effect of the modulated radiant flux is simplified.



Fig. 4.6. Caption next page.

Fig. 4.6. Pyroelectric receivers: a) the longitudinal type; b) cross type.

Page 121.

In this case $\eta d \gg 1$, $\tanh \eta d$ is close to unity.

Equation (4.59) takes the following form:

$$\begin{aligned} \Theta_2(y, t) = & \frac{\epsilon_1 W_0 [1 + h_2 (d - y)]}{4\sigma_C T_0^3 (\epsilon_1 + \epsilon_2)} + \\ & + \frac{\epsilon_1 W_0 e^{i\omega t} \left[\frac{h_2}{\eta} \operatorname{sh} \eta (d - y) + \operatorname{ch} \eta (d - y) \right]}{k_2 h_2 \operatorname{ch} \eta d \left[1 + \frac{4\epsilon_1 \sigma_C T_0^3 b l + i\omega c_0}{k_2 b i \eta} \right]}. \end{aligned} \quad (4.66)$$

Expression (4.66) is correct for both types of pyroelectric radiation detectors. But relationship/ratios for pyroelectric currents are different. Pyroelectric current, which appears in volume

element $\delta x \cdot \delta z \cdot d$, one and the same for two forms of receivers. However, of longitudinal type pyroelectric receiver the currents, removed from elementary volumes along face b , are connected in parallel (combined), and for cross type receiver the currents, removed from volume elements along this same face, are connected in series. Along face b the currents of volume elements in both cases store/add up. If pyroelectric receiver works far from Curie point $\left(\frac{\theta_s(y, t)}{T_K - T_s} \ll 1\right)$ ^{approximation} for the volt-watt sensitivity of longitudinal type pyroelectric receiver, obtained from formula (4.52), takes the form

$$S_{np} = \frac{\gamma \epsilon_1 R_n}{c_2 d (1 + i\omega C'_0 R_n) \left[1 + \frac{4\epsilon_1 \sigma_C T_0^3 + i\omega C'_0}{k_2 \lambda} \right]}, \quad (4.67)$$

where $C'_0 = c_0/bd$, $C_0 = C_{nx} + C_{kp}$.

The experimental studies showed that in work lower than the Curie point the noises of ferroelectric were close to their Johnson noises. Then expression for a threshold of response in accordance with equation (4.33) can be written thus:

$$\mathcal{P}_{rp} = \sqrt{\frac{4KT\Delta f}{R_{11}}} \cdot \frac{c_2 d \left[1 + \frac{4\epsilon_1 \sigma_C T_0^3 + i\omega c_0'}{k_2 \eta} \right]}{\epsilon_1 \gamma}. \quad (4.68)$$

Expression for the complex volt-watt sensitivity of cross type pyroelectric receiver (see Fig. 4.6b):

$$S_{non} = \frac{\gamma \epsilon_1 R_{11}}{c_2 b (1 + i\omega c_0' R_{11}) \left[1 + \frac{4\epsilon_1 \sigma_C T_0^3 + i\omega c_0'}{k_2 \eta} \right]}, \quad (4.69)$$

a threshold of response it will be written as

$$\mathcal{P}_{non} = \sqrt{\frac{4KT\Delta f}{R_{11}}} \cdot \frac{\left[1 + \frac{4\epsilon_1 \sigma_C T_0^3 + i\omega c_0'}{k_2 \eta} \right] c_2 b}{\epsilon_1 \gamma}. \quad (4.70)$$

Page 122.

The comparison of the constructions of pyroelectric detectors of the emission/radiation of the longitudinal and cross types with identical crystals let us conduct by the estimation of their thresholds of sensitivity.

From equations (4.68) and (4.70) it follows:

$$\frac{\mathcal{P}_{np}}{\mathcal{P}_{non}} = \frac{d}{b}. \quad (4.71)$$

Since virtually $d \ll b$, the threshold of response of longitudinal type pyroelectric receiver is always better than cross one.

The volt-watt receiver sensitivity of longitudinal type when $\omega C_0 R_n \ll 1$ and $\omega C_0 R_n \ll 1$, is higher than cross

$$\frac{S_{np}}{S_{non}} = \frac{b}{d}. \quad (4.72)$$

With $\omega C_0 R_n \gg 1$ and $\omega C_0 R_n \gg 1$ we will obtain

$$\frac{S_{np}}{S_{non}} = \frac{\left(C_{nx} + \frac{eld}{4\pi b}\right)b}{\left(C_{nx} + \frac{ebl}{4\pi d}\right)d}. \quad (4.73)$$

If we input capacitance C_{px} is considerably less than the self-capacitance of crystal for two types of receivers, then

$$\frac{S_{np}}{S_{non}} = \frac{d}{b}. \quad (4.74)$$

Relationship/ratio (4.74) conversely to relationship (4.72). This is explained themes that during transition from the longitudinal type of receiver to cross under the conditions pointed out above a decrease in the pyroelectric current is proportional to ratio d/b , and by a decrease in capacity d^2/b^2 . Therefore the volt-watt receiver sensitivity of cross type is theoretically higher than longitudinal one, if $C_{nx} = 0, \omega C_0 R_n \gg 1$ and $\omega C_0 R_n \gg 1$.

With utilized in real constructions sensing elements 50-500 μ thickness the capacity of cross type receiver is very small $C_{nx} \approx (0,5 \div 5)$ ($10^{-1} \sim 10^{-3}$ pF) in comparison with the capacity of input device \wedge pF. In connection with this relationship/ratio (4.73) takes the form

$$\frac{S_{np}}{S_{non}} \approx \frac{C_{nx}}{\frac{el}{4\pi}}. \quad (4.75)$$

Is concealed by form, in real developments the receiver sensitivity of longitudinal type higher than cross one. Furthermore, technology of receivers with end electrodes is more complex, since transverse before blackening it is necessary to the irradiated crystal boundary to apply separating dielectric layer [4].

Page 123.

In this case grow/rises specific heat capacity of the irradiated electrode c_0'' in comparison with heat capacity c_0' . However as it will be said on its own absorption without the application/use of a black are less inertia, than longitudinal type receivers.

Analysis of the basic parameters of pyroelectric receivers. Let us characterize (see Chapter I, §1) the inertness of pyroelectric detector of cut-off frequency $f_{0.5}$, at which its threshold of response grow/rises double in comparison with the minimum threshold by low frequencies. From equation (4.68) we obtain

$$\left| 1 + \frac{4\epsilon_1\sigma_C T_0^3 + i\omega\epsilon_0'}{k_1\eta} \right| = 2. \quad (4.76)$$

Hence under condition $\omega\epsilon_0' \gg 4\epsilon_1\sigma_C T_0^3$ we find simple expression for

AD-A046 669

FOREIGN TECHNOLOGY DIV WRIGHT-PATTERSON AFB OHIO

F/G 17/5

FERROELECTRIC RADIATION DETECTORS, (U)

JUL 77 L S KREMENCHUGSKIY

FTD-ID(RS)T-0846-77

NL

UNCLASSIFIED

4 OF 6
ADA
046669



cut-off frequency $f_{0.5}$:

$$\left(\frac{2\pi f_{0.5}}{c_0 k_2} \right)^{0.5} c_0 \sim 1. \quad (4.77)$$

The frequency dependence of threshold of response \mathcal{P} (and also the volt-watt sensitivity with $\omega C_0 R_u \ll 1$) will be noticeably exhibited, when the complete thermal conductivity of the irradiated electrode \wedge $(4\pi\sigma_C T_0^3 + i\omega c_0)$

becomes comparable with the complete thermal conductivity of part of the crystal $k_2\eta$, to which it penetrates thermal wave.

As said in chapter I, §1, heat radiation detectors it is accepted to characterize by time constant $\tau_{ep} = \sqrt{3/2\pi} f_{0.5}$. If the heat capacity of the irradiated electrode is decreased down to the heat capacity of gold black, so that $c_0 = 2.5 \cdot 10^{-5} \text{ J/deg}\cdot\text{cm}^2$ [5], then the computed value of the time constant of receiver τ_{ep} will be 10^{-7} s .

The analysis of the threshold of response of pyroelectric radiation detector of formulas (4.68) and (4.70) makes it possible to draw the conclusion that for a reduction in the value of threshold of response it is necessary to select pyroactive material with the minimum value of ratio c_2/γ , to prepare sensing elements of the minimum thickness d , and also to utilize in load circuit the maximum values of resistance R_H . If the equivalent resistance of the losses of pyroactive crystal R_{kp} considerably greater load resistance R_H ($R_{kp} \gg R_H$),

the threshold of response of pyroelectric detector does not depend on modulation frequency into sufficiently wide frequency band, as long as $\left| \frac{4\epsilon_1\sigma_C T_0^3 + i\omega\epsilon_0'}{k_2\eta} \right| < 1$ (see 4.68) and the noises of measuring device less than noises of detector, and also does not depend on the value of the receiving area/site b_1 .

Page 124.

As the criterion of the quality of pyroactive material in this case serves value

$$M_{R_{kp} > R_H} = \frac{\gamma(d)}{c_2}. \quad (4.78)$$

Since during transition to thin layers pyroelectric coefficient becomes the function of the thickness of crystal, the maximum of the criterion of quality is caused by the maximum of ratio $\gamma(d)/d$.

If the equivalent resistance of losses R_{kp} of pyroactive crystal becomes lower than the load resistance R_H , then the threshold of response of receiver will express by the formula, similar to relationship/ratio (4.68), in which value R_H is replaced by value R_{kp} . After accepting into consideration, that $R_{kp} = (\omega C_{kp} \operatorname{tg} \delta)^{-1}$, we will obtain (when the capacity of detector is described by formula for a parallel-plate capacitor)

$$\mathcal{P}_{np} = \sqrt{\frac{KT\Delta f \omega \epsilon b l \operatorname{tg} \delta \cdot d}{\pi}} \cdot \frac{c^2}{\epsilon_1 \gamma} \left[1 + \frac{4\epsilon_1\sigma_C T_0^3 + i\omega\epsilon_0'}{k_2\eta} \right]. \quad (4.79)$$

In this case the threshold of response of receiver depends on the modulation frequency ω , of size/dimensions of the receiving area b_l , of dielectric loss angle $\text{tg} \delta$ and of dielectric constant ϵ . The criterion of the quality of material is value

$$M_{R_{\text{kp}} < R_n} = \frac{V}{c_2 (\epsilon \text{tg} \delta)^{0.5}} \quad (4.80)$$

During irradiation of pyroelectric receiver by powerful radiation fluxes occurs the displacement of operating point. Expression for the average constant value component of the temperature increment of pyroelectric detector on solid base at sinusoidally the modulated flow according to formula (4.58) takes the form

$$\Theta_{\text{avr}} = \frac{\epsilon_1 W_0 \left| \frac{d}{2} + \frac{k_2}{k_3} (l-d) \right|}{k_2 + 4\epsilon_1 \sigma_0 T_0^3 \left| h + \frac{k_2}{k_3} (l-d) \right|} \quad (4.81)$$

For the vacuum receiver

$$\Theta_{\text{ввк}} = \frac{\epsilon_1 W_0 \left| 1 + \frac{h_2 d}{2} \right|}{4\sigma_c T_0^3 (\epsilon_1 + \epsilon_2)} \quad (4.82)$$

Under the pulse influence on crystal, the temperature of the irradiated surface is bonded with radiation flux by following relationship/ratio [9]:

$$\Theta_{\text{нмп}} = \frac{d}{c_2 (\pi k_2)^{0.5}} \int_0^t \frac{W(\tau) d\tau}{(t-\tau)^{0.5}} \quad (4.83)$$

By knowing the experimental dependence of pyroelectric coefficient γ and of dielectric constant ϵ on temperature, it is possible to find the half-breadths of the temperature intervals, in which a change in the parameters does not exceed $\pm 50\%$.

Page 125.

After determining thus value $\Theta_{\text{нмп}}$, it is possible according to equations (4.81); (4.83) to rate/estimate the value of the maximum radiant flux W_{max} , at which the disturbance/breakdown of linearity it does not exceed the assigned value.

The amplitude and frequency characteristics of the volt-watt sensitivity of the pyroelectric receiver S depend on the value of load resistance and circuit diagram. In connection with this it is presented by the more rational introduction of another conversion factor - the ampere-watt sensitivity, which does not depend on this

$$S_a = \frac{J}{W_0 b l e^{i\omega t}} \quad (4.84)$$

Expression for the total pyroelectric receiver current can be obtained from equations (4.47) and (4.58) / far from Curie point, when length as the temperature of wave λ_2 is considerably less than the thickness of crystal $d(\lambda_2 \ll d)$, this expression takes the sufficiently simple form, and the ampere-watt sensitivity

$$S_a = \frac{e_1 \gamma}{c_2 d \left[1 + \frac{4e_1 \sigma_c T_0^3 + i\omega c_0}{k_2 \eta} \right]} \quad (4.85)$$

The pyroelectric receiver current J is complex function of the physical characteristics of crystal, its geometric dimensions and conditions of heat exchange of crystal with the environment. Value J is form/shaped under the action/effect of two basic factors - the value of the average temperature increment of the sensitive element of receiver and rate of change in the temperature increment.

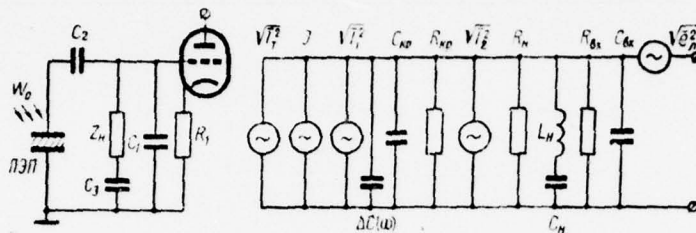


Fig. 4.7. The complete equivalent replacement scheme of the pyroelectric detectors: PEP - pyroelectric receiver; Z_H - the complex resistance of load; R_1 - the resistance of the matching cascade/stage; I - the generator of pyroelectric current V_T^2 , $V_{I_1}^2$, $V_{I_2}^2$ - the equivalent generators of noise current, caused by temperature fluctuations by the Johnson fluctuations of crystal and input circuit respectively; $V_{I_3}^2$ - the equivalent voltage generator of the noises of the measuring device, led to the grid of input time; C_1 - C_3 are capacities for a tuning into resonance in work with inductive load.

Page 126.

The average temperature increment of the pyroelectric receiver of as

any other thermal receiver, inversely proportional to the frequency of modulation, but the rate of its change directly proportional to modulation frequency. The action/effect of these two factors is balanced into sufficiently wide frequency interval. Of this consists qualitative explanation of the rapid response of pyroelectric detector in comparison with other heat radiation detectors.

The uniformity of the frequency characteristic of pyroelectric receiver is disturbed at the very small frequencies, when the thermal waves, created by radiation flux, in passing by through pyroelectric cell/element 2 (see Fig. 4.4), they reach support/base 3, and at the high modulation frequencies, code thermal waves, without reaching pyroactive crystal 2, they extinguish in absorbing layer 1 (for example, see expression (4.76)).

If radiation absorption, which falls to pyroelectric detector, occurs on the absorptive bands of crystal (fundamental absorption of crystal (fundamental absorption of pyroactive crystal), then the inertness of detector is determined by the inertness of pyroelectric effect, i.e., by the set-up time of spontaneous polarization under the influence of thermal waves on crystal.

In above given calculations it is assumed that the noises of pyroelectric receiver the only Johnson. If one takes into account

temperature and supplementary receiver noise, and also noises of measuring device, then complete equivalent receiver circuit taking into account all sources of signal and noises it takes the form, presented in Fig. 4.7.

It should be noted that the pyroelectric receiver is the transformer of energy analogous with thermocouple or photo-voltaic detector, and in work do not require power supplies.

BIBLIOGRAPHY.

1. Кременчугский Л. С. — Оптико-мех. пром., 1966, 10, 17.
2. Кременчугский Л. С., Ройцина О. В. — В кн.: Электрические и оптические свойства диэлектриков. Изд. УкрНИИТИ. К., 1966, 61.
3. Кременчугский Л. С., Ройцина О. В. — ЖПС, 1967, 6, 5, 569.
4. Кременчугский Л. С., Лысенко В. С., Мальнев А. Ф., Ройцина О. В. — ЖПС, 1966, 4, 4, 298.
5. Кременчугский Л. С., Лысенко В. С., Мальнев А. Ф., Ройцина О. В. — Инж. физ. журн., 1964, 7, 2, 3.
6. Новик В. К. — Изв. вузов. Приборостроение, 1966, 9, 5, 137.
7. Ройцина О. В. — В кн.: Тепловые приемники излучения. «Наукова думка», К., 1967, 84, 89.
8. Burdick G. A., Arnold R. T. — J. Appl. Phys., 1966, 37, 8, 3223.
9. Cooper J. — J. Scient. Instrum., 1962, 39, 9, 467; Rev. Scient. Instrum., 1962, 33, 1, 92; Nature, 1962, 194, 4825, 269.
10. Hadni A., Henninger G., Thomas R., Vergnat P., Wyncke B. — C. r. Ac. Sc., 1965, 260, 15, 4186; J. Phys., 1965, 28, 6, 345.

Page 127.

Chapter ~~1~~^V.

PYROELECTRIC RADIATION DETECTORS.

The first attempts at the creation of pyroelectric radiation detectors are related to 1938-40 [92, 102]. However, these works were noticed. the basic jerk/impulse, which woke up interest in pyroelectricity, will be the work of Chaynoviz, which left into 1956 [62]. The author of work will propose dynamic method of the study of spontaneous polarization in single crystals BaTiO_3 and will predict the possibility of recording with the aid of this method of changes in temperature on the order of 10^{-4}°C .

Subsequently Meyts Perls [87] abroad I. M. Silvestrov in the USSR [39] will be indicated the possibility of designing of the receivers of infrared emission/radiation on the basis of ferroactive ceramicist of single crystals of TGS. By Cooper [58] was proposed the first theory of the work of pyroelectric radiation detectors and is theoretically predicted the possibility of the achievement of the threshold of response of receivers on the basis of of single crystals

BaTiO_3 , comparable with the threshold of response of superconducting bolometers from nitride of niobium.

During 1964-1968 were developed highly sensitive pyroelectric receivers with the standardized/normalized threshold sensitivity $\mathcal{D}^* = (10^8 - 10^9) \text{ cm} \cdot \text{Hz}^{1/2} / \text{W}$ [1, 6, 49, 70, 93, 100].

The pyroelectric receiver of Meyts and Perls [87] (Fig. 5.1) is ceramic the disk from polarized ceramics BaTiO_3 or $\text{Pb}(\text{TiZr})\text{O}_3$, condensed with the by means of of glass fiber in the shielding metallic housing.

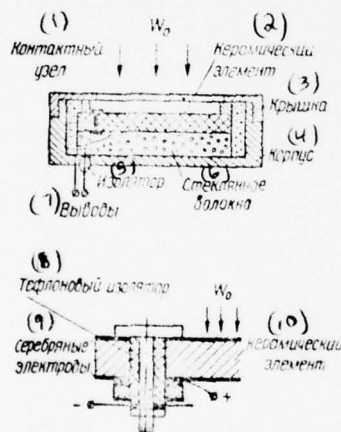


Fig. 5.1. Pyroelectric radiation detector on the basis of ferroelectric the ceramicists [87]. Is below shown contact node/unit.

Key: (1). Contact node/unit. (2). Ceramic cell/element. (3). Cap/cover. (4). Housing. (5). Insulator. (6). Glass fiber. (7). Conclusions. (8). Teflon insulator. (9). Silver electrodes. (10). Ceramic cell/element.

Page 128.

To both sides of disk are plotted/applied silver electrodes. For the equalization of the spectral characteristic of sensor the irradiated electrode was covered with Glyptal enamel 25 μ thickness, possessing the coefficient of absorption $\epsilon_0 = 0,9 \pm 0,05$ in the range of wavelengths 0.3-24 μ and in temperature range 0-100°C. The presence of the thick irradiated electrode will condition the time constant of receiver of approximately 1 ms.

The irradiated electrode is grounded with the aid of the bolt, passing through ceramic cell/element and isclate/insulated from positive electrode by teflon packing. The reliability of contacts is provided by the flat springs between current terminals.

Shown, that the utilized pickup was capable to maintain/withstand heat flows of approximately 100 W/cm² during 0.5 s. The authors of development assert that initially the calibration conducted is retained during one year with accuracy $\pm 50\%$. The calibration of sensor is conducted with the aid of standard calorimeter from 200-watt electric lamp.

Into 1964 in the institute of physics of AS UkSSR were developed the high-speed and highly sensitive receivers of radiant energy on the basis of fine-grained ceramics BaTiO_3 [1], and then with the utilization of thin-layer single crystals TGS [15, 16].

§1. Receivers on the basis of ceramics BaTiO_3 .

Sensing element of receiver is thin layer (40-100 μ) the ceramicists of titanate of barium of receiving area/site 1-20 mm^2 in size/dimension. By atomization in vacuum to sensing element will be deposited metal electrodes thickness than 1000 Å. to the irradiated electrode is spray-coated the layer of that absorbing in the assigned spectral interval of coating, for example the layer of gold black. Sensing element is fastened to holder with the aid of the braces from phosphor bronze 20-30 μ thickness. Holder with sensing element is placed in heat container (Fig. 5.2). In immediate proximity of sensing element is placed the input time of preamplifier in order to reduce to a minimum parasitic wiring capacitance. The temperature of container of pyroelectric receiver is connected to a standard thermostat of the type TS-15, with the aid of which in container is

establish/install the desired temperature, controlled copper - by constantan thermocouple.

Figure 5.3 gives the dependences of the volt-watt sensitivity S and of threshold of response \mathcal{P} the pyroelectric receiver, prepared from ceramics BaTiO_3 with impurity/admixture CO , at the room temperature depending on modulation frequency f of radiant flux during different load resistances R_H . With a decrease in the value of load resistance R_H volt-watt sensitivity descends, and the threshold of response grow/rises.

Page 129.

With $\omega CR \gg 1$ volt-watt sensitivity obeys the law f^{-1} , which will agree well with formula (4.52). Analogously changes the RMS value of receiver noise (see 4.53). Therefore threshold of response barely depends on modulation frequency, as long as $R_{\text{sp}} \gg R_H$. In this a difference of the pyroelectric receiver, which is is capacitance cell/element, from other thermal radiation detectors.

A small increase in the threshold of response at low frequencies is bonded with the low-frequency component of acoustic interferences. Analogously an increase in the threshold of response with $R_H = 10$ Gohms in the range of frequencies 500-1000 Hz is bonded with certain

decrease in the equivalent resistance of the losses of crystal

$$(R_{kp} = (\omega C_{kp} \operatorname{tg} \delta)^{-1}), \text{ when } R_{kp} \sim R_n.$$

By utilizing a differentiator amplifier, it is possible, in principle, to correct the amplitude-frequency characteristic of pyroelectric receiver, after preserving signal-to-noise ratio in that range of frequencies, in which the threshold of response remains constant/invariable.

The spectral density of the noises of pyroelectric receiver is given in Fig. 5.4.

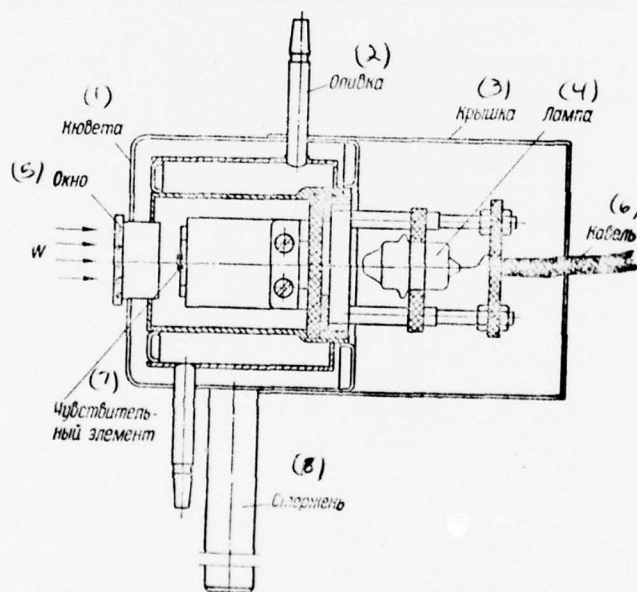


Fig. 5.2. Pyroelectric receiver in heat container.

Key: (1). Container. (2). Olive. (3). Cap/cover. (4). Lamp. (5). Window. (6). Cable. (7). Sensing element. (8) Rcd.

Page 130.

Lower curve presents the dependence of the RMS value of noise voltage $\sqrt{e_{\text{yer}}^2}$ measuring unit from frequency, average - Johnson noises of equivalent to receiver RC network, upper - the inherent noise of pyroelectric receiver $\sqrt{e_{\text{osp}}^2}$ at temperature of 300°K.

To it is evident from the figure, the inherent noise of pyroelectric receiver do not exceed the noises of equivalent RC network more than by 50o/o. This it makes it possible in a number of cases simple to calculate receiver noise from Nyquist's formula, without conducting measurements. With an increase of noise frequency of installation, caused in the main by the effect of glimmer, drops more slowly than receiver noise. Therefore in designing input units for a work with pyroelectric receivers special attention follows specific reduction in the noises of installation at frequencies above 100 Hz.

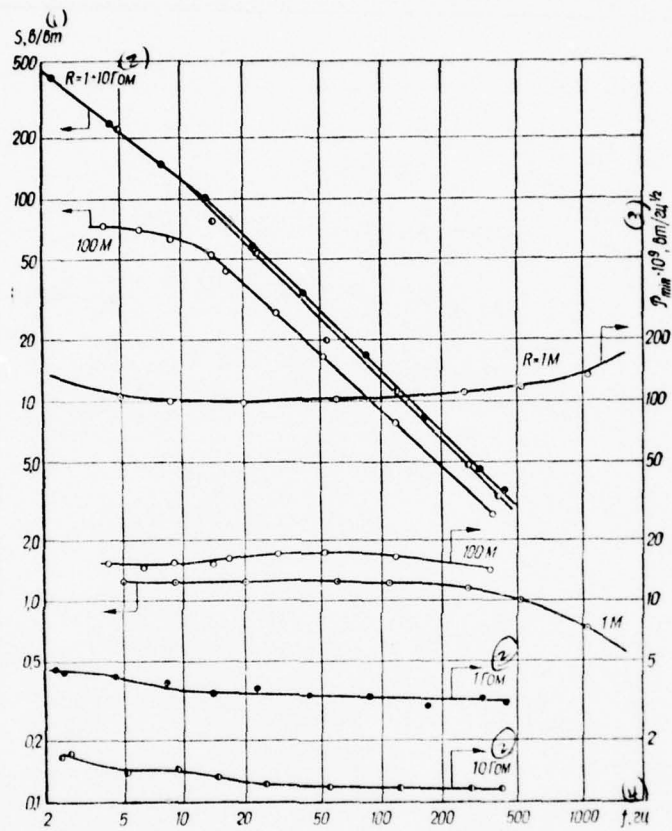


Fig. 5.3.

Fig. 5.3. Dependence of the volt-watt sensitivity S of receiver on the basis of ceramics BaTiO_3 on frequency f at different values of load resistance: R_H ($A_0 = 1 \text{ mm}^2$).

Key: (1). V/W. (2). Gohms. (3). W/Hz^{1/2}. (4). Hz.

Page 131.

The stability of the characteristics of pyroelectric receiver can be studied by the observation of the temperature dependences of the dynamic pyroelectric coefficient γ_d (or pyroelectric current I) with the consecutive cycles of heating and cooling (Fig. 5.5).

After the polarization of specimen/sample with the first cycle of heating to 70°C and subsequent cooling occurs the aging process of specimen/sample. During the subsequent cycles of heating to this temperature the process of aging virtually is finished and the points, which correspond to identical temperatures, they coincide with accuracy of $\pm 5\%$. The work of pyroelectric receiver in this temperature interval is stable.

Pyroelectric coefficient reaches the maximum value at temperature of 85-90°C, which exceeds 2.5-3 times its value at room

temperature.

Since pyroelectric coefficient γ_R and the dielectric constant similarly grow/rise with an increase in the temperature to 70°C , the volt-watt sensitivity S , proportional to their relation during high load resistances, changes insignificantly in this temperature interval. Therefore the pyroelectric receiver, prepared from ceramics of titanate of barium, it is expedient to utilize at room temperature. The conducted investigations of the subsequent aging of receiver responses showed that during half-year of any substantial changes in the parameters it is not observed.

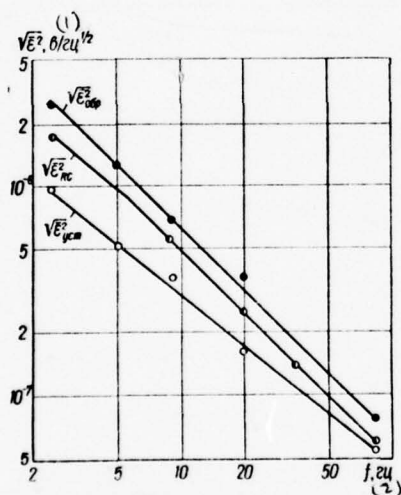


Fig. 5.4.

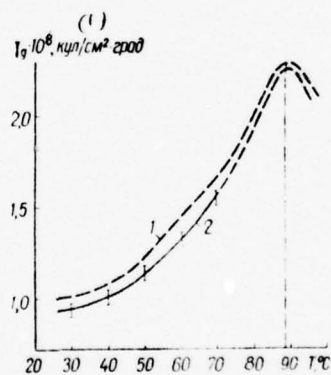


Fig. 5.6.

Fig. 5.4. Spectral noise density of receiver on the basis of ceramics BaTiO_3 ($R_H = 1 \text{ Gohms}$).

Key: (1). $\text{V}/\text{Hz}^{1/2}$. (2). Hz .

Fig. 5.5. Dependence of pyroelectric coefficient γ_n from temperature of T: 1 - the original cycle of heating and cooling; 2 - following.

Key: (1) - coul/cm²•deg.

Page 132.

The basic parameters of receivers on the basis of ceramics BaTiO₃ with impurity/admixture CO the following:

1) threshold of response in frequency range 5-200 Hz during load resistance $R_H = (1-10)$ Gohms in the circuit of cathode follower on a lamp of the type "acorn" is equal to $5 \cdot 10^{-9}$ W/Hz^{1/2}.

2. the time constant, caused by thickness and the thermal characteristics of the irradiated electrode, is 1-20 μ s; in work on fundamental absorption, the inertness of receiver descends to $10^{-7}-10^{-8}$ s and in some constructions is limited to piezoresonance phenomena of sensitive layer;

3) volt-watt sensitivity on modulation frequency 10 Hz and the value of load resistance $R_H = 10$ Gohms compses 100 V/W t with the size/dimensions of receiving area/site 1 mm².

4) dynamic range compose 10^{-1} - 10^{-8} W/mm².

Sensors can be made in the form of the figures of arbitrary form - by the forging, mechanical processing, etc.

Utilization of single crystals BaTiO₃ for the creation of pyroelectric receivers did not yield positive results, in spite of the fact that c-domain crystals can be obtained in free state by area several millimeters with thicknesses of approximately 20 μ . The basic reason is the instability of characteristics, bonded with the instability of domain of structure.

Positive results were obtained with the use of industrial piezoelectric the ceramicist of the type "central telephone exchanges" and KNBS. Prepared on their basis receivers possess approximately the same threshold of response, so and receivers from ceramics BaTiO₃; however, with wider dynamic range.

§2. Receivers on the basis of single crystals TGS.

Pyroelectric coefficient γ_n and relation γ_n/ϵ for TGS are higher than for ceramics BaTiO_3 . Single crystals easily are treated and can be grown to sufficiently large size/dimensions. In connection with this most sensitive pyroelectric receivers are obtained with the use of single crystals TGS [3, 15, 16, 18-23, 47, 49, 70, 93]. Exception is the report/communication of Glass [50, 67] about the development of highly sensitive pyroelectric receiver on the basis of single crystals SNB ($\text{Sr}_{1-x}\text{Ba}_x\text{Nb}_2\text{O}_6$).

Sensing element of pyroelectric receiver is the plate, prepared from the large single crystal TGS, by area 1-5 mm^2 by thickness 50-150 μ . With smaller thicknesses of sensing element becomes mechanically fragile and its pyroelectric coefficient falls faster than it is thinned crystal. Structural/design formulation is the sensing cell/element to analogously described for crystals BaTiO_3 . General view of sensing element is given in Fig. 5.6.

Page 133.

Of pyroelectric receivers, released by firm Barnes Engineering CO, the construction of sensing element differs from preceding/previous themes that the crystal TGS is fastened to the metallized mylar film, which, in turn, is fastened on carrier ring (Fig. 5.7). The irradiated electrode, covered with black, is connected with the

entrance of solid-body preamplifier.

The frequency dependence of volt-watt sensitivity and threshold of response of the pyroelectric receiver, developed in the institute of physics of AS UkSSR, with the size/dimensions of receiving area/site 1 mm^2 and the thickness of crystal $50 \text{ } \mu$ during different load resistances is given in Fig. 5.8.

During load resistance $R_H = 10 \text{ Gohms}$ Are threshold of response $\mathcal{P} = 10^{-9} \text{ W/Hz}^{1/2}$. In the measured frequency band the dependence of value \mathcal{P} from frequency is insignificant.

The amplitude frequency characteristics of pyroelectric receiver are given in Fig. 5.9. During load resistance $R_H = 100$ anyone cut-off frequency $f_{0.5} = 13 \text{ kHz}$. The calculation of cut-off frequency according to formula (4.77), when the heat capacity of the irradiated electrode is equal to $7 \cdot 10^{-5} \text{ cal/(deg} \cdot \text{cm}^2)$, gives value $f_{0.5} = 20 \text{ kHz}$. This inaccuracy in the calculation was explained [to 15] themes that is not considered the time constant of the input circuit, which composes $2 \cdot 10^{-6} \text{ s}$.

The work of pyroelectric detector near the point of phase transition is described in [21]. Did arise the question: will not be an increase in the fluctuations of polarization at Curie point the

fundamental limitation of threshold receiver sensitivity? For explanation were carried out the measurements of the noises of detector on the crystals TGS in an interval of temperatures 20-60°C. Investigations were carried out on frequency analyzer with time constant of approximately 100 s during an uniform increase in the temperature at a rate of 1 deg/min. The RMS value of noise is record/written on automatic recorder. The measurements will show that receiver noise as at Curie point, that and outside it was equal to the noise of equivalent RC network.

$$\sqrt{\overline{e^2}} = f(T).$$

Figure 5.10 gives the written on automatic recorder dependences Δ taken at frequency 350 Hz at the different values of load resistance and upon blocked entrance.

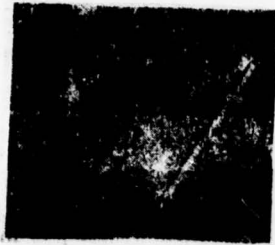


Fig 5.6.

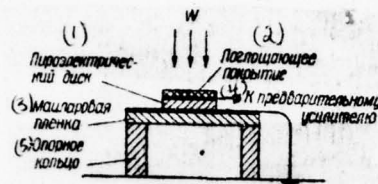


Fig. 5.7.

Fig. 5.6. Sensing element of pyroelectric receiver.

Fig. 5.7. Circuit of sensing element of receiver Barnes Engineering CO [47].

Key: (1). Pyroelectric disk. (2). Absorbing coating. (3). Maiparovaya film. (4). To preliminary amplifier. (5). Carrier ring.

Page 134.

An increase in the capacity at Curie point leads to a decrease in the noise. In this case the course of the temperature dependence of the RMS value of noise is qualitatively such/similar to the course of

reciprocal value of dielectric constant. Connection to the specimen/sample of constant voltage does not cause supplementary electrical fluctuations both at the room temperature and near Curie point

D During rapid heating on the order of 10 deg/min and above sensing element of pyroelectric receiver in the range of phase transition appear the supplementary noises, caused by the effect, analogous to the Barkhausen effect [16]. No longer appear also during a sign change of the applied stationary field. They after the application/appendix of field can be continued for several minutes.

Figure 5.11 depicts the curves of the threshold of response of pyroelectric receiver with room temperature and near Curie point, and also the calculated curve is assumed that receiver noise is purely Johnson [54]. The designed threshold values of the sensitivity of pyroelectric receiver with 48°C show that it in sensitivity approaches an ideal thermal receiver. The real threshold of response of receiver near Curie point with an increase of frequency is raised, that its as noises are determined by the noises of measuring circuit.

The comparison of the sensitivity of pyroelectric receiver IF of AS UkSSR, that works at room temperature, with the vacuum and gas-filled nickel bolometers, used for spectral target/purposes,

conducts according to signal-to-noise ratio at frequency 9 Hz by the radiation flux $W_0 = 3 \cdot 10^{-7} \text{ W/mm}^2$. During the comparison of receivers is utilized the meter low energies [11, 29].

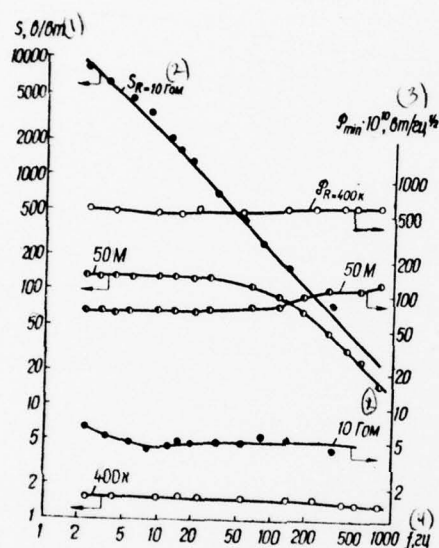


Fig. 5.8. Frequency dependences of volt-watt sensitivity and threshold of response and threshold of response of pyroelectric detector on the basis of the single crystal TGS at different values R_N .

Key: (1). V/W. (2). Gohms. (3). W/Hz^{1/2}. (4). Hz.

Page 135.

With weakening by the grid of radiant flux W_0 25 times the signal, taken from the gas-filled nickel bolometer, it was hardly let us distinguish against the background of noise (is in form not RMS value of noise $\sqrt{\overline{e^2}}$, a the maximum amplitude value noise- "spread/scope", that exceeds this value approximately 5 times).

Vacuum nickel bolometer and pyroelectric receiver distinguish signal against the background of noise with the weakening of flow 150 times. But the threshold sensitivity of vacuum nickel bolometer will be above. The amplitude characteristic of the pyroelectric receiver with $R_H = 10$ Gohms is linear in the range of flows $W_0 = (10^{-3}-10^{-9})$ W/mm².

In spite of an increase in the pyroelectric coefficient near Curie point, volt-watt receiver sensitivity during high load resistances R_H descends, since simultaneously occurs an increase in the dielectric constant. However, in the course of experimental and calculated curves there is the disagreement (Fig. 5.12), which is bonded with certain displacement of the maximum pyroelectric

coefficient γ_A with respect to maximum ε to the side of lower temperatures. on the basis of the curves of Fig. 5.12, optimum operating temperatures of triglycinesulfate receiver one should select in area 46-47°C, near maximum γ_A .

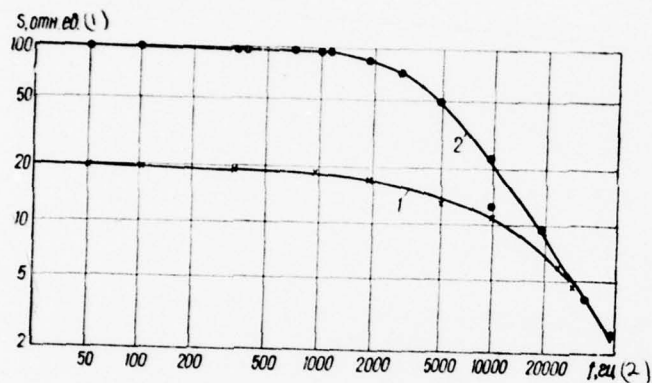


Fig. 5.9.

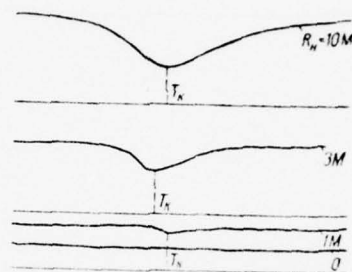


Fig. 5.10

Fig. 5.9. Amplitude-frequency characteristics of longitudinal type pyroelectric receiver on the basis of TGS: 1 - $R_H = 100$ anyone; 2 - $R_H = 400$ anyone.

Key: (1). rel. un. (2). Hz.

Fig. 5.10. The written on automatic recorder dependences $V_e^2 = f(T)$ at different values R_H (value of the Curie temperature is shown by dotted line).

Page 136.

Figure 5.13 gives the fundamental characteristics of the pyroelectric receiver of firm Barnes Engineering CO [47] with the size/dimensions of whose receiving area/site is $0.5 \times 0.5 \text{ mm}^2$ and whose capacity is 4 pF. Measurements conducted with the aid of solid-body amplifier with the entry impedance 10^{12} ohm (electrical time constant was 4 s). The contributions different the component of noises - temperature noise U_t , the Johnson noise of entry impedance U_0 , the noise of the equivalent resistance of the receiver (dispersive losses) U_d , of the noise of amplifier U_a are determined at different modulation frequencies. Calculated value of the standardized/normalized threshold sensitivity of ideal thermal radiation detector with the receiving area/site indicated at room temperature $\mathcal{D}^* = 5.2 \cdot 10^9 \text{ (cm} \cdot \text{Hz}^{1/2}) / \text{W}$.

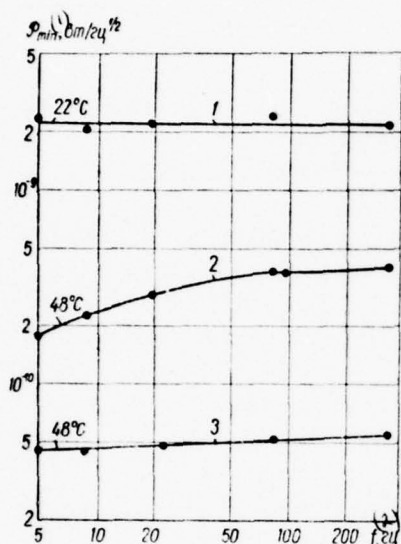


Fig. 5.11.

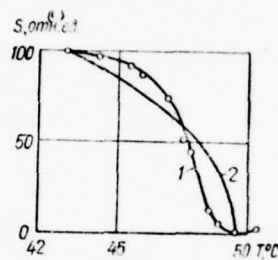


Fig. 5.12.

Fig. 5.11. Dependence of the threshold of sensitivity of pyroelectric receiver on the basis of TGS on modulation frequency: 1. , 2.

experimental curves; 3 - calculated curve.

Key: (1). $W/Hz^{1/2}$. (2). Hz.

Fig. 5.12. The temperature dependence of relative volt-watt receiver sensitivity on the basis of TGS:

1 - experimental; 2 - designed by formula (4.44).

Key: (1). rel. un.

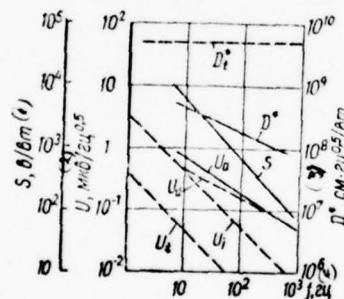


Fig. 5.13. Frequency dependences of noises, volt-watt and threshold sensitivities of TGS- pyroreceiver Barnes Engineering CO [47]: S -

volt-watt sensitivity; D_t^* - the standardized/normalized threshold sensitivity ideal type; U_n - receiver noise TGS-; U_j - the Johnson noises of entry impedance; U_a - to the shim of solid-body amplifier; U_{λ} - temperature noise. Solid lines showed experimental curves, by broken lines - calculated.

Key: (1) - V/W. (2) - $\mu V/Hz^{0.5}$. (3) - $cm \cdot Hz^{0.5}/V$.

Page 137.

This value considerably exceeds the threshold sensitivity of pyroelectric receiver. At the frequency of modulation 0.06 Hz the volt-watt sensitivity S_0 was equal to 10^6 V/W.

It should be noted that the threshold sensitivity D_t^* TGS = receiver in Fig. 5.13 with an increase of frequency descends according to the law $f^{-0.5}$, while in Fig. 5.3 and 5.8 is not observed a noticeable incidence/drop in the threshold of response \mathcal{P} receiver IF AS UkSSR. This is connected with the fact that the value of the load resistance of receiver IF AS UkSSR $R_H = 10$ G Ω , and the entry impedance of the solid-body amplifier Earnes Engineering Co was equal to 1000 G Ω . Therefore the threshold of response of the last/latter receiver was proportional to its equivalent resistance, depending on

frequency, dielectric constant and dielectric loss angle (see (4.79)), while the threshold of response of receiver IF AS UKSSR was caused by the value of load resistance (see (4.68)).

§3. Receiver with high value of receiving area/site.

The threshold sensitivity of the majority of thermal radiation detectors deteriorates with an increase in the size/dimensions of receiving area. Therefore in recent years was outlined the tendency of the development of receivers with the minimum value of receiving area/site (less than 1 mm^2), and also of the creation of the immersion systems, offering the possibilities of a further size decrease of sensing elements of receivers.

However, there is a series of problems in radiometry [48], where they are required receivers with large size/dimensions of sensing element (on the order of 100 mm^2) and by uniform zonal sensitivity.

The conducted in work [48] investigations with thermocouples indicate that an increase in the receiving area desensitize of detector and its uniformity over surface. In this same article was proposed the gold sprayed bolometer with area of approximately 80

mm².

The measurements of the zonal sensitivity of metallic bolometers and dependence of their characteristics on the size/dimensions of receiving area/site [2] showed that the bolometers barely suitable for these purposes.

As shown in chapter IV (see (4.68)), the threshold sensitivity of pyroelectric receivers is proportional to the thickness of crystal and does not depend on the value of sensitive area, if the value of load resistance $R_n \ll R_{kp}$ and if thermal agitations do not limit the limit of their sensitivity.

Page 138.

Experimental studies establish/installed that receiver noise on the basis of crystals TGS and BaTiO₃ in temperature range 20-70°C are Johnson. This it indicates the possibility of the production of receivers with large size/dimensions of sensitive area without fundamental deterioration in their threshold sensitivity. Unlike the bolometers, the nonuniformity of sensitivity of which is caused by the temperature distribution along film, the zonal sensitivity of pyroelectric receivers depends on the arrangement of domain fields.

The conducted investigations of the zonal sensitivity $S(x, y)$ of the pyroelectric receivers, prepared on the basis of single crystals of TGS, LiNbO_3 , and fine-grained ceramics BaTiO_3 , they showed that they are more promising than bolometers and thermocouples, for the creation of detectors with large size/dimensions of receiving area/site [19, 26].

The method of measurement $S(x, y)$ consisted of the irradiation of sensing elements by narrow light beam and the fixing of pyroelectric signal of the place of irradiation. The specimen/samples being investigated had thickness 100-300 μ and receiving area/site from 1 to 100 mm^2 .

The observation of the place of illumination on receiver and the checking of the value of light probe were realized by using stereomicroscope.

In order that the length of temperature wave by crystal would not exceed its thickness, necessary correctly to select the modulation frequencies of luminous flux. With the thickness of the specimen/samples being investigated more than 50 μ the frequency 40 Hz satisfied these requirements. Otherwise could arise supplementary errors due to nonuniform thermal contact on crystal boundary - support/base.

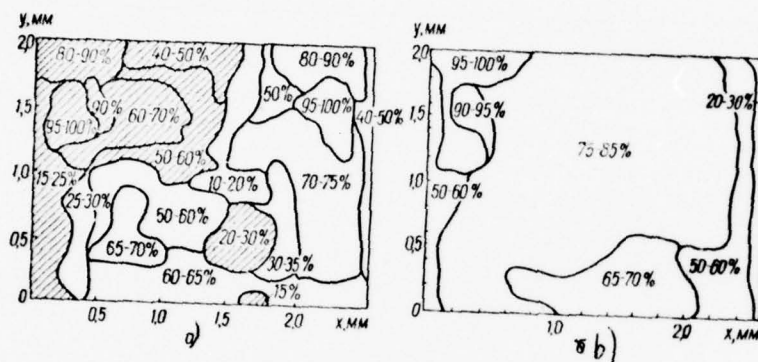


Fig. 5.14. Relative zonal sensitivity of pyroelectric receiver on the basis of the poly-domain single crystal of TGS: a) without electric field; b) with field.

Page 139.

Cell with pyroelectric receiver and preamplifier was placed under microscope object lens and was moved in horizontal plane in two directions with the aid of micrometer screw/propellers. Pyroelectric

signal was amplified by the amplifier, tuned to a frequency of modulation 40 Hz, and by the phasemeter F2-1 was determined gas. For a feed to the phasemeter of reference voltage was utilized the circuit: incandescent lamp is a photodiode.

Fig. 5.14a gives the zonal sensitivity of the poly-domain single crystal of TGS. Signals in shaded and that which was not shaded fields are located in antiphase. During the illumination of entire receiver the total signal is close to zero, that as areas with the opposite signs of polarization nearly equal. During appendix to the crystal of electric field 50-100V the domains are run up/turned in the direction of field. The general volt-watt sensitivity considerably grow/rises, and zonal becomes more uniform (see Fig. 5.14b). If not to consider an incidence/drop in the sensitivity in narrow field (0.1 mm) at the edges of receiver and about contacts (due to the nonuniformity of black at the edges of receiver and to heat withdrawal on contacts), area with the sensitivity, which differs by 20o/o from the maximum, composes more than 2/3 values of an entire receiving area/site.

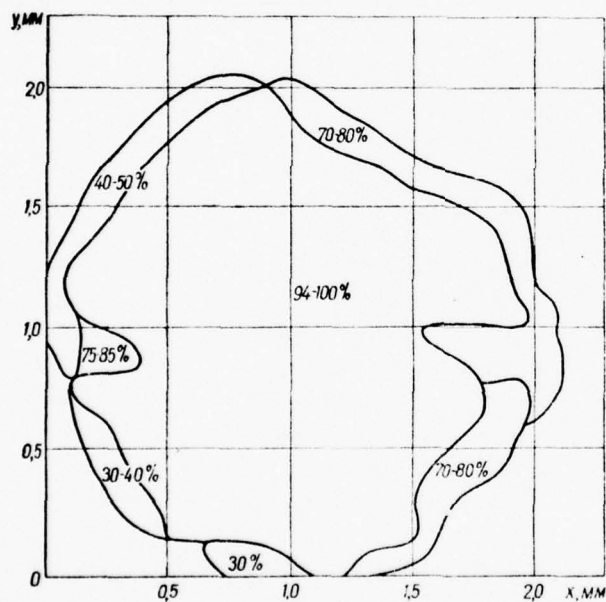


Fig. 5.15. Distribution of relative zonal sensitivity according to

the area of the pyroelectric receiver, prepared from ceramics BaTiO_3 .

Page 140.

Frequently are encountered the sufficiently large monodomain crystals of TGS, which remain such even after warm-up higher than the Curie point and subsequent cooling down to room temperature. The stabilization of domain structure it is possible to realize by dusting/deposition/spraying to the crystal of metal electrodes with different work function (for example, indium is gold). In this case the area with the zonal sensitivity which differs by 100/o from the maximum, is 0.8 entire receiving area/sites.

Sometimes of crystals of TGS is observed the unsteady state, which is characterized by many domains, but it rapidly transfer/converts to stable, that contains 2-3 domains. Probably, the deposition of electrodes (even silver is silver) and the circuit diagram of receiver stabilize its polarization.

Zonal receiver sensitivity on the basis of ceramics BaTiO_3 is represented in Fig. 5.15. The nonuniformity of sensitivity is 60/o of mA of 9/10 areas of receiver. only at the edges of specimen/sample and of contacts sensitivity falls to 300/o. Uniform zonal sensitivity

is observed also of receiver and single crystal LiNbO_3 . The nonuniformity of sensitivity of this receiver does not exceed 1-2% in an entire area.

During the investigation of single crystals BaTiO_3 , map/charts of the distribution of the sensitivity did not coincide with the map/charts of the arrangement of domain fields, taken before dusting/deposition/spraying electrodes and blackening. In a-domain fields were not observed the sharp dips of sensitivity as it was possible to expect. It is possible that into the process of the deposition of electrodes on crystal boundary appear local electrical and mechanical stresses, which it leads to the rearrangement of domain structure.

The investigations showed that the best zonal sensitivity possess the receivers from niobate of lithium, ceramics of titanate of barium and single crystals of triglycine sulfate with the stabilized polarization.

Pyroelectric receivers with large receiving area, developed in IF AS UkSSR, are shown in Fig. 5.16. The sensitive cell/element, prepared from fine-grained ceramics BaTiO_3 , is fastened on the conducting supports, which perform the role of ground electrode. Permalloy housing safeguards receiver from electromagnetic

focusing/inductions. Window is made from the material, transparent in the assigned spectral interval.

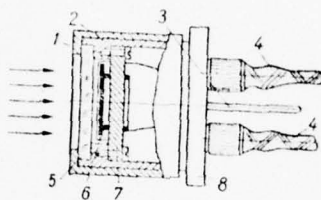


Fig. 5.16. Pyroelectric receiver with the high value of the receiving area/site: 1 - housing; 2 - insert/bushing; 3 - filler; 4 - conclusions; 5 - window; 6 - sensing element; 7 - holder; 8 - flange.

Page 141.

The threshold of response of pyroelectric receiver, if the length of temperature wave in crystal considerably shorter than its thickness and more than the thickness of the irradiated electrode, it is possible to write in the form

$$\mathcal{P} = \left\{ \frac{4KT\Delta f}{R_n} \cdot \frac{c^2 d^3}{\gamma^2} + 16A_0 \sigma_0 K (\epsilon_1 + \epsilon_2) T \Delta f \right\}^{0.5}. \quad (5.1)$$

The second term in equation (5.1) is considerably lower than the

first with the reasonable size/dimensions of receiving area/site. The value of the quantity of the receiving area/site of the receiver, at whose equivalent power of Johnson noises is comparable with temperature, is determined by the expression

$$A_0 = \frac{c^2 d^2}{\gamma^2} \cdot \frac{1}{4R_{00}(\epsilon_1 + \epsilon_2) T^4} \quad (5.2)$$

For the developed at present pyroelectric receivers, which work far from Curie point, expression (5.2) is made at values $A_0 = 10^5 - 10^6$ mm². a virtually considerable increase in the receiving area/site leads to an increase in the microphonic noises (piezonoise) and lowering of the value of load resistance (due to a decrease in value R_{KN}).

Pyroelectric receivers on the basis of ceramics of titanate of barium of sensor 10-100 mm² in size/dimension possess threshold of response $5 \cdot 10^{-9} - 5 \cdot 10^{-8}$ W/Hz^{1/2} with the nonuniformity of zonal sensitivity $\pm 50\%$.

§4. Pyroelectric targets for image converters.

Of the nonscanning image converters of infrared region the sensor usually consists of two layers. In the first layer the incident radiation is absorbed, in the second - is created the

temperature image of object, which then is record/fixed either visually or by photographic method (for example, in recording evaporimeter). Such systems are inertial ($\tau = \overset{0.1}{\cancel{0.1}}-50$ s) and are insufficiently are sensitive.

In recent years appeared the report/communication about the possibility of designing of image converter on the basis of pyroelectric effect in lamellar ferroelectric. Although at present these instruments are located in the initial stage of their development, is of interest the study of the possibilities of pyroelectric transformers. The already preliminary estimations showed that the developed image converters are potentially more sensitive and less inertia than recording evaporimeters [12, 33].

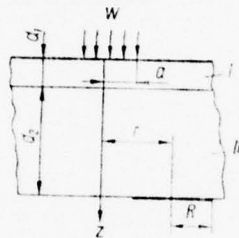


Fig. 5.17. The circuit of the pyroelectric target: d_1 is thickness of upper electrode (I); d_2 - the thickness of crystal (II); a - the radius of the falling/incident light ray; R - the radius of lower electrode.

Page 142.

Let us conduct study of the structure of the temperature image, which appears in crystal during irradiation of it by the light probe of a small diameter, to evaluate the resolution of this target.

Let us examine the system, which consists of two plates with

different thermophysical properties (Fig. 5.17). The surface of upper electrode (plate I) is irradiated by modulated radiant flux W through the circle of radius a . As a result of a change in the temperature of plate II, which is pyroactive crystal with the special polar axis, parallel to the coordinate z axis, in it appears pyroelectric current whose density can be calculated from the formula

$$j(r, t) = \gamma \frac{\partial \bar{\theta}_2(r, t)}{\partial t}, \quad (5.3)$$

where γ is a pyroelectric coefficient; $\bar{\theta}_2(r, t) = 1/d_2 \int_{d_1}^{d_1+d_2} \theta_2(r, z, t) dz$ - the increase in the temperature of crystal, averaged according to thickness; r, z are cylindrical coordinates.

For the determination of the distribution in crystal, it is necessary to solve the equation of thermal conductivity for a two-layered system, which in cylindrical coordinates taking into account the axial symmetry of task is taken in the form

$$\frac{\partial^2 \theta}{\partial r^2} + \frac{1}{r} \cdot \frac{\partial \theta}{\partial r} + \frac{\partial^2 \theta}{\partial z^2} = \frac{1}{\psi} \cdot \frac{\partial \theta}{\partial t}, \quad (5.4)$$

where ψ is coefficient of thermal diffusivity.

If the initial increase in the temperature equal to zero and

heat losses can be disregarded, then boundary conditions they take the following form:

$$\begin{aligned} z = 0, \quad -k_1 \frac{\partial \Theta_1}{\partial z} &= \begin{cases} \varepsilon_0 W_0 e^{-i\omega t} & (0 < r < a), \\ 0 & (r > a); \end{cases} \\ z = d_1, \quad k_1 \frac{\partial \Theta_1}{\partial z} &= k_2 \frac{\partial \Theta_2}{\partial z}, \quad \Theta_1 = \Theta_2; \\ z = d_1 + d_2, \quad \Theta_2 &= 0, \end{aligned} \quad (5.5)$$

where Θ_1 and Θ_2 are increases in the temperature; k_1 and k_2 - the coefficient of the thermal conductivity of electrode and crystal respectively; W_0 - the amplitude of the falling/incident radiant flux; ε_0 - the coefficient of the absorption of upper electrode; ω - cyclic modulation frequency.

The periodic part of the solution to equation (5.4), carried out by M. A. Itskovskiy [12], under boundary conditions (5.5) for a crystal takes the following form:

$$\Theta_1(r, z, t) = a \varepsilon_0 W_0 e^{-i\omega t} \int_0^\infty J_0(\xi, r) J_1(\xi, a) \times$$

$$\times \frac{\operatorname{sh}(d_1 + d_2 - z) \eta_1 d_2^2}{k_1 \eta_1 \operatorname{sh} \eta_2 d_2 + k_2 \eta_2 \operatorname{ch} \eta_1 d_1 \operatorname{ch} \eta_2 d_2},$$

$$\eta_{1,2} = \sqrt{\xi^2 - \frac{i\omega}{\psi_{1,2}}}, \quad (5.6)$$

where $J_0(\xi, r)$ and $J_1(\xi, a)$ - the Bessel function of zero and first orders respectively; ψ_1 and ψ_2 - the coefficients of thermal diffusivity of upper electrode and crystal.

With $d_1 = 0$, $\psi_2 \rightarrow \infty$ and $\omega = 0$ from formula (5.6) is obtained the solution of problem for a semi-restricted body with the constant heat flux W_0 through circle $0 < r < a$, lying/horizontal at plane $z = 0$, and zero flow through surface of $r > a$;

$$\Theta_1(r, z) = \frac{a r_0 W_0}{k_2} \int_0^\infty J_0(\xi, r) J_1(\xi, a) e^{-\xi z} \frac{d\xi}{\xi}. \quad (5.7)$$

With $d_1/d_2 \ll 1$ (thickness of upper electrode considerably shorter than the thickness of crystal) and $k_1/k_2 > 1$ (thermal conductivity of

upper electrode greater the thermal conductivity of crystal) from expression (5.6) we obtain

$$\Theta_2(r, z, t) = a\varepsilon_0 W_0 e^{-i\omega t} \int_0^\infty J_0(\xi, r) J_1(\xi, a) \frac{\text{sh}(d_2 - z) \eta_2 d_2}{k_2 \eta_2 \text{ch} \eta_2 d_2} d\xi. \quad (5.8)$$

It should be noted that formula (5.8) is applied for the calculation of the temperature in the crystal even at $k_1/k_2 \sim 10^3$, if $d_1/d_2 \sim 10^{-5}$. In this case the first term in the denominator of formula (5.6) is negligible as compared with the second. However, when indicated relationship/ratios are not fulfilled, calculation one should produce precise formula (5.6).

For the density of pyroelectric current we obtain

$$j(r, t) = -i\omega \bar{\Theta}_2(r, t), \quad (5.9)$$

where

$$\bar{\Theta}_2(r, t) = \frac{a\varepsilon_0 W_0 e^{-i\omega t}}{d_2 k_2} \int_0^\infty J_0(\xi, r) J_1(\xi, a) \frac{\text{ch} \eta_2 d_2 - 1}{\eta_2^2 \text{ch} \eta_2 d_2} d\xi. \quad (5.10)$$

- the average increase in the temperature of crystal.

Page 144.

Expression (5.10) can be presented in the form

$$\bar{\Theta}_2(r, t) = \frac{a\varepsilon_0 W_0 e^{-i\omega t}}{k_2 N} (M_2 + 2iM_1) = \frac{a\varepsilon_0 W_0}{k_2} F(r) e^{-i(\omega t - \varphi(r))}, \quad (5.11)$$

where

$$F(r) = \frac{1}{N} \sqrt{4M_1^2 + M_2^2}; \quad \varphi(r) = \arctg(2M_1/M_2);$$

$$M_1 = \int_0^\infty J_0(R, t) J_1(A, t) \times$$

$$\times \frac{\operatorname{ch} 2NT_+ + \cos 2NT_- - 2\operatorname{ch} NT_+ \cos NT_- - t^2 \operatorname{sh} NT_+ \sin NT_-}{(t^4 + 4)(\operatorname{ch} 2NT_+ + \cos 2NT_-)} dt;$$

$$M_2 = \int_0^\infty J_0(R, t) J_1(A, t) \times$$

$$\times \frac{t^3 (\operatorname{ch} 2NT_+ + \cos 2NT_- - 2\operatorname{ch} NT_+ \cos NT_-) + 4 \operatorname{sh} NT_+ \sin NT_-}{(t^4 + 4)(\operatorname{ch} 2NT_+ + \cos 2NT_-)} dt;$$

$$T_{\pm}(t) = \sqrt{\frac{1}{2}(\sqrt{t^4 + 4} \pm t^2)}$$

$$(t = \xi \lambda_2),$$

$$R = \frac{2}{\lambda_2}; \quad A = \frac{a}{\lambda_2}; \quad N = \frac{d_2}{\lambda_2};$$

$$\lambda_2 = \sqrt{\frac{2\psi}{\omega}}$$

is a temperature wavelength in crystal.

Thus, the basic difficulty during the analysis of the obtained

results is the calculation of integrals M_1 and M_2 . These integrals were calculated on computer for some values of parameters D_2 and λ_2 at the radius of light ray $a = 20 \mu$. Figure 5.18 depicts the dependence of function F (and, consequently, the average increase in the temperature of crystal, value of pyroelectric signal and volt-watt sensitivity, which are proportional to value F) of distance between centers of incident ray/beam and lower point electrode r .

The experimental study of the structure of the temperature image was conducted on the crystals of TGS and BaTiO_3 by thickness 100-500 μ [19]. During the determination of the resolution of pyroelectric target with a thickness of of electrode varied within the limits (0.05-1) μ . The effective thickness of gold black was 0.03 μ . For measurement was utilized the method, described above. The modulated emission/radiation of laser source by power 10^{-4} W was focused by microscope into small circle 20 μ in radius. Coordinate displacement/movement was conducted through every 5 μ . The appearing during irradiation pyroelectric signals were remove/taken with the aid of acicular electrode with effective diameter (20-50) μ .

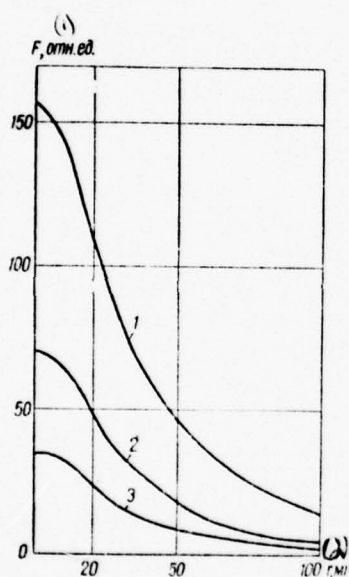


Fig. 5.18. The dependence of the relative value of pyroelectric voltage from distance to the center of light ray r at the different thicknesses of the crystal: 1 - $d/2 = 100 \mu$; 2 - $d/2 = 200 \mu$; 3 - $d/2 =$

400 μ ($\lambda_2 = 50 \mu$; this value it corresponds to modulation frequency for BaTiO₃, 80 Hz, for TGS - 36 Hz).

Key: (1). rel. un. (2). μ .

Page 145.

Was investigated the effect of the different parameters of pyroelectric target (thickness of crystal, the thickness of upper electrode and modulation frequency) on the character of a decrease in the pyroelectric signals at an increase in the distance between the laser ray/beam and the lower point electrode, measured in the direction, perpendicular to the direction of the laser ray/beam.

With the connection of target to measuring circuit the voltage, removed from load resistance R_n with $R_{kp} \gg R_n$,

$$U = \frac{IR_n}{1 + i\omega C_0}, \quad (5.12)$$

where $I = jA_0$ - the pyroelectric current through the electrode with an area of A_0 ; C_0 - the total capacitance of crystal and input time.

From (5.8) and (5.12) we obtain (with $\omega C_0 R_n \gg 1$)

$$U(r) = -\gamma \frac{A_0}{C_0} \Theta_2(r) \quad (5.13)$$

The measurements conducted did not reveal/detect any noticeable dependence of the relative value of the pyroelectric voltage

$$N_0(r) = \frac{|U(r)|}{|U(0)|} = \frac{F(r)}{F(0)} \quad (5.14)$$

from the thickness of crystal D_2 within the limits of the utilized thicknesses of crystals ($d = 100-500 \mu$). However, the volt-watt sensitivity of target as in usual pyroelectric receivers [15], depends substantially on the thickness of crystal and grow/rises with its decrease.

The calculated values of relative sensitivity confirm these experimental results. The width of the curve of relative pyroelectric stress, measured at the height where the signal falls into e once, can serve as the parameter to evaluate resolution. In this case the resolution of pyroelectric target let us call the number of widths that are placed of cut 1 mm long. The experimental dependence of parameter $N_0(r)$ on the thickness of the upper sprayed electrode d_1 is given in Fig. 5.19. With a decrease in the thickness of upper electrode the slope/transconductance of decrease $N_0(r)$ considerably grow/rises, i.e., is increased the permission of target.

The permission of target also substantially grow/rises with an

increase in the modulation frequency of laser beam. Figure 5.20 gives characteristic dependence for crystals of TGS. The disagreement of theoretical and experimental curves is explained themes that during numerical calculation on computer was not taken into account the effect of upper electrode. Mathematically this indicates the account of the first term in the denominator of formula (5.6) that greatly complicates the calculation.

With the aid of these Fig. 5.20 it is possible to produce the estimation of the resolution of target.

Page 146.

For a frequency 285 Hz permission composes 20 lines/mm (theoretical value) even 17 lines/mm (experimental value). In separate specimen/samples with very fine/thin point electrode ($\phi = 15 \mu$) was obtained experimentally the permission 20-30 lines/mm.

The conducted investigation of pyroelectric target makes it possible to make the determined conclusions about the possibilities of the conversion of image. The pyroelectric effect during probe irradiation is determined by the structure of the appearing nonuniform distribution of temperature according to crystal plate. For estimating the value of the volt-watt sensitivity of pyroelectric

target one should introduce the representation of its single cell/element, which presents the cylinder, cut out along the polar axis, with the area of basis/base, equal to area lower-q of electrode. The volt-watt sensitivity of the cell/element of pyroelectric target is increased both with the decrease in the thickness of crystal and with a decrease in the frequency of modulation (with $\omega C_2 R_n \gg 1$). For the crystal of TGS with thickness $D_2 = 100 \mu$, the diameter of lower electrode $\phi = 50 \mu$ and with value $R = 10 \text{ G}\Omega$ at modulation frequency 10 Hz the volt-watt sensitivity of cell/element $S = 2000 \text{ V/W}$. For ceramics BaTiO_3 , value S for an order lower threshold of response in this case composes $5 \cdot 10^{-9} \text{ W/Hz}^{1/2}$.

It should be noted that the sensitivity of the cell/element of pyroelectric target can be improved during the optimum agreement with measuring device.

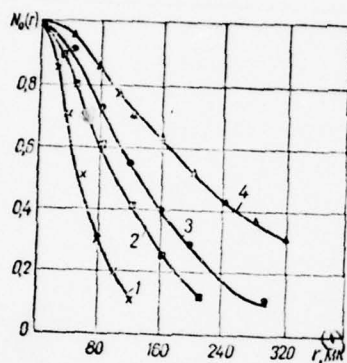


Fig. 5.19.

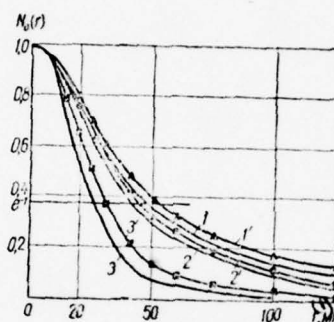


Fig. 5.20

Fig. 5.19. Experimental dependence of the relative value of the pyroelectric voltage N_0 from distance between centers of light ray and point electrode for the crystal of TGS at the different thicknesses of upper electrode d_1 : 1 - 0.1; 2 - 0.15; 3 - 0.5; 4 - 0.9 mm.

Key: (1). μ .

Fig. 5.20. Dependence of parameter N_0 on distance between centers of

light ray and point electrode r for the crystal of TGS at different modulation frequencies: 1 - 13; 2 - 36; 3 - 285 Hz (1-3 - calculated curves; 1'-3' - experimental).

Key: (1) - μ .

Page 147.

The calculation conducted shows that use of the field triode with the entry impedance 10^{14} ohm inherent noise level, lower than the Johnson noise of the cell/element of pyroelectric target from TGS, makes it possible to obtain value $S = (10^5 - 10^6)$ V/W at low modulation frequencies. Threshold of response also decreases to 10^{-10} W/Hz $^{1/2}$.

Its own time constant of the cell/element of target as for all pyroelectric receivers, is $10^{-5} - 10^{-6}$ s.

The permission of system in practice does not depend on the thickness of crystal, but sufficiently substantially it is increased with an increase in the modulation frequency of light ray (with $\omega C_0 R_n \gg 1$) and with a decrease in the thickness of the upper sprayed electrode.

§5. Receivers of complete radiation absorption.

In connection with the amplification of works on absolute spectrometry and radiometry in recent years arose the need for the creation of the standard meters, making it possible to determine the spectral receiver responses of emission/radiation and independently used for these purposes.

For an example let us examine the process of spectral measurement by the scanning spectrometer - the instrument, performance characteristics of which are the complex composition of the characteristics of optical and electrical node/units [30].

In general form the result of optical and electrical effects on the spectrum being investigated can be presented in the form

$$U = \Lambda h S W, \quad (5.15)$$

where Λ is the apparatus function, which characterizes the distortion of the true spectrum W under the influence on it of the scanning optical system; h - the transient function, which describes system response to unit step. In this case one should consider the

distortions of intensity and form of true noise spectrum of receiver and by the nonlinearity of the entire receiving-recording system.

Obtaining the true spectrum W with measured U is called reduction to ideal instrument. This problem is the central task of spectrometry and in the general case is solved very complicatedly.

However, task is simplified, if receiver completely absorbs emission/radiation in the assigned spectral interval and has low inertia, since development of amplifying recorders, which do not distort the spectrum, is technically solved. For the absolute measurements of emission/radiation in the ultraviolet, visible and infrared regions of the spectrum in many instances are used thermal radiation detectors. Many researchers, assuming that the thermal radiation detectors in principle are nonselective, if are covered with the layers, which completely absorb emission/radiation, during measurements with by industrial thermocouples, bolometers or acousto-optical detectors frequently refer to their one hundred percent "blackness".

end section.

Page 148.

Are at present many works, dedicated to technology of obtaining and to investigation of the characteristics of the absorbing coatings and optical materials. It would seem, not difficult to foresee the spectral characteristics of thermal radiation detectors. However, the conditions of the formation of the absorbing coatings on transparent in this spectral interval plates and sensing elements different can change in time. Therefore the question of the determination of the spectral characteristic of completely ready radiation detectors has important value.

The recently conducted investigations of the spectral characteristics of bolometers and radiation thermocouples showed that their utilization as standards can lead to large errors [7.55-57, 65, 66, 95].

Are possible two methods of determining the spectral receiver responses of the emission/radiation:

1) the method of standard source [8, 37, 40, 45, 61, 79, 80, 82, 86, 95];

2) the method of the standard receiver of complete radiation absorption [7, 24, 25, 34, 44, 55, 57, 60, 64-66, 68, 78, 89, 94, 95, 99].

the first method consists of the calibration of the receiver being investigated on the basis of source with the known spectral distribution of intensity (tungsten lamp or specimen blackbody) with the aid of the monochromator, the transmission function of which is determined.

In the second calibration method of receivers consists of the comparison of the spectral characteristic of the receiver being investigated with the spectral characteristic of standard thermal radiation detector, establish/installed on the output/yield of monochromator.

Were outlined in essence two tendencies in the creation of the thermal radiation detectors of the total absorption: the development of radiation microcalorimeters [55, 65, 66, 68] and of the ferroelectric receivers, having the form of blackbodies [23, 24-26, 43, 44].

The pyroelectric receivers of total absorption can be made in the form of conical, tapered or spherical blackbody (Fig. 5.21).

The calculation of the emissivity of wedge- or cone-shaped receiver can be conducted by geometric construction (see Fig. 5.21a) and according to the data on the absorption and reflectivities of the material of the internal surface of cone.

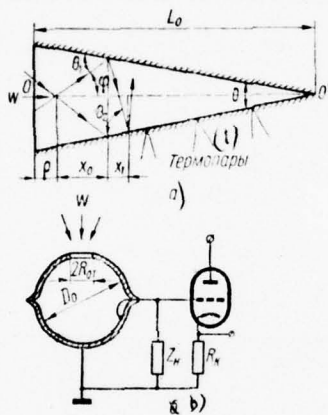


Fig. 5.21. Pyroelectric receivers of complete radiation absorption:
a) conical or wedge-shaped; b) spherical.

Key: (1). Thermocouples.

It is possible to obtain [65, 66] the following relationship/ratios:

$$\begin{aligned} \theta_n &= \varphi + (2n + 1)\theta; \\ l_0 &= \rho + \sum_{i=0}^n x_i; \\ x_n &= 2 \left[(L_0 - \rho_0) - \sum_{i=0}^{n-1} x_i \right] \operatorname{tg} \theta / \operatorname{tg} \theta + \operatorname{tg} (\varphi + 2n\theta), \end{aligned} \quad (5.16)$$

where θ_n is the angle, hearth by which the entering ray/beam will be reflected from the internal surface of cone after n of reflections; l_0 is a projection of distance on the axis of cone OO' , passed by ray/beam after n of reflections and measured from O to O' ; x_n - the projection of the path of ray/beam on axis CO' between n about $n + 1$ by reflections.

If $\theta_n > \pi/2$, ray/beam emerges the cone. The number of reflections and the covered path can be described by the equations, analogous (5.16). Under these conditions the relationship/ratio between the number of reflections, after the ray/beam emerges the cone, and the distance along axis OO' to the side of the basis/base of cone takes the form

$$\begin{aligned} \xi &= (L_0 - l_0) + \sum_{i=1}^k z_i; \\ z_k &= 2 \left[(L_0 - l_0) + \sum_{i=1}^{k-1} z_i \right] \operatorname{tg} \theta / \operatorname{tg} [\alpha_0 - (2k - 1)\theta] - \operatorname{tg} \theta, \end{aligned} \quad (5.17)$$

where $\alpha_0 = \pi - (0_k - 2\theta)$.

The authors [65, 66] calculated the values of the absorptive ability of cone for some materials in the case of mirror and diffuse reflection. During an increase in the value of the mirror reflection coefficient in comparison with diffuse is observed an increase in the absorptivity of wedge or cone. The computed values of absorptivity ϵ_0 can reach value of 0.999.

Develop in IF AS UkSSR cone-shaped pyroelectric receivers of longitudinal type emission/radiation (Fig. 5.22a) possess the following characteristics:

1) the volt-watt sensitivity $S = (0.5-1)$ V/W at modulation frequency 10 Hz during the load resistance $R_n = 1$ G Ω ;

2) threshold of response $\mathcal{P} = (5 \cdot 10^{-8} - 10^{-7})$ W/Hz^{1/2};

3) time constant $\tau < 50 \mu\text{s}$;

4) absorptivity $\epsilon_0 \approx 0.8-0.9$.

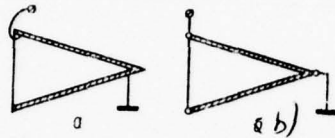


Fig. 5.22. Cone-shaped pyroelectric receivers: a) the longitudinal type; b) cross.

Page 150.

Cross type cone-shaped pyroelectric receivers (see Fig. 5.22b) prepared from ceramics of titanate of barium, are characterized by these parameters:

1) the volt-watt sensitivity $S = (0.2-0.4) \text{ V/W}$ at modulation frequency 10 Hz during the load resistance $R_L = 1 \text{ G}\Omega$;

2) threshold of response $(5 \cdot 10^{-7} - 10^{-7}) \text{ W/Hz}^{1/2}$;

3) time constant $\tau \sim 20 \text{ ns}$;

4) absorptivity $\epsilon_0 \approx (0.85-0.95)$ in the range $0.4-20 \mu$;

5) geometric dimensions: $L_0 = 20 \text{ mm}$, $2\theta = 15^\circ$, $d = 200 \mu$, the diameter of inlet 6 mm .

The possibility of the production of pyroelectric receivers in the form of the figures of complex form with large area was used for developing the standard receivers of spherical form with high absorptivity [23-36]. Standard pyroelectric receiver is spherical condenser/capacitor (Fig. 5.23) with round or rectangular inlet. Receiver consists of two cemented/glued hemispheres, prepared from pyroactive ceramics with internal and external metal electrodes. For an increase in the absorptive ability internal surface is cover/coated with the layer of gold black.

The evaluation of the quality of receiver as an absolute absorber of emission/radiation can be carried out in accordance with the calculated relationship/ratios, recommended in works [9, 59, 64, 69].

The principle of the calculation of absorptivity is of the calculation of emission/radiation of the assigned direction from arbitrary cell/element within sphere, the consisting of intrinsic emission this cell/element and reflected it emission/radiation from

all other cell/elements of cavity. Then conducts integration for all cell/elements of cavity.

According to [64], the absorptivity of this receiver is determined by the approximate relationship/ratio

$$\epsilon_0 = 1 - \frac{\pi r_0}{\left(\frac{D_0}{R_{or}}\right)^2}, \quad (5.18)$$

where D_0 and R_{or} - the diameter of sphere and the radius of inlet; r_0 is a reflection coefficient. Table 5.1 gives the computed values of the absorptivity of different spherical pyroelectric receivers (in accordance with relationship/ratio 5.18) in spectral range 0.2-150 μ , when the internal surface of sphere is covered with gold black or silverplated.



Fig. 5.23.
Are standard spherical type pyroelectric receiver.

Page 151.

As can be seen from Table 5.1; in ratio $D_0/R_{01} > 10$ the absorptivity, ϵ_0 , of receiver independent of value r_0 so close to unity that in a number of cases there is no need for for the

deposition of black on the internal surface of sphere.

By G. A. Puchkovskoy et al. [7] on indicatrices of scattering from the surfaces, adequate to the internal surfaces of sphere, are experimentally obtained the values of coefficients r_0 and is calculated the absorptivity of sphere in spectral range 1-25 μ . The obtained values of absorptivity for the developed receivers were 0.98-0.99.

Natural interest is of the experimental check of absorptivity ϵ_0 spherical pyroelectric receivers. Thus far it was not impossible to find any reliable and simple method of experimental determination ϵ_0 . However, the qualitative investigations, which confirm the correctness of the calculations, were conducted. Were made [23, 26] receivers by diameter $D_0 = (3.5-10)$ mm and wall thickness 100-300 μ with the input window of round and rectangular form 0.3-1.5 mm² in area. By the authors was investigated receiver sensitivity to the emission/radiation, when its internal surface was covered with gold black, then with the restored/reduced black after heating to 150°C and with removed by its mechanical method. The value of volt-watt sensitivity during these measurements remained constant/invariable within the margins of error in measurements ($\pm 20\%$). The spectral receiver responses, written with respect to one of them in region 1-25 μ , also they differed not more than by 20%, which corresponded

to the accuracy of measurements.

In the spectral dependent absorbing and reflectivity of the internal surface of spherical receiver are essential the uniformities of its zonal sensitivity and the linearity of amplitude characteristic.

The conducted investigations with the pyroelectric receivers of large area showed that of 95o/o of area of receiver the divergence of sensitivity from its average value does not exceed 5o/o, but the linearity of amplitude characteristic is retained with an accuracy to 1-2o/o within the limits of the rate of flow of emission/radiation $10^{-1}-10^{-7}$ W/mm².

Table 5.1.

D_0 , мм	$R_{(1)0T}$ мм	ϵ_0	
		(2) Серебро	(3) Золотая чернь
10	0,75	0,983	0,998
10	0,5	0,992	0,999
7	0,5	0,984	0,998
5,5	0,65	0,95	0,996
5	0,35	0,984	0,998
3,5	0,3	0,977	0,998

Note. For silver $r_{\max} \approx 0.98$, for the gold black $r_{\max} \approx 0.1$.

Key: (1). from. (2). Silver. (3). Gold black.

Page 152.

Under such conditions output signal in practice does not depend on that, in which part of the receiver is absorbed the incident radiation: over an entire surface it is evenly or in one place. The washed away and focused image of standard source gave one and the same signal within the limits of accuracy of measurements.

The fundamental characteristics of spherical pyroelectric radiation detectors are the following:

- 1) the volt-watt sensitivity $S = (2-5) \text{ V/W}$ at modulation frequency 10 Hz during the load resistance $R_n = 1 \text{ drive}$;
- 2) threshold of response $\mathcal{P} = 5 \cdot 10^{-8} \text{ W/Hz}^{1/2}$;
- 3) time constant $\tau < 50 \text{ } \mu\text{s}$;
- 4) the geometric dimensions of the sensor: $D_0 = 5 \text{ mm}$, $R_{or} = 0.5 \text{ mm}$, $d = 150 \text{ } \mu$;
- 5) absorptivity $\epsilon \approx 0.99$.

The measured threshold of response 1.5-2 times is worse than calculated due to acoustic noises, since pyroelectric receiver simultaneously is piezoelectrick pickup.

Pyroelectric receivers of total absorption can be used for the measurement of intense radiation fluxes. But for this their internal surface is cover/coated with high-melting layer with high

reflectivity (for example, by the layer of platinum 1000 Å thickness). During irradiation occurs the redistribution of radiation flux, passing through the input window, over an entire internal surface of sphere, is expanded the dynamic range of receiver it is safeguarded the surface of the primary incidence/impingement of ray/beams from destruction.

During the study of intense radiation fluxes, by selecting $\omega C_0 R_n \ll 1$, it is possible to measure directly the emission impulses of approximately 50 μ s.

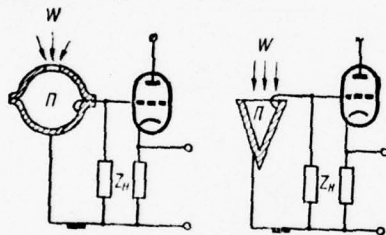


Fig. 5.24.

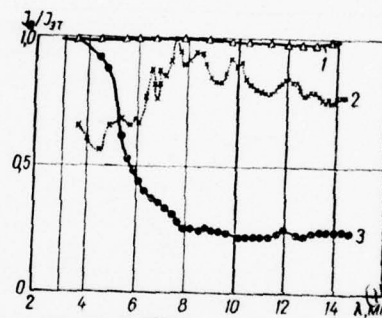


Fig. 5.25.

Fig. 5.24. Circuit diagram of the receivers of total absorption.

Fig. 5.25. Relative spectral characteristics of some thermal radiation detectors (measured with respect to standard pyroelectric receiver): 1) pyroelectric receiver (nickel bolometer); 2) semiconductor bolometer; 3 - bismuth bolometer.

Key: (1). μ .

Page 153.

If is required high volt-watt receiver sensitivity, it should be worked at low modulation frequencies 10-20 Hz, selecting $\omega C_0 R_{\parallel} \gg 1$.

The circuit diagram of the pyroelectric receivers of total absorption is given in Fig. 5.24.

Pyroelectric radiation detectors are intended for recording modulated and pulsed radiation fluxes [31, 36, 41, 42, 46, 51-53, 63, 71-74, 77, 81, 83, 84, 88, 90, 91, 97, 101, 103-106]. In the case, when cannot be modulated radiation flux, for measurements can be used ferroelectric bolometers. However, their threshold of response with the same thickness of sensing elements is worse than of pyroelectric. The pyroelectric receivers of total absorption were used for determining the spectral characteristics of thermal radiation detectors [7].

The conducted investigations showed that the spectral characteristics of some TPI possess considerable selectivity, although according to the specifications frequently is guaranteed the uniformity of their spectral characteristic. Spherical pyroelectric receivers of total absorption can be recommended as standards during investigation in wide spectral integral from extreme ultraviolet to

the far-infrared region of the spectrum. Figure 5.25 gives the relative spectral characteristics of some thermal receivers of emission/radiation.

§6. Coordinate-sensitive pyroelectric radiation detectors.

Coordinate-sensitive (position-sensitive) and servo transformers find wide application in electro-optical equipment. there is a series of works, dedicated to the description of optical position detectors with photosensitive receivers [27, 35, 38].

The main advantage of the optical sensors of the position before other instruments is the absence of mechanical communication/connection with the controlled/inspected object and the possibility of remote control.

There exists two types of photoelectric coordinate-sensing apparatus. The first type is the electrooptical bridge, which is specific composition of optical, electrical and mechanical cell/elements. one of basic parts of first type instruments is the analyzer of image, which gives information about the position of the controlled/inspected object. The presence of the analyzer of image

considerably complicates the design of the sensor of position and impedes its microminiaturization.

In the second type coordinate- of delicate apparatus are combined the functions of analyzer and receiver in one solid-body cell/element.

Page 154.

The photoelectric receivers with coordinate-dependent sensitivity are those which move rapidly and comparatively small. In them during the local illumination of sensitive surface the value of output signal depends on the position of gate of entry on the surface of receiver.

One of the basic parameters of the coordinate-sensitive apparatus is the characteristic of displacement. In a number of cases it is desirable that this parameter would have in operating region the linear section whose slope/inclination determines instrument sensitivity - the value of the signal, which appears in moving ray/beam per unit of dyne. It is desirable also in order that in operating region the characteristic of displacement would pass through the zero point, and then it changed its sign to opposite.

Requirements for the linearity of response of displacement

mainly are presented to the receivers, designed for the direct measurement of the appearing displacement. In the case, when coordinate-sensitive receiver plays the role of null indicator, requirements for linearity are not necessary.

Are distinguished the coordinate-sensitive photoreceivers whose action/effect is based on photoconductive effect, and semiconductor photoreceivers on p-n junctions [32]. The photoconductive coordinate-sensitive receivers include differential photoresistors and photopotentiometers. Multielement photodiodes, the longitudinal photocells and bicrystal photoreceivers with coordinate sensitivity, which appears during irradiation of p-n junction, are advanced, than photoconductive, due to their operating speed, the stability of characteristics and increased sensitivity.

A deficiency/lack in the photoelectric coordinate-sensitive receivers of radiation is spectrally the narrow working range at room temperature. Their sensitivity is limited to the visible and near IR spectral region.

Pyroelectric coordinate-sensitive radiation detectors, developed/processed recently, can be used nonselectively in a wide spectral interval. Receiver consists of pyroactive crystal in the form of plane-parallel plate III (Fig. 5.26), irradiated electrode

II, which is layer of silver of thickness 0.1μ , to which is plotted/applied the layer of gold black I of the same equivalent thickness. The opposite (acicular) electrode IV has a form of circle as diameter $D_0 = 50 \mu$.

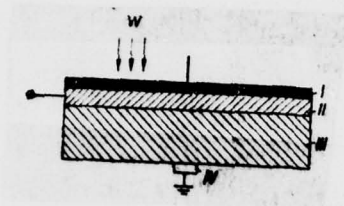


Fig. 5.26. Circuit of the pyroelectric coordinate-sensitive receiver: I - black; II - electrode; III - pyroactive crystal; IV - point electrode.

Page 155.

As pyroactive material can be used the single crystals of TGS and polarized ceramics BaTiO_3 of approximately 100μ thickness. Sensing element is placed into the Permalloy housing, which screens from electromagnetic fields and which shields from mechanical damage. In housing there is an input window from transparent in a spectral interval being investigated material. The operating principle of coordinate-sensitive radiation detector consists of the following. The modulated radiant flux in the form of the focused with optical

system narrow beam, being absorbed by the layer of black, produces local heating continuous electrode and pyroactive crystal. As a result of a change in the temperature of crystal on its surfaces appear changing with modulation frequency the polarized charges, which lead to the emergence of pyroelectric voltage between the upper the continuous and lower by point electrodes. Pyroelectric voltage will be maximum, if the centers of incident beam and point electrode lie on one vertical line. With the removal/distance of beam from this vertical line the voltage falls. Radial dependence of the relative receiver sensitivity is shown in Fig. 5.27. Changing the thickness of the irradiated electrode, it is possible to change the form of curved relative sensitivity. With the very fine/thin irradiated electrodes and the at high modulation frequencies of radiant flux this curve it has resonance character. By decreasing the modulation frequency and by increasing the thickness of upper electrode, it is possible to obtain the quasi-linear curve of relative sensitivity.

Pyroelectric coordinate-sensitive radiation detector has the following fundamental characteristics:

1) the volt-watt sensitivity of the cell/element, when the center of incident beam and point electrode lie/rest on one vertical line, at the frequency of modulation 20 Hz it composes 2000 V/W; radial sensitivity $5 \cdot 10^3$ V/ (W.mm);

2) threshold of response under these conditions comprises $5 \cdot 10^{-9}$ $W/Hz^{1/2}$;

3) disconnection/cutoff from the linearity of amplitude characteristic does not exceed $\pm 50\%$ in the range of radiant fluxes $(10^{-8} - 10^{-2}) W/mm^2$;

4) time constant is $10^{-5} - 10^{-6}$ s;

5) the spectral range of sensitivity is characterized by the spectral characteristic of the absorbing coating (for example, by gold black); therefore receiver, in principle, can be used in any section of the electromagnetic spectrum.

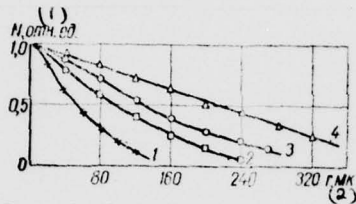


Fig. 5.27. Radial dependence of the relative sensitivity of the coordinate-sensitive receiver $N = N(r)$: 1 - 0.1; 2 - 0.15; 3 - 0.5; 4 - 0.9 μ .

Key: (1). rel. un. (2). μ .

Page 156.

The smallest possible displacement, which can be reveal/detected with the aid of pyroelectric coordinate-sensitive receiver (its maximum resolution), is determined by inherent noise level. It is possible to introduce the concept of threshold sensitivity on displacement, defined as value of displacement of the radiation beam, which causes the signal, equal to the RMS value of noise. In turn,

the threshold of response on displacement is the function of coordinate, after grow/rising with removal/distance from point electrode. Therefore for determining the resolution of these receivers it suffices to know the small value of its threshold of response and the radial dependence of output signal.

The coordinate dependence of the sensitivity of pyroelectric receiver can be obtained with use of a pyroactive crystal with a nonuniform thickness of d . The volt-watt sensitivity of longitudinal type pyroelectric receiver (4.67)

$$|S_{np}| \approx \frac{\gamma_{\pi} e_0 R_n}{cd (1 + \omega^2 C_0^2 R_n^2)^{0.5}}$$

inversely proportional to the thickness of crystal, if $\omega^2 C_0^2 R_n \ll 1$.

However, the execution of this inequality is bonded with deterioration in the volt-watt sensitivity; therefore in the general case the dependence S_{np} on thickness d has a complex character.

Figure 5.28 gives the coordinate sensitivity of the pyroactive crystal, which has the form of wedge, from the position of the illuminated zone. The quasi-linear sections of curve can be used for the creation of coordinate-sensitive receiver.

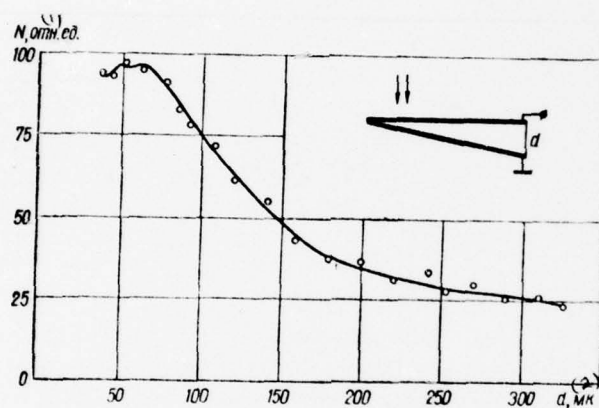


Fig. 5.28. The coordinate sensitivity of the pyroelectric receiver, which has the form of wedge, from the position of the illuminated zone.

Key: (1). rel. un. (2). μ .

§7. Receivers for emission/radiation measurement by substitution method.

The measurement of electromagnetic radiation with the aid of thermal receivers can be realized by two methods - by direct measurement and by substitution method (comparison in the process of measurement).

The method of direct measurement consists of the determination of unknown radiated power from the exit dial face, which is calibrated with the aid of the standard emitter before measurements. Reliability of such measurements is caused by the stability of the receiver responses of emission/radiation and many cell/elements of amplifier circuit in the period between calibrations. In connection with this this method possesses low accuracy and in essence is used for the indication of radiation flux.

Substitution method consists of the comparison (during measurement) of the radiated power being investigated with the power of the calibrated heat flux, supplied to receiver from the radiation source or of another heat source. The accuracy of measurements with

the aid of substitution method is determined in essence by the stability of the characteristics of the source of the heat flux, which consists of one or a few cell/elements, and the radiation detector and the amplifier unit determine the only sensitivity of meter. Therefore the accuracy of the measurement by substitution method is considerably higher than by the method of direct measurement.

The calibrated sources of heat flux can be optical or electrical. as an example of optical source can serve calibrated black body or incandescent bulb. The principle of measurement consists in consecutive comparison with the aid of the covering device or the circuit of modulation of the radiated power and of the standard sources being investigated. Measurements can be conducted by compensation method, by changing the emission/radiation of standard source with calibrated attenuator - optical wedge. The measure of the weakening of standard source is proportional to the power of the radiation of unknown emitter. This substitution method can be call/named optical.

The utilization of the electrical calibrated sources of heat flux, arrange/located in immediate proximity of sensing element, considerably simplifies measuring device. The majority of receivers with the calibrated sources of heat fluxes work during constant

irradiation, and the amplification of the removed from sensing transducer conducts by dc amplifier. Such systems are very inertia and insufficiently sensitive.

Page 158.

More preferable are the receivers, which work on the modulated radiation flow and the utilized electrical substitution of this flow of with a power Joule losses of alternating current [5].

The pyroelectric radiation detector, intended for the measurement of electromagnetic radiation by the method of substitution, is shown schematically in Fig. 5.29. The principle of its work consists of the following. The radiant flux W being investigated, modulated by mechanical timer, falls in receiver. Appearing in the absorbing coating thermal oscillations are spread through the heating element 2, separating dielectric layers 3 and they reach sensing element 4. During a change in the temperature of crystal in it appears the signal, which is supplied to input amplifier stage.

If the thermal pulses created by alternately entering to sensing element by the rectangularly modulated radiant flux and right-angled by electric current, is identical, then output signal from receiver

will become equal to zero. However, the method of the irradiation of sensing transducer right-angled suffers essential deficiency/lack. Heating element is arranged in immediate proximity of sensing element, and the voltage, supplied to heating element, it excites in receiver parasitic signal. Since the power of Joule losses is proportional to the square of stress on heating element, and spurious signal - the first degree of voltage, the effect of focusing/induction will be large with low signals. To get rid of the focusing/induction, which coincides in frequency with the signal of imbalance, is difficult.

In connection with this more rational is the utilization of sinusoidal modulation of radiation flux with the frequency, two times exceeding the frequency of the sine voltage, supplied to heating element.

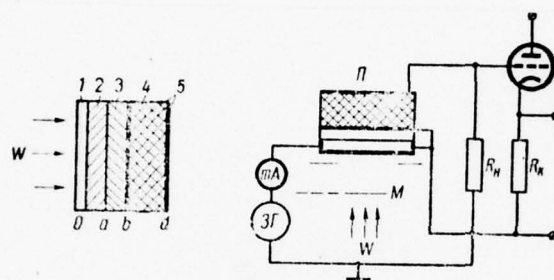


Fig. 5.29. Pyroelectric receiver for emission/radiation measurement according to substitution method: 1 - the absorbing coating; 2 - heating element; 3 - separating layer; 4 - pyroelectric; 5 - electrodes; p - receiver; m - modulator; ZG - generator.

Page 159.

In this case the signal frequencies of imbalance, proportional to a difference in the amplitudes of thermal radiant flux with the thermal flow of Joule losses, and spurious signal also differ double. By utilizing the narrow-band amplifier, tuned to a frequency of the

signal of imbalance, it is possible to remove spurious signal.

The selection of the geometric and thermophysical characteristics of the layers of sensing element is essential during the development of receiver. heating element must be so fine/thin in order that the length of temperature wave in working frequency band would be considerably more than his thickness. Under this condition it is possible to assume the equivalency of the action of the radiation flow of the heat flux of Joule losses with respect to sensing element of receiver.

Requirements for the geometric characteristics of layer are contradictory. On one hand, the small thickness of layer leads to an increase in the stray capacitance of communication/connection between heater and sensing element. With another, an increase in the thickness of the dielectric interlayer limits the frequency range of receiver.

Let us find the calculated relationship/ratios, which relate geometric, thermophysical and frequency receiver responses.

Let in the heater be released the power of alternating current

$$W_s = \frac{U_0^2 \sin^2 \theta}{R} \cdot \quad (5.10)$$

where $U_0 \omega_0$ is voltage and the frequency of alternating current; t is time; R - the resistance of heater.

For the determination of temperature increment in dielectric layer and sensing element, is solved the equation of thermal conductivity [14]

$$\frac{\partial \Theta_n(x, t)}{\partial t} = \eta_n \frac{\partial^2 \Theta_n(x, t)}{\partial x^2} \quad (5.20)$$

with the following boundary conditions

$$\begin{aligned} \Theta(x, t)_{x=a} &= \Theta_a e^{2i\omega_0 t}; \\ \Theta(x, t)_{x=b} &= \Theta_b e^{2i\omega_0 t}; \\ \Theta_3(x, t)_{x=b} &= \Theta_4(x, t)_{x=b}; \\ k_3 \left(\frac{\partial \Theta_3(x, t)}{\partial x} \right)_{x=b} &= k_4 \left(\frac{\partial \Theta_4(x, t)}{\partial x} \right)_{x=b}; \\ \Theta_4(x, t)_{x=d} &= 0. \end{aligned} \quad (5.21)$$

In equations (5.20) and (5.21) are conducted the following designations; Θ is a temperature increment; $n = 2, 3, 4$ the numbering of the compound/composite layers (parts) of receiver; $\eta_n = \frac{k_n}{c_n}$ - thermal diffusivity, k and c - the thermal conductivity and the heat capacity of unit volume.

As a result of the solution of system of equations (5.20) under boundary conditions (5.21) let us find that

$$\Theta_4(x, t) = \Theta_b \frac{\text{sh } \mu (d-x)}{\text{sh } \mu (d-b)} e^{2i\omega t}. \quad (5.22)$$

In equation (5.22)

$$\begin{aligned} \Theta_b &= \frac{\Theta_a}{\text{ch } m(b-a) [1 + H \text{cth } \mu (d-b) \text{th } m(b-a)]}; \\ \mu &= (1+i) \sqrt{\frac{\omega_0}{\eta_4}}; \quad m = (1+i) \sqrt{\frac{\omega_0}{\eta_3}}; \\ i &= \sqrt{-1}; \quad H = \sqrt{\frac{k_4 c_4}{k_3 c_3}}. \end{aligned} \quad (5.23)$$

During irradiation of the absorbing coating by the sinusoidally modulated radiation flux $W_1 = A_0 e_0 W_0 e^{i\omega t}$ (e_0 - the absorptivity of black; W_0 - the density of radiation flux; ω - modulation frequency A_0 - the area of sensor) the appearing in sensing element temperature increment is defined by equation [17]:

$$\Theta'_4(x, t) = \Theta'_b \frac{\text{sh } m_4 (d-x)}{\text{sh } m_4 (d-b)} e^{i\omega t}, \quad (5.24)$$

where

$$\begin{aligned} \Theta'_b &= \Theta'_a / \text{ch } m_3(b-a) [1 + H \text{cth } m_4(d-b) \text{th } m_3(b-a)]; \\ m_3 &= (1+i) \sqrt{\frac{\omega}{2\eta_3}}; \quad m_4 = (1+i) \sqrt{\frac{\omega}{2\eta_4}}. \end{aligned} \quad (5.25)$$

From comparison (5.22) - (5.23) with (5.24) - (5.25) we see that a change in the temperature of sensing element will be one and the same under the influence on the receiver both of variable electric current and radiant flux, if

$$\omega = 2\omega_0; \quad (5.26)$$

$$eA_0W_0 = U_0^2/R. \quad (5.27)$$

During heating of pyroactive crystal in it appears the pyroelectric current

$$J = \frac{\gamma hl}{(d-b)} \int_b^d \frac{d\theta(x, t)}{dt} dx, \quad (5.28)$$

where γ - pyroelectric coefficient, h and l - the width and the length of pyroactive crystal. By substituting in (5.28) values $\theta(x, t)$ from (5.22) or (5.25), we will obtain the value of the pyroelectric current, which appears in crystal with the transmission through the heater of alternating of the electric current

$$J = A \frac{\text{th} \mu \frac{d-b}{2}}{\mu (d-b) \text{ch} m (b-a) [1 + H \text{cth} \mu (d-b) \text{th} m (b-a)]}, \quad (5.29)$$

$$A = 2i\omega_0 \gamma hl \Theta_0 e^{2i\omega_0 t}.$$

Page 161.

Now let us establish/install communication/connection between the sensitivity of pyroelectric receiver, the thickness of dielectric layer, its thermophysical properties and the characteristics of pyroactive crystal. The thickness of dielectric layer we select in such a way that receiver sensitivity as a whole would decrease not more than in N once.

From (5.29) follows that in the absence of the layer

$$\mathcal{T}_1 = A \frac{1 - \operatorname{sch} \mu(d-b)}{\mu(d-b) \operatorname{th} \mu(d-b)}. \quad (5.30)$$

The introduction of the dielectric layer between the heater and the pyroactive crystal lowers the taken from crystal signal in N once,

i.e.,

$$|\mathcal{T}_1| = N |\mathcal{T}|. \quad (5.31)$$

Substituting in (5.31) the values \mathcal{T} and \mathcal{T}_1 from (5.29) and (5.30) and by expanding hyperbolic functions in a series in $\left[\sqrt{\frac{\omega_0}{\eta_4}} (b-a) \right]$, we will obtain with $\sqrt{\frac{\omega_0}{\eta_4}} (d-b) \gg 2$

$$\Lambda^2 = \frac{2(b-a) \sqrt{\omega_0 k_4 \epsilon_4}}{k_3} + 1. \quad (5.32)$$

From condition (5.32) it follows that for an increase in the thickness of dielectric layer without a considerable reduction in the removed from sensing transducer and deterioration in the working frequency range it is necessary to select the material of dielectric layer with the largest possible thermal conductivity k_3 , but the values of the quantities of pyroactive crystal k_4 and C_4 must be as far as possible smaller.

Table 5.2 gives the corrected values of the thicknesses of dielectric layers from the different materials with different ω_0 whose introduction lowers the removed from pyroactive crystal signal not more than 1.5 times.

Table 5.2.

(1) Материал прослойки	(2) $\frac{W}{cm \cdot ^\circ C}$ k_2	(3) Толщина прослойки для $N = 1,5$, см					(4) Примечание
		ω_a					
		10	10^2	10^3	10^4	10^5	
LiF [4]	0,142	0,275	0,067	0,0275	0,0067	0,00275	(6) Пироактивным кристаллом выбран ТГС, у которого $c_4 = 2,548 \frac{W \cdot \text{сек}}{cm^3 \cdot ^\circ C}$ $k_4 = 6,872 \times 10^{-1} \frac{W}{cm \cdot ^\circ C}$
(*) Кварц [4]	0,070	0,137	0,033	0,0137	0,0033	0,00137	
Al ₂ O ₃ [28]	0,296	0,580	0,139	0,058	0,01390	0,0058	
BeO [76]	2,310	4,53	1,09	0,453	0,109	0,0453	

Key: (1). the material of layer. (2). W/cm·deg. (3). Thickness of layer for. (4). Note. (5). Quartz. (6). By pyroactive crystal is selected the TGS, which has. (7). W·s/cm³·deg. (8). W/cm·deg.

The block diagram of installation with receiver is represented

in Fig. 5.30. On sensing element of receiver 1 simultaneously act two heat fluxes, out of phase: the measured radiant flux W , sinusoidal modulation of which is realized with the aid of modulator 7, and the heat flux \dot{W} , created by alternating current, passing through the heating element of receiver. The frequency of alternating current ω_0 is assigned by generator 5. Simultaneously this generator supplies frequency doubler 4 and through phase inverter 6 voltage is fed to the modulator, that interrupts itself radiant flux with frequency $2\omega_0$.

two heat fluxes - measured and compensative - affect the sensing element, creating in it a resulting signal. This signal is then amplified with selective amplifier 2 and is supplied to recording instrument 3.

Measurements can be conducted through zero-method. By changing the stress level, which feeds heating element, and the controls of phase displacement it is possible to attain equality zero of resulting signal. The power of the falling/incident radiant flux is determined by formula (5.27).

zero-method detail with the high accuracy of measurements possesses essential deficiency/lack - inertness, since is required considerable time for compensation.

Promising can turn out to be the phase-meter method, in which the relation of two heat fluxes is proportional to the phase angle between their vectors [10]. during the rational selection of the initial phase angle it is possible to obtain the quasi-linear dependence of the relation of two values within the limits of two orders of change in one of them. This method of measurement is, in principle, high-speed/velocity.

The described pyroelectric radiation detector can be used as the absolute meter, which completely absorbs electromagnetic radiation and which does not require any calibration. the latter is provided by the very principle of its work. Total absorption of the falling/incident to radiation detector can be attained because of geometric form. If pyroelectric receiver is prepared in the form of 15-degree wedge, its emissivity can be drawn nearer the absorptivity of absolute blackbody ($\epsilon_0 \sim 0,95$).

The creation of "black" pyroelectric receiver for emission/radiation measurement by substitution method can be one of the methods of the realization of the standard receiver optical range.

AD-A046 669

FOREIGN TECHNOLOGY DIV WRIGHT-PATTERSON AFB OHIO

F/G 17/5

FERROELECTRIC RADIATION DETECTORS, (U)

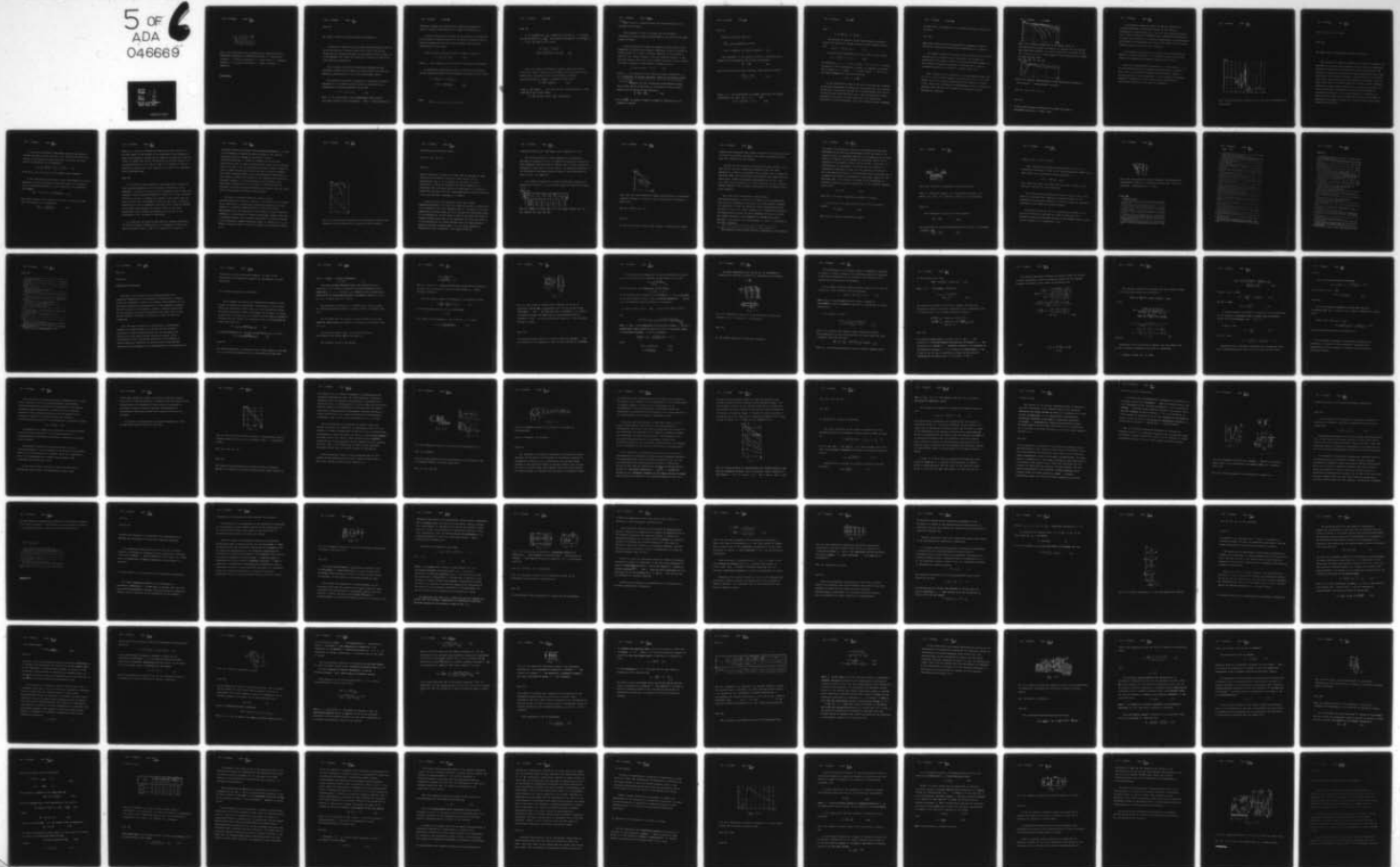
JUL 77 L S KREMENCHUGSKIY

FTD-ID(RS)T-0846-77

UNCLASSIFIED

NL

5 OF
ADA
046669



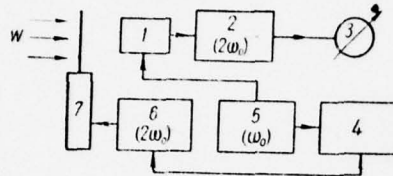


Fig. 5.30. Block diagram of installation for emission/radiation measurement according to substitution method: 1 - pyroelectric receiver; 2 - selective amplifier; 3 - output meter; 4 - frequency doubler; 5 - the master oscillator; 6 - phase inverter; 7 - modulator.

~~end section.~~

Page 163.

§8. Work of receivers on high modulation frequencies.

Already first works [58] on recording emission impulses with the aid of pyroelectric receivers showed that in the range of high frequencies are observed resonance of pyroelectric current, which, as it was assumed, will limit the threshold of response of receiver at high modulation frequencies.

Let us examine the work of pyroelectric receiver on high modulation frequencies and examine the contribution of primary and secondary pyroelectricity to the total pyroelectric effect.

the electrical induction of crystal D as function of elastic deformations u , of electric field E and of an increase in the temperature θ in matrix notations has the form

$$D = e^{\theta, E} u + \varepsilon^{\theta, u} E + \gamma^{u, E} \theta, \quad (5.33)$$

where $e^{\theta, E}$ is a matrix/die of the coefficients, which connect electrical induction with deformation $\varepsilon^{\theta, u}$ and $\gamma^{u, E}$ are matrix/dies of

dielectric constant and pyroelectric coefficient (superscript indicate constant conditions of the change of coefficients).

Let the crystal plate, attached on support/base, be irradiated by the modulated radiant flux ΔW . In the plate, irradiated side of which is covered with the thin layer of black, polar axis is perpendicular to its plane.

Current density, passing through the plate, is equal to:

$$j_x = \sigma_{xx} E_x + \frac{1}{4\pi} \cdot \frac{\partial D_x}{\partial t}, \quad (5.34)$$

where σ_{xx} - the component of the tensor of electrical conductivity.

By substituting expression (5.33) in (5.34) and by averaging current density according to the thickness of crystal, we will obtain

$$\begin{aligned} d \cdot j = & \sigma \int_0^d E_x dx + \frac{1}{4\pi} \cdot \frac{\partial}{\partial t} \left(e \int_0^d u_{xx} dx + \right. \\ & \left. + \varepsilon \int_0^d E_x dx + \gamma^u \int_0^d \Theta(x) dx \right), \end{aligned} \quad (5.35)$$

where

$$e_{xxx}^{\Theta, E} = e; \quad \sigma_{xx} = \sigma; \quad j_x = j; \quad e_{xx}^{\Theta, u} = \varepsilon \text{ и } \gamma_x^{u, E} = \gamma^u.$$

Page 165.

If we designate $R_{kp} = \frac{d}{\sigma A_0}$ - resistance of plate; R_n - the value of load resistance; $C_{kp} = \frac{\epsilon A_0}{4\pi d}$ - the capacitance/capacity of plate; $\int_0^d E_x dx = -IR_n$ ($I = jA_0$), then we will obtain

$$\begin{aligned} I \left(1 + \frac{R_n}{R_{kp}} \right) + \frac{\partial}{\partial t} (C_{kp} R_n I) = \\ = \frac{A_0}{4\pi} \gamma^* \frac{\partial}{\partial t} \left(\frac{1}{d} \int_0^d \Theta(x) dx + \frac{e}{d} \int_0^d u_{xx} dx \right). \end{aligned} \quad (5.36)$$

Thus, the complete pyroelectric current, which takes place through the plate, consists of two members: the first member in the right side of expression (5.36) is determined by primary pyroelectricity, the second - secondary. In this case

$$J_{py} = \frac{A_0 e}{4\pi d} \cdot \frac{\partial}{\partial t} \int_0^d u_{xx} dx. \quad (5.37)$$

Since $u_{xx} = \frac{\partial u_x}{\partial x}$, where u_x - the shift of plate into direction x , from equation (5.37) we will obtain

$$J_{py} = \frac{A_0 e}{4\pi d} \cdot \frac{\partial}{\partial t} [u_x(d) - u_x(0)] = - \frac{A_0 e}{4\pi d} \cdot \frac{\partial}{\partial t} [u_x(0)] \quad (5.38)$$

$(u_x(d))$

equal to zero in connection with the rigid attachment of one end/lead of the plate).

From expression (5.38) it follows that the secondary pyroelectric current completely determined by the shift of the upper surface of plate.

During irradiation of plate by simulated radiant flux at high modulation frequencies the radiation absorption occurs in essence in surface layer. As a result of thermal expansion on the surface of plate act the thermal stresses, which are balanced elastic, so that the total stress, which acts on the surface of plate in the direction of X-axis, is equal to zero (surface of plate is free):

$$\sigma_{xx}^0 = c_{xx} u_{xx} - c_{xx} \alpha_T \Theta = 0 \quad (x=0), \quad (5.39)$$

where c_{xx} - the component of the tensor of elastic hardnesses, α_T is a coefficient of thermal expansion. Change in the thermal stress in the remaining cross sections of the plate can be disregarded since $\Theta(x) \ll \Theta(0)$.

. Therefore for the calculation of the shifts of plate, which appear during irradiation, it is possible to use the usual equation of the theory of the elasticity

$$\frac{1}{v^2} \cdot \frac{\partial^2 u_x}{\partial t^2} = \frac{\partial^2 u_x}{\partial x^2}, \quad (5.40)$$

where $v = \sqrt{\frac{c_{xx}}{\rho}}$ - the speed of sound in crystal in direction x; ρ is density of crystal.

Page 165.

Boundary conditions they are

$$\left. \frac{\partial u_x}{\partial x} \right|_{x=0} = \alpha_r \Theta(0, t) \text{ (surface is free);}$$

$$u_x(d) = 0 \text{ (surface is rigidly attached).} \quad (5.40 \text{ a})$$

The temperature of the surface of plate is located from the solution to the equation of the thermal conductivity

$$\frac{\partial \Theta}{\partial t} = \kappa \frac{\partial^2 \Theta}{\partial x^2} \quad (5.41)$$

under the following boundary conditions (heat losses are small):

$$\begin{aligned} -k \left. \frac{\partial \Theta}{\partial x} \right|_{x=0} &= \Delta W(t), \\ \Theta|_{x=d} &= 0, \end{aligned} \quad (5.42)$$

where κ , k - the coefficients of thermal diffusivity and thermal conductivity. If $\Delta W(t) = W_0(1 + e^{-i\omega t})$, that

$$\Theta_-(0, t) = \frac{W_0}{hk} \operatorname{th} h d e^{-i\omega t} = \Theta_0 e^{-i\omega t}, \quad (5.43)$$

where

$$h = (1 + i) \sqrt{\frac{\omega}{2\kappa}}; \quad \Theta_0 = \frac{W_0}{hk} \operatorname{th} hd.$$

The solution of equation (5.40) under boundary conditions (5.40a) and taking into account solution (5.43) assumes the form [13]

$$u_x(0, t) = -\frac{\alpha_r \Theta_0 v}{\omega} \operatorname{tg}\left(\frac{\omega}{v} d\right) e^{-i\omega t}. \quad (5.44)$$

By substituting expression (5.44) in (5.38), we will obtain

$$J_{\text{sr}} = -i \frac{A_0 \Theta_0(\omega)}{4\pi d} \alpha_r v \operatorname{tg}\left(\frac{\omega}{v} d\right) e^{-i\omega t}. \quad (5.45)$$

At frequencies $\omega = \omega_n = v \pi (2n + 1)/2d$, $n = 0, 1, 2, 3, \dots$, begins resonance of second pyroelectric current. For example, for crystal TGS, in which $\rho = 1.7 \text{ g/cm}^3$, $c_{22} = 0.5 \cdot 10^{11} \text{ dyn/cm}^2$, $d = 2 \cdot 10^{-2} \text{ cm}$, the cyclic frequency of the first resonance

$$\omega_1 = \frac{\pi}{d} \sqrt{\frac{c_{22}}{\rho}} = 1 \cdot 10^7 \frac{\text{Hz}}{\text{sec}}.$$

For the experimental study of the work of pyroelectric receiver on the high frequencies of modulation [13] was utilized dual optical modulation of laser beam from OKG-12: in high frequency with the aid of the modulator OLMSH-100 and on low - with the mechanical timer, assembled on the basis of polar relay RP-4. The removed from pyroelectric sensing transducer after the cathode follower, assembled

on lamp 6S1Zh, was supplied to the selective microvolt meters V6-6 and V6-1).

Page 166.

After dual detection and the contraction of passband to several hertzes the signal was recorded being investigated by voltmeter.

The sensing elements of receivers were fastened during fine/thin suspensions are attached to solid basis/base. Was studied the dependence of the relative value of output signal from frequency at the different irradiated electrodes of receiver and at work on fundamental absorption of pyroactive crystal (Fig. 5.31).

With a decrease in the thickness of the blackening coating from 50 to 3.5 μ the cut-off frequency f_{05} grow/rises from 0.9 to 20 kHz (curves 1-4). These results qualitatively will agree with formula (4.77). During the production of semitransparent silver electrodes of thickness 1400, 300 and 180 Å (curves 5-7) frequency receiver responses are improved.

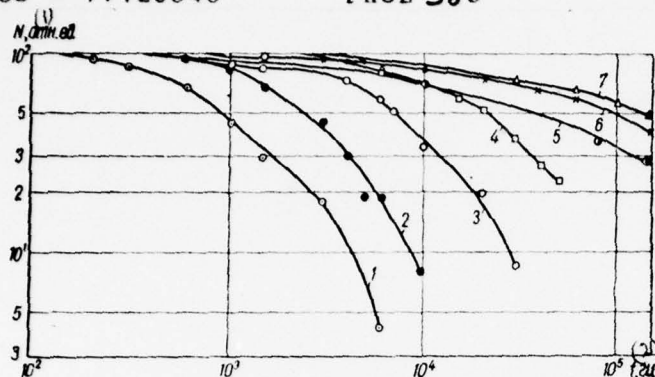


Fig. 5.31. Frequency dependence of the output signal of TGS-pyroelectric receiver as function of thickness and material of the irradiated electrode: 1-4. zloty black with a thickness of 50; 30; 11 and 3.5 μ ; 5-7 - semitransparent silver electrode with length of 1400, 300 and 180 \AA .

Key: (1). rel. un. (2). Hz.

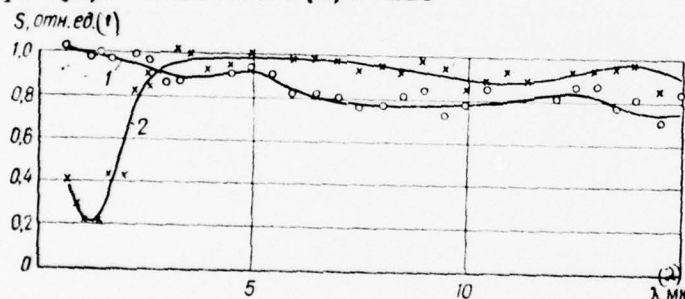


Fig. 5.32. Spectral characteristics of the pyroelectric receivers: 1 - gold black; 2 - semitransparent electrode.

Key: (1). rel. units. (2). μ .

In this case spectral characteristic is made only worse at wavelengths less than 3 μ (Fig. 5.32).

At modulation frequencies above 100 kHz are observed the resonance phenomena, especially powerful of the crystals, strengthened to solid basis (Fig. 5.33). It was established/installed [by 13] that a quantity of maximums, their amplitude and position on frequency scale depend on the geometric dimensions of specimen/sample and method of its attachment, but they do not depend on the value of electric field and value of load resistance.

By decreasing the thickness of crystal and by eliminating the effect rc - of input circuit, it is possible to lower its own time constant of pyroelectric receiver to values less $5 \cdot 10^{-8}$ s.

That as at antiresonance frequencies $\omega = v \pi n/d$ (where $n = 1, 2, 3$) the contribution of the secondary pyroelectricity is equal to zero, that it is possible to experimentally determine primary pyroelectricity at these frequencies. in the presence of resonance appears the possibility of an increase in the sensitivity of pyroelectric receivers in the range of resonance.

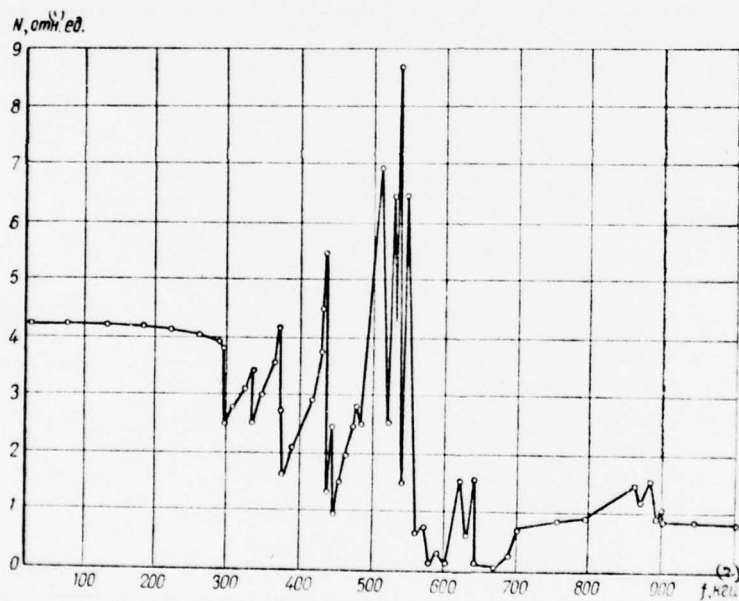


Fig. 5.33. Pyroelectric resonance in the plate TGS, strengthened to solid basis.

Key: (1). rel. un. (2). kHz.

Page 168.

§9. Input units to pyroelectric radiation detectors.

The pyroelectric radiation detectors are capacitor elements, and therefore they possess high resistance. This creates the determined complexities during their agreement with input cascade/stage. The matching cascade/stage must have high entry impedance and small input capacitance, the necessary frequency characteristic and low inherent noise level. These requirements are difficult to combine, since the lamps, which work in the mode/conditions of high of entry impedance, usually have large noises. Therefore it is difficult to develop the universal low-noise preamplifier, which would be suitable for pyroelectric receivers of any type. however, it is possible to propose several types of the preamplifiers, which are suitable for pyroelectric receivers, intended for recording rapidly and slowly elapsing processes [22].

if we use the equivalent replacement scheme of pyroelectric receiver and input circuit (see Fig. 4.7), then the RMS value the current of the equivalent noise generator of receiver and input circuit is determined by the expression

$$\sqrt{I_w^2} = \sqrt{4KT \left(\frac{1}{R_{kp}} + \frac{1}{\operatorname{Re}(Z_u)} + \frac{1}{R_{ax}} \right) \Delta f_{s.m.}} \quad (5.46)$$

where $\operatorname{Re}(Z_u)$ is a real part of the composite load impedance.

At the sufficiently large values of the load impedance and input impedance of a tube, the RMS value of noise current is determined only by capacitance/capacity C_{kp} and by value $\operatorname{tg} \delta$ the reception cell/element:

$$\sqrt{I_{kp}^2} = \sqrt{4KT \Delta f_{s.m.} / R_{kp}} = \sqrt{8KT \pi C_{kp} \operatorname{tg} \delta \Delta f_{s.m.}} \quad (5.47)$$

The signal-to-noise ratio taking into account the noises of input time is determined by the expression

$$\frac{U_c}{\sqrt{U_w^2}} = \frac{J_c |Z_{om}|}{\sqrt{I_w^2} |Z_{om}|^2 + e_n^2}, \quad (5.48)$$

where Z_{out} - the total impedance of detector and input circuit, \bar{e}_n^2 - the mean square of the voltage of the equivalent noise generator of lamp. From equivalent diagram and the analysis of equation (5.46) and (5.48) it follows that as the criterion of the optimum character of the mode/conditions of the work of lamp it is possible to take the maximum the ratio of the input impedance of a tube to its equivalent noise resistance, $R_{\text{in}}/R_{\text{w}}$.

Page 169.

If in work with the pyroelectric receivers, which possess the small capacitance/capacity 1-10 pF, appear difficulties in the agreement of receiver and input unit on resistance, then in work with receivers, whose capacitance/capacity is equal to 1-10 nF, the basic difficulty consists in matching for noises. In the latter case the noise of input time considerably exceeds its own noise of receiver, especially in work at frequencies more than 100 Hz. With an increase in the capacitance/capacity of receiver falls its volt-watt sensitivity, which creates supplementary difficulties in the realization of the threshold of sensitivity.

In order that the noise of lamp would not manifest themselves the value of signal-to-noise ratio, it is necessary to attain the largest possible value Z_{out} . This it is possible to achieve, by

including instead of the ohmic load resistance inductance L . In work on the frequency of modulation which is equal to the resonance frequency of circuit formed by inductance L and by capacitance/capacity C_{kp} , occurs an increase in the volt-watt sensitivity in $tg\delta)^{-1}$ once in comparison with usual circuit diagram (point 0 on Fig. 5.34). So many times grow/rises receiver noise. If noise of lamps considerably exceeds the noise of sensing element, then after supplying instead of the load resistance inductance, we will obtain a considerable increase in the signal-to-noise ratio at resonance frequency. a deficiency/lack in this diagram is the narrow-band characteristic, due to which it cannot be used for recording the rapidly elapsing processes and suitable only for a work with the periodically modulated radiant fluxes.

The shift of resonance frequency conducts by the connection/inclusion of series capacitor. Are possible three versions of the connection of supplementary capacitance/capacities (C_1-C_3). Capacitor C_1 displaces operating point to the side of lower frequencies. Since the resistance of the losses of sensing element of receiver R_{kp} , corresponding to parallel replacement scheme, falls with a frequency division, the volt-watt sensitivity of resonance diagram on low frequencies somewhat decreases (curve 1). Adding C_2 or C_3 , we displace operating point to the side of more high frequencies (curves 2, 3).

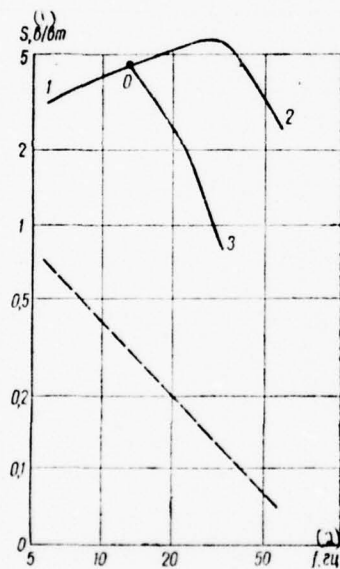


Fig. 5.34. The volt-watt sensitivity of pyroelectric receiver with inductive load (by dotted line is shown volt-watt receiver

sensitivity with resistive load).

Key: (1). V/W. (2). Hz.

Page 170.

However, addition C_3 leads to the fact that the entrance of lamp enters not all resonance stress, but only the part of it, proportional $C_3/C_2 + C_3$. A decrease in the curve 2 at high frequencies is caused by by-passing the stray capacitance of inductance coil. the given curves are constructed for a spherical pyroelectric receiver with the capacitance/capacity 6000 pF value $\text{tg}\delta = 0.05$, and also with inductance $L = 20000$ H.

During work with the receivers, which have a small capacitance/capacity (1-10 pF), the primary attention one should give to an increase in the entry impedance and to a decrease in the input capacitance. Receiver noise and input circuits are sufficiently great at low frequencies, and the noise of lamp do not affect the value of signal-to-noise ratio. Best of all approaches for this lamp 6S12h in the mode/conditions of cathode follower with the lowered/reduced anode and filament voltages (Tabl. 5.3). It input capacitance determined by grid capacitance - the anode and by the

capacitance/capacity of lead wires, can be lowered to 1.5 pF.

The active component of entry impedance it is possible to determine at frequency 0.1 Hz. Is observed the powerful dependence of entry impedance from the value of cathode load. the best results are obtained at values of $R_k = (15-20)$ anyone. The frequency dependence of the RMS value of the noise voltage of lamp in these conditions is given in Fig. 5.35 (curve 1).

In a number of cases for the larger operational stability of pyroelectric receiver to it one should supply the small bias voltage 1-2 v.

Table 5.3.

Номер кривой рис. 5.35	Тип лампы	U_a , в (1)	U_n , в (2)	R_a , ком (3)	R_k , ком (4)	R_{nx} , ом (5)	$R_{nx}/R_{ш}$ ($f = 20$ гц) (6)
1	6C1Ж	50	2,5	0	18	10^{11}	$8 \cdot 10^3$
2	6C15П	65	2,5	8,2	0,03	10^9	10^5
3	6C51Н	50	2,5	13	0,13	10^9	10^4
4	6C1Ж	50	2,5	100	5,6	10^{10}	$3 \cdot 10^4$
5	6Ж1Ж	100	2,5	820	24	10^{10}	$5 \cdot 10^3$

Key: (1). Number of curve, Fig. 5.35. (2). Type of lamp. (3). in.
(4). anyone. (5). ohm. (6). Hz.

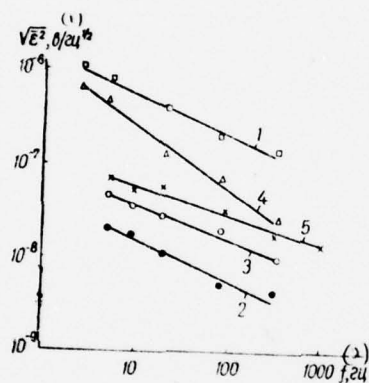


Fig. 5.35. The noise spectrum of input cascade/stages to pyroelectric receivers (numbers of curves in figure corresponds to numerals in Table 5.3).

Key: (1). $V/Hz^{1/2}$. (2). Hz.

Page 171.

In order not to place special power supply, in diagram with cathode

repeater load resistance they connect up not to the earth/ground, but to part of the cathode resistance. The noises of cascade/stage in this case virtually are not changed.

In work with the receivers, which possess great capacity (1-10 nf), when is not used diagram with inductive load, the input impedance of a tube it can be small (0.1-1 Gohms), but is necessary low noise level. The best results were obtained with lamps 6S15P and 6S51Yu [22], working in amplifier mode/conditions (curved 2 and 3 Fig. 5.35). The inclusion of the lamps indicated into the circuit of cascade amplifier gives essential improvement not on noises, but on entry impedance.

For a work with the receivers, which possess capacitance/capacity 0.1-1 nf, it is possible to use preamplifiers with the entry impedances of 10 Gohms. For these purposes approach the amplifiers to 6S1Zh and 6Zh1Zh in triode connection/inclusion (curved 4, 5 Fig. 5.35). Here especially it is exhibited contradicts the requirements for high for entry impedance and low noise level. For example decrease in the resistance of cathode bias gives a decrease in the noises, but simultaneously it leads to a decrease in the entry impedance.

For work in the pulsed made most suitable is a cathode follower on a 6S1Zh since it possesses a large passband.

In connection with the fact that for a decrease in the threshold

of response of pyroelectric receiver is necessary the high input resistance of the matching cascade/stage on the low level of its inherent noise, the promising solution to this question can be found during the creation of the composition instrument, which is the combination of pyroactive crystal and MDP (metal - dielectric is a semiconductor) of transistor. The possibility of designing of composition instruments of such type was published in works [75, 107]. The operating principle of pyroelectric field instrument (so it is possible to call/name instruments of such type) consists of the following (Fig. 5.36). During the change in the temperature of pyroactive crystal, caused by irradiation, on its armatures appears charge [107]

$$\Delta q = \gamma A_0 \Delta \bar{T}, \quad (5.49)$$

where $\Delta \bar{T}$ - the average temperature increment of crystal.

In the case of the plane-parallel plate of the pyroactive crystal

$$\Delta q = \frac{\epsilon A_0}{4\pi d} \Delta V, \quad (5.50)$$

where ΔV is a change in the stress on gate.

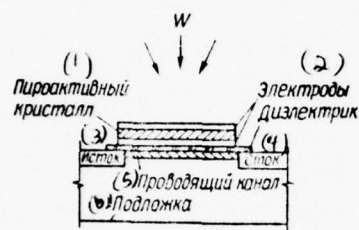


Fig. 5.36. Schematic of pyroelectric field instrument.

Key: (1). Pyroactive crystal. (2). Electrodes dielectric. (3). Source. (4). Flow. (5). Conducting channel. (6). Support/base.

Page 172.

From expressions (5.49) and (5.50) we obtain

$$\frac{\Delta V}{\Delta T} = \frac{4\pi\gamma d}{\epsilon}. \quad (5.51)$$

If we designate the slope/transconductance of the field of instrument

$$g_m \text{ (a/ohm)}, \text{ then} \quad \frac{\Delta J_{\text{МДП}}}{\Delta T} = \frac{4\pi\gamma d g_m}{\epsilon}, \quad (5.52)$$

where ΔJ_{MII} is a current of flow.

With sinusoidally modulated radiation flux $W = W_0 (1 + e^{i\omega t})$ according to expression (5.52) and to relationship/ratio $i\omega C\Delta T = W$ we will obtain for an alternating current component

$$|\Delta J_{MII}| = \frac{4\pi\gamma d g_m}{c\omega} W_0. \quad (5.53)$$

Thus, under the action of radiant flux W_0 occurs a change in the current of the flow of field instrument.

one of the possible electrical circuits is shown in Fig. 5.37, where is represented the composition instrument, which is the combination of pyroactive crystal with the MOS transistor, connected according to the diagram of cathode repeater.

Relationship about the use of a pyroelectric receiver in the circuit of solid-body amplifier are given in work [85]. The distinctive special feature/peculiarity of the developed meter is the uniform response up to frequencies 1 MHz.

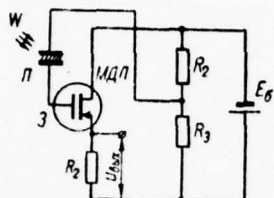


Fig. 5.37. The electrical circuit diagram of the pyroelectric semiconductor device; p - pyroactive crystal; MDP - metal is a dielectric - semiconductor; H - gate.

Page 172

BIBLIOGRAPHY

1. Артюховская Л. М., Кременчугский Л. С., Мальнев А. Ф., Самойлов В. Б., Яценко А. Ф. — Изв. АН СССР, сер. физ., 1965, 29, 11, 2110.
2. Артюховская Л. М., Кременчугский Л. С., Мальнев А. Ф., Ройцина О. В. — УФЖ, 1964, 9, 11, 1240.
3. Беляев Л. М., Набатов В. В., Писаревский Ю. В., Сильвестрова И. М., Шалдин Ю. В. — В кн.: Нелинейная оптика. «Наука», М., 1968, 222.
4. Воронкова Е. М., Гречушников Б. Н., Дистлер Г. И., Петров И. П. — Оптические материалы для инфракрасной техники. «Наука», М., 1965.
5. Валитов Р. А., Дюбко С. Ф., Кузьмичев В. М., Свич В. А. Авторское свидетельство № 218250. Бюллетень изобретений, 1968, 17.
6. Гассанов Л. Г., Кременчугский Л. С., Мальнев А. Ф., Шульга А. Я., Ящишин П. И. — В кн.: Тепловые приемники излучения. «Наукова думка», К., 1967, 111.
7. Гордиенко Т. А., Коновалов Е. В., Кременчугский Л. С., Пучковская Г. А., Столяров В. М., Фролков Ю. А. — В кн.: Тепловые приемники излучения. «Наукова думка», К., 1967, 199.

8. Герасимова Н. Г., Гусев Д. А., Старцев Г. П. — Оптико-механическая промышленность, 1965, 11, 24.
9. Гордов А. Н. — Труды ВНИИМ, 1959, 9 (69), 5.
10. Дианов-Клоков В. И. — Заводская лаборатория, 1955, 21, 3, 361.
11. Есельсон М. П., Мальнев А. Ф. — ПТЭ, 1961, 1, 137.
12. Ицковский М. А., Кременчугский Л. С., Скляренко С. К. — ЖПС, 1969, 11, 2, 320.
13. Ицковский М. А., Кременчугский Л. С., Скляренко С. К. — УФЖ, 1971.
14. Кременчугский Л. С., Лисенко В. С., Мальнев А. Ф., Ройцина О. В. — Инж. физ. журн., 1964, 7, 2, 3.
15. Кременчугский Л. С. — Оптико-механическая промышленность, 1966, 10, 17.
16. Кременчугский Л. С., Мальнев А. Ф., Самойлов В. Б. — В кн.: Электрические и оптические свойства диэлектриков «Наукова думка», К., 1966, 68.
17. Кременчугский Л. С., Лисенко В. С., Мальнев А. Ф., Ройцина О. В. — ЖПС, 1966, 2, 298.
18. Кременчугский Л. С., Мальнев А. Ф. — В кн.: Тепловые приемники излучения «Наукова думка», К., 1967, 75.
19. Кременчугский Л. С., Мальнев А. Ф., Скляренко С. К. — В кн.: Тепловые приемники излучения «Наукова думка», К., 1967, 95.
20. Кременчугский Л. С., Мальнев А. Ф., Самойлов В. Б. — ПТЭ, 1966, 6, 169.
21. Кременчугский Л. С., Ройцина О. В. — ЖПС, 1967, 6, 5, 559.
22. Кременчугский Л. С., Мальнев А. Ф., Самойлов В. Б., Столяров В. М., Шульга А. Я. — ПТЭ, 1969, 2, 111.
23. Кременчугский Л. С. — В кн.: Новые пьезо- и сегнетоматериалы и их применение. Изд. МД НТН, М., 1969, 142.
24. Кременчугский Л. С., Мальнев А. Ф. — Авторское свидетельство № 187357. Бюллетень изобретений, 1966, 20.
25. Кременчугский Л. С., Мальнев А. Ф. — Авторское свидетельство № 206859. Бюллетень изобретений, 1968, 1.
26. Кременчугский Л. С., Мальнев А. Ф. — ПТЭ, 1968, 3, 165.
27. Кроливец К. М. — Слідуючі фотоелементи. «Техніка», К., 1965.
28. Кэй Дж., Лэби. Таблицы физических и химических постоянных ГИФМИ, М., 1962.
29. Мальнев А. Ф., Есельсон М. П., Кременчугский Л. С. — УФЖ, 1961, 6, 6, 881.
30. Непорент Б. С., Дмитриевский О. Д., Никитин В. А. — УФН, 1958, 64, 3, 447.
31. Новик В. К., Гаврилова Н. Д. — В кн.: Новые пьезо- и сегнетоматериалы и их применение. Изд. МД НТН, М., 1969.
32. Полунов Ю. Л. — Оптико-механическая промышленность, 1969, 3, 5.
33. Пельц С. Д., Дуи Л. М., Новик В. К., Рез И. С. — Радиотехника и электроника, 1968, 13, 61, 183.
34. Панкратов Н. А., Робачевский М. В. — В кн.: Тепловые приемники излучения «Наукова думка», К., 1967, 191.
35. Полупроводниковые фотоприемники и преобразователи излучения. «Мир», М., 1966.
36. Ройцина О. В. — В кн.: Тепловые приемники излучения. «Наукова думка», К., 1967, 84, 99.
37. Роговой И. Д. — Оптико-механическая промышленность, 1966, 6.
38. Свешников С. В. — Фотодухполосники. «Техніка», К., 1965.
39. Сяльвестрова И. М. — Изв. АН СССР, сер. физ., 1960, 24, 10, 1213.

Page 174.

40. Станевич А. Е., Ярославский Н. Г.—Оптико-механическая промышленность, 1966, 5, 1.
41. Харченко А. М., Дун Л. М., Смирнов Е. В., Боголюбова И. В.—В кн.: Тепловые приемники излучения. «Наукова думка», К., 1967.
42. Alday J. R., Everett G. E., White D. J.—IEEE Trans., 1966, MTT-14, 2, 100.
43. Astheimer R. W., Buckley R. E.—Rev. Scient. Instrum., 1967, 38, 12, 1761.
44. Astheimer R. W., Buckley R. E.—IEEE J. of Quantum Electronics, 1967, 6, 267.
45. Aart J. F. M., DeHeer F. J., Luyken B. F. J., Saris F. W., Vriens L., Vroom D. A.—Physica, 1969, 41, 1, 209.
46. Alday I. R.—IEEE Trans. Electron Devices, 1969, 16, 6, 598.
47. Astheimer R. W., Schwarz F.—Appl. Optics, 1968, 7, 9, 1687.
48. Blewin W. R., Brown W. J.—J. Scient. Instr., 1965, 42, 1, 19.
49. Beerman H. P.—Amer. Ceram. Soc. Bull., 1967, 46, 8, 737.
50. Bell Laboratories record, 1969, 47, 1, 33.
51. Berkner K., Myers B. R., Pyle V.—Rev. Scient. Instrum., 1968, 39, 8, 1201.
52. Burdick G. A., Arnold R. T.—J. Appl. Phys., 1966, 37, 8, 3223.
53. Burdick G. A., Arnold R. T., Hickman T. G.—J. Appl. Phys., 1966, 37, 1287.
54. Brophy J., Webb S. L.—Phys. Rev., 1962, 128, 2, 584.
55. Betts D. B.—J. Scient. Instrum., 1965, 42, 4, 243.
56. Bischoff K.—Optik, 1968, 28, 2, 183.
57. Bischoff K.—Optik, 1964, 21, 10, 521.
58. Cooper J.—J. Scient. Instrum., 1962, 39, 9, 467; Rev. Scient. Instrum., 1962, 33, 1, 92; Nature, 1962, 194, 4825, 269.
59. Campanaro P., Ricolfi T.—Appl. Optics, 1965, 5, 929.
60. Canfield L. R., Johnson R. G., Codling K., Madden R. P.—Appl. Optics, 1967, 6, 11, 1886.
61. Christensen R. L., Ames I.—J. Opt. Soc., America, 1961, 51, 2, 224.
62. Chynoweth A. G.—J. Appl. Phys., 1956, 27, 1, 78.
63. Dulye W. W.—J. Scient. Instrum., 1967, 44, 8, 629.
64. De Vos J. C.—Physica, 1954, 20, 669.
65. Eisenman W. L., Bates R. L., Merriam J. D.—J. Opt. Soc., America, 1963, 53, 6, 729.
66. Eisenman W. L., Bates R. L.—J. Opt. Soc., America, 1964, 54, 10, 1280.
67. Glass A. M.—Appl. Phys. Lett., 1968, 13, 4, 147.
68. Gillham E. J.—Proc. Roy. Soc., 1959, 12, 10, 404; 1962, 269, 1337, 249, 1945, 24, 1.
69. Gouffe A.—Rev. Optique, 1945, 24, 1.
70. Hadni A., Henninger G., Thomas R., Vergnat P., Wyncke B.—C. r. Ac. Sc., 1965, 260, 15, 4186; J. Phys., 1965, 26, 6, 345.
71. Hadni A., Thomas R., Perrin J.—C. r. Ac. Sc., 1969, 268, 4, 325.
72. Hadni A., Charlemaque D., Thomas R.—C. r. Ac. Sc., 1968, 266, 18, 1230.
73. Rev. Radio Res. Labs., 1965, 11, 6, 252.
74. Hickman T. G., Burdick G. A.—IEEE Trans. Instrum. Meas., 1968, 1M-17, 2, 106.
75. Heyman P. M., Heilmeier G. H.—Proc. IRE, 1966, 54, 6, 30.
76. Hessinger P. S.—Electronics, 1963, 2, 39.
77. Ingrao H. C., Kahn F. J., Menzel D. H.—Mem. Soc. Roy. Sci. Liege, 1964, 9, 105.
78. Johnston R. G., Madden R. P.—Appl. Optics, 1965, 4, 12, 1574.

Page 175.

79. Jones H. W., Perkins W. D., Siegler E. H.—J. Opt. Soc. America, 1963, 53, 11, 1354.
80. Karoli A. R., Hickey J. R., Nelson R. E.—Appl. Optics, 1967, 6, 7, 1183.
81. Kimmitt M. F., Ludlow J. H., Putley E. H.—Proc. IEEE, 1968, 56, 7, 1250.
82. Lichtenberg A. J., Sesnic S.—J. Opt. Soc., America, 1966, 56, 1, 77.
83. Laser focus, 1967, 3, 34.
84. Leiba E.—C. r. Ac. Sc., 1969, 268, 1, 31.
85. Ludlow J. H., Mitchell W. H., Putley E. H., Shaw—J. Scient. Instr., 1967, 44, 9, 694.
86. Merrill J. J., Layton R. G.—Appl. Optics, 1966, 5, 11, 1818.
87. Mattes B. L., Perls T. A.—Rev. Scient. Instrum., 1961, 32, 3, 332.
88. Maling G. C., Ingard U.—Rev. Scient. Instrum., 1967, 38, 3, 119.
89. Packer D. M., Lock C.—J. Opt. Soc., America, 1951, 41, 10, 699.
90. Perls T. A., Diesel T. J., Dobrov W. L.—J. Appl. Phys., 1958, 29, 9, 1297.
91. Putley E. H.—J. Scient. Instrum., 1966, 43, 12, 857.
92. Rosetti C.—C. r. Ac. Sc., 1950, 231, 2, 126.
93. Stanford A. L.—Solid-state Electr., 1965, 8, 8, 747.
94. Stair R., Schmider W. E., Waters W. R., Jackson J. K.—Appl. Optics, 1963, 2, 11, 1151.
95. Schmider W. E., Stair R.—J. Opt. Soc., America, 1963, 53, 11, 1354.
96. Schmider W. E., Garvey J. A.—Appl. Optics, 1968, 7, 6, 1141.
97. Shimazu M., Suzuki G., Takatsuji, Takami K.—J. Appl. Phys., Japan, 1967, 6, 120.
98. Stanford A. L.—Solid-states Electr., 1965, 8, 9, 747.
99. Treharue R. W., Trolander H. W.—J. Scient. Instr., 1965, 42, 9, 699.
100. Таками К., Суда К., Коча М.—Объединенный Опыты, 1968, 37, 2, 147.
101. Toole J. M., Henisch H. K.—Solid-state Electr., 1968, 11, 8, 743.
102. Tau—C. r. Ac. Sc., 1938, 207, 1042.
103. White D. J., Weider H. H.—J. Appl. Phys., 1963, 34, 8, 2487.
104. White D. J.—J. Appl. Phys., 1964, 35, 12, 3536.
105. Woodtill D., Andrews J. C.—IEE Trans. Aerospace and Electron Syst., 1967, 3, 20, 356.
106. Wünsche C.—Z. f. angew. Phys., 1967, B22 H5, 399.
107. Wooten E. T.—Proc. IEEE, 1967, 55, 564.

Page 176.

Chapter VI.

FERROELECTRIC BOLOMETERS.

The idea of the creation of the bolometers, which use a temperature dependence of the impedance of dielectrics, is proposed by Moon and Steinhardt in 1938 [10]. Somewhat later appeared [8], in which were described the characteristics of the bolometers, prepared from the thin film of nitrobenzine. However, threshold sensitivity and the inertness of dielectric bolometers were worse than of other thermal radiation detectors, and interest in them for some time disappeared.

Into 1961 Henel conducted the calculation of ferroelectric bolometer as lumped systems and it showed that the threshold sensitivity of ideal thermal receiver [9]. The calculation was carried out by the author without taking into account of the nonuniformity of the distribution according to the thickness of sensing element at modulation of radiation flux, electrothermal interaction and dependence of the characteristics of ferroelectric on

temperature, electric field and frequency. In work [4] the calculation of ferroelectric bolometer is approximated to actual conditions.

§1. Volt-watt sensitivity of bolometer.

Let us examine the work of the ferroelectric bolometer, which consists of working and compensative cell/elements, in the bridge circuit of alternating current (Fig. 6.1) near equilibrium. During irradiation of sensing element of bolometer its impedance Z_1 changes by value ΔZ_1 . If changes ΔZ_1 are so small that the value of current I_1 virtually does not change, an incremental stress in the diagonal of bridge takes form [6]

$$\Delta U = \frac{-Z_4 \Delta Z_1 Z_n U}{[Z_n (Z_2 + Z_4) + Z_2 (Z_3 + Z_4)] (Z_1 + Z_3)}. \quad (6.1)$$

If before irradiation $Z_1 = Z_2$ and, correspondingly, $Z_3 = Z_4$, then

$$\Delta U = \frac{-Z_3 \Delta Z_1 Z_n U}{(Z_1 + Z_3) [Z_n Z_3 + Z_1 (Z_n + 2Z_3)]}. \quad (6.2)$$

Page 177.

The optimum conditions of transmission are reached, when $Z_3 \gg Z_1$ and $Z_n \gg Z_3$. In this case equation (6.2) is record/written in the form

where $V = Z_1/Z_3$, U - stress on bolometer.

$$\Delta U = \frac{\Delta Z_1}{Z_1} V, \quad (6.3)$$

Virtually optimum conditions easily are realized with the connection of the bridge of bolometer to electron tube with input capacitance $C_{BX} = (3 \div 4)$ by pF $(Z_H \approx \frac{1}{\omega C_{BX}})$. Equation (6.3) is sufficiently correct with the capacitance/capacity of bolometer 1000 pF and with $Z_3 = Z_4 = 1/i\omega_0 C_3$, where $C_3 = 100$ pF.

For determining value $\Delta Z_1/Z_1$ in equation (6.3) let us examine the parallel replacement scheme of sensing element of bolometer (Fig. 6.2).

Let us assume that the crystal is heated because of the heat, caused by Joule losses, and because of irradiation by radiation flux $W_0 (1 + e^{i\omega t})$.

Let us break crystal into n of the series-connected cell/elements with surface b and thickness Δy .

The impedance of the k cell/element

$$Z_k = \frac{R_k}{1 + i\omega_0 C_k R_k} = \frac{1 + i \operatorname{tg} \delta_k}{i\omega_0 C_k (1 + \operatorname{tg}^2 \delta_k)}, \quad (6.4)$$

where C , R and $\operatorname{tg} \delta$ - capacitance/capacity, resistance and tangent of the angle of the dielectric losses of cell/element; ω_0 - supply frequency of bridge.

Then for sensing element of bolometer it is possible to write

$$Z_1 = \sum_{k=1}^n Z_k = \sum_{k=1}^n \frac{1 + i \operatorname{tg} \delta_k}{i\omega_0 C_k (1 + \operatorname{tg}^2 \delta_k)}. \quad (6.5)$$

If the capacitance/capacity of any cell/element

$$C_k = \frac{\epsilon_k b l}{4\pi \Delta y},$$

and the number of cell/elements $n \rightarrow \infty$ with $\Delta y \rightarrow 0$, then

$$Z_1 = 4\pi \int_0^d \frac{[1 + i \operatorname{tg} \delta(T)] dy}{i\omega_0 \epsilon(T) b l [1 + \operatorname{tg}^2 \delta(T)]}. \quad (6.6)$$

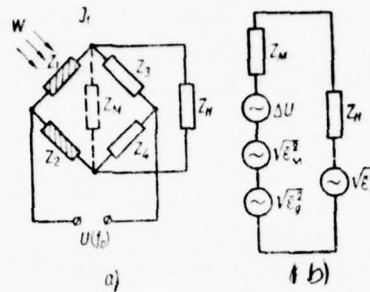


Fig. 6.1.

Fig. 6.1. The bridge of ferroelectric bolometer (a) and its equivalent diagram of substitution (b): Z_1 , Z_2 , Z_3 and Z_4 are ratio arms; Z_M and Z_H are exit and load resistances; $\sqrt{\epsilon_M^2}$, $\sqrt{\epsilon_B^2}$ and $\sqrt{\epsilon_A^2}$ are noise of bridge, the loads and the supplementary noises of bolometer; $U(f_0)$ - the supply voltage of bridge; ΔU - the equivalent voltage of signal.

Page 178.

The dielectric power factor $\tan \delta$ and the dielectric constant ϵ are the function of the temperature, which in turn, depends on coordinate y -

To irradiation the temperature of any cell/element was equal to T_0 , and the resistance of bolometer can be written in the form

$$Z_1 = \frac{1 + i \operatorname{tg} \delta(T_0)}{i \omega_0 C(T_0) [1 + \operatorname{tg}^2 \delta(T_0)]} = Z_1(T_0). \quad (6.7)$$

During irradiation the temperature of the crystal

$$T = T_0 + \Theta(y, t). \quad (6.8)$$

If one assumes that increases in the temperature $\Theta(y, t)$ are small due to weak radiation fluxes, then temperature dependences ϵ and $\operatorname{tg} \delta$ can be presented linearly depending on temperature

$$\epsilon[T_0 + \Theta(y, t)] = \epsilon(T_0) [1 + \alpha_\epsilon \Theta(y, t)] \quad \text{and} \quad \operatorname{tg} \delta[T_0 + \Theta(y, t)] = \operatorname{tg} \delta(T_0) [1 + \gamma_\delta \Theta(y, t)].$$

Then

$$Z_1[T_0 + \Theta(y, t)] = \int_0^d \frac{4\pi [1 + i \operatorname{tg} \delta(T_0) [1 + \gamma_\delta \Theta(y, t)]] dy}{i \omega_0 \epsilon(T_0) b l [1 + \alpha_\epsilon \Theta(y, t)] [1 + \operatorname{tg}^2 \delta(T_0) [1 + \gamma_\delta \Theta(y, t)]^2]}, \quad (6.10)$$

where α_ϵ and γ_δ are temperature coefficients of values ϵ and $\operatorname{tg} \delta$ respectively. Being limited in equation (6.10) to the terms, linear on temperature increment $\Theta(y, t)$, we obtain

$$\frac{\Delta Z_1[\Theta(y, t)]}{Z_1(T_0)} = \left\{ \alpha_\epsilon + \frac{\gamma_\delta \operatorname{tg} \delta(T_0) e^{i\varphi}}{[1 + \operatorname{tg}^2 \delta(T_0)]^{0.5}} \right\} \bar{\Theta}(y, t), \quad (6.11)$$

where

$$\bar{\Theta}(y, t) = \frac{1}{d} \int_0^d \Theta(y, t) dy; \quad (6.12)$$

$$\varphi = \operatorname{arctg} \left[\frac{1}{\operatorname{tg} \delta(T_0)} \right]. \quad (6.13)$$

By using expressions (6.3) and (6.11), it is possible to determine the volt-watt sensitivity of bolometer by the formula

$$S = \frac{\Delta U}{\Delta W}.$$

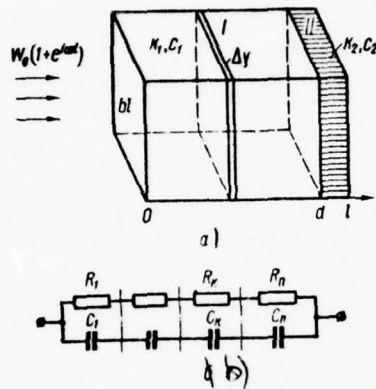


Fig. 6.2.

Fig. 6.2. Replacement scheme (b) of the irradiated ferroelectric bolometer (a); I - crystal; II - support/base.

Page 179.

§2. The thermal design of ferroelectric bolometer.

The determination of the average value of temperature increment in crystal in transit through it of alternating current of frequency ω_0 and during irradiation of its surface by the radiation flux W composes the thermal design of bolometer.

Let us examine arbitrary crystal element (see Fig. 6.2) bldy and compose for it the equation of the heat balance:

$$cbl\delta y \frac{\partial \Theta}{\partial t} = kbl\delta y \frac{\partial^2 \Theta}{\partial y^2} + Q(y, \Theta), \quad (6.14)$$

where $Q(y, \Theta)$ is the power of Joule losses, isolated in cell/element; c and k is specific heat and the coefficient of thermal conductivity.

It is possible to write

$$Q(y, \Theta) = v^2(\Theta, y) \omega_0 C(y, \Theta) \lg \delta(\Theta, y) \approx \frac{4\pi q^2 \omega_0 \lg \delta(T_0) [1 + (\gamma_\delta - \alpha_e) \Theta] \delta y}{\epsilon(T_0) bl}, \quad (6.15)$$

where q is a charge. Then equation (6.14) taking into account relationship/ratio (6.15) during division into value $cbl\delta y$ for range I (crystal) will take the form

$$\frac{\partial \Theta_1}{\partial t} = \frac{k_1}{c_1} \cdot \frac{\partial^2 \Theta_1}{\partial y^2} + \frac{E_0^2 \omega_0 \lg \delta(T_0) [1 + (\gamma_\delta - \alpha_e) \Theta_1] \epsilon(T_0)}{4\pi c_1}, \quad (6.16)$$

where E_0 - the average strength of field in crystal. Equation (6.16)

can be written in the form

$$\frac{\partial \Theta_1(y, t)}{\partial t} = \eta_1 \frac{\partial^2 \Theta_1(y, t)}{\partial y^2} + A \Theta_1(y, t) + B, \quad (6.17)$$

where $\eta_1 = \frac{k_1}{c_1}$ - the thermal diffusivity

$$A = (\gamma_\delta - \alpha_e) \frac{F_0^2 \omega_0 \varepsilon(T_0) \operatorname{tg} \delta(T_0)}{4 \pi c_1};$$

$$B \approx \frac{A}{\gamma_\delta - \alpha_e}. \quad (6.17a)$$

The solutions to equation (6.17) for a crystal, and also the homogeneous equation of thermal conductivity for a support/base can be conducted under the following boundary conditions:

$$k_1 \left[\frac{\partial \Theta_1(y, t)}{\partial t} \right]_{y=0} + H_1 |\Theta_1(y, t)|_{y=0} - \varepsilon_0 W_0 (1 + e^{i\omega t}) = 0;$$

$$k_1 \left[\frac{\partial \Theta_1(y, t)}{\partial y} \right]_{y=d} + H_2 |\Theta_1(y, t)|_{y=d} = k_2 \left[\frac{\partial \Theta_2(y, t)}{\partial y} \right]_{y=d}; \quad (6.18)$$

$$|\Theta_2(y, t)|_{y=l} = 0.$$

Page 180.

The adopted designations: $H_1 = 4\sigma_C \varepsilon_1 T_0^3$; $H_2 = 4\sigma_C \varepsilon_2 T_0^3$; ε_1 and ε_2 - the emissivity of the front/leading and back side of receiver; ε_0 - the absorptivity of "black", σ_C - Stephan's constant; d is thickness of ferroelectric crystal; $l - d$ the thickness of support/base; $\Theta_1(y, t)$ and $\Theta_2(y, t)$ are a temperature increment in any point of ferroelectric and support/base in the moment of time t .

The average temperature increment of sensing element of receiver in steady conditions, caused by dielectric losses and the constant component of radiation flux, takes the following form:

$$\begin{aligned} \Theta_1(y, t) = & \frac{F \left\{ \operatorname{th} \kappa d + \frac{(1 - \operatorname{sch} \kappa d) 2h_1 \left[h_2(l-d) + \frac{k_2}{k_1} \right]}{\kappa \left[(h_1 + h_2)(l-d) + \frac{k_2}{k_1} \right]} \right\}}{\kappa d \left\{ 1 + \frac{\operatorname{th} \kappa d \left[(h_1 h_2 + \kappa^2)(l-d) + \frac{h_1 k_2}{k_1} \right]}{\kappa \left[(h_1 + h_2)(l-d) + \frac{k_2}{k_1} \right]} \right\}} + \\ & + \frac{W_0 e_0 \left\{ \left[h_2(l-d) + \frac{k_2}{k_1} \right] \frac{(1 - \operatorname{sch} \kappa d)}{\kappa} + (l-d) \operatorname{th} \kappa d \right\}}{k_1 \kappa \left[(h_1 + h_2)(l-d) + \frac{k_2}{k_1} \right]} - \\ & + \frac{\frac{k_2}{k_1}}{\left\{ 1 + \operatorname{th} \kappa d \frac{(h_1 h_2 + \kappa^2)(l-d) + h_1 \frac{k_2}{k_1}}{\kappa \left[(h_1 + h_2)(l-d) + \frac{k_2}{k_1} \right]} \right\}} - \\ & - (\gamma_\delta - \alpha_e)^{-1}, \end{aligned} \quad (6.19)$$

where

$$F = \frac{A}{B}; \quad \kappa = \sqrt{-\frac{A}{k_1}}; \quad h_1 = \frac{H_1}{k_1};$$

$$h_2 = \frac{H_2}{k_1}.$$

The variable component of radiation flux heats sensing element on the value whose value can be written so

$$\Theta_1(y, \omega, t) = \frac{\text{ch } \beta_1 d}{\beta_1 d} [M(1 - \text{sch } \beta_1 d) + N \text{ th } \beta_1 d] e^{i\omega t}, \quad (6.20)$$

where

$$M = \frac{\epsilon_0 W_0 \left[1 + \frac{k_1}{k_2} \cdot \frac{h_2}{\beta_2} \text{ th } \beta_2 (l-d) \right]}{k_1 \beta_1 \text{ ch } \beta_1 d \left\{ 1 + \frac{k_1}{k_2} \cdot \frac{(h_1 - h_2)}{\beta_2} \text{ th } \beta_2 (l-d) + \left[\frac{h_1}{\beta_1} + \frac{k_1}{k_2} \cdot \frac{(\beta_1^2 + h_1 h_2)}{\beta_1 \beta_2} \text{ th } \beta_2 (l-d) \right] \text{ th } \beta_1 d \right\}};$$

$$N = \frac{\epsilon_0 W_0 \text{ th } \beta_2 (l-d)}{k_2 \beta_2 \text{ ch } \beta_1 d \left\{ 1 + \frac{(h_1 + h_2)}{\beta_2} \text{ th } \beta_2 (l-d) + \left[\frac{h_1}{\beta_1} + \frac{k_1}{k_2} \cdot \frac{\beta_1^2 + h_1 h_2}{\beta_1 \beta_2} \text{ th } \beta_2 (l-d) \right] \text{ th } \beta_1 d \right\}};$$

$$\beta_1 = (1+i) \sqrt{\frac{\omega}{2\eta_1}} (1+iA)^{0.5}; \quad \beta_2 = (1+i) \sqrt{\frac{\omega}{2\eta_2}};$$

$$\eta_2 = \frac{k_2}{c_2}. \quad (6.21)$$

age 181.

Expressions (6.19) and (6.20) in general form are complex, but or two in practice realizable cases they are simplified.

1. Bolometer vacuum ($k_2 = 0$). Then

$$\bar{\Theta}_{1-\text{Bak}} = \epsilon_0 W_0 e^{i\omega t} \left[\frac{\epsilon_1 (1 + \text{sch } \beta_1 d)}{k_1 \beta_1} + \frac{\text{th } \beta_1 d}{4\sigma_C T_0^3} \right] (\epsilon_1 + \epsilon_2) \left[1 + \frac{\beta_1^2 + h_1 h_2}{\beta_1 (h_1 + h_2)} \text{th } \beta_1 d \right] \beta_1 d. \quad (6.22)$$

If $|\beta_1 d| \gg 1$ and $\epsilon_1 \gg \epsilon_2$, that

$$\bar{\Theta}_{1-\text{Bak}} = \frac{\epsilon_0 W_0 e^{i\omega t}}{\beta_1^2 d k_1} = \frac{\epsilon_0 W_0 e^{i\omega t}}{\omega \epsilon_1 d (1 - A)}. \quad (6.23)$$

If $|\beta_1 d| \ll 1$, that

$$\bar{\Theta}_{1-\text{Bak}} = \frac{\epsilon_0 W_0 e^{i\omega t}}{4\sigma_C T_0^3 (\epsilon_1 + \epsilon_2)}. \quad (6.24)$$

2. Sensing element of bolometer is mounted on solid support/base and the length of temperature wave in support/base considerably shorter than its thickness, i.e., $|\beta_2 (l - d)| \gg 1$.

If $|\beta_1 d| \gg 1$, that

$$\bar{\Theta}_{1-\text{TB}} = \frac{\epsilon_0 W_0 e^{i\omega t}}{\beta_1^2 d k_1}. \quad (6.25)$$

If $|\beta_1 d| \ll 1$, that

$$\bar{\Theta}_{1-\text{TB}} = \frac{\epsilon_0 W_0 e^{i\omega t}}{(k_2 \beta_2 + k_1 h_1)} = \frac{\epsilon_0 W_0 e^{i\omega t}}{k_2 \beta_2 + 4\sigma_C \epsilon_0 T_0^3}. \quad (6.26)$$

Expressions for a volt-watt sensitivity can be obtained, after using relationship/ratios (6.3), (6.11), (6.20), and also (6.22) -

(6.26).

For the vacuum ferroelectric bolometer

$$S_{\text{vak}} = \frac{\epsilon_0 E_0}{b l \omega c_1 (1 - A)} \left\{ \alpha_e + \frac{\gamma_\delta \operatorname{tg} \delta (T_0) e^{i\varphi}}{|1 + \operatorname{tg}^2 \delta (T_0)|^{0.5}} \right\}. \quad (6.27)$$

If $\alpha_e \gg \gamma_\delta \operatorname{tg} \delta / (1 + \operatorname{tg}^2 \delta)^{0.5}$, that

$$|S_{\text{vak}}| = \frac{\alpha_e \epsilon_0 E_0}{\omega c_1 (1 + A^2)^{0.5} b l}. \quad (6.28)$$

Page 182.

For a ferroelectric bolometer on solid basis volt-watt sensitivity with $|\beta_1 d| \gg 1$ and $|\beta_2 (l - d)| \gg 1$ also is described by formula (6.28).

If $|\beta_2 (l - d)| \gg 1$, but $|\beta_1 d| \ll 1$, that

$$S_{\text{TB}} = \frac{\epsilon_0 E_0 d}{b l (k_2 \beta_2 + 4 \sigma_{\text{C}} \epsilon_0 T_0^3)} \left\{ \alpha_e + \frac{\gamma_\delta \operatorname{tg} \delta (T_0) e^{i\varphi}}{|1 + \operatorname{tg}^2 \delta (T_0)|^{0.5}} \right\}. \quad (6.29)$$

§3. Electrical fluctuations in ferroelectrics

The fluctuation phenomena in ferroelectric bolometers are determined, in essence, by the processes of dissipation and repolarization with the supply of bolometer from the source of alternating current.

The fluctuation- dissipation theorem, demonstrated by G. Kallen and T. Velton in 1951 [5], establish/install single-valued communication/connection between the fluctuations of the physical quantities, which characterize the medium, and its dispersive properties. For the spectral density of the fluctuation of the voltage in dielectric is derive/concluded the following relationship/ratio, which is the generalization of Nyquist's formula:

$$\bar{U}^2(\omega) = \frac{4KT \operatorname{tg} \delta}{(1 + \operatorname{tg}^2 \delta) \omega C} \quad (6.30)$$

As shown by P. V. Bunkin [3], fluctuation- dissipation theorem is used for the description of the spectral intensity of thermodynamically equilibrium fluctuations in arbitrary (nonlinear) passive systems.

Ferroelectric bolometer is nonlinear system, since its capacitance/capacity C and the tangent of the angle of the dielectric losses $\operatorname{tg} \delta$ are the functions of electric field. The experimental check of the applicability of formula (6.30) showed a good coincidence with theory (Fig. 6.3).

In real ferroelectric crystals in transit through them of alternating current appear the supplementary noises, which

considerably exceed the noises, calculated by Nyquist's formula. Basic part of these fluctuations is connected with the process of the repolarization of ferroelectric. These noises are analogous to Barkhausen's noises, observed during the repolarization of ferromagnetic materials, although their nature up to now is not explained.

The noises of repolarization are caused nonrepetition of the process itself from one period to the next.

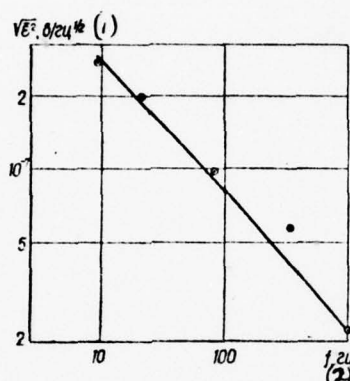


Fig. 6.3.

Fig. 6.3. The noises of dielectric losses of specimen/sample made of ceramics BaTiO_3 : solid line is a calculated curve; \odot experimental points.

Key: (1). V/Hz. (2). Hz.

Page 183.

The current of repolarization has complex discrete-continuous spectrum. It contains the discrete (regular) part, which consists of

the harmonics, to the multiple frequency of repolarization, and continuous (fluctuation) part. The investigation of fluctuation phenomena during the periodic repolarization of ferroelectric is carried out by I. A. Andronovoy [1, 2]. By the author was emitted the spectral density of the fluctuations of current under the varied conditions of repolarization. Measurements conducted according to bridge circuit (Fig. 6.4). Bridge consisted of two ferroelectric condensers C_1 and C_2 and two low resistances $R_1 = R_2 = 100$ ohm.

The noise spectrum of repolarization (without taking into account of effects near harmonics) is represented in Fig. 6.5. The spectrum of ceramic specimen/samples (see Fig. 6.5a) is characterized by frequency f_1 , lower than which the value of spectral noise density $\overline{e^2}$ (f) falls, and by frequency f_2 , above by which also is observed incidence/drop. For ferroelectric single crystals the noise spectrum (see Fig. 6.5b) differs themes that he does not have expressed flat/plane section with the uniform density of fluctuations.

During temperature change the noise spectrum both for the ceramic specimen/samples and for single crystals changes, but in Curie point special changes are not observed [2].

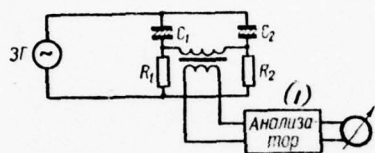


Fig. 6.4.

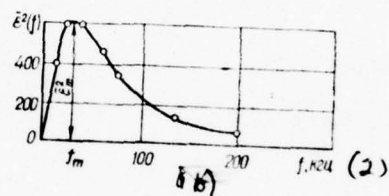
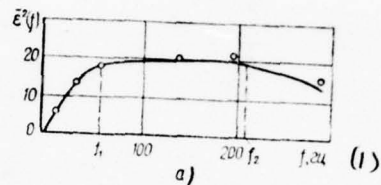


Fig. 6.5.

Fig. 6.4. Measuring circuit of the noises of repolarization [1].

Key: (1). Analyzer.

Fig. 6.5. Noise spectrum of the repolarization of ferroelectric [2]:
a) ceramicist BaTiO_3 ; b) single crystal TGS.

Key: (1). Hz. (2). kHz.

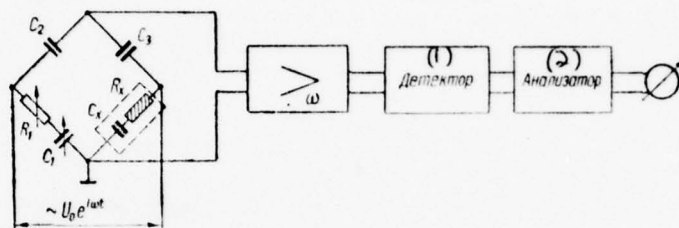


Fig. 6.6.

Fig. 6.6. Measuring circuit of the noises of the stress of repolarization.

Key: (1). Detector. (2). Analyzer.

Page 184.

For explaining the obtained dependences was proposed the model, analogous to the model of the processes of the magnetic reversal of ferromagnetic materials. It was assumed that the specimen/sample consists of the determined number of identical domains. The form and the value of current pulse, which appears during the repolarization of separate domain, is identical for all domains, repolarized during

one half-period. The appearing noises are caused by lax recurrence from period to the period of the torque/moments of the repolarization of separate domains. In this case the fluctuations of the torque/moments of the repolarization of different domains are independent and independent the fluctuation of the torque/moments of the repolarization of one domain in different periods.

The noise spectrum, designed on this model, takes the form, close to experimental. The process of the repolarization of ferroelectric according to the existing representations consists of two mechanisms: the nucleation of the domains of opposite polarity and intergrowth of domain through crystal. The mechanism of the origin/conception/initiation of antiparallel domains bears statistical character and, in essence, responsible for the emergence of the fluctuations of the value of the current of repolarization.

V. B. Samoilov [7] investigated the noises of the stress of repolarization in ferroelectric bolometer near fundamental harmonic. For measurements was used the circuit, presented in Fig. 6.6. The specimen/sample being investigated was included in capacitance bridge. In this case was observed the following relationship/ratio between the capacitance/capacities: $C_1 = \frac{C_2 C_x}{C_3}$ ^{and} $C_x \gg C_1$. Bridge was balanced on the fundamental harmonic of the supply voltage of bridge. Noise voltage was supplied to the selective amplifier, tuned to a

frequency of the supply of bridge f_0 . Then the intensive noise voltage entered the linear detector and the detected signal - the low-frequency analyzer of the spectrum, with the aid of which was investigated the noise spectrum in the area of supply frequency of the bridge of bolometer. Figure 6.7 depicts the noise spectrum of repolarization in the area of the fundamental harmonic of the supply voltage of bridge ($f_0 = 15$ kHz) for the crystal of TGS.

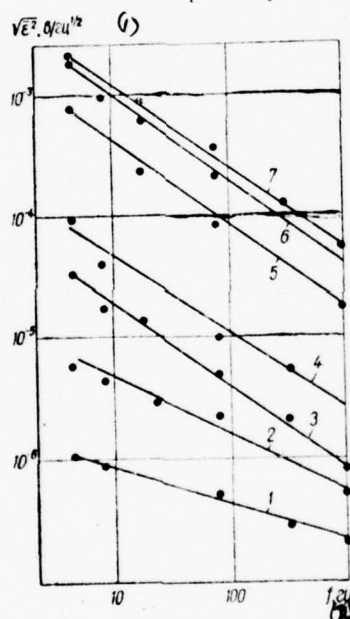


Fig. 6.7.

Fig. 6.7. Noise spectrum of repolarization for ceramics BaTiO_3 in the area of fundamental harmonic with the different supply voltages of the bridge: 1 - 1 V; 2 - 2.5; 3 - 5; 4 - 10; 5 - 20; 6 - 30; 7 - 50.

Key: (1). V/Hz. (2). Hz.

Page 185.

§4. Threshold of response of bolometer.

The output resistance of the bridge of bolometer near the equilibrium, when the resistance of power supply is great, is equal to:

$$Z_M = \frac{(Z_1 + Z_2)(Z_3 + Z_4)}{(Z_1 + Z_2) + (Z_3 + Z_4)} = \frac{Z_1 + Z_2}{1 + \frac{Z_1 + Z_2}{Z_3 + Z_4}} \approx \frac{2Z_1}{1 + \frac{Z_1}{Z_3}} \quad (6.31)$$

If $Z_3 \gg Z_1$, then $Z_M \approx 2Z_1$ (with $Z_1 = Z_2$). Then the RMS value of the noise of the bridge of bolometer by Nyquist's generalized formula is written:

$$V_{e_6}^2 = V \frac{8KT \operatorname{tg} \delta \Delta f}{(1 + \operatorname{tg}^2 \delta) \omega_0 C_1} \quad (6.32)$$

Analogously it is possible to present the noise of the load resistance:

$$V_{e_n}^2 = \frac{V 4KT \Delta f}{\omega_0 C_{BX} R_{BX}^{0.5}} \quad (6.33)$$

When $Z_H = \left(\frac{1}{i\omega_0 C_{RX}} + R_{RX} \right) \gg 2Z_1$, the Johnson noise will be, in essence, determined by expression (6.23).

The threshold of response of ferroelectric bolometer takes the form

$$\mathcal{P} = \left(4KT^2 G \Delta f + \frac{8KT \operatorname{tg} \delta \Delta f}{\omega_0 C_1} S^{-2} + \overline{W_A}^2 \right)^{0.5}. \quad (6.34)$$

The first term in expression (6.34) characterizes the actions of temperature noises (G - the total coefficient of heat losses), the second term is determined by Johnson noises, and the third is caused by the supplementary fluctuations, from which most significant the noises of repolarization. The value of the fluctuations, described $\overline{W_A}^2$, is especially noticeable with the incorrectly selected operating point. Besides the noises of repolarization, significant role can play the noises, connected with the dependence of dielectric constant on electric field during the fluctuations of the supply voltage of bridge.

If value $\overline{W_A}^2$ is low, then, by increasing the frequency of the supply of bridge ω_0 , it is possible the second term in equation (6.34) to make comparable with the first, if the dielectric power factor $\operatorname{tg} \delta$ and the volt-watt sensitivity S in this case are not

strongly change.

The analysis of the obtained expressions makes it possible to make some conclusions in the selection ratio of the operating temperature and supply voltage of bridge. The expression for A (see (6.17a) , proportional $(\gamma_0 - \alpha_c)$, characterizes electrothermal interaction. Depending on the sign of temperature capacitance coefficient α_c electrothermal communication/connection either decreases value A (in work after Curie point), or it increases it. For an increase in volt-watt sensitivity (6.27) one should approach decrease in A.

Page 186.

For the purpose of an increase in the sensitivity desirable is the application/use of high electric fields, close to disruptive. But in this case grow/rises the dielectric power factor $\text{tg } \delta$ and they can appear supplementary noises (for example, repolarization). The large values of quantities $\text{tg } \delta$ are always undesirable, since this leads to an increase in the Johnson noises. Under real conditions for the selecting of operating point requires detailed analysis. But from common considerations it is expedient to select operating point somewhat higher than phase transition, where α_c is still sufficiently great, $\text{tg } \delta$ small, but their dependence on electric

field is not very considerable.

To evaluate the characteristics of ferroelectric bolometers let us examine temperature dependences ϵ and $\operatorname{tg} \delta$ ceramics BaTiO_3 (Fig. 6.8). Calculation of the volt-watt sensitivity S and of threshold of response \mathcal{P} for the vacuum bolometer, prepared from ceramics BaTiO_3 with the thickness of sensing element $d = 100 \mu$ at temperature of 130°C , modulation frequency 10 Hz and the frequency of the supply of bridge 10 kHz, and also in the absence of supplementary noises ($\bar{W}_a = 0$), gives such, the value: $S = 200 \text{ V/W}$ and $\mathcal{P} = 5 \cdot 10^{-10} \text{ W/Hz}^{1/2}$.

One of the special feature/peculiarities of ferroelectric bolometer is that it is capacitor elements. This, in principle, makes it possible to lower Johnson noises and, if it is possible to exclude supplementary noises, to obtain ideal thermal radiation detector.

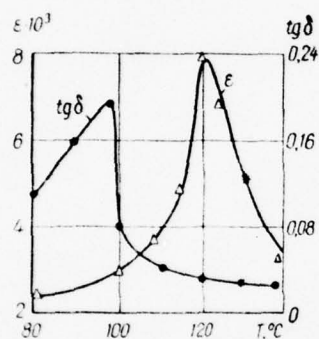


Fig. 6.8.

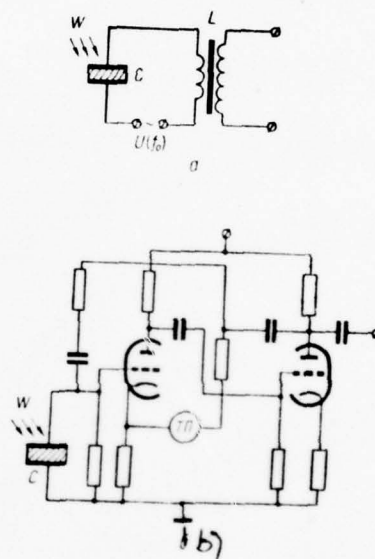


Fig. 6.9.

Fig. 6.8. Dependence of dielectric constant ϵ and of the dielectric power factor $\operatorname{tg} \delta$ on temperature for ceramics BaTiO_3 (* - operating point [4]).

Fig. 6.9. Circuit diagrams of the ferroelectric bolometer: a)

resonant circuit; b) the frequency-dependent output/yield.

Page 187.

As the criterion of the quality of the selected material of ferroelectric bolometer according to formulas (6.28) and (6.34) serves value

$$M_{\text{eq}} = \sqrt{\frac{\alpha_r^2}{C_1^2 \lg \delta (1 + A^2)}} \quad (6.35)$$

Ferroelectric bolometer can be used in bridge circuits (see Fig. 6.1), in the circuits of resonant circuit [11] (Fig. 6.9a) and in circuits with the frequency-dependent output/yield (Fig. 6.9b). The last/latter method of parametric measurement is most interesting in view of the simple transformation of analog value into digital code.

The threshold of response of ferroelectric bolometers worse is at present than of the better/best thermal receivers. However, ferroelectric bolometers possess some special feature/peculiarities, which give to them the determined advantage over other receivers during the solution of series of problems. Sensing elements of ferroelectric bolometers from ceramics can be made in the form of the figures of complex form with large area. Unlike the pyroelectric receivers, which possess the same advantage, ferroelectric bolometers

can work during the unmodulated irradiation. The receivers, prepared in the form of spheres (4 π -detectors), can be utilized for research on the radiation fields, created by many radiation sources.

Bibliography

1. Андропова Н. А.— ДАН СССР, 1958, 119, 1, 68.
2. Андропова Н. А.— Изв. вузов. Радиофизика, 1961, 4, 1, 90.
3. Букин Ф. Б.— Радиотехника и электроника, 1961, 6, 1, 3.
4. Кременчугский Л. С., Ройцина О. В.— В кн.: Тепловые приемники излучения. «Наукова думка», К., 1967, 249.
5. Ландау Л. Д., Лифшиц Е. М. Электродинамика сплошных сред. ГИИЛ, М., 1957.
6. Нестеренко А. Д. Основные расчеты измерительных схем уравнивания. Изд-во АН УССР, К., 1960.
7. Самойлов В. Б.— В кн.: Тепловые приемники излучения. «Наукова думка», К., 1967, 265.
8. Ewles J.— J. Scient. Instrum., 1947, 24, 57.
9. Hanai R.— J. Opt. Soc., America, 1961, 51, 2, 220; 1961, 51, 8, 916.
10. Moon P., Steinhardt L. R.— J. Opt. Soc., America, 1938, 28, 148.
11. Takami K., Matsuura K.— Rev. Scient. Instrum., 1966, 37, 11, 1505.

~~End Section.~~

Page 188.

Chapter VII.

EQUIPMENT AND PROCEDURES FOR DETERMINING THE CHARACTERISTICS OF MATERIAL AND PARAMETERS OF FERROELECTRIC RADIATION DETECTORS.

The fundamental characteristics of the material of sensing elements of ferroelectric receivers are the pyroelectric coefficient γ dielectric constant ϵ and the dielectric power factor $\operatorname{tg} \delta$. These three characteristics in essence predetermine the parameters of receivers.

§1. Static method of the determination of pyroelectric coefficient.

The static compensation method of the measurement of pyroelectric coefficient γ is described by Ackerman [39] into 1915. This method was preserved up to now, not having undergone fundamental changes, with the exception of the introduction of the automatic

compensation for electrostatic charge instead of the manual.

The principle of the measurement of the pyroelectric coefficient of ferroelectric by static method consists of the compensation for the electrostatic charge, which appears on the electrodes of pyroactive crystal during its heating or cooling.

Figure 7.1 gives the installation diagram for research on pyroelectric effect by static method. The specimen/sample $C_{\text{кп}}$ being investigated with two electrodes, plotted/applied to opposite sides of crystal and perpendicular to the determined crystallographic orientation, is placed into thermostat. The appearing during heating or cooling in pyroactive specimen/sample $C_{\text{кп}}$ electric charge is compensated for with the aid of calibration capacitor C_0 , which is placed for an interference elimination into electrostatic shield. Electrometer E serves as zero-adjustment instrument. Its motionless plates are connected with battery E_1 through the auxiliary resistances R_1 and R_2 , which safeguard battery from short circuit.

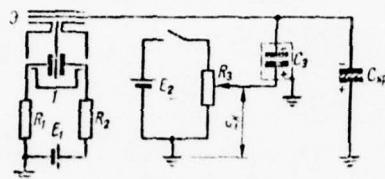


Fig. 7.1.

Fig. 7.1. Schematic diagram of setting for determining pyroelectric coefficient statically [39].

Page 189.

If at the initial moment of measurements potential in the specimen/sample C_{sp} being investigated is equal to zero earth referenced, then the wiper is located in lower position and the arrow/pointer of electrometer is establish/installled to zero.

When changes the temperature of specimen/sample, on its electrodes are formed the charges and it appears potential earth referenced. The arrow/pointer of electrometer differs from zero position. In moving the arm of potentiometer P upward to specimen/sample is supplied the potential, which is the result of the

division of the removed from potentiometer voltage between capacities C_s and C_{kp} . However, since the sign of the potential, caused by voltage from potentiometer, is opposite to the sign of the potential, which arose as a result of the formation of pyroelectric charges, occurs their compensation. When the rifleman/gunner of electrometer it is establish/installed to zero, the total potential on C_{kp} earth referenced also becomes zero.

Value of the pyroelectric coefficient

$$\gamma_c = \frac{q}{\Delta T A_0} = \frac{C_s U_s}{\Delta T A_0} = \frac{E_k C_s C_{kp}}{\Delta T A_0 (C_s + C_{kp})}. \quad (7.1)$$

If $C_s \ll C_{kp}$,

$$\gamma_c = \frac{E_k C_s}{\Delta T A_0}, \quad (7.2)$$

where E_k is compensative voltage on potentiometer; ΔT - the temperature increment of specimen/sample; A_0 - the area of electrodes. In obtained expression (7.2) is not taken into account the electrostatic leakage with C_{kp} for the time of heating, or the inertness of thermal process. The accuracy of measurements depends not only on the quality of calibration capacitor and correctness of the selection of the geometric dimensions of specimen/sample, but also on the rate of the compensation for pyroelectric charge.

In connection with this to N. D. Gavrilovoy [6] was proposed the circuit with the automatic compensation for pyroelectric potential. The block diagram of this setting is given in Fig. 7.2.

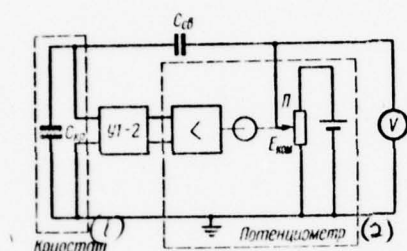


Fig. 7.2.

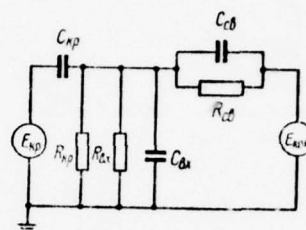


Fig. 7.3

Fig. 7.2. Block diagram of setting for determining pyroelectric coefficient γ_c with automatic compensation [6]: $C_{кр}$ the capacity of crystal; $C_{сб}$ the capacity of coupling capacitor; У1-2 - electrometric amplifier.

Key: (1). Cryostat. (2). Potentiometer.

Fig. 7.3. Equivalent diagram of the compensation method of the measurement of pyroelectric coefficient [6].

Page 190.

The ferroelectric being investigated is placed into the thermostat.

in which the temperature varies from 190 to 120°C, and it is connected to the electrometric amplifier U1-2.

The pyroelectric potential, which appears in specimen/sample during a change in the temperature of crystal, is compensated for by the potential, supplied from auxiliary battery E_{KOM} through the potentiometer ρ whose arm is bonded with the rheochord of automatic recorder, and through the coupling capacitor C_{cb} . The signal of imbalance, taken from amplifier, is supplied to automatic recorder EPP-09, the arm of rheochord of which is moved until the signal of imbalance becomes equal to zero.

Figure 7.3 gives the equivalent diagram of compensation method. Pyroelectric crystal is represented in the form series-connected the source of electromotive force E_{kp} and of its capacity C_{kp} , shunted by leakage resistance R_{kp} , C_{bx} and R_{bx} they are input capacitance and the resistance of the electrometer U1-2; C_{cb} and R_{cb} - the capacity and the resistance of coupling capacitor.

In work [6] was obtained the expression for the calculation of the static pyroelectric coefficient:

$$\gamma_c = \frac{E_{\text{KOM}} C_{\text{CB}}}{\Delta T A_0} \cdot \frac{1}{1 - \exp\left[-\frac{(t + t_1)}{\tau_0}\right]} + \frac{U_0 t}{R \Delta T A_0} \cdot \frac{1}{1 - \exp\left[-\frac{t + t_1}{\tau_0}\right]}, \quad (7.3)$$

where t is the time, calculated off the beginning of heating; t_1 - time of the delay of compensation; τ_0 - the time constant of thermal process (set-up time of the temperature in crystal); R is the total resistance of crystal R_{LD} and of entrance R_{BX} ; U_0 - the sensitivity of electrometer.

Under conditions of experiment time $t = 300$ s, t_1 equal to the time constant of recorder it is 1-3 s. Thermal time constant $\tau_0 = (5-50)$ s and $C_{\text{CB}} R_{\text{CB}} = 25 \cdot 10^3$ s; therefore expression (7.3) is fulfilled sufficiently accurately. An error of measurement is 2-30/o.

Expression (7.3) transfer/converts in (7.2), if we disregard the second term. Special attention one should give to the selection of coupling capacitor - its resistance must be not less than 10^{17} ohm with the capacity 0.25 pF.

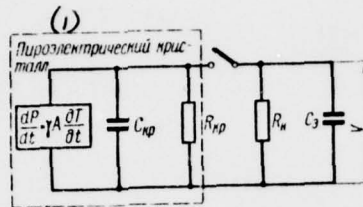


Fig. 7.4.

Fig. 7.4. The installation diagram for determining pyroelectric coefficient by the quasi-static method: dP/dt is a generator of pyroelectric current; C_{np} and R_{np} the capacitance and the resistance of specimen/sample; R_n - load resistance; C_3 - the capacity of electrometer.

Key: (1). Pyroelectric crystal.

Page 191.

During the measurement of pyroelectric coefficient by static method it is necessary that the electrometer would possess high entry impedance in order that the charge would not flow from specimen/sample. Electrometer U1-2 possesses the entry impedance chm , and therefore with small capacities of specimen/sample

electrostatic leakage becomes especially perceptible, if the processes of a change in the polarization last dozen minutes. In connection with this was proposed the circuit with the utilization of vibrating condenser [35].

Recently frequently began to be utilized the quasi-static method of the determination of pyroelectric coefficient.

If in static method the measurement of pyroelectric coefficient is conducted at the establish/installated discrete value of temperature, then in quasi-static the measurement of pyroelectric potential conducts during a continuous change in temperature [3, 7, 8, 50]. Measuring circuit is given in Fig. 7.4. Pyroelectric crystal is represented as current generator

$$I_n = \frac{dP}{dt} = \gamma A_0 \frac{dT}{dt} \quad (7.4)$$

The equation of Kirchhoff for the above-mentioned circuit can be written in the form

$$\gamma A_0 \frac{dT}{dt} = C \frac{dV}{dt} + \frac{V}{R} \quad (7.5)$$

Considering that the thermal time constant of process under the initial conditions $V_{(t=0)} = 0$ much more RC , after the integration of equation (7.5) we will obtain

$$V = \gamma A_0 R \left(\frac{dT}{dt} \right)_0 \left(1 - e^{-\frac{t}{RC}} \right), \quad (7.6)$$

where $C = C_{kp} + C_s$; $R^{-1} = R_{kp}^{-1} + R_n^{-1}$; $\left(\frac{dT}{dt}\right)_0$ - temperature increment at $t = 0$.

Are possible two limiting cases: $t \gg RC$ and $t \ll RC$. In the first case, if $R_{kp} < R_n$, we obtain

$$V = \gamma A_0 R_n \left(\frac{dT}{dt} \right)_0. \quad (7.7)$$

If RC very greatly ($R \approx R_{kp}$), that expression (7.6) assumes the form

$$V = \gamma A_0 \left(\frac{dT}{dt} \right)_0 \left(\frac{t}{C} - \frac{t^2}{2C^2 R_{kp}} \right). \quad (7.8)$$

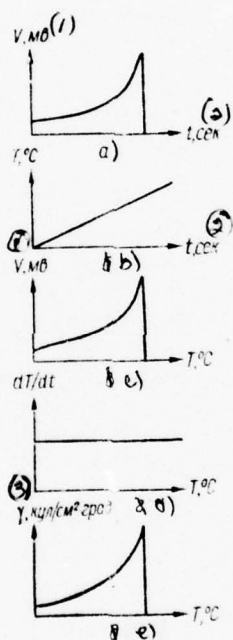


Fig. 7.5.

Fig. 7.5. Plotting dependence $\gamma = \gamma(T)$ with quasi-static method.

Key: (1). mV. (2). s. (3). C/cm²•deg

Page 192.

By putting to use equations (7.6) - (7.8), it is possible to calculate, besides the value of pyroelectric coefficient, also the volume resistivity of crystal and its dielectric constant.

The process of the measurement of pyroelectric coefficient is reduced to the following. To specimen/sample will be fed heat flux in such a way that the rate of its heating would be that which was assigned. The last/latter condition none is necessary, but raises the accuracy of measurements.

Figure 7.5 gives the graphic sequence of the construction of function $\gamma = \gamma(T)$ by quasi-static method. Are recorded the curves $V(t)$ and $T(t)$ are given in Fig. 7.5a and 7.5b. On these dependences are constructed the curves $V(T)$ and dT/dt (Fig. 7.5c and 7.5d) and finally the unknown dependence $\gamma = \gamma(T)$ (Fig. 7.5e).

§2. Dynamic method of the determination of pyroelectric coefficient.

The dynamic method of the measurement of pyroelectric coefficient is described for the first time by Chaynoviz [43]. The essence of method is of periodic heating and cooling specimen/sample the modulated radiation flux and the measurement of the appearing in specimen/sample signal during a change in its temperature. The equation of heat balance for the specimen/sample, heated by radiation flux, takes the form

$$\frac{dQ}{dt} + G\Delta T = W(t). \quad (7.9)$$

The first term indicates a change in the enthalpy of specimen/sample, the second describes its heat losses (G - the coefficient of heat losses) and the third characterizes radiation flux. If $Q = c\Delta T$ (c is heat capacity of specimen/sample, ΔT - temperature increment) and specimen/sample is irradiated by the sinusoidally modulated flow, the temperature increment of the specimen/sample

$$\Delta T = \frac{A_0 W_0 e^{i\omega t}}{G + i\omega c} + \Delta T_0 e^{-\frac{c}{G}t} + \frac{W_0}{G}, \quad (7.10)$$

where ω is a cyclic modulation frequency $i = \sqrt{-1}$; W_0 - the radiation flux density; ΔT_0 - value ΔT with $t = 0$; A_0 = the area of specimen/sample. Pyroelectric current in steady state

$$J = A_0 \frac{dP}{dt} = A_0 \gamma_A \frac{dT}{dt} = A_0^2 \frac{i\omega \gamma_A W_0 e^{i\omega t}}{G + i\omega c}, \quad (7.11)$$

a its module/modulus

$$|J| = A_0^2 \frac{\gamma_A \omega W_0}{(G + \omega^2 c^2)^{0.5}}. \quad (7.12)$$

Page 193.

Expression (7.12) for determining dynamic pyroelectric coefficient γ_A is derived on the assumption that value ΔT is certain average value of the temperature of specimen/sample without the analysis of the conditions of heat transfer on boundaries and therefore bears the qualitative character. More exact expression for the determination of value γ can be obtained during detailed analysis [18].

Let us examine the pyroactive crystal, which has the form of rectangular prism (Fig. 7.6). Its front face, irradiated by radiation flux, is covered with the absorbing layer of black, which simultaneously fulfills the functions of electrode. The back side of crystal is found on the massive heat withdrawal, which is absolute heat sink and the second electrode. The vector of the spontaneous polarization of crystal is directed perpendicular to electrodes. The pyroelectric current, which appears in arbitrary crystal element $\delta x \delta y \delta z$, is determined by a change of polarization $P(y)$ in this volume and is equal to:

$$i_0(y) = \delta x \delta z \frac{dP(y)}{dt}. \quad (7.13)$$

Average value of pyroelectric current in elementary rectangular prism $\delta x \delta z d$ [23]

$$\bar{i}_0 = \frac{\delta x \delta z}{d} \int_0^d \frac{dP(y)}{dt} dy = \frac{\delta x \delta z}{d} \int_0^d \gamma_{\pi} \frac{dT(y)}{dt} dy. \quad (7.14)$$

If the polarization of crystal is uniform in volume and the pyroelectric coefficient $\gamma_{\pi} = \frac{dP}{dT}$ to place by constant/invariable during weak irradiation, disregarding the corrections of the second and of the higher orders of smallness, we will obtain

$$\bar{i}_0 = \gamma_{\pi} \frac{\delta x \delta z}{d} \int_0^d \frac{dT(y)}{dt} dy. \quad (7.15)$$

For the determination of value $dT(y)/dt$ the irradiated crystal it is necessary to solve the equation of thermal conductivity.

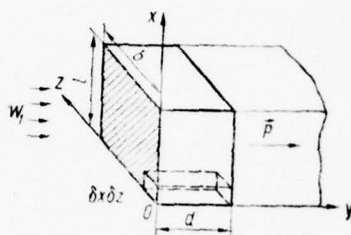


Fig. 7.6.

Fig. 7.6. Circuit of pyroactive crystal.

Page 194.

If the thickness of crystal d considerably shorter than its length and the widths, but heat losses from the lateral faces can be disregarded, the thermal problem, solved for a homogeneous and an isotropic medium, it is reduced to the one-dimensional case

$$\frac{\partial T}{\partial t} = n \frac{\partial^2 T}{\partial y^2} \quad (7.16)$$

under the following boundary conditions:

$$c_0 \frac{dT}{dt} = e_0 W_0 (1 + e^{i\omega t}) + k \frac{\partial T}{\partial y} - 4\varepsilon_0 \sigma_c T_0^3 (T - T_0)$$

with $y = 0$, $T - T_0 = 0$ with $y = d$, where c_0 is heat capacity of one

of the surface of black; ϵ_0 - its absorptivity; σ_C is constant of stefana - Boltzmann; T - the temperature of crystal; T_0 - the temperature of the medium; n - thermal diffusivity ($n = k/c$); k - the coefficient of thermal conductivity; c is specific heat of one volume of crystal.

The first boundary condition is the equation of the heat balance of crystal boundary, heated by the sinusoidally modulated flow $W_0(1 + e^{i\omega t})$ and cooled because of thermal conductivity $k \frac{\partial T}{\partial y}$ and by emission/radiation $4\epsilon_0\sigma_C T_0^3$, when crystal is located in vacuum.

After changing to new alternating/variable $\theta = T - T_0$ and by solving equation (7.16), we will obtain

$$\theta(y, \omega, t) = \frac{\epsilon_0 W_0 (d - y)}{k + 4\epsilon_0 \sigma_C T_0^3 d} + \frac{\epsilon_0 W_0 \operatorname{sh} h (d - y) e^{i\omega t}}{kh \left[\operatorname{ch} hd + \frac{4\epsilon_0 \sigma_C T_0^3 + i\omega c_0}{kh} \operatorname{sh} hd \right]} \quad (7.17)$$

where $h = (1 + i) \sqrt{\frac{\omega}{2n}}$; $\sqrt{\frac{2n}{\omega}} = d_0$ the length of temperature wave. By substituting equation (7.17) in equation (7.15) and by producing integration for the volume of crystal, we will obtain expression for the complete pyroelectric current of the crystal:

$$J = \frac{\gamma_{\pi} \epsilon_0 W_0 b l e^{i\omega t} (1 - \operatorname{sch} hd)}{cd \left[1 + \frac{4\epsilon_0 \sigma_c T_0^3 + i\omega c_0}{kh} \operatorname{th} hd \right]}, \quad (7.18)$$

where b and l are width and the length of crystal; $bl = A_0$. The irradiated by the modulated flow pyroactive crystal can be presented in the form of equivalent circuit (Fig. 7.7) as generator of the pyroelectric current J with in in parallel connected capacity $C_{\kappa p}$ and the resistance of losses $R_{\kappa p}$. Then input voltage of the lamp

$$U = \frac{JR}{1 + i\omega CR} = \frac{\gamma_{\pi} \epsilon_0 W_0 A_0 e^{i\omega t} (1 - \operatorname{sch} hd) R}{cd (1 + i\omega CR) \left[1 + \frac{4\epsilon_0 \sigma_c T_0^3 + i\omega c_0}{kh} \operatorname{th} hd \right]}. \quad (7.19)$$

In the sonic frequency band of modulation expression (7.19) is simplified [19]. We examine equation (7.19) for the cases of crystals BaTiO_3 and TGS. The parameters of these crystals are given in Table 7.1.

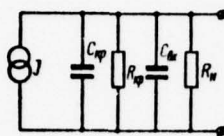


Fig. 7.7.

Fig. 7.7. The equivalent replacement scheme of the irradiated pyroelectric: T is a generator of pyroelectric current; C_{kp} - the capacity of crystal; R_{kp} - the equivalent resistance of losses; C_{vx} the input capacitance of meter; R_n - load impedance.

Page 195.

From table it is evident that product $hd \geq 2$ is fulfilled at the frequencies, which exceed 20 Hz. If $hd \gg 1$, $\sin hd \rightarrow 0$.

Furthermore, the term, which stands in brackets in the denominator of equation (7.19), is close to unity at least to frequencies 20 kHz, if the heat capacity of the irradiated electrode $c_0 \approx 2.5 \times 10^{-5} \text{ J/}(\text{deg} \cdot \text{cm}^2)$.

Then expression (7.19) is simplified:

$$|U| = \frac{\gamma \pi^2 \epsilon_0 W_0 A_0 R}{(1 + \omega^2 C^2 R^2)^{0.5} c_d} \quad (7.20)$$

Are possible two operating modes: $\omega CR \ll 1$ and $\omega CR \gg 1$. When load resistance $R_n = 10^6$ ohm, $C = 10$ pF and modulation frequency is equal to 40 Hz, with larger degree of accuracy it is possible to write

$$U_1 = \frac{\gamma \pi \epsilon_0 W_0 A_0 R_1}{cd} \quad (7.21)$$

If load resistance $R_n = (10^8 \div 10^{10})$ to ohm with the same capacity, expression (7.20) takes the form

$$U_2 = \frac{\gamma \pi \epsilon_0 W_0 A_0}{cd\omega C} = \frac{2\gamma_A}{e} \cdot \frac{\epsilon_0 W_0}{lc} \quad (7.22)$$

By putting to use expressions (7.21) and (7.22), let us find the value of pyroelectric coefficient γ_A and relation γ_A/e . On this is based the radiation method of the simultaneous measurement of pyroelectric coefficient and dielectric constant of pyroactive crystals.

Table 7.1.

(2) Материал	(1) Параметры						(9)					
	(3) Удельная плотность ρ , г/см ³	(4) Удельная теплоем- кость c' , кал/г·град	(5) Теплоем- кость единицы объема $c = \rho c'$, кал/см ³ ·град	(6) Коэффициент теплопровод- ности k , кал/см·сек·град	(7) Температу- ропровод- ность $n = \frac{k}{c}$, см ² /сек	(8) Длина тем- пературной волны $\lambda = \sqrt{\frac{2n}{\omega}}$, см $f = 1$ гц	(9) $\lambda \lambda_0 = \frac{\sqrt{2}}{f} \cdot a$ ($a = 10^{-2}$ см) при разных частотах модуляции, гц					
							1	10	10 ²	10 ³	10 ⁴	10 ⁵
(10) BaTiO ₃ поликри- сталлический	6	0,12	0,75	$4,5 \cdot 10^{-3}$	$6,25 \cdot 10^{-3}$	$1,41 \cdot 10^{-2}$	1	3,16	10	31,6	100	316
ГТС	1,69	0,36	0,608	$1,64 \cdot 10^{-3}$	$2,7 \cdot 10^{-3}$	$2,93 \cdot 10^{-2}$	0,48	1,52	4,8	15,2	48	152

Key: (1). Parameters. (2). Material. (3). Specific density ρ , g/cm³.
 (4). Specific heat c' cal/g·deg. (5). Heat capacity of unit volume $c = \rho c'$ cal/cm³·deg. (6). Coefficient of thermal conductivity k ,
 cal/cm·s·deg. (7). Thermal diffusivity $n = k/c$, cm²/s. (8). Length of
 temperature wave cm. $f = 1$ Hz. (9). at the
 different modulation frequencies, Hz. (10). BaTiO₃ polycrystalline.

The calculated relationship/ratios have following form [16]:

$$\varepsilon = 1,82 \cdot 10^{12} \frac{d}{A_0} \left(\frac{U_1}{U_2} \times \right. \\ \left. \times \frac{1}{R_1 f} - 2\pi 10^{-12} C_{nx} \right); \quad (7.23)$$

$$\gamma_A = U_1 \frac{cd}{\varepsilon_0 R_1 W_0 A_0}; \quad (7.24)$$

$$\gamma_A/\varepsilon = U_2 \frac{cf}{\varepsilon_0 W_0} 10^{-12} \left(0,55 + \frac{2\pi d}{\varepsilon_0 A_0} C_{nx} \right), \quad (7.25)$$

where C_{nx} is the capacity of input circuit, measured in picofarads.

Schematic electrical diagram for the investigation of pyroactive crystals is given in Fig. 7.8. The specimen/sample being investigated K , placed into thermostat, is irradiated by the modulated radiant flux $W(t)$. The removed from crystal pyroelectric signal is supplied to the entrance of amplifier (lamp 6S12h). Switch P_1 serves for the consecutive connection of resistances $R_1 = 1 \text{ M}\Omega$ and $R_2 = 1 \text{ Gohm}$. In this case exit pyroelectric voltage is proportional either to $\gamma_A (R_1 = 1 \text{ to } \text{M}\Omega)$ or $\gamma_A/\varepsilon (R_2 = 1 \text{ Gohm})$. Then signal is supplied to amplifying tube 6Zh1P and through the attenuator P_2 (one-to-one; 1:10; 1:100) to the selective cascade/stage, assembled on lamps 6N2P with dual T-shaped bridge in feedback loop. Switch P_3 serves for the connection of the filters, adjusted to 10, 40 and 10⁴ Hz.

By the authors [24] were proposed procedure and setting for the investigation of pyroelectric coefficient and dielectric constant of ferroelectric in infralow-frequency range (0.05-10 Hz). The specimen/sample being investigated was placed into the vacuum container, where was maintained pressure 10^{-3} torr. The pyroelectric signal, taken from the changed over load resistances, was amplified by the electrometric instrument V2-5. The measuring instrument of electrometer was disconnected and instead of it was utilized low-frequency oscillograph S1-4.

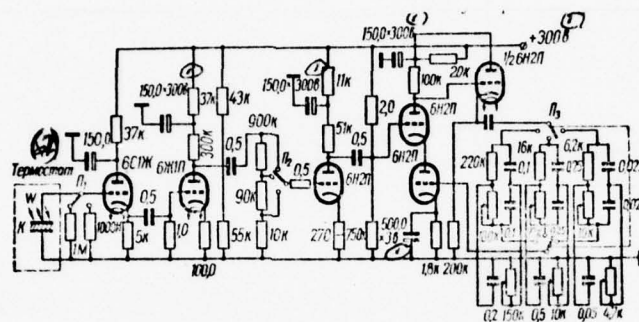


Fig. 7.8.

Fig. 7.8. Schematic electrical diagram of setting for the measurement of pyroelectric coefficient and dielectric constant by dynamic method.

Key: (1) - Volts (2) - Thermostat.

Page 197.

The calculated relationship/ratios for values

$$\gamma_A = U_1 \frac{cd}{\epsilon_0 R_1 W_0 A_0} \Gamma; \quad \gamma_A/e = U_2 \frac{cf}{\epsilon_0 W_0} 10^{-12} \left(0,55 + \frac{2nd}{\epsilon A_0} C_{nx} \right) \Gamma$$

differ from expressions (7.24) and (7.25) in terms of the correction factor

$$\Gamma = \frac{\frac{h_0}{h(hd)} + 1 - \frac{1}{3}(hd)^2 + \frac{2}{15}(hd)^4}{1 - \frac{1}{3}(hd)^2 + \frac{2}{15}(hd)^4}, \quad (7.26)$$

where

$$h_0 = \frac{4\epsilon_0\sigma_C T_0^3}{k}.$$

The described dynamic method of the determination of pyroelectric coefficient is not the only possible (for exam. [49]). One of the versions of this method is represented in Fig. 7.9. In this version the mean temperature is determined from a change in the resistance of the irradiated electrode, which simultaneously plays the role of bolometer. A change in the electrode resistance R_6 can be written thus:

$$\Delta R = \alpha_c R_6 \Delta T, \quad (7.27)$$

where α_c is temperature specific resistance of the irradiated electrode; ΔT - the temperature increment of electrode.

When switch \mathcal{P} is located in position of 2, the voltage, taken from load resistance R_{n_1} , takes the form

$$\Delta U = \frac{\alpha_c R_6 \Delta T i_0 R_{n_1}}{(R_{n_1} + R_6)} = \frac{\alpha_c R_6 \Delta T R_{n_1} U}{(R_{n_1} + R_6)^2}, \quad (7.28)$$

where U is voltage in the circuit of bolometer.

From expression (7.28) it follows

$$\Delta T = \frac{\Delta U (R_n + R_0)^2}{U \alpha_c R_0 R_n}. \quad (7.29)$$

Measuring value ΔU at modulation frequency, and also value α_c and R_0 as functions of temperature, by formula (7.29) we determine the temperature of the irradiated electrode on pyroactive crystal.

The temperature of the irradiated electrode whose thickness does not exceed 0.5μ , it is possible with a high degree of accuracy to consider identical in the thickness of electrode at sonic modulation frequencies [22]. According to [20], the temperature of the back side of electrode T_r is bonded with the temperature of the front T_n by the relationship/ratio

$$T_r = T_n e^{-\frac{d}{d_0}}. \quad (7.30)$$

If we use data by Table 7.2 for nickel, bismuth and germanium, then it is not difficult to see that at frequencies less than 200 Hz, a difference in the temperature of the front/leading and back sides of the irradiated electrode will not exceed 10/c.

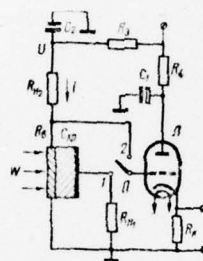


Fig. 7.9.

Fig. 7.9. The circuit of the determination of pyroelectric coefficient by the dynamic method, in which the irradiated electrode serves as bolometer.

Page 198.

Thus, the obtained values of the temperature of film can be considered the temperature of the front face of pyroactive crystal.

Let us determine the mean temperature of crystal, if it is known that on its face the temperature changes according to the law $\theta = \Delta T_0 e^{i\omega t}$. For this is solved the equation of the thermal conductivity

$$\frac{\partial \theta}{\partial t} = n \frac{\partial^2 \theta}{\partial y^2} \quad (7.31)$$

under the following boundary conditions:

$$\Theta = \Delta T_0 e^{i\omega t} \quad \text{when} \quad y = 0, \quad (7.32)$$

$$\Theta = 0 \quad \text{with} \quad y = d.$$

The solution to equation (7.31) takes the form

$$\Theta(y) = \Delta T_0 e^{i\omega t} \frac{\operatorname{sh} h(d-y)}{\operatorname{sh} hd}. \quad (7.33)$$

Then the average value of the temperature of the crystal

$$\bar{\Theta} = \frac{1}{d} \int_0^d \Delta T_0 e^{i\omega t} \frac{\operatorname{sh} h(d-y)}{\operatorname{sh} hd} dy = \frac{\Delta T_0 e^{i\omega t}}{hd} \cdot \frac{(\operatorname{ch} hd - 1)}{\operatorname{sh} hd}, \quad (7.34)$$

whence

$$\frac{\partial \bar{\Theta}}{\partial t} = i\omega \Delta T_0 \frac{e^{i\omega t}}{hd} \operatorname{th} \frac{hd}{2}. \quad (7.35)$$

With $hd \geq 4$ and $\operatorname{th} hd/2 \rightarrow 1$ expression (7.35) is simplified:

$$\frac{\partial \bar{\Theta}}{\partial t} = i\omega \Delta T_0 \frac{e^{i\omega t}}{hd} \quad (7.36)$$

The value of pyroelectric input voltage of lamp taking into account equations (7.11) and (7.36) takes the form

$$|U_n| = |J_n| R_{n_1} = A_0 \gamma_n |\Delta T_0| \sqrt{n\omega} \frac{R_{n_1}}{d}, \quad (7.37)$$

whence

$$\gamma_n = \frac{|U_n| d}{|\Delta T_0| \sqrt{n\omega} A_0 R_{n_1}}. \quad (7.38)$$

Table 7.2 [20].

(1) Вещество	(2) Теплоемкость ед. нц объема с, кал град·см ³	(3) Коэффициент теплопровод- ности k кал град·см·сек	(4) Длина температурной вол- ны λ_0 (см) для двух частот модуляции	
			10 гц	200 гц
Никель (5)	0,140	0,930	0,068	0,015
Висмут (6)	0,019	0,286	0,047	0,010
Германий (7)	0,136	0,358	0,105	0,022

Key: (1). Substance. (2). Heat capacity of unit volume c , cal/deg·cm³. (3). Coefficient of thermal conductivity k cal/deg·cm·s. (4). Length of the temperature wave λ_0 (cm.) for two modulation frequencies. (5). Nickel. (6). Bismuth. (7). Germanium.

Page 199.

After substituting into equation (7.38) the value of quantities $|\Delta T| = |\Delta T_0|$, from (7.29) we will obtain

$$\gamma_A = \frac{\{U_n \{ U \alpha_c R_0 R_{n_1} \}}{|\Delta U(\omega) | (R_{n_1} + R_0)^2 | n \omega} \cdot \frac{d}{A_0 R_{n_1}} \quad (7.39)$$

In equation (7.39) value $\Delta U(\omega)$ is the complex function of the modulation frequency and thermophysical characteristics of crystal. Its precise value was obtained by O. V. Roytsina et al. [34]. However, in the described case the value $\Delta U(\omega)$, just as α_c , is determined experimentally.

The determination of pyroelectric coefficient is reduced to measurement $\Delta U(\omega)$ and R_0 at the fixed/recorded temperature in the position of switch 2, and then to the measurement of pyrovoltage U_n in the position of switch 1. The calculation V_n conducts by formula (7.39).

The determination of the temperature dependence of pyroelectric coefficient is the work consuming process, which is continued several hours. In work [17] is proposed the rapid method of research on pyroelectric effect in ferroelectric. By authors was utilized dynamic method during rapid heating specimen/sample by radiation flux. Measurements were conducted on the setting, analogous that which was described above. Measuring flow with a power $W_0 = 10^{-5} \text{ W/mm}^2$ from the calibrated radiation source, modulated by frequency 20-50 Hz, it was headed for the specimen/sample being investigated, which was being located in vacuum glass container. The appearing during irradiation

signal was supplied to amplifier and to the memory oscillograph with the long afterglow, on screen of which it was possible to observe and to photograph the kinetics of pyroelectric effect. Heating specimen/sample was realized by the instantly supplied powerful source radiation constant with the density of flow $W = (10^{-2} - 10^{-3})$ W/mm². Under the action/effect of luminous flux the specimen/sample 50-300 μ thickness was heated on 15-25°C in 1-5 s. Since heating the specimen/sample, irradiated by instantly connected radiation flux W , occurs exponentially, one should fit such conditions of the works, which would correspond to the linear section of the exponential of heating. In this case the average temperature increment it is possible to obtain by solving of the equation of the heat balance

$$\Delta T = \frac{W}{G} (1 - e^{-\frac{G}{c} t}), \quad (7.40)$$

where G is a coefficient of heat losses; c - the heat capacity of specimen/sample; t - time from the torque/moment of the connection/inclusion of radiant flux.

Page 200.

Expanding $e^{-\frac{G}{c} t}$ in a series under condition $t / (c/G) < 1$ approximately we will obtain

$$\Delta T \approx \frac{W}{c} t. \quad (7.41)$$

For uniform heating specimen/sample in the assigned temperature interval ΔT it is necessary that time t be less than the thermal time constant of specimen/sample $\tau = c/G$, and the intensity of emission/radiation W was sufficient for obtaining the desired temperature increment for this time. The calculation of value ΔT is obtained simply and does not require the knowledge of the coefficient of heat losses.

Time for temperature balance according to the thickness of specimen/sample can be written [14] in the form

$$\tau_0 = \frac{d^2 c}{\pi^2 k} \quad (7.42)$$

For the specimen/samples being investigated less than 300μ thickness $\tau_0 \leq 10^{-2}$ s, the sweep length on oscilloscope face 1-5 s; therefore difference of the temperature states at the different points of specimen/sample in practice is not observed.

A change of the signal, taken the irradiated specimen/sample, in temperature dependence is proportional to a change in the pyroelectric coefficient. During linear changes in the temperature the envelope of the pyroelectric signal, written on oscillograph, will present the temperature dependence of pyroelectric coefficient.

The comparisons of the different methods of the determination of

pyroelectric coefficients, carried out in recent years, they showed that the obtained values of these quantities can considerably differ [2, 3]. The pyroelectric coefficients, measured by static method, are caused both by the rapid and slow processes of polarization. During the measurement of pyroelectric coefficients by dynamic method the basic contribution introduce the rapid processes of polarization. The measurements, carried out by quasi-static method, to a considerable degree depend on the rate of heating [8, 35] crystal. Ambiguity in measurements can be bonded with the complexity of the course of the slow processes of polarization and uneven heating crystal. The latter fact it can lead to the emergence of mechanical stresses in crystal and the appearance of a tertiary pyroelectric effect. Analogous description could arise, also, during the investigation of pyroelectric effect by dynamic method, since at different modulation frequencies the depth of penetration of temperature wave (7.17) was different. However, in the literature still not were given any quantitative measurements of tertiary pyroelectric effect.

Page 201.

Conducted investigations [24] of pyroelectric coefficients by dynamic method showed that the tertiary pyroelectric effect was small. Focus into point and the washed away over surface one and the same radiant flux at modulation frequencies 20-500 Hz gave one and

the same signal.

An error of measurement of pyroelectric coefficients by static method is 2-50/o. The determination of pyroelectric coefficients by the dynamic method is done with smaller accuracy, since in the calculated relationship/ratios enters more the parameters, than at static method. In this case errors of measurement are 10-150/o.

However, dynamic method makes it possible to conduct the measurements of the dispersion of pyroelectric coefficient. And main, for the calculation of pyroelectric radiation detectors in wide frequency range it is necessary to know dynamic pyroelectric coefficient.

§3. Methods of the measurement of dielectric constant.

For the calculation of ferroelectric radiation detectors it is necessary to know dielectric constant ϵ and the dielectric power factor $\tan \delta$. The dielectric constant of ferroelectric ϵ strongly depends on the value of the external field E (Fig. 7.10).

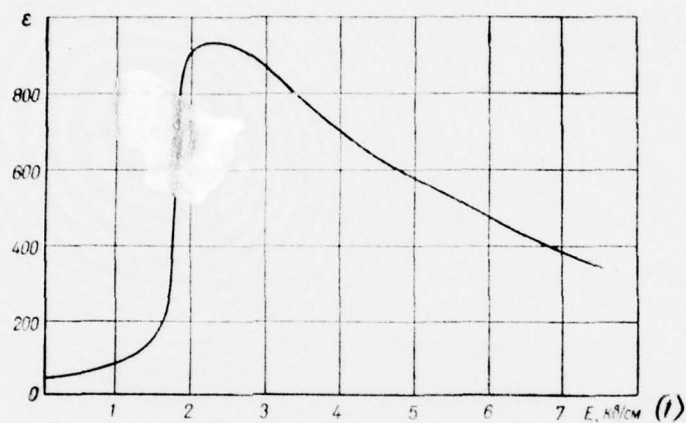


Fig. 7.10.

Fig. 7.10. Dependence of dielectric constant ϵ for the single crystal TGS on external electric field.

Key: (1). kV/cm.

Since the dielectric constant ϵ loses the uniqueness with of measurement depending on value and character of electric field [52], there is a number of concepts of the capacity of ferroelectric condenser [13]:

a) static capacity is the capacitance of capacitor, measured with constant stress with the aid of the ballistic galvanometer:

$$C_{\text{st}} = \frac{q_{\text{st}}}{U_{\text{st}}}, \quad (7.43)$$

where U_{st} - constant stress, applied to condenser/capacitor; q_{st} is the conservative value of charge on the capacity of specimen/sample;

b) the differential (dynamic) capacity is determined by the expression

$$C_{\text{d}} = \frac{\partial P}{\partial E} = \frac{\partial q}{\partial U} \quad (7.44)$$

and is the tangent of tangent angle to the curved loop of charge q (U);

c) the effective capacity is measured on alternating current and is defined as capacitance of this linear capacitor whose charge at the maximum value of voltage U_{max} is equal to the charge of nonlinear capacitor with the same voltage:

$$C_{\text{eff}} = \frac{q_{\text{max}}}{U_{\text{max}}}; \quad (7.45)$$

d) the reversible capacity is determined with the aid of low measuring variable field U_{m} in high stationary field

$$C_p = \left(\frac{q_H}{U_H} \right)_{U_{\text{m}}} \quad (7.46)$$

Figure 7.11 gives circuit for the measurement of reversible dielectric constant. Constant adjusted with potentiometer R_1 voltage through the throttle/choke D_r is supplied to the capacitor C_{kp} being investigated. Measuring voltage U_{m} through isolating capacitor C_1 is supplied to the capacitor C_{kp} being investigated and the standard resistance R_s . With low alternating voltages and low losses the current, which takes place through the capacitor, approximately is equated by the capacitive component of the current

$$I = \omega C_p U_{\text{m}} \quad (7.47)$$

Hence

$$C_p = \frac{U_s}{\omega U_{\text{m}} R_s} \quad (7.48)$$

where U_s is voltage on standard capacity.

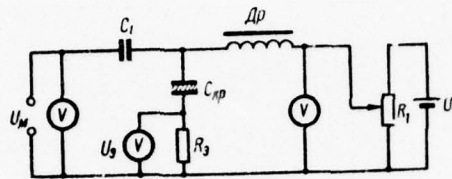
*Fig. 7.11.*

Fig. 7.11. Measuring circuit of reversible dielectric constant.

Page 203.

At the low values of effective stress the measurement of capacity and tangent of the angle of dielectric losses can be conducted by resonance or bridge method.

If measuring frequencies exceed several kilohertz, then convenient and precise is the resonance method. At lower frequencies the effectiveness of bridge method is higher.

Figure 7.12 gives bridge circuit for the measurement of dielectric constant ϵ and of the dielectric power factor $\tan \delta$ in the range from 2 to 5000 Hz with voltage on specimen/sample of

approximately 50 MV. For the purpose of an increase in the sensitivity the circuit has two output/yields. For frequencies less than 100 Hz, is applied the RC-filter, which cuts off high frequencies. Wave trap on 50 Hz serves for the elimination of focusing/inductions.

It should be noted that only in weak electric fields in the ferroelectric of the form of the voltage are close to sinusoidal. Therefore values ϵ and $\tan \delta$ under these conditions can be determined as for linear dielectrics, with the aid of the equivalent replacement scheme of real ferroelectric by ideal capacity with the consecutively or in parallel connected resistance.

The method of the simultaneous determination of dielectric constant and pyroelectric coefficient of crystals was described in the preceding/previous paragraph.

Page 204.

§4. Equipment for determining receiver responses.

Industry does not discharge standard installations for determining the parameters of radiation detectors. Are absent any systematic descriptions of procedures on this question. The rare published works are related to the description of the testing units, intended for characteristic measurement of a defined class of radiation detectors [15, 21, 25, 27, 28, 29, 38, 40, 48, 51].

The creation of universal installations is connected with the considerable difficulties of the agreement of the equivalent resistance of receiver with the noises of input time, since the internal resistance of receivers changes depending on their type in the range from 0.1 to 10^{10} ohm at the temperature of sensing element 2-300°K.

Will be described below the complex of metering equipment for determining the parameters of ferroelectric receivers. The block diagram of installation is given in Fig. 7.13. Installation consists

AD-A046 669

FOREIGN TECHNOLOGY DIV WRIGHT-PATTERSON AFB OHIO
FERROELECTRIC RADIATION DETECTORS, (U)

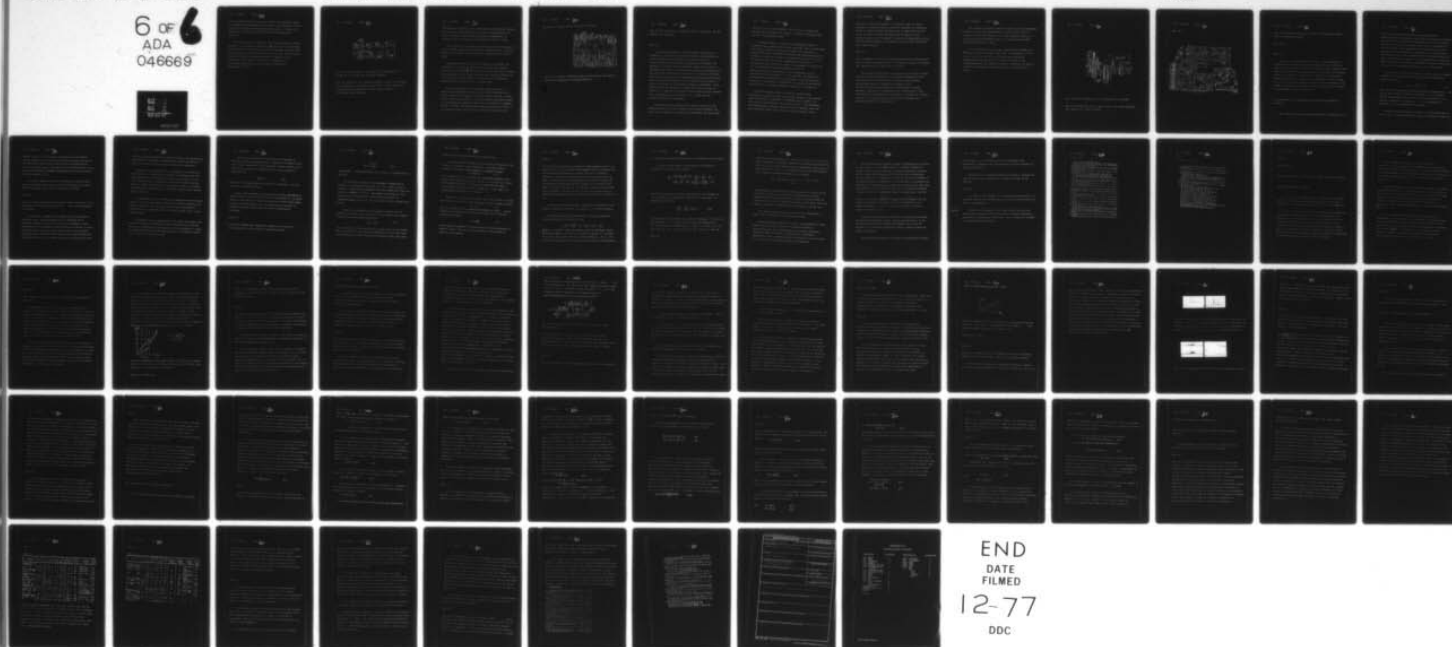
F/G 17/5

UNCLASSIFIED

JUL 77 L S KREMENCHUGSKIY
FTD-ID(RS)T-0846-77

NL

6 OF 6
ADA
046669



END
DATE
FILMED
12-77
DDC

of the standard emitter, as which is utilized the cylindrical model of blackbody with temperature of 400-600°K. It is possible to utilize a model of spherical or tubular blackbody; however, to obtain the uniformity of temperature within this body structurally more difficult.

The evaluation of the quality of the model of blackbody conducts according to the procedure, proposed by De Vose [45]. For temperature balance along the core tube of the model of blackbody Nichrome spiral at its end/leads is coiled more densely. If the ratio of the depth of cavity to a radius of radiating aperture is equal to 30, the temperature of the cavity of the model of blackbody, up to front/leading wall, remains constant with accuracy $\pm 5^\circ$ to temperatures of 450°K.

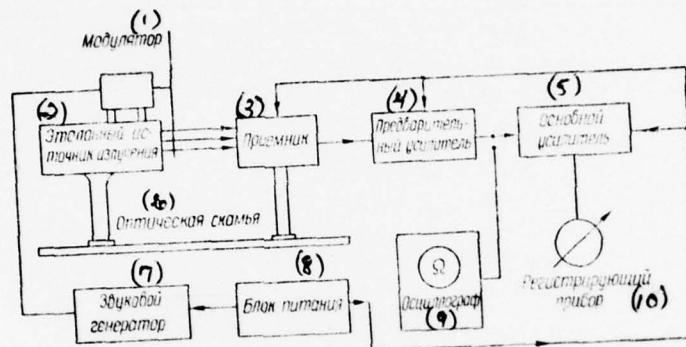


Fig. 7.13. Block diagram of installation for determining the parameters of ferroelectric radiation detectors.

Key: (1). Modulator. (2). Standard radiation source. (3). Receiver. (4). Preamplifier. (5). Basic amplifier. (6). Optical bench. (7). Audiofrequency oscillator. (8). Power supply units. (9). Oscillograph. (10). Recorder.

Page 205.

Calculation of the value of the coefficient of the radiating capacity of model gives value larger than 0.99. The front/leading wall of model is cooled by water. During operation the temperature of modulator must not exceed room temperature more than by 1.5°C.

The setting up of the model of blackbody, which can be moved in three mutually perpendicular directions, conducts in such a way that normal to the surface of receivers would coincide with the axis of model.

Preamplifier serves for impedance matching of receiver with resistance of the basic amplifier. The basic amplifier contains cascade/stage with dual π -section filter or with synchronous detector for measurements in the narrow frequency band. Visual observation of the form of the measured signal is realized by an oscillograph. Audiofrequency oscillator supplies chopper motor.

For the investigation of the dynamic characteristics of ferroelectric bolometers and partly pyroelectric receivers can be used the setting up, schematic electrical diagram of which is given in Fig. 7.14 [21]. At setting up can be determined amplitude-frequency and phase-frequency receiver responses in the interval of pressures $5 \cdot 10^{-6}$ - 760 torr, the temperatures, which vary from 77 to 400°K, in the different gaseous media with the sinusoidal and square-wave

modulation of radiant flux in the range 2-5000 Hz.

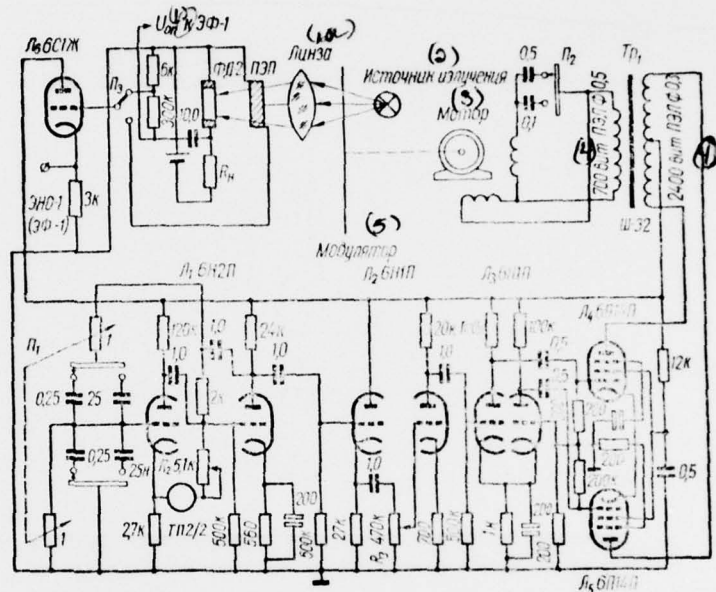


Fig. 7.14. Schematic electrical diagram of setting for the study of the receiver responses of emission/radiation.

Key: (1) ^{to} K. (1A). Lens. (2). Radiation source. (3). Motor. (4). ^{is} twisted. (5). Modulator.

Page 206.

The emission/radiation of standard source, interrupted by modulator, is focused by lens on the receiver being investigated, which is placed into the special glass cryostat, where is establish/installated the necessary temperature and pressure. The appearing in receiver during irradiation signal with the aid of cathoderepeater (lamp L₆) is supplied to electron oscillograph ENO-1 (or vacuum tube voltmeter) and phasemeter EF-1 with the introduced low-frequency correction. The simultaneously modulated radiant flux falls in germanium photodiode FD-2. The removed from the load of diode signal serves as the reference voltage of phasemeter. On the entrance of cathode follower is located the switch P₃, which in position of 1 connects to measuring circuit signal from the receiver being investigated, and in position of 2 ~ signal from the divider/denominator of photodiode.

The audiofrequency oscillator (L₁) controls the work of the asynchronous motor ASM-100, connected with reducer modulator. The value of exit voltage is regulated by potentiometer R₃. After phase

inverter (L_3) and power amplifier (L_4 and L_5) the voltage from audiofrequency oscillator is supplied to matching transformer Tr_1 , and then to asynchronous motor.

As standard emitter is utilized the incandescent bulb of automobile type, supplied from storage batteries. Bulb is placed into the metallic cylinder, strengthened together with modulator on optical bench. With square-wave modulation the front/leading wall of cylinder, illuminated by bulb, has rectangular groove (8×1) mm², the length of the mean line of a trapezium of the groove of modulator, passing through the center of illuminator, is equal to 25 mm. For obtaining sinusoidal modulation of flow is establish/installed the covering to the front/leading wall of cylinder with opening/aperture 10 mm in diameter. The diameter of opening/aperture corresponds to the diameter of the inscribed into the groove of interrupter circumference. At an angle of perforation less than 30°, is obtained modulation, very close to sinusoidal.

The glass cryostat, where is placed the receiver being investigated, is shown in Fig. 7.15. Sensing element of the receiver being investigated is fastened to molybdenum rod 1, sealed in in glass tube 2, which concludes with hollow section 3. The molybdenum input/introductions, passing through the body of section, serve for test connection. Dewar flask fills with liquid nitrogen. Vacuum

tap/crane 4 serves for filling of the chamber, where is placed receiver, by different gases at different pressures. For obtaining vacuum is utilized carbon adsorptive pump 5. Before work into the cavity of pump is inserted the heater for the warm-up of the activated angle. After 15 minutes of warm-up and evacuation with fore pump the system overlaps, but adsorptive pump and Dewar flasks fill with liquid nitrogen.

Page 207.

After 10 minutes in system is establish/installed the pressure $5 \cdot 10^{-6}$ torr. By heating molybdenum rod, it is possible to report to receiver any temperature in the range from 90 to 400°K.

The described installation for determining the dynamic receiver responses of emission/radiation is completely sufficient for the investigation of the ferroelectric bolometers, which possess considerable inertness. However, for research on the amplitude-frequency characteristics of pyroelectric receivers mechanical modulation is insufficient. For determining the time characteristics of pyroelectric receivers it is possible to utilize a gas laser in conjunction with electro-optical modulator and a selective amplifier of the type V6-6.

The schematic electrical diagram of setting [15] for determining receiver noise of emission/radiation is given in Fig. 7.16. It consists of input unit (lamp L_1), the basic amplifier (lamps $L_2 - L_8$), monitoring oscillograph (lamps $L_9 - L_{12}$ and L_{18}) and power supply unit (lamps $L_{13} - L_{17}$).

For the selectivity of the basic amplifier are utilized dual π -sections filter in feedback loop, tuned to frequencies 5, 9, 15, 20, 35, 83, 335 and by 10000 Hz. The wave trap between the cascade/stages of lamp L_3 by 50 Hz lowers the level of the focusing/inductions of commercial frequency. Attenuator P_2 makes it possible to investigate the receivers, which strongly differ in noises.

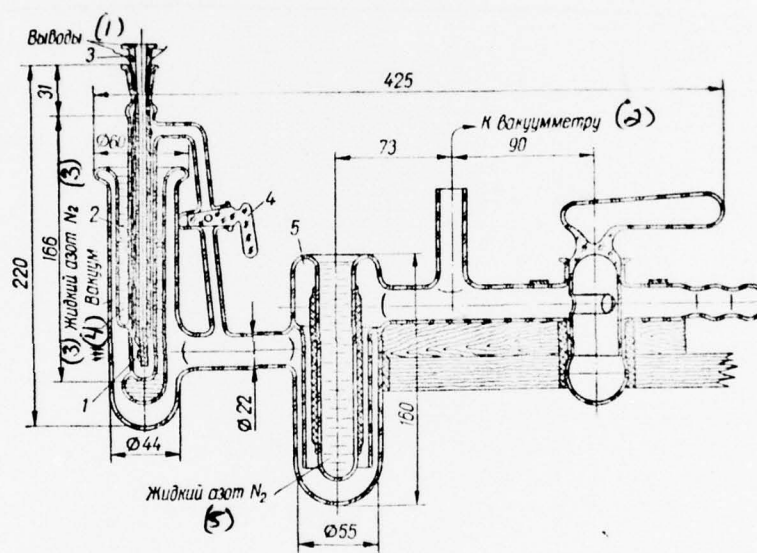


Fig. 7.15. Glass cryostat for the investigation of receivers.

Key: (1). Conclusions. (2). To vacuum gauge. (3). Liquid nitrogen.
(4). Vacuum. (5). Liquid nitrogen.

Fig. 7.16. Electrical circuit of setting for determining receiver noise of emission/radiation.

Key: (1). V.

Page 209.

During the investigation of the noises of the ferroelectric bolometers whose bridge is supplied by high frequency, before the lamp L₆ it is necessary to supply the detector of high frequency with filter. After filter the envelope, which characterizes low-frequency noises, is amplified by lamp L₆ and is supplied to low-frequency detector, and then it is recorded by a measuring meter of the type M-82 or by the automatic recorder EPP-09. For the measurement of the noises of pyroelectric receivers at high frequencies it is possible to use standard setting the type V6-1.

§5. Procedures of the determination of the basic parameters of receivers.

The conversion factor of receivers (volt-watt sensitivity) it is

expedient to determine during the sinusoidal-modulated emission/radiation, expressing output and input signals in effective values. This is connected with convenience in the use of standard equipment and exit dial instrument whose scale is calibrated in effective values. The second reason is connected with the very principle of the measurements in question. If is known volt-watt sensitivity of TPI on the sinusoidal-modulated emission/radiation, then, by using Fourier transform in the examination of receiver as linear system, it is possible to calculate the response (reaction) of receiver to the arbitrarily modulated or pulse radiant flux.

The amount of incident on bolometer radiation power is computed according to the Stefan-Boltzmann formula and is multiplied by modulation factor g :

$$W = g \frac{\sigma_C}{\pi} \cdot \frac{A_0 A_1}{l_0^2} (T_1^4 - \epsilon_0 T_0^4), \quad (7.49)$$

where A_0 is an area of the receiving area/site of bolometer; A_1 - the area of the radiating aperture of blackbody; l_0 - the distance between the blackbody and the receiver being investigated; T_0 is absolute temperature of modulator; ϵ_0 - the absorptivity of modulator; T - the temperature of blackbody.

Distance from black body to receiver is selected more than 20 cm, in order to ensure sufficiently precise calculation according to

formula (7.49). If we the radiant flux modulate by rectangular emission impulses at the narrow-band measuring circuit, adjusted to the fundamental harmonic, the amount of the falling/incident to receiver radiation power is determined by the effective value of the fundamental harmonic of radiant flux, decomposed in Fourier series. Modulation factor $g = \frac{\sqrt{2}}{\pi}$.

One should consider that at the temperature of emitter 400°K appear the smaller errors due to radiation absorption by the water vapors and carbonic acid, than at temperature of 600°K.

Page 210.

But at the higher temperature of blackbody descend errors due to the inaccurate determination of absorptivity ϵ_0 and of the temperature of modulator.

The RMS value of noise $\sqrt{\epsilon^2}$. The measurement of this parameter represents one of complex problems both in instrument and in systematic relation [9, 26, 33, 42]. For the measurement of weak fluctuations it is necessary to enforce them and to detect. In radio engineering this problem is solved with the use of the low-noise linear amplifiers and square law detectors with measuring meter [4]. Convenience in the use of a square law detector consists in the fact

that the noises, generated from different sources, are statistically independent and store/add up quadratically. Square law detector it makes it possible by their easy to divide simple subtraction.

However, the requirements for the squareness of detector and even linearity of amplifier are optional. Is compulsory only that that output meter was calibrated in the units of noise, and it is also desirable that the calibration curve will be simple analytic function. Square law detectors are capricious in work, for example thermocouple and thermistors [36]. Therefore frequently are applied linear detectors.

The requirements for the linearity of amplifier are sufficiently rigid. In this case one should consider that checking linearity must conduct oversized, since the peak value of noise approximately 5 times exceeds the amplitude value of the sine voltage, which has the same RMS value.

The inherent noise of preamplifier - the noises of glimmer, shot noise, the noises of redistribution and microphonic noiser must be brought to the minimum. To the question of the investigation of lamps in infralow-frequency and low-frequency ranges is dedicated a series [4, 5, 10, 11, 12, 30, 37, 41, 46].

Fundamental question is the selection of the passband of measuring device and averaging time of detector. The relative error of the single measurement of the intensity of noise, caused by its statistical properties, is determined for a linear detector by expression [4]

$$(2\Delta f_{\text{э.ш}}t)^{-0.5}, \quad (7.50)$$

where $\Delta f_{\text{э.ш}}$ - the equivalent noise passband of amplifier; t is time constant of measuring device.

During the measurement of spectral noise density (dependence of receiver noise on frequency) the width of transmission $\Delta f_{\text{э.ш}}$ one should select so that within its limits spectral noise density would remain constant. The determination of the equivalent noise passband of frequency analyzer conducts with the aid of audiofrequency oscillator.

Page 211.

One should remember that value $\Delta f_{\text{э.ш}}$ is connected with factor of amplification K_{yc} by the following relationship/ratio:

$$\Delta f_{s.m} = \frac{\int_0^{\infty} K_{yc}^2(f) df}{K_{yc}^2 \max}, \quad (7.51)$$

where $K_{yc} \max$ - the maximum value of the factor of amplification of analyzer.

The virtually equivalent noise bandwidth is determined as follows. Is remove/taken dependence $K_{yc} = K_{yc}'(f)$. Then in curve is selected a series of the ordinates, which are raised into square for plotting dependence $K_{yc}^2 = K_{yc}'^2(f)$. Area under the last/latter curve graphically is integrated and is led to rectangle with the height/altitude, equal to $K_{yc}^2 \max$. The second side of rectangle will be $\Delta f_{s.m}$.

Between the equivalent noise passband of analyzer and the passband of analyzer $\Delta f_{0.7}$, during the use resonance of the adjusted T-filter there communication/connection

$$\Delta f_{s.m} = \frac{\pi}{2} \Delta f_{0.7}. \quad (7.52)$$

It is necessary to still consider that during the use of an analyzer with linear detector and during the measurement of the noise, which is subordinated to normal distribution (Gaussian noise), the output

value of noise one should multiply by factor 1.13.

The output meter of analyzer can be directly calibrated in the values of equivalent noise resistance R_{eq} . The latter makes it possible to calculate noise according to Nyquist's formula

$$\bar{e}^2 = 4KTR_{eq}\Delta f_{n.m.} \quad (7.53)$$

For calibration one should select the wire-wounds resistor whose noise purely Johnson and does not depend on the passage of current. This calibration method is convenient in work with the phase discriminator, which has narrow passband ($\Delta f_{n.m.} = 1$ Hz), when it is experimentally difficult it to measure.

Threshold of response of receiver. This value, knowing volt-watt sensitivities and the RMS value of noise, we find by simple indexing:

$$\mathcal{P} = \bar{e}^2/S. \quad (7.54)$$

The more reliable and more precise measurements of value \mathcal{P} can be obtained, by determining signal-to-noise ratio with the assigned radiation flux W . Then

$$\mathcal{P} = W / \frac{\text{Signal}}{\text{noise}} \quad (7.55)$$

In this case is eliminated the heterochronism of the measurements of values $\sqrt{\bar{e}^2}$ and S , and also the determination of these values by different output meters.

Page 212.

For determining threshold of response \mathcal{P} from equation (7.55) it is convenient to use the recording potentiometer EFP-09. Irradiating the receiver being investigated by the known flux W , we determine according to the scale of automatic recorder in relative units the value of signal. Then emission/radiation from source overlaps, the amplification of measuring circuit increases in m once and on the scale of automatic recorder is record/written during several minutes noise path/track. The value of the RMS value of receiver noise is calculated graphically also in relative units and is led to band in 1 Hz.

One should rate/estimate errors during the determination of the luminous sensitivity threshold of a receptor - its basic parameter.

The luminous sensitivity threshold of a receptor taking into account expression (7.49) takes the form

$$\mathcal{P} = \frac{V^2}{\pi^2} \sigma_c \frac{\sqrt{\bar{\epsilon}_1^2 - \bar{\epsilon}_2^2}}{K_{yc}} \cdot \frac{K'_{yc}}{V} \cdot \frac{A_0 A_i}{L_0^2} (T_1^4 - \epsilon_0 T_0^4), \quad (7.56)$$

where $\bar{\epsilon}_1^2$ - the mean square of receiver noise and measuring device;
 $\bar{\epsilon}_2^2$ - the mean square of the noises of measuring device; V - the value of signal at the output/yield of measuring device; K'_{yc} and K_{yc} are factors of amplification of measuring device during the determination

of volt-watt sensitivity and during the determination of noise level.

Then the relative error in determination of threshold of response can be found by the formula

$$\begin{aligned} \frac{\Delta \mathcal{P}}{\mathcal{P}} = & \frac{\Delta V \sqrt{\epsilon_1^2} \cdot V \sqrt{\epsilon_2^2} + \Delta V \sqrt{\epsilon_2^2} \cdot V \sqrt{\epsilon_1^2}}{\epsilon_1^2 + \epsilon_2^2} + \frac{\Delta K_{yc}}{K_{yc}} + \frac{\Delta K_{yc}}{K_{yc}} + \frac{\Delta V}{V} + \\ & + \frac{\Delta A_0}{A_0} + \frac{\Delta A_1}{A_1} + \frac{2\Delta l_0}{l_0} + \frac{4T_1^3 \Delta T}{T_1^4 - \epsilon_0 T_0^4} + \frac{4\epsilon_0 T_0^3 \Delta T}{T_1^4 - \epsilon_0 T_0^4}. \quad (7.57) \end{aligned}$$

The relative error of the single measurement of the intensity of noise, caused by its statistical properties, is determined by expression (see (7.50))

$$\frac{\Delta V \sqrt{\epsilon_1^2}}{V \sqrt{\epsilon_1^2}} = \frac{\Delta V \sqrt{\epsilon_2^2}}{V \sqrt{\epsilon_2^2}} = (2\Delta f_{s.m} t)^{0.5}. \quad (7.58)$$

If equivalent noise bandwidth of measuring device $\Delta f_{s.m} = 2$ Hz, and its time constant $t = 50$ s, then error according to formula (7.57) composes 40%. Let us assume that $T_1 = 550^\circ\text{K}$, $T_0 = 300^\circ\text{K}$, $A_0 = (2 \times 0.3) \cdot 10^{-2} \text{ cm}^2$, $A_1 = (0.9 \times 0.45) \text{ cm}^2$, $l_0 = 20 \text{ cm}$, $V = 35.2 \text{ mV}$.

With errors of measurement: $\Delta T = 1^\circ\text{C}$, $l_0 = 0.2 \text{ cm.}$, $\Delta V = 0.5 \text{ mV}$; the linear dimensions of radiating aperture and receiving area/site 0.001 cm. , and also with the relative error in determination the factors of amplification K'_{yc} and $K_{yc} \pm 40\%$ general error in the determination of the luminous sensitivity threshold of a receptor

$$\frac{\Delta \bar{P}}{\bar{P}} = 6\% + 4\% + 4\% + 1.5\% + 2\% + 5\% + 0.41\% + 0.01\% \approx \\ \approx 23\%$$

If we moreover consider the error, which appears as a result of the fact that the axis of the model of the blackbody not strictly perpendicular to receiving area/site and does not pass through its center, or errors due to radiation absorption by the water vapors and carbon dioxide, then relative error will comprise $\pm (30-35) \%$.

The maximum errors appear as a result of the measurement of noises and size/dimensions of receiving area/site.

Amplitude-frequency receiver response. The measurement of these characteristics conducts during the sinusoidal-modulated emission/radiation from standard source by different modulation frequencies [2]. The obtained dependences are conveniently constructed on dual logarithmic scale. By formulas (1.10) and (1.11) it is possible to find phenomenological time constant.

The phase-frequency receiver response is determined by the value of phase angle $\phi = \phi(\omega)$. Phase angle ϕ is measured between the signal, taken from photo detector, the being inertia-free receiver, and the signal, which appears in the receiver being investigated during irradiation. To account for errors due to the nonuniformity of the phase-frequency characteristic of preamplifier is recommended the measurement of single angle ϕ_2 between the voltage/stress, taken from photo detector, and the voltage, taken from the divider/denominator of photo detector and intensified themes by preamplifier. With this

$$\varphi = \varphi_1 - \varphi_2 \quad (7.59)$$

where φ_1 - the angle between the voltage of photo detector and the signal of receiver, intensified themes the preamplifier. From relationship/ratio $\varphi = \arctg \omega r(\omega)$ it is possible to find the factor of inertness $r(\omega)$.

Spectral receiver response. For this is necessary the specimen receiver, which possesses uniform spectral characteristic. As the recommended receiver for absolute measurements can be used the developed in IF AS UkSSR pyroelectric receiver, sensing element of which is blackbody.

Zonal receiver sensitivity is measured by analogously volt-watt.

The developed in IF AS UkSSR setting for determining zonal sensitivity is assembled on stereomicroscope and has a diameter of light probe 20-100 μ .

The value of the receiving area/site, utilized in formulas for determining the basic parameters, is measured by usual optical methods.

Page 214.

The range of the linearity of the amplitude characteristic L of radiation detector can be determined, by using standard emitter with the set of attenuators.

Estimate of the magnitude L for pyroelectric receivers and ferroelectric bolometers can be conducted, by knowing temperature dependence of pyroelectric coefficient γ and of dielectric constants in formulas (4.81) and (6.19).

Bibliography

1. Акопян Н. Г.— ПТЭ, 1959, 1, 157.
2. Бородин В. З., Гах С. Г., Крамаров О. П., Кременчугский Л. С., Ливанская Л. П., Мальнев А. Ф.— Электронная техника (материал), 1967, сер. 14, в. 8, 141.
3. Бородин В. З., Берберова Л. М., Гах С. Г., Крамаров О. П., Кременчугский Л. С., Мальнев А. Ф.— Изв. АН СССР, сер. физ., 1967, 31, 1818.
4. Вандер Зил А. Флуктуации в радиотехнике и физике. Госэнергоиздат, М.— Л., 1958.
5. Войшвилло Г. В., Давыдов В. С.— ПТЭ, 1958, 6, 82.
6. Гаврилова Н. Д.— Кристаллография, 1965, 10, 3, 346.
7. Гаврилова Н. Д., Новик В. К.— ПТЭ, 1964, 3, 186.
8. Гладкий В. В., Желудев И. С.— Кристаллография, 1965, 10, 1, 63.
9. Давыдов В. С., Пустовойт В. Г.— ЖПС, 1968, 8, 4, 619.
10. Дианов-Клоков В. И., Палицына И. А., Стаховский А. Д.— ПТЭ, 1963, 6, 89.
11. Есельсон М. П., Кременчугский Л. С., Мальнев А. Ф.— УФЖ, 1962, 7, 1, 46.
12. Жестковский В. М., Чеканников Б. А.— ПТЭ, 1968, 3, 228.
13. Казарновский Д. М. Сегнетоэлектрические конденсаторы. Госэнергоиздат, М.— Л., 1956.
14. Карслон П., Егер Д. Теплопроводность твердых тел. «Наука», М., 1964.
15. Кременчугский Л. С., Мальнев А. Ф., Самойлов В. Б.— УФЖ, 1963, 7, 7, 762.
16. Кладкевич М. Д., Кременчугский Л. С.— УФЖ, 1968, 13, 4, 629.
17. Кременчугский Л. С., Самойлов В. Б.— УФЖ, 1968, 13, 2, 215.
18. Кременчугский Л. С.— Оптико-механическая промышленность, 1966, 10, 17.
19. Кременчугский Л. С., Самойлов В. Б.— Кристаллография, 1967, 12, 6, 1077.
20. Корнфельд М. И.— ЖТФ, 1960, 30, 1137.
21. Кременчугский Л. С., Мальнев А. Ф.— ПТЭ, 1963, 5, 182.
22. Кременчугский Л. С., Лысенко В. С., Мальнев А. Ф., Ройцина О. В.— Изв. физ. журнал, 1964, 7, 2, 3.
23. Кременчугский Л. С.— Оптико-механическая промышленность, 1966, 10, 17.
24. Кладкевич М. Д., Кременчугский Л. С.— УФЖ, 1969, 14, 5, 814.
25. Лукьянчикова Н. Б., Гарбар Н. П.— ПТЭ, 1966, 2, 178.

Page 215.

Bibliography continued.

26. Лихтер Л. Н., Прокуменщиков С. М., Соболев Л. П.— ПТЭ, 1961, 1, 96.
27. Мальнев А. Ф., Кременчугский Л. С.— УФЖ, 1959, 4, 4, 522.
28. Мальнев А. Ф., Кременчугский Л. С.— Измерительная техника, 1961, 6, 26.
29. Марков М. Н.— ПТЭ, 1956, 3, 70.
30. Малахов А. Н.— ПТЭ, 1958, 1, 74.
31. Мирлин Д. Н.— Полупроводники в науке и технике, 1958, 2, 516.
32. Марков М. Н.— Оптика и спектроскопия, 1957, 3, 2, 158.
33. Потапов А. В., Чекалов В. В., Чернявский А. Ф.— ПТЭ, 1968, 5, 7.
34. Ройцина О. В., Кременчугский Л. С., Мальнев А. Ф.— Оптико-механическая промышленность, 1965, 12, 9.
35. Сильвестрова И. М., Сильвестров Ю. Н.— Кристаллография, 1958, 3, 1, 57.
36. Тихонов В. И.— ЖТФ, 1960, 30, 1137.
37. Чикин Л. И.— Изв. вузов. Радиофизика, 1960, 3, 3, 419.
38. Экспресс-информация, КИТ, 1958, в. 48, 186.
39. Askermann W.— Ann. Phys., 1915, 46, 217.
40. Brandshaw P. R.— Electr. Industr., 1963, 22, 10, 82.
41. Brower R.— Electronics, 1955, 26, 11, 1076.
42. Brower R.— Electronics, 1968, 41, 14, 3.
43. Chynoweth A. G.— J. Appl. Phys., 1956, 27, 1, 78.
44. Cooper J.— Rev. Scient. Instrum., 1962, 33, 1, 92.
45. De Vos J. C.— Physica, 1951, 20, 10, 669.
46. Firlie T. E.— Rev. Scient. Instrum., 1956, 27, 3, 140.
47. Hans H. A.— J. Appl. Phys., 1961, 32, 3, 493.
48. Kramer L.— Expt. Techn. Phys., 1962, 10, 3, 207.
49. Krajewski T.— Acta Phys. Polon., 1966, 30, 6, 1015.
50. Lang S. B., Steckle F.— Rev. Scient. Instrum., 1965, 36, 7, 929.
51. Rev. Scient. Instrum., 1961, 32, 2, 127.
52. Sinka J. K.— J. Scient. Instrum., 1965, 42, 9, 696.

Page 216.

Chapter VIII.

LIMITED APPLICATIONS OF FERROELECTRIC THERMAL RADIATION DETECTORS.

§1. Pyroelectric SHF receivers.

One of the first application/uses of pyroelectric radiation detectors is their use for recording the power SHF centimeter, millimetric and submillimeter ranges [3, 17, 20, 38, 41, 42, 44].

Special effectiveness in the use of pyroelectric receivers in comparison with other receivers SHF one should expect in the submillimeter wavelength range in the quasi-optical lines of the transmission, when receivers must be equally sensitive to the electromagnetic radiation of different wavelengths. The latter is reached during the use of sensing elements of receivers with the size/dimensions of receiving area/site, which exceed the wavelengths of different modes of vibration, spread in waveguide.

White and Vider [44] utilized the crystals of the y-section/shear of TGS with the size/dimensions of the receiving area/site $A_0 = 4.8 \text{ mm}^2$ and thickness $d = 0.4 \text{ mm}$ as radiation detector in centimeter band. Receiver sensitivity composed 1.6 V/W during load resistance $R_n = 10^9 \text{ ohm}$. The range of linearity was retained up to power 1.2 W .

Shteyer and Yumashita [38] developed the detector of millimeter and submillimeter waves on the basis of single crystals of TGS and BaTiO_3 with the size/dimensions of sensor $(2 \times 2 \times 0.5) \text{ mm}^3$. During measurements at wavelengths 8.15 and 4.10 mm the threshold of response comprised for TGS-receivers $8 \cdot 10^{-7} \text{ W/Hz}^{1/2}$ and for BaTiO_3 -receivers $8.7 \cdot 10^{-6} \text{ W/Hz}^{1/2}$ with the value of load resistance R_n to $2 \text{ M}\Omega$.

The use of pyroactive crystals of TGS, BaTiO_3 , and its derivatives for the detection of electromagnetic radiation in wide spectral range from microwave range to the visible region of the spectrum was made by Stanford [39]. The best threshold of response - $(1.5-2) \cdot 10^{-9} \text{ W/Hz}^{1/2}$ - at frequencies of modulation to 100 Hz possessed receivers on the basis of crystals of TGS with the size/dimensions of sensor $A_0 = 3.15 \text{ mm}^2$ and $d = 50.8 \text{ }\mu$.

Page 217.

Time constants did not exceed 50 μ s and the range of linearity it composed 10%.

Eldey, Iveret and White [17] reported the development of pyroelectric receiver with sensing element from the cryst 1 of TGS, working at wavelengths 4 and 12.5 mm. The time constant of device was 2 μ s. They utilized a preamplifier with high input impedance and a differentiator amplifier for the equalization of the total frequency characteristic. Although they did not succeed in achieving the maximum sensitivity, they all the same could determine peak pulse power 10^{-5} W for duration 10^{-5} s with the front of growth/build-up and drop 40 ns, in signal-to-noise ratio equal to 1 dB.

The first Soviet report/communication about the development of pyroelectric receiver for the detection of the SHF-emission/radiation of millimetric range ((0.8-10) mm) both in the waveguides and in free space was made into 1966 [3]. As sensing elements were utilized the specimen/samples of single crystals of TGS and of ceramic BaTiO_3 . The irradiated electrode had the assigned skin drag for the optimum absorption of electromagnetic radiation.

The dependences of the output signal of pyroelectric receiver and thermistor knob/cap of the type M5-24 on the amplitude of the supplied power are represented in Fig. 8.1. Curve 2 is taken during the use of a source by power of order (1-2) W at modulation frequency 50 Hz, and curves 1 and 3 are taken at source power 10 mW at modulation frequency 20 Hz. From figure is visible a good linearity of the amplitude characteristic of pyroelectric receiver, whereupon the range of rated power considerably greater of pyroelectric receiver, than of thermistor knob/cap (with a weakening less than 20 dB, thermistor knob/cap it goes out of order).

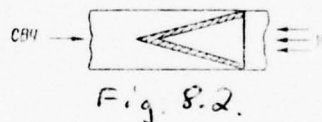
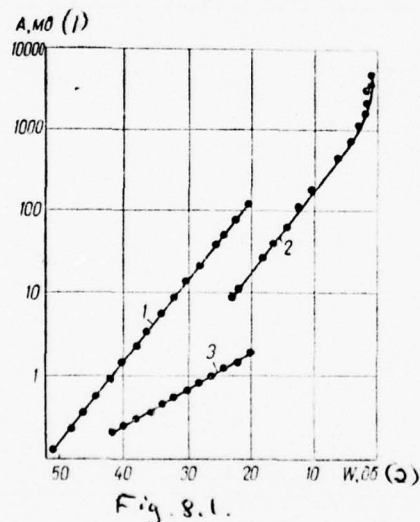


Fig. 8.1. Dependence of the output signal of pyroelectric receiver (curves 1 and 2) and of the thermistor knob/cap M5-24 (curve 3) on the value of the amplitude of power SHF.

Key: (1). mV. (2). dB.

Fig. 8.2. Pyroelectric radiation detector, which works on the principle of the comparison with a power SHF with radiated power of optical range (W).

Page 218.

The results of the comparison of these characteristics indicate the prospect of the development of the highly sensitive output meters of microwave range with the use of pyroelectric receivers, comparatively simple by construction and in operation, more resistant to overloads in comparison with thermistor and metallic bolometers.

Threshold of response for a receiver on the basis of crystals of TGS is not worse than $10^{-3} \text{ W/Hz}^{1/2}$ with the volt-watt sensitivity of 200 V/W at modulation frequency 20 Hz.

The pyroelectric receiver, which makes it possible to compare the intensity SHF with radiated power of the optical range, in which the calibration of receivers conducts by comparatively simple methods, is given in Fig. 8.2. The outer side of pyroactive cone or wedge is the matched load for radiation absorption SHF-, and internal is blackbody for visible or infrared radiation. Measurement can be carried out by zero or phase-meter method.

sensitivity of microcalorimeters is low.

In connection with this the development of the new instruments, which make it possible to determine the energy and time characteristics of laser emission/radiation in wide spectral interval, is actual/urgent.

as one of such instruments, which do not require cooling, can serve pyroelectric radiation detector. The high-speed absolute meter of the short-term momentum/impulse/pulses of flashbulbs and laser emission/radiation on the basis of pyroelectric receiver was developed in the institute of physics of AS UkSSR [6, 8].

Page 219.

The distinctive special feature/peculiarity of the developed device is the use in it of a pyroelectric radiation detector with sensing element in the form of the spherical blackbody whose characteristics were described in chapter V.

The block diagram of setting is given in Fig. 8.3. In the instrument is provided of two operating modes - pulse and continuous. During recording pulse emission/radiation the preamplifier is connected to wideband amplifier with output/yield to oscillograph

CI-29 (OK-17) and peak voltmeter V4-3. In continuous operation vibration modulator is establish/installed next to laser, and preamplifier is changed over to narrow-band amplifier with synchronous detector. The latter has a output/yield to an automatic recorder of the type EPP-09 or dial instrument.

The value of load resistance R_n also changes depending on the operating mode. In pulsed operation for determining time structure of laser pulse the value of resistance R_n is selected by such that would be satisfied condition $R_n C_0 < \tau$ (where C_0 is general input capacitance of receiver and lamp, a τ is its own time constant of receiver). The capacitance/capacity of the spherical pyro electric receiver, prepared from ceramics BaTiO_3 , is approximately 1000 pF. In order that the time constant of input circuit would be less than $5 \cdot 10^{-6}$ s, load resistance R_n must be less than 5 anyone. As shown in chapter IV, the threshold of response of pyroelectric receiver deteriorates with decrease R_n ($\mathcal{P} \sim R_n^{-0.5}$). Therefore for the preservation/retention/maintaining of the high sensitivity of device during the measurement of the time structure of momentum/impulse/pulse it is possible to utilize a receiver from TGS with the size/dimensions of whose receiving area/site is 1-2 mm² and whose self-capacitance is 5-10 pF.

For determining energy of momentum/impulse/pulse is selected the

mode/conditions of integration, in this case $R_n C_0 \gg t_n$ (where t_n - the pulse duration). If $R_n = 100 \text{ M}\Omega$, the time constant of input circuit during the use of a spherical receiver is equal to 0.1 s. This time is greater than the duration of the virtually observed momentum/impulse/pulses of laser emission/radiation.

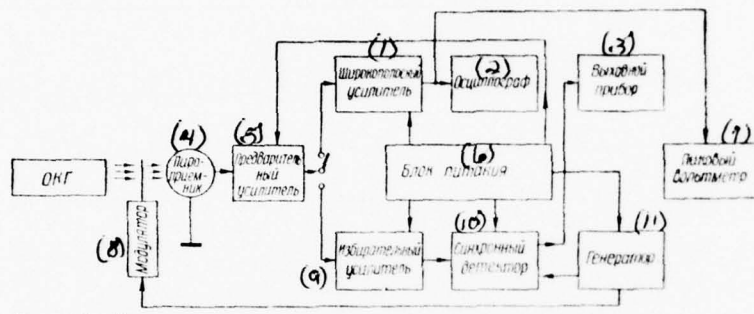


Fig. 8.3. Block diagram of setting for the measurement of laser emission/radiation.

Key: (1). Wideband amplifier. (2). Oscillograph. (3). output instrument. (4). pyroreceiver. (5). Preliminary amplifier. (6). Block/module/unit of power. (7). Peak voltmeter. (8). Modulator. (9). Selective amplifier. (10). Synchronous detector. (11). Generator.

Page 220.

In the mode/conditions of the integration, when its own time constant

of receiver is lower than the pulse duration, the peak value of output pulse proportional to energy of momentum/impulse/pulse. In addition to this, by observing momentum/impulse/pulse on oscilloscope face, it is possible by the duration of its front to determine the total duration of laser emission/radiation.

In work in continuous duty is connected the load $R_n = 100 \text{ M}\Omega$ for obtaining the high sensitivity of device.

The calibration of the device, which works in continuous duty, is carried out from blackbody. In this case the threshold of response at modulation frequency 10 Hz composes $10^{-7} \text{ W/Hz}^{1/2}$ with a receiver from BaTiO_3 of the spherical type and $5 \cdot 10^{-9} \text{ W/Hz}^{1/2}$ by receiver from IGS.

For calibrating device in pulsed operation it is possible to utilize an incandescent lamp and a gate of camera.

According to the volt-watt sensitivity of pyroelectric receiver, determined with the sinusoidally modulated radiant flux from blackbody, is measured the radiant flux from incandescent lamp at the open gate of camera and the same modulation frequency. On known time of exposure, which is monitored by oscillograph CI-29, and to the output signal of peak voltmeter it is possible to determine the pulse

volt sensitivity of device. For a spherical receiver whose diameter is 8 mm, the of whose wall thicknesses are 0.2 mm by the radius of whose inlet is 0.5 mm, prepared from ceramics BaTiO_3 , pulse volt sensitivity composes 15.2 V/J. This value considerably exceeds the sensitivity of known laser microcalorimeters.

Meter retains the linearity of the amplitude characteristic up to of radiant fluxes 10 W/mm².

Analogous results can be obtained, by utilizing conical or tapered pyroelectric receivers. Although the emissivity of the latter somewhat lower than of spherical, they possess larger voltage sensitivity with the same value of inlet.

With large radiant fluxes (energies of momentum/impulse/pulse) is disrupted the linearity of the amplitude characteristic of meter both because of the displacement of operating point into the range of the powerful temperature dependence of pyroelectric coefficient and as a result of the failure of the irradiated electrode. By decreasing the radiant density with the aid of the scattering cell/elements and by increasing the working surface of pyroelectric receiver, it is possible to expand dynamic range to 10 - 100 J. In this case the material of sensing element of receiver it is desirable to select with higher Curie point, for example ceramics of titanate of

zirconate of lead.

Figure 8.4 gives the dependence of the output signal, taken from receiver with the diameter of sphere 30 mm, a radius of inlet $R_0 = 6$ mm wall thickness $d = 0.8$ mm. The linearity of amplitude characteristic is retained up to the maximum energies of the "pumping" of laser or pulse energy of emission/radiation is 3.5 J.

Page 221.

The main disadvantage in longitudinal type pyroelectric receivers (with the irradiated electrode) is insufficiently fast time constant ($\tau = 10^{-5} - 10^{-6}$ s). This limits the time/temporary resolution of meter, making it possible to measure the momentum/impulse/pulses only in the mode of "free generation" (by duration more than 10 μ s).

For the measurement of shorter laser pulses (mode/conditions with "q-switching") were used conical- and tapered end type pyroelectric receivers, described in chapter V. The linearity of amplitude characteristic during the use of 15-degree cone shaped pyroelectric receivers with inlet 8 mm in diameter was retained up to energies 1.5 J. Figure 8.5 gives the oscillogram of emission impulse by duration to 20 ns, written in the mode of the measurement of energy. For a comparison is given to the right this same

value of receiving area/site was 15 mm².

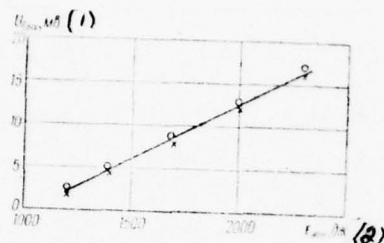


Fig. 8.4. Dependence of the output signal of spherical pyroelectric receiver U_{max} on energy of the "pumping" of ruby laser E_{ruby} : \times and \circ measuring point, conducted into different days.

Key: (1) - mV. (2) - J.

Page 222.

In work in continuous duty the calibration conducted at modulation frequency 104 Hz, and in pulse - with the aid of camera shutter.

In work [30] is described the pyroelectric detector, utilized for research on the generation of CO₂-laser, ch-maser ($\lambda = 337 \mu$) and

laser emission/radiation on water vapors ($\lambda = 28 \mu$). The pyroelectric receiver, assembled on the basis of the plate of sulfate of lithium whose diameter is 7 mm whose thickness is 50μ , was placed in immediate proximity of the solid-body operational amplifier, leveling its frequency characteristic in the range from 20 Hz to 2 MHz. The time constant of this system was 100 ns, volt-watt sensitivity is 3 V/W. The noise level in the frequency band in question did not exceed 15 mV. The measured by pyroelectric receiver momentum/impulse/pulse of CO₂-laser by duration 1 μ s was compared with the measurement, carried out with the aid of the cooled to 77°K detector on the basis of germanium, alloyed Zn and Sn. The operating speed of pyroelectric receiver with solid-body amplifier was insufficient for the reproduction of leading impulse front.

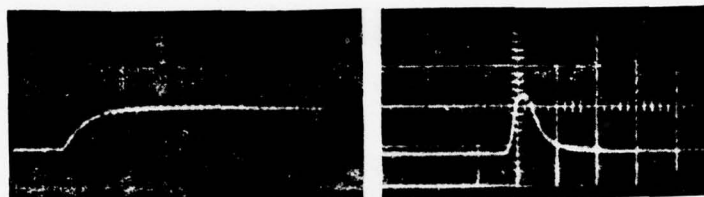


Fig. 8.5. Oscillogram of the momentum/impulse/pulse of ruby laser by duration 20 ns: to the left - written with the aid of transverse type cone-shaped pyroelectric receiver in the mode of the measurement of energy; to the right - with the aid of the photoreceiver FEK-09.

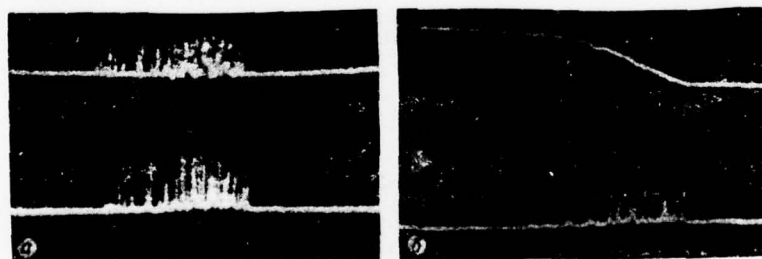


Fig. 8.6. Oscillograms of the mode of the "free generation" of ruby

laser ($t_m = 250$ ns): a) written with the aid of transverse type pyroelectric receiver in mode/conditions $R_{th}C \ll \tau$ (above) and the photoelectric receiver F-5 (below); b) with the aid of transverse type pyroelectric receiver in mode/conditions $R_{th}C \gg t_m$ (above) and by the photoreceiver F-5 (below).

Page 223.

The proposed by the authors construction of receiver was free from piezoelectric resonance in operating range. The designed the lowest resonance frequency was 100 MHz. However, at frequency 20 kHz were observed small oscillations.

Glass [29] utilized as sensing element of receiver crystals SBN ($Sr_{1-x}Ba_xNb_2O_6$),

Λ possessing the large value of the pyroelectric coefficient at values of $0.25 < x < 0.5$ in the range of room temperatures. With the size/dimensions of the receiver: $A_0 = 5$ mm² and $d = 100$ μ low-frequency volt-watt sensitivity composed 10^4 V/W with threshold of response $\dot{P} = 4 \cdot 10^{-9}$ W/Hz^{1/2}cm. The author recorded momentum/impulse/pulses by duration 25-30 ns from the CO₂-laser, when the time constant of input circuit was less than 10^{-8} s. The time constant of pyroelectric receiver was determined with the aid of detector on the basis of the germanium, alloyed by copper and working

at 4°K.

To the use of pyroelectric receivers for the measurement of laser emission/radiation are dedicated also [2, 13, 28, 3, 34].

§3. Other application/uses of pyroactive crystals.

The use of pyroelectric crystals for the creation of the image converters of television type was suggested by Khadni, etc. [27]. The investigations of the zonal sensitivity of pyroelectric targets and their resolution [7], determined with the aid of light probes, indicate long-range for the creation of the image converters of nonscanning type.

Estgeymer and Schwarz [16] utilized a pyroelectric receiver in thermal image converter with optical-mechanical scanning. The developed by the authors infrared thermograph with the field of view $10 \times 10^\circ$ and with angular resolution 0.1° with 10000 cell/elements, which possess temperature resolution 0.2°C , record/writes thermogram in 30 s.

The taken from pyroelectric sensing transducer is supplied to

the modulator of auxiliary ray/beam, the latter is synchronized by the single system of scanning and is projected to photographic film. They are utilized two methods of modulation of auxiliary ray/beam. In the first method conducts direct modulation of the intensity of the glow-discharge tube, which leads to the appearance of a white-black image on photographic film. In other, more advanced, method is utilized the source of the fixed/recorded intensity, which projects on the mirror of galvanometer the image of light filter. During the rotation of the mirror of the galvanometer, controlled from the signal of pyroelectric receiver, through exit slit is focused the emission/radiation of the determined color, which then falls on colored photographic film. Is establish/installated the one-to-one correspondence between the temperature of the determined section of object and the color of the corresponding section of image.

Page 224.

This instrument was used for relieving the temperature map/charts of objects, which are located at the temperature lower than red heat ($T < 700^\circ\text{K}$), in particular for the analysis of the structures, having active thermal radiation sources (electronic circuits and node/units), rubbing parts, volumes with those which pass in them exo- and endothermal reactions, and also for the analysis of the passive structures, requiring supplemental heat or

cooling.

Among other uses of pyroelectric receivers one should note their application/use of as detectors of the beams of rapid atoms [18], for purposes of the dosimetry of ultraviolet radiation [37], for recording heat fluxes [26], in particular for research on the characteristics of wood [36], for the measurement of complete thermal emission/radiation in astronautics [14].

The use of pyroelectric crystals for the creation of highly sensitive temperature sensors [32, 33] offers the possibility of recording temperature changes from 10^{-7} to 10^{-8}°C with volt-degree sensitivity 20 V/deg. If one considers that the sensitivity of Sb-Bi-thermocouples is approximately 300 $\mu\text{V}/\text{deg}$, then pyroelectric thermometers more sensitive than 10^5 times. The connection of pyroelectric crystal with Mos transistor open/discloses the possibilities of designing of miniature supersensitive temperature-sensing devices [43].

§4. Comparison of thermal radiation detectors.

The basic requirement, presented to TFI, consists of obtaining

the maximum threshold sensitivity with best possible frequency and spectral characteristics. Sometimes essential is the broad band of the linearity of the amplitude characteristic of TPI. In this case, of course, one should consider the operating temperature of receiver, since cooling TPI is connected with considerable operational difficulties.

Into 1947-1949 Jones indicated the need for the comparison of receivers with the different parameters and formulated the single conditions of comparison [21-25]. By him it was suggested to determine the value of the RMS value of noise $\sqrt{\epsilon^2}$ by the amplifier, frequency characteristic of which corresponds to the frequency characteristic of the receiver being investigated, and volt-watt sensitivity at the zero frequency S_0 . Then the threshold of response under conditions of comparison A is determined by the constant value of the falling/incident radiation, which causes in sensin transducer, equal to the RMS value of the noise:

$$\mathcal{P} = \frac{\sqrt{\epsilon^2}}{S_0} |em / 2u^{0.5}|. \quad (8.1)$$

Page 225.

If we assume the equivalence of all sections of sensor in the creation of signal and noise, then, as showed Jones, threshold of

response H_m under conditions of comparison B inversely proportional to square root of the value of the receiving area/site A_0 :

$$H_m = \frac{\mathcal{P}}{A_0^{0.5}} \{ \text{cm} / (\text{cm} \cdot \text{cm})^{0.5} \}. \quad (8.2)$$

Value H_m characterizes the threshold of response, led to receiver with single receiving area/site.

For the comparison of receivers with different time constants and by receiving area/sites is proposed the factor of quality M - the parameter, which does not depend neither on A_0 nor on τ , but having different values for different detectors. Parameter M is conveniently normalized, i.e., to express in unity the qualities of very good receiver. For ideal thermal and acousto-optical (pneumatic) receivers with $T = 300^\circ\text{K}$

$$\mathcal{P} = 2.76 \cdot 10^{-12} \left(\frac{A_0}{\tau} \right)^{0.5}. \quad (8.3)$$

If we accept the factor of quality of this receiver for unity, then is the factor of quality of any receiver of this class

$$M_1 = 2.76 \cdot 10^{-12} \left(\frac{A_0^{0.5}}{\mathcal{P} \tau^{0.5}} \right). \quad (8.4)$$

Carrying out the evaluation of the characteristics of bolometers and thermocouples, Havens it showed (see [5]), that their smallest possible threshold of response

$$\mathcal{P} = 3 \cdot 10^{-12} \left(\frac{A_0^{0.5}}{\tau} \right). \quad (8.5)$$

The factor of quality of this receiver Jones also accepted for

unity. Therefore for any other receiver of this class

$$M_2 = 3 \cdot 10^{-12} \left(\frac{A_0^{0.5}}{P_1} \right). \quad (8.6)$$

The conditions of the comparison of receivers according to Jones are not complete, if receiver noise differ from the thermal and threshold of response complexly depends on the value of receiving area/site. The quality factor is not any universal parameter, which would make it possible to compare receivers not only with the different size/dimensions of receiving area/sites and different time constants, but also different spectral sensitivity, different mechanical strength, the different technological processes of manufacture and the cumulative methods of the taken from sensing transducer.

Factor of quality M not found wide acceptance among developers and the users of receivers. Knowing the factor of quality of receiver and without disposing of other information about receiver, user it could not accurately say: approaches to it this receiver or not.

Page 226.

Into the qualities of an example let us examine two TPI - bolometer and pyroelectric receiver. For a bolometer the threshold of response at frequency 10 Hz with passband 1 Hz is equal to $5 \cdot 10^{-10}$

$W/Hz^{1/2}$ and time constant 10 ms, while for a pyroelectric receiver threshold of response is equal to $5 \cdot 10^{-9} W/Hz^{1/2}$ and time constant 10 μs . Calculation of quality factor for a bolometer gives $M_2 = 0.12$, and for the pyroelectric receiver $M_2 = 0.37$.

By comparing these data, it is possible to draw the conclusion that the pyroelectric receiver three times is better than the bolometer. However, in work on low modulation frequencies for the notation of the slowly changing processes bolometer is better than the pyroelectric receiver, although in high-frequency operation it is inferior to it. Therefore Jones into 1959 [21-25] again returned to threshold sensitivity as to the more convenient criterion of the comparison of receivers. He proposed as the parameter of comparison the standardized/normalized threshold sensitivity \mathcal{D}^* , equal to signal-to-noise ratio to the rate of flow of emission/radiation and led to receiving area/site in 1 cm^2 and to band 1 Hz (comparison under conditions E):

$$\mathcal{D}^* = \mathcal{D}(\lambda_0, \Delta f)^{0.5}. \quad (8.7)$$

In the general case \mathcal{D}^* is the function of many variables:

$$\mathcal{D}^* = \mathcal{D}^*(f, \lambda, T, \tau_d, g).$$

where λ is a wavelength of emission/radiation; f - modulation frequency; T - absolute temperature; τ_d - is time constant; g - the amplification of receiver (parameter, which controls its sensitivity). It is possible to count that parameter g is selected in

such a way that value \mathcal{D}^* would be maximum.

Communication/connection between values M_1 and M_2 and by threshold sensitivity \mathcal{D}^* is record/written in the form

$$\mathcal{D}_{M_1}^* = \left(1,81 \cdot 10^{10} \frac{cM \cdot cM'^{1/2}}{am} \right) M_1; \quad (8.8)$$

$$\mathcal{D}_{M_1}^* = \left(1,67 \cdot 10^{13} \frac{cM}{am} \right) \tau^{0,5} M_2. \quad (8.9)$$

The direct/straight determination of parameters M_1 and M_2 according to Jones is conjugate/combined with considerable experimental difficulties. This is explained themes that the measurement of the RMS value of receiver noise at zero frequency is hinder/hampered by slow changes in the temperature of the medium. But if are known the receiver responses during the modulated emission/radiation, measured by narrow-band diagram, and frequency receiver response is approximated by one time constant, then communication/connection of factor of quality M_2 with the measured threshold of response \mathcal{P}_i it is determined by relationship/ratio [9]

$$M_2 = \frac{3 \cdot 10^{-12} \sqrt{4A_0 \Delta f (1 + 4\pi^2 f^2 \tau^2)}}{\mathcal{P}_i \sqrt{\tau}}. \quad (8.10)$$

Page 227.

For the comparison of the TPI, which operate on a pulsed basis, Jones introduced the standardized/normalized threshold sensitivity on the energy

$$\Delta^* = \Delta A_0^{0.5} \left| \frac{c\eta}{\partial \kappa} \right|. \quad (8.11)$$

Since passband by complex form affects the parameter Δ^* , this value is not led to single band.

For the purpose of the comparison of TPI, whose threshold of response is limited to radiation noise, Jones introduced [25] the factor of the standardized/normalized threshold sensitivity on solid angle (comparison under conditions F):

$$\mathcal{D}^{**} = \mathcal{D} \left(\frac{\Omega}{\pi} \right)^{0.5}, \quad (8.12)$$

where Ω is the effective solid angle, hearth by which sensing element was observable through the aperture in radiation shield.

If receiver possesses circular symmetry and its solid angle can be represented by cone with angle 2θ , that relationship/ratio between values Ω and θ it takes the form

$$\text{Then} \quad \Omega = \pi \sin^2 \theta, \quad (8.13)$$

$$\mathcal{D}^{**} = \mathcal{D}^* \sin \theta. \quad (8.14)$$

Of Lambert receiver $\theta = 90^\circ$ and

$$\mathcal{D}^{**} = \mathcal{D}^*. \quad (8.15)$$

Factor \mathcal{D}^{**} can turn out to be suitable for the comparison not only of the cooled and superconducting receivers, but also for immersion type receivers.

The thermal radiation detector is optical instrument and is intended for obtaining the information about radiation sources. Therefore during the comparison of TPI it is interesting to know, is such their to transmissivity the information about changes in the radiant flux and is which the volume of information, transferred TPI, per the unit of power of incident radiation. For this purpose Jones introduced new characteristic TPI - informational effectiveness [21-25]. This value determines quantity of information in bits, transferred by receiver to one watt of the incident radiation:

$$J^* = \frac{\int_0^\infty \log_2 [1 + w_p(f) |\mathcal{D}^*(f)|^2] df}{\left[\int_0^\infty w_p(f) df \right]^{0.5}}; \quad (8.16)$$

$$w_p(f) = 2 \langle T^{-1} | F(f) |^2 \rangle, \quad (8.17)$$

where $F(f)$ - the component of the expansion of Fourier the rate of flow of emission/radiation $W(t)$. Value $w_p(f)$ represents square $F(f)$, divided into period of T and averaged on ensemble T of similar duration [25].

Page 228.

In two procedurally important cases it is possible to obtain simple expressions for the informational effectiveness:

a) when measurement conduct in the narrow passband of amplifier, then

$$J^* = \mathcal{D}^*(f); \quad (8.18)$$

b) when $\mathcal{D}^*(f) = \text{const}$ in the range of frequencies from 0 to a outside this interval $\mathcal{D}^*(f) = 0$, then

$$J^* = \frac{1}{2} \Delta_m, \quad (8.19)$$

where

$$(\Delta_m)^2 = 4 \int_0^a [\mathcal{D}(f)]^2 df.$$

The given analysis of the criteria of the comparison of the quality of TPI shows that by one parameter it is not possible to describe TPI completely so that user on the basis of these data could foresee the characteristics of the develop/processed optical equipment. However, it is possible to indicate the set of the

fundamental characteristics of thermal radiation detector, necessary for the solution to the question concerning the selection of TPI for the determined target/purposes.

1. Threshold of response (or threshold sensitivity)

$$\mathcal{P} = \mathcal{P}(f, \tau, \Delta f, A_0); \quad \mathcal{D} = \mathcal{D}(f, \tau, \Delta f, A_0). \quad (8.20)$$

2. Conversion factor (volt-watt sensitivity)

$$S = S(f, \lambda, A_0) \text{ and } S(x, y). \quad (8.21)$$

These dependences are contained the frequency, spectral and zonal sensitivities of TPI, and also the dependence of TPI on the size/dimensions of receiving area/site. If the frequency dependence of the volt-watt sensitivity of TPI it is possible to approximate the curve of form (1.9), then time constant τ is sufficient for the description of high-speed/velocity receiver response.

3. Dynamic range L , and also the information about the effect of mechanical, radiation and thermal effects on receiver.

In a number of cases the set of characteristics can be substantially decreased. If noise TPI is Johnson, then it suffices to know values $S = S(f, \lambda)$, τ and $\mathcal{P}(f)$ in order to solve in principle the question concerning the use of this receiver in

spectral and radiometric instrumentation.

§5. Prospects for development and applying thermal radiation detectors.

Thermal radiation detectors find wide application in the technology of the physical experiment and industry.

Page 229.

The infrared spectrometers, radiation detector in which in the majority of cases it is thermal, they became some of the basic analytical instruments, giving information about structure and state of substances and which obtained wide acceptance during physicochemical investigations. Low-temperature radiation pyrometers (thermometers) confidently enter in the minimum of physical instruments, which is necessary for the work of contemporary research laboratory. Infrared spectrometry and radiometry, measurement of laser generation, diagnostics of plasma, research on the generation of microwave range, astrophysical and space investigations, automatic control and direction compose the incomplete enumeration of application/uses of TPI. Table 8.1 gives the comparative

characteristics of bolometers, while Table 8.2 - other thermal radiation detectors.

Creation of highly sensitive and low-inertia TPI - the main direction in their development. In connection with the development of the new methods of spectrometry, in particular interferen e spectrometry of the high resolving power with Fourier transform, special attention is given to the linearity of amplitude and spectral receiver responses. Unlike usual dispersive monochromators in interferometers the radiation detector receives a comparatively wide spectral interval of wavelengths in sufficiently high signal-to-noise ratios. Therefore requirements for the width of the dynamic range of receiver are often are more rigid, than to sensitivity.

By a special feature/peculiarity of TPI in the far-infrared region of the spectrum [4], where the standard sources of noncoherent radiation are weak, and therefore are utilized large mirrors and wide slots, are the considerable size/dimensions of receiving area/site. For this region of the spectrum they are required TPI, the threshold of response of which strongly does not deteriorate with an increase in the size/dimensions of receiving area/site. Promising for these purposes are the pyroelectric radiation detectors along with the acousto-optical and cryogenic bolometers, utilized in long-wave spectrometers.

The creation of intense radiation sources - quantum generators and the SHF generator/oscillators of millimetric and submillimeter ranges assigned the new missions before the developers of receivers. Arose the need for receivers with the high absorption coefficient, capable of measuring the powerful radiant fluxes 10^2-10^6 W/cm² or the energy of momentum/impulse/pulses $10^{-2}-10^2$ J for their duration $10^{-4}-10^{-8}$ s. The utilized for these purposes calorimeters make it possible to measure energy or power of intense radiant fluxes, but the determination of the pulse duration is realized by photoreceivers. In this case the photoreceivers in the distant and middle regions of optical spectrum require cooling. Pyroelectric receivers (among other things receivers of total absorption) make it possible to carry out the simultaneous measurements of energy and duration of laser pulses and can be used for these purposes in wide spectral interval (0.1-1000 μ) without cooling.

Page 230.

Table 8.1.

Тип болометра (1)	A_0 , мм ²	t , °K	R_0 , ом (2)	S , в/см (3)	λ , м (4)	$\lambda_{ср}$, м (5)	$\mathcal{P} \cdot 10^{-10}$, вт/см ² /°K (6)	$\mathcal{D} \cdot 10^8$, см ² /°K·см (7)	Изготовитель (фирма) (8)	Литера- тура к табл. (9)
Висмутовый (сплав Bi с Pb) (10)	2,25	295	260	20	0	18	1	1,5	ФИАН СССР	[35]
То же (11)	1,9×0,4	295	200	15	9	25	1,4	0,62	ЛОМО (БМК-3)	[8]
Никелевый вакуумный (12)	1,9×0,4	295	10	4	9	20	1	0,87	ИФАН УССР	[8]
То же (11)	1	100	5	7	9	25	0,4	0,4	То же (11)	[120]
Никелевый газонаполненный (13)	4×0,55	295	10	0,6	80	5	10	0,15	" "	[120]
Платиновый (14)	7×0,3	295	40	—	—	16	—	0,14	Baird Atomic	[263]
Полупроводниковый (15)	4,34	295	0,7·10 ⁶	76	—	3	20	0,1	БКМ-2	[35]
То же (15)	1	295	0,6·10 ⁶	50	9	10	26	0,038	ИФАН УССР	[8]
Термисторный (16)	—	295	2,5·10 ⁶	—	—	1—10	—	0,16	Barnes Engineering	[263]
Термисторный (иммерсионный) (17)	0,1×0,1	295	4·10 ⁶	3,6·10 ⁴	15	2,3	0,5	0,17	То же (11)	[102]
Угольный (18) (19)	19,3	2,1	1,2·10 ⁵	1,4·10 ⁴	13	10	0,12	37	Bell Telephone Lab. (20)	[117]
Сверхпроводящий (Sn)	3	3,8	1	230	10	10	0,012	140	Колледж королевы Марии (QMC) (21)	[116, 124]
То же (11)	10	3,7	2	760	10	110	0,0026	1200	—	[8]
Германиевый с галлием (22)	15	2	1,2·10 ⁶	4,5·10 ⁶	200	0,4	0,05	800	Texas Instrum.	[128]
То же (11)	10	2	—	—	—	1	0,0003	10 000	То же (11)	[135]
" "	2,3	2,15	1,3·10 ⁶	10 ⁴	200	0,3	0,0045	330	—	[8]

Key: (1). Type of bolometer. (2). ohm. (3). V/W. (4). Hz. (5). ms.
 (6). W/Hz^{1/2}. (7). Hz^{1/2}·cm²/W. (8). Producer (firm). (9). Literature
 to chapter 1. (10). Bismuth (alloy Bi with Pb). (11). The same. (12).
 Nickel vacuum. (13). Nickel gas-filled. (14). Platinum. (15).
 Semiconductor. (16). Thermistor. (17). Thermistor (immersion). (18).
 Carbon. (19). Superconducting. (20). Queen's college. (21). Mary.
 (22). Germanium with gallium.

Page 231.

Table 8.2.

Тип ТПИ (1)	$A, \text{мм}^2$ (2)	$T_{\text{ср}}, \text{К}$ (3)	$R_0, \text{ом}$ (4)	$S, \text{el/cm}$ (5)	$L, \text{мГ}$ (6)	$\tau, \text{мсек}$ (7)	$\beta \cdot 10^{-10}, \frac{\text{вт/см}^2}{\text{м}^2}$ (8)	$D^* \cdot 10^8, \frac{\text{Вт}^{1/2}}{\text{м}^2 \cdot \text{с} \cdot \text{см}}$ (9)	Изготовитель (фирма) (10)	Литера- тура (11)
Пневматический (10)	7,06	295	—	—	10	15	—	3	Unicam Eppley	I[263] I[189]
Неселективный оптико- акустический (11)	4,5 × 2,5	295	—	3 · 10 ⁴	10	20	1	3	ГОИ	I[226]
Термоэлемент биметал- лический (12)	1	295	10	4,4	5	36	0,7	1,4	Ferrant Opt. Compt., Beck- man	I[6]
То же (13)	—	295	150	—	—	40	6,6	0,34	Instrum. Reader Barnes Engene- ring Co	I[185]
„ „	3	295	78	7,1	9	87	1,6	0,34	ЛОМО	I[8]
„ „	3	295	27	3,7	9	58	2	0,27	ЦЕЙСС	I[8]
Термоэлемент полупро- водникового типа (14)	0,4	295	42,9	38,5	5	20—55	0,46	1,4	Hilger, Perkin- Elmer, Reader	I[6] I[172]
То же (15)	0,09	295	36	18	0	40	0,45	0,6	—	I[8]
„ „	1,4	295	10	2,9	9	87	1,4	0,84	ЛОМО	V[70]
Пирозлектрический (15)	400	295	—	—	—	—	40	0,5	—	V[47]
То же (16)	0,25	295	—	10 ⁴	10	—	—	0,5	Barnes Engene- ring Co	V[98] V[16] V[15]
„ „	3	295	—	—	—	0,01	15	0,11	ИФАН УССР	V[16]
„ „	4	295	10 ¹²	2 · 10 ³	10	0,02	20	0,1	То же (17)	V[15]
„ „	1	295	10 ¹²	—	—	0,0001	—	0,05	—	V[26] V[65]
Пирозлектрический (16) «черный»	1,5	295	10 ¹⁰	5	9	0,05	500	0,0025	„ „	—
Термопарный «черный» (17)	3,14	295	—	0,05	1	170	—	—	„ „	—
Пирозлектрический «черный» (поперечно- го типа) (18)	100	295	10 ¹⁶	0,5	10	0,00002	2000	—	„ „	—
Пирозлектрический (19) (координатно-чув- ствительный)	—	—	—	5 · 10 ³	10	0,01	20	—	„ „	—

Key: (1). Type. (2). ohm. (3). V/W. (4). Hz. (5). ms. (6). $W/Hz^{1/2}$.
(7). $Hz^{1/2} \cdot cm/W$. (8). Producer (firm). (9). Literature. (10).
Pneumatic. (11). Nonselective optico acoustic. (12). Thermal element
is composite. (13). The same. (14). Semiconductor type thermal
element. (15). Pyroelectric. (16). Pyroelectric "black". (17).
Thermocouple "black". (18). Pyroelectric "black" (transverse type).
(19). Pyroelectric (coordinate-sensitive).

Page 232.

For the measurement of weak laser emission/radiations are required thermal receivers with high sensitivity, for example cryogenic bolometers or narrow-band photoreceivers. Is promising also the use of pyroelectric receivers, which work near Curie point and with the low temperature of phase transition.

The increased interest in absolute radiometry and spectrometry, which woke up in recent years, will require the development of TPI with uniform spectral characteristic with the coefficient of absorption $\epsilon_0 \approx 0,99$ in the wide interval of the spectrum and by the stable in time parameters.

For developing TPI can be used any properties of materials,

which depend on temperature. It is desirable to obtain the reaction of receiver to radiation exposure in the form of the electrical signal, convenient for amplification by known methods. This necessary condition is also the large conversion factor in order that the threshold of response of receiver would be minimum and so its measuring device did not impair.

Up to now is not realized the thermodynamic sensitivity threshold of TPI. The obtained threshold values of sensitivity more than by an order exceed the value, characterized by the temperature fluctuations of sensing element. Therefore the search for the effective parameters, which depend on temperature, it continues. In recent years was proposed a series of principles for the creation of the TPI, of which thus far still not one gave the desired results.

On the possibility of applying ferrites as thermal materials in the infrared region of the spectrum it is reported in work [1].

Estimation of the parameters of the TPI, which can be created on the basis of the temperature dependence of the Hall coefficient InSb P-type with $T = 135^\circ\text{K}$, gives value for the standardized/normalized threshold sensitivity $\mathcal{S}^* = (10^{10}-10^{11}) (\text{cm}\cdot\text{Hz}^{1/2})/\text{W}$ with conversion factor $S = (10^3-10^4) \text{ V/W}$, but for Ge N-type with $T = 293^\circ\text{K}$ - by an order is worse [12].

To the determination of the possibility of emission/radiation measurement on the basis of the use of thermomagnetic effects in the crystals of gadolinium in the range of Curie point is dedicated [35]. The analysis of the powerful temperature dependence of the magnetization of layers from gadolinium fusion with magnesium in range 1020K indicated the possibility of recording the power of order 10^{-8} W/Hz^{1/2}. The report/communication about the powerful temperature dependence of the coefficient of the self-induction of some alloys and the practical application/appendices of this effect is given in work [40].

The anomalous course of the resistance of semiconductor titanate of barium in the field of phase transition can be used for the creation of sensitive bolometer.

Page 233.

The positive temperature specific resistance (TKS [- triple coordinate test stand]) of this material reaches 500/o [10, 11]. If one takes into account, that TKS of metallic bolometers composes 0.35-0.50/o, thermistor - 4-50/o, it is open/disclosed the prospect for the creation of receiver with large conversion factor Be managed

to preserve large TKS during transition to thin layers and they will not current noises limit the sensitivity threshold posistor bolometer, will show the further investigations.

It is natural that the development of the new sections of metrology, connected with development powerful radiation sources and with the investigation of super-weak radiation signals, will entail the new development of thermal receivers. Apparently, the basic effort/forces of the producers will be directed toward the creation of low-inertia receivers with high threshold sensitivity and with wide dynamic range with the high absorption coefficient. From this viewpoint ferroelectric thermal radiation detectors are promising.

Literature

1. Бокринская А. А., Захаров В. П., Слободянюк А. Н., Комлик В. П.— В кн.: Тепловые приемники излучения. «Наукова думка», К., 1967, 236.
2. Дюбко С. Ф., Свич В. А., Валитов Р. А.— ЖЭИФ (письма в редакцию), 1968, 7, 11, 408.
3. Гассанов Л. Г., Кременчугский Л. С., Мальнев А. Ф., Шульга А. Я., Яценкин П. И.— В кн.: Тепловые приемники излучения. «Наукова думка», К., 1967, 111.
4. Длинноволновая инфракрасная спектроскопия. «Мир», М., 1966.
5. Кременчугский Л. С.— В кн.: Тепловые приемники излучения. «Наукова думка», К., 1967, 3.
6. Кременчугский Л. С., Мальнев А. Ф., Столяров В. М., Шульга А. Я.— В кн.: Тепловые приемники излучения. «Наукова думка», К., 1967, 191.
7. Кременчугский Л. С., Мальнев А. Ф., Скаляренко С. К.— В кн.: Тепловые приемники излучения. «Наукова думка», К., 1967, 95.
8. Кременчугский Л. С., Мальнев А. Ф., Столяров В. М., Шульга А. Я.— ЦЭ, 1969, 4, 167.
9. Мальнев А. Ф., Кременчугский Л. С., Скачко М. А.— УФЖ, 1960, 5, 5, 631.
10. Тектер-Проскурякова Г. Н., Шефтель И. Г.— Радиотехника и электроника, 1966, 5, 907.
11. Тектер-Проскурякова Г. Н.— Приборостроение, 1966, 10, 21.
12. Трифонов В. И.— Физика и техника полупроводников, 1967, 1, 9, 1342.
13. Харченко А. М., Дуи Л. М., Смирнов Е. В., Боголюбова И. В.— В кн.: Тепловые приемники излучения. «Наукова думка», К., 1967, 105.
14. Allen D. W., Andrews J. C.— IEE Trans. Aerospace, 1967, 3, 20, 356.
15. Astheimer R. W., Buckley R. E.— Rev. Scient. Instrum., 1967, 38, 12, 1761; IEEE J. of Quantum Electronics, 1967, QE — 3, 6, 267.
16. Astheimer R. W., Schwarz E.— Appl. Optics, 1968, 7, 9, 1687.

17. Alday I. R., Everett G. E., White D. J.—IEEE Trans. Instrum. Meas., 1966, **14**, 2, 100.
18. Berkner K. H., Myers B. R., Pyle V.—Rev. Scient. Instrum., 1968, **39**, 8, 1204.
19. Duley W. W.—J. Scient. Instrum., 1967, **44**, 8, 629.
20. Ивасаки Х.—J. Radio Res. Labs., 1964, **11**, 55, 155; 1964, **10**, 47, 62.
21. Jones C. R.—J. Opt. Soc., America, 1946, **36**, 6, 355; 1947, **37**, 11, 888; 1949, **39**, 5, 327, 344.
22. Jones C. R.—Nature, 1952, **170**, 29, 937.
23. Jones C. R.—Advances in Electronics, 1953, **5**, 1.
24. Jones C. R.—Proc. IRE, 1959, **47**, 9, 1495.
25. Jones C. R.—J. Opt. Soc., America, 1960, **50**, 9, 883; 1960, **50**, 11, 1058; 1960, **50**, 12, 1166; 1962, **52**, 11, 1193.
26. Hickman T. G., Burdick G. A.—IEEE Trans., Instrum. Meas., 1968, **17**, 2, 165.
27. Hadni A., Henninger Y.—J. Phys., 1965, **26**, 6, 345.
28. Hadni A., Charlemagne D., Thomas R.—C. r. Ac. Sc., 1968, **266**, 18, 1230.
29. Glass A. M.—Appl. Phys. Lett., 1968, **13**, 4, 147.
30. Kimmitt M. F., Ludlow J. H., Putley E. H.—Proc. IEEE, 1968, **56**, 7, 1250.
31. Leiba E.—C. r. Ac. Sc., 1969, **268**, 1, 31.
32. Lang S. B., Steckel F.—Rev. Scient. Instrum., 1965, **36**, 12, 1817.
33. Дэнг С.—В кн.: Измерение нестационарных температур и тепловых потоков. «Мир», М., 1966, 261.
34. Ludlow J. H., Mitchell W. H., Putley E. H.—J. Scient. Instrum., 1967, **44**, 9, 694.
35. Ohman Y.—Optica Acta, 1959, **6**, 4, 372.
36. Maling G. C., Ingard U.—Rev. Scient. Instrum., 1967, **38**, 3, 119.
37. Toole J. M., Henisch H. K.—Solid-State Electr., 1968, **11**, 8, 743.
38. Steier W. H., Yamashita E.—Proc. IRE, 1963, **51**, 8, 1145.
39. Stanford A. L.—Solid-State Electr., 1965, **8**, 2, 747.
40. Willeus R. H., Buehler E., Nesbitt E. A.—Rev. Scient. Instrum., 1968, **39**, 2, 194.
41. White D. J.—J. Appl. Phys., 1964, **35**, 12, 3536.
42. Wünsche C.—Z. f. Angew. Phys., 1967, **22**, 5, 399.
43. Wooten F. T.—Proc. IEEE, 1967, **55**, 564.
44. White D. J., Weider H. H.—J. Appl. Phys., 1963, **34**, 8, 2487.

UNCLASSIFIED

SECURITY CLASSIFICATION OF THIS PAGE (When Data Entered)

REPORT DOCUMENTATION PAGE		READ INSTRUCTIONS BEFORE COMPLETING FORM
1. REPORT NUMBER FTD-ID(RS)T-0846-77	2. GOVT ACCESSION NO.	3. RECIPIENT'S CATALOG NUMBER
4. TITLE (and Subtitle) FERROELECTRIC RADIATION DETECTORS		5. TYPE OF REPORT & PERIOD COVERED Translation
		6. PERFORMING ORG. REPORT NUMBER
7. AUTHOR(s) L. S. Kremenchugskiy		8. CONTRACT OR GRANT NUMBER(s)
9. PERFORMING ORGANIZATION NAME AND ADDRESS Foreign Technology Division Air Force Systems Command U.S. Air Force		10. PROGRAM ELEMENT, PROJECT, TASK AREA & WORK UNIT NUMBERS
11. CONTROLLING OFFICE NAME AND ADDRESS		12. REPORT DATE 1971
		13. NUMBER OF PAGES 538
14. MONITORING AGENCY NAME & ADDRESS (if different from Controlling Office)		15. SECURITY CLASS. (of this report) UNCLASSIFIED
		15a. DECLASSIFICATION/DOWNGRADING SCHEDULE
16. DISTRIBUTION STATEMENT (of this Report) Approved for public release; distribution unlimited		
17. DISTRIBUTION STATEMENT (of the abstract entered in Block 20, if different from Report)		
18. SUPPLEMENTARY NOTES		
19. KEY WORDS (Continue on reverse side if necessary and identify by block number)		
20. ABSTRACT (Continue on reverse side if necessary and identify by block number) 18; 20		

DD FORM 1 JAN 73 1473

EDITION OF 1 NOV 65 IS OBSOLETE

UNCLASSIFIED

SECURITY CLASSIFICATION OF THIS PAGE (When Data Entered)

DISTRIBUTION LIST

DISTRIBUTION DIRECT TO RECIPIENT

ORGANIZATION	MICROFICHE	ORGANIZATION	MICROFICHE
A205 DMATC	1	E053 AF/INAKA	1
A210 DMAAC	2	E017 AF/ RDXTR-W	1
B344 DIA/RDS-3C	8	E404 AEDC	1
C043 USAMIIA	1	E408 AFWL	1
C509 BALLISTIC RES LABS	1	E410 ADTC	1
C510 AIR MOBILITY R&D	1	E413 ESD	2
LAB/FIO		FTD	
C513 PICATINNY ARSENAL	1	CCN	1
C535 AVIATION SYS COMD	1	ETID	3
C557 USAIIC	1	NIA/PHS	1
C591 FSTC	5	NICD	5
C619 MIA REDSTONE	1		
D008 NISC	1		
300 USAICE (USAREUR)	1		
ERDA	1		
CIA/CRS/ADD/SD	1		
NAVORDSTA (50L)	1		
NAVWPNSCEN (Code 121)	1		
NASA/KSI	1		
AFIT/LD	1		